MICROBIAL CELL IMMOBILIZED BIOCHAR FOR BIOREMEDIATION OF METAL IONS AND PESTICIDE FROM WATER AND SOIL

Thesis

Submitted in partial fulfilment of the requirements for the degree of

DOCTOR OF PHILOSOPHY

by

SOUMYA K M

Registration No. 197126CH004

DEPARTMENT OF CHEMICAL ENGINEERING

NATIONAL INSTITUTE OF TECHNOLOGY KARNATAKA,

SURATHKAL, MANGALORE

April, 2024

DECLARATION

I hereby declare that the research thesis entitled **"MICROBIAL CELL IMMOBILIZED BIOCHAR FOR BIOREMEDIATION OF METAL IONS AND PESTICIDE FROM WATER AND SOIL"** which is being submitted to the **National Institute of Technology Karnataka, Surathkal** in partial fulfilment of the requirements for the award of the degree of **Doctor of Philosophy** in Chemical Engineering is a *bonafide report of the research work carried out by me*. The material contained in this research thesis has not been submitted to any University or Institution for the award of any degree.

Soumya K M

197126CH004

Department of Chemical Engineering

Place: Surathkal

Date: 08-04-24

CERTIFICATE

This is to certify that the research thesis entitled **"MICROBIAL CELL IMMOBILIZED BIOCHAR FOR BIOREMEDIATION OF METAL IONS AND PESTICIDE FROM WATER AND SOIL"** submitted by **SOUMYA K M (197126CH004)** as the record of the research work carried out by her *is accepted as the research thesis submission* in partial fulfilment of the requirements for the award of degree of **Doctor of Philosophy.**

Research Guide

Dr. Vaishakh Nair

Assistant professor

Department of Chemical Engineering

NITK, Surathkal

Chairman DRPC

Head of the Department
विभागाध्यक्ष
Department of Chemical Engineering
रासायनिक अभियांत्रिकी विभाग
National Institute of Technology Karnataka - Surathkal
राष्ट्रीय प्रौद्योगिकी संस्थान कर्नाटक, सुरत्कल
PO Srinivasnagar, Mangalore - 575025 Karnataka
पी.ओ. श्रीनिवासनगर, मंगलौर – ५७५०२५, कर्नाटक

ACKNOWLEDGEMENT

I take this opportunity to acknowledge each and every individual who has contributed in different ways for my research work carried out in the Department of Chemical Engineering at NITK, Surathkal.

I wish to express special gratitude to my research guide, Dr. Vaishakh Nair, Assistant Professor, Department of Chemical Engineering, NITK, Surathkal for his valuable guidance, unwavering support, constant encouragement, and providing me the cognitive liberty throughout my PhD.

I sincerely thank and express my gratitude to the RPAC committee members, Dr. Lekshmi Vellanki, Department of Chemistry and Dr. Keyur Raval, Department of Chemical Engineering. Their insightful suggestions and expert guidance have helped me to improve the quality of my research work.

I express my sincere gratitude to the Director, NITK. I wish to extend my gratitude to all the HODs (Dr. Prasanna Belur, D., Dr. P. E. JagadeeshBabu and Dr. I. Regupathi) for providing support throughout the research work. I also wish to thank all teachers and research scholars in the Department of Chemical Engineering for their support and encouragement. I thank MoE, GOI for providing stipend throughout my research work.

I am deeply grateful to Dr. Hari Mahalingam for providing access to the laboratory facility and Prof. Vidya Shetty K., for the ICP OES facility.

I would like to extend my thanks to Mrs. Vijetha, Mrs. Bhavya Shree, Mrs. Shashikala, Mr. Jnaneshwar, Mr. Mahadeva, and all other non-teaching staff of the Department of Chemical Engineering for their timely help and support in the laboratory for the research work. I exclusively thank Mr. Suresh for his constant availability to rectify the issues in operating instruments. I also thank Central Research Facility (CRF), STIC (Kochi), SAIF IITM (Chennai), JNCASR (Bengaluru) for providing instrumentation facilities.

I would also like to extend my sincere gratitude to all my friends particularly Minimol M and the entire Energy and Environment Research Lab (EERL) group members. I deeply appreciate the invaluable support I received throughout my PhD, as they were always by my side with their honest appreciation and assistance, helping me to progress in my

academic journey. I am also indebted to my sister Remya K M, brother Midhun K M, and my sisters-in-law, Mrs. Smitha Suresh and Mrs. Kavitha Sivadasan, for their valuable support.

I also extend my heartfelt thanks to my parents for their constant support, which has made this challenging journey possible. I owe a debt of gratitude to my husband, Mr. Sumesh Mani, for his persistent encouragement and for pushing me to achieve my goals. Finally, I would like to thank my son, Master Ishan Sumesh, for his unwavering support and understanding throughout the research work.

Soumya K M

ABSTRACT

The escalating water and soil contamination, due to industrialization and urbanization, poses significant threats to human health and ecological safety. Among various pollutants, pesticides and heavy metals, are alarming due to their potential to bioaccumulate in organisms, disrupting the food chain and exposing humans. Bioremediation with microbial cells is promising but faces challenges such as microbial loss or reduced survival due to high pollutant concentration, uneven growth, cell washout and prolonged process time. In recent years, microbial immobilization technology has rapidly advanced for pollutant removal, with a focus on low-cost carriers with high removal efficiency. Biochar stands out as an efficient carrier due to its high porosity and strong adsorption capabilities, providing a habitat for microorganisms. This work explores the potential of microbial cell-immobilized biochar in removing cadmium, nickel, and chlorpyrifos from contaminated water and soil. Different combinations of biochar and microbial cells were tested, with the most efficient biochar selected for further pollutant removal experiments. The effect of various operating conditions, pH, temperature, biocatalyst dosage, and initial metal ion concentration, on cadmium and nickel removal efficiency were examined. *Pseudomonas stutzeri* immobilized on rice husk biochar showed significant efficacy, removing up to 95% of cadmium and 92% of nickel. Moreover, efficiently remediated cadmium-contaminated soil, converting exchangeable cadmium to less bioavailable residual fractions. Other combinations of microbial cell-immobilized biochar, such as *Pseudomonas stutzeri* immobilized sawdust biochar, *Bacillus* sp immobilized rice husk biochar, and *Pseudomonas stutzeri* immobilized coconut shell biochar were also efficient in metal ion removal. Additionally, *Aeromonas veronii* immobilized on rice husk biochar effectively degraded chlorpyrifos, with a removal rate of 96.25% in water within 24 h and 92.4% in soil within 42 days. The mechanism of metal ion and pesticide removal involves biochar-mediated adsorption, microbial cell-mediated bioaccumulation for metal ions, and microbial metabolism and biochar-mediated adsorption for pesticides. This combined biochar and immobilized microbial cell approach presents an innovative, sustainable solution for remediating metal ions and pesticide-contaminated environments.

Keywords: Biochar, immobilization, microbial cells, metal ions, chlorpyrifos, bioremediation, biodegradation, bioavailability, plant growth studies.

CONTENTS

LIST OF FIGURES

LIST OF TABLES

NOMENCLATURE

A. veronii	*Aeromonas veronii*
AAS	Atomic Absorption Spectroscopy
AFM	Atomic force microscopy
AOP	Advanced Oxidation Processes
ARHB	*Aeromonas veroni* immobilized rice husk biochar
BCR	European Community Bureau of Reference
BET	Brunauer-Emmett Teller
BET	Brunauer–Emmett–Teller
BRHB	*Bacillus* immobilized rice husk biochar
Cd	Cadmium
CFU	Colony forming units
CP	Chlorpyrifos
CSB	Coconut shell biochar
DETP	diethyl thiophosphoric acid
DTPA	diethylenetriamine pentaacetic acid
EDTA	Ethylenediaminetetraacetic acid
EDX	Energy Dispersive X-ray analysis
EPS	Extracellular polymeric substances
eV	Electron volt
FESEM	Field Emission Scanning Electron Microscopy
FID	flame ionization detection
FTIR	Fourier transform infrared spectroscopic
FYM	Farm yard manure
GC MS	Gas chromatography
GP	Germination percentage
GRI	Germination rate index
HPLC-UV	High per liquid chromatography with ultraviolet detection
HR-FESEM	High Resolution-Field Emission Scanning Electron Microscopy

HR-LCMS	High-resolution liquid chromatography-mass spectrometry
ICP-OES	Inductively Coupled Plasma – Optical Emission Spectrometry
LB	Luria Bertani broth
LC MS	Liquid chromatography
MCB	Microbial cell immobilized biochar
mg L^{-1}	Microgram per lite
MGR	Mean germination rate
MGT	Mean germination time
MSM	Minimal salt medium
MTCC	Microbial Type Culture Collection and Gene Bank,
NCBI	National centre for biotechnology information
Ni	Nickel
OD	Optical density
OP	Organophosphates
P. stutzeri	*Pseudomonas stutzeri*
PCSB	Pseudomonas stutzeri immobilized coconut shell biochar
PFO	pseudo-first order
PPSB	*Pseudomonas stutzeri* immobilized peanut shell biochar
PRHB	*Pseudomonas stutzeri* immobilized rice husk biochar
PS	Peanut shell
PSB	Peanut shell biochar
PSCB	*Pseudomonas stutzeri* immobilized sugarcane bagasse biochar
PSDB	*Pseudomonas stutzeri* immobilized sawdust biochar
PSO	pseudo-second order
QTOF	Quadruole time of flight
RH	Rice husk
RHB	Rice husk biochar
SC	Sugarcane
SCB	Sugarcane biochar
SD	Sawdust
SDB	Sawdust biochar

SEM	Scanning electron microscopy
SVI	Seed vigor index
TCP	3, 5, 6-trichloropyridinol
TEM	Transmission electron microscopy
TGA	Thermogravimetric Analysis
UV Vis	Ultraviolet visible
WHO	World health organization
XPS	X-ray photoelectron spectroscopy
XRD	X-ray diffraction
XRF	X-ray Fluorescence

CHAPTER 1

INTRODUCTION

1.1 HEAVY METAL AND PESTICIDE POLLUTION: AN ENVIRONMENTAL MENACE

Rapid industrialization, urbanization, and intensive agricultural activities have resulted in the depletion of natural resources and the production of vast volumes of hazardous waste that pollute water and soil, threatening the environment and human health (Razzak et al. 2022). Heavy metals, mainly originate from industrial processes like mining, smelting, and disposal of storage battery effluents (Deng et al. 2023) which are not biodegradable and tend to accumulate in living organisms through the food chain (Manikandan and Nair 2022). Heavy metals exhibit bioaccumulation and biomagnification characteristics despite their low concentrations and are toxic to living organisms (Adnan et al. 2022). Aside from the harm to humans, heavy metals in water bodies destroy aquatic habitats and cause harm across the food chain when contaminated water is absorbed by plants (Alengebawy et al. 2021).

Heavy metal contamination presents a significant global challenge, with studies revealing varying concentrations across continents, such as Europe (14%), America (30%), Africa (2%), and notably high levels in Asia (53%) (Roy et al. 2022). Factors like urban development, population density, and economic conditions influence these variations. Asian countries like China, India, Bangladesh, Jordan, and Pakistan report widespread heavy metal pollution, impacting groundwater, air quality, and agricultural lands (Elumalai et al. 2023). The Ministry of Environment, Forest and Climate Change has identified 320 high-risk sites for heavy metal contamination and pesticide pollution nationwide, with Uttar Pradesh, West Bengal, and Odisha having the highest concentration of affected areas. Industrialization is a key factor in this contamination, with the Ganga River being particularly affected by pollutants such as

chromium, copper, and nickel. Three-quarters of river monitoring stations in India report alarming levels of heavy toxic metals. The Ganga, a focal point of the Centre's Namami Gange mission, exhibits elevated levels of lead, iron, nickel, cadmium, and arsenic, according to the State of Environment Report 2022 by the Centre for Science and Environment (Simon and Joshi 2022). Recent studies from Bengaluru highlight significant heavy metal contamination in vegetables, urging immediate action for effective soil remediation. Research by the Environment Management and Policy Research Institute indicates that the use of wastewater for vegetable cultivation exceeds permissible limits set by the Food and Agriculture Organization, resulting in elevated concentrations of heavy metals in samples obtained from various outlets, posing substantial health risks to consumers.

Cadmium (Cd) and nickel (Ni) are common carcinogenic pollutants, relatively widespread in the environment, and can reach the aquatic ecosystem through wastewater discharges (Wang et al. 2020b). Cd is commonly found in mining, smelting, and rechargeable battery sewage (Agoro et al. 2020). WHO recommended Cd levels in drinking water is 0.005 mg L^{-1} (Guidi et al. 2020). Exposure to Cd causes liver damage, renal dysfunction, and bone degeneration (Rahman et al. 2022) (**Figure 1.1**). Ni is another potentially toxic element commonly found in soil and water systems and can be discharged into the environment from nickel alloy industries, pigment manufacturing processes, tannery industry wastewater, etc. Ni levels in fresh water and oceans are typically less than 0.02 mgL^{-1} (Hadzi et al. 2024). It mainly targets the respiratory tract, cardiovascular system, and immune system, resulting in the outbreak of diseases like allergies and asthma (Sharma et al. 2021).

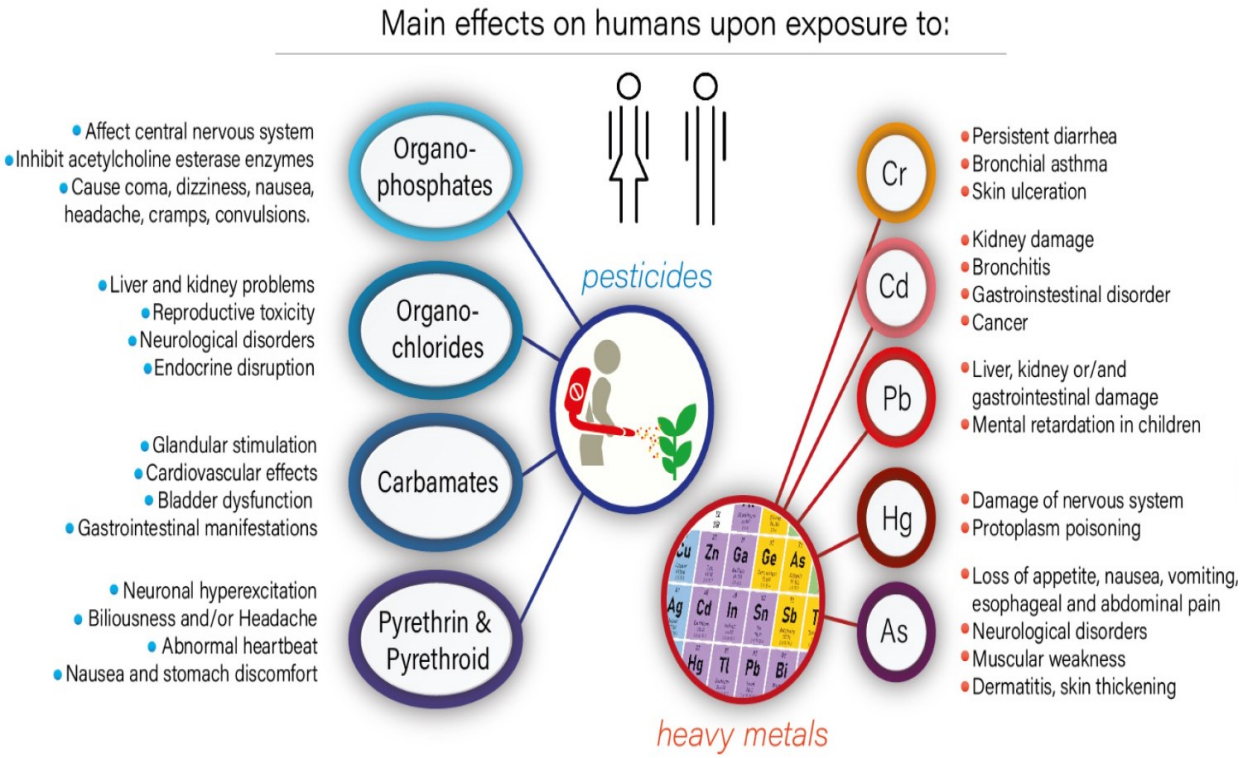

Figure 1.1. The effects of pesticides and heavy metal exposure on humans (Manikandan et al. 2023) .

India has played a pivotal role in ensuring crop protection and enhancing productivity through chemical pesticides, particularly during the green revolution (Gupta et al. 2022). However, the extensive application of pesticides has resulted in notable environmental issues, including soil and water pollution, adverse effects on non-target organisms, and potential health hazards. These chemicals, designed to improve food security, often release toxic materials into the surrounding environment, leading to detrimental consequences. Alarmingly, a significant portion of pesticides, up to 90 %, harm non-target organisms and can spread through air and soil pollution (Yang et al. 2023).

Chlorpyrifos (CP), a broad-spectrum chlorinated organophosphate pesticide widely used against a large number of insects and pests, infesting economically important crops, beetles, along with earth inhabitants (Hamadeen and Elkhatib 2022; Jacob et al. 2020). Despite being insoluble in aqueous solutions, CP and their by-products have been found to migrate into soil, water, and food chains (Mali et al. 2022). While some developed countries have banned CP, it continues to be widely used in developing countries, leading to its detection in various food

products (Yadav et al. 2021). CP, a banned pesticide in multiple countries due to its severe health risks, has garnered international attention, notably with the European Commission raising concerns over its detection in imported turmeric powder from India (Carrasco Cabrera and Medina Pastor 2022). Despite being among 27 deadly pesticides initially proposed for banning by the Indian government in 2020, pressure from the agrochemical industry led to a scaled-back decision, allowing its continued use alongside similar toxic pesticides (Yang et al. 2023). Numerous Indian studies have highlighted CP's detrimental effects on crops, human health, and the environment. A study conducted in Punjab in 2015 found CP residues in 6.4% of milk samples, accounting for 20.2% of all pesticide residues detected. Environmental research from West Bengal and Tamil Nadu indicated the genotoxic effects and histological alterations in organisms exposed to CP (Ray and Shaju 2023). Additionally, the main biodegraded product of CP, 3,5,6-trichloro-2-pyridinyl (TCP), is categorized as toxic and persistent, leading to secondary pollution. Various studies showed that less than 1 % of organophosphate pesticides are sufficient for controlling pests, and the remaining part contaminates the natural resources in the environment (Yadav et al. 2021). The high persistence and migration of CP in the environment have raised concerns about their impact on ecosystems.

1.2 SYNERGISTIC EFFECT OF HEAVY METAL AND PESTICIDE POLLUTION

The synergistic effect of heavy metals and pesticides presents a multifaceted threat to environmental health, impacting water, soil, plants, and ultimately human well-being (Alengebawy et al. 2021). Studies have shown that simultaneous exposure to heavy metals and pesticides can lead to increased toxicity in living organisms, affecting various physiological systems. For instance, in aquatic ecosystems, combined pollution of heavy metals and pesticides can disrupt water quality and harm aquatic life. In soil systems, the presence of pesticides alongside heavy metals can alter metal species behavior, potentially increasing their solubility of metal ions and bioavailability to plants (Alengebawy et al. 2021). This can result in contaminated crops and subsequent human exposure through food consumption. Uwizeyimana et al. (2017) found that combinations of cadmium with certain insecticides exhibited synergistic effects on earthworm mortality. Similarly, in plants, the synergistic effect of 2,4-dichlorophenol with zinc and copper in ryegrass-planted soil led to increased solubility

and toxic activity of heavy metals compared to 2,4-DCP-free samples (Chen et al. 2004). These interactions can affect various aspects of plant physiology, such as root and shoot growth inhibition, changes in tissue structure, and alteration of enzyme activities. Daily exposure to a combination of heavy metals and pesticides poses an increased threat to human organs also but limited knowledge exists about the toxicity of these mixtures. Animal studies indicate severe consequences, due to combined exposure to Cd and diazinon. Cytotoxicity analyses reveal lipid accumulation in hepatocytes when exposed to a mixture of Cd and CP, intensifying hepatic toxicity (Wallace and Buha Djordjevic 2020).

1.3 CONVENTIONAL REMEDIATION APPROACHES

During the last few decades, the separation of pollutants from water systems and soil via several methods has been developed and successfully applied (Manikandan et al. 2022). Technologies such as membrane filtration, ion exchange, and chemical precipitation have been utilized to remove pollutants. Chemical precipitation is a frequently used method because it is simple, inexpensive, and effective. However, chemical precipitation results in secondary pollution and eventually leads to additional difficulties in cleaning up the trace contaminants from large areas. Ion-exchange resin offers fast kinetics and is highly efficient for pollutant removal. However, the need for an acidic environment restricts their application in various contexts (Wu et al. 2021). Membrane filtration-based technologies can remove toxic substances with high efficiency, but the production of membrane materials is typically intricate and comes with a substantial cost. Hence it is observed that conventional pollutant remediation methods are not eco-friendly and produce toxic chemical sludge, as a result, there is an urgent need to improve sustainable, efficient, and low-cost technologies for monitoring and treating toxic environmental pollutants. A sustainable remediation method should exhibit high pollutant removal performance, economical, simple operation, and environmentally friendly processes. One such promising alternative is the use of biological methods for remediation. These methods involve using microorganisms, plants, or enzymes to naturally degrade, accumulate, or immobilize pollutants, making it a more environmentally friendly and sustainable option.

1.4 BIOREMEDIATION: A SUSTAINABLE SOLUTION

Bioremediation, a cost-effective and eco-friendly technique, relies on microorganisms to utilize organic pollutants as carbon sources for oxidation and decomposition and by reducing the toxicity of metals through various mechanisms. Diverse microorganisms play pivotal roles in bioremediation, with bacteria emerging as particularly advantageous in various studies as it targets a broad range of contaminants with specific metabolic pathways. Bioremediation can be effective even for contaminants in low concentrations that cannot otherwise be removed by chemical or physical methods.

Various bacterial strains, including *Bacillus cereus*, *Enterobacter* sp., *Pseudomonas aeruginosa*, *Bacillus licheniformis*, fungi such as *Penicilium notatum*, *Trichoderma brevicompactum*, *Aspergillus niger*, and microalgae like *Chlorella vulgaris*, are employed for heavy metal removal (Sharma and Shukla 2021; Zhang et al. 2020). Bacteria can bio adsorb, bioaccumulate, or bio-transform the heavy metals permanently at a low operating cost and without the generation of harmful secondary products (Huang et al. 2020). The diversity and metabolic activity of the microorganisms are influenced by the presence of heavy metal ions, which compels the microorganisms to develop resistance systems for overcoming this toxic metal ion stress. Furthermore, microorganisms convert toxic metal ions into inactive forms and can thus be utilized for bioremediation. One approach involves bioremediation through redox state change. This method transforms pollutants such as arsenic, mercury, and hexavalent chromium Cr (VI)) into less toxic forms through alteration of their oxidative states. Bacterial enzymes like arsenite oxidase catalyze the oxidation of toxic As (III) to less harmful forms, while Cr (VI)-reducing enzymes convert toxic Cr (VI) into non-toxic Cr (III) (Rahman et al. 2023). Various microorganisms, including bacteria like *Bacillus* and *Pseudomonas*, participate in these transformations. Biomineralization is another effective strategy where microorganisms facilitate mineral synthesis, immobilizing heavy metals in the mineral phase (Robles-Fernández et al. 2022). Bacteria such as *Staphylococcus epidermidis* and *Sporosarcina ginsengisoli* utilize biomineralization to immobilize lead and chromium, respectively. Fungi like *Penicillium chrysogenum* also contribute to biomineralization. Bio-volatilization involves microbial enzymatic activities that convert pollutants into volatile compounds. Bacterial enzymes like arsenic methyltransferases and mercury reductases facilitate the transformation of arsenic and mercury into less toxic volatile species, aiding in their removal from

contaminated sites. Filamentous fungi such as *Scopulariopsis brevicaulis* also participate in bio-volatilization, Biosorption processes involve the attachment of pollutants to active components of microbial cell walls through various binding mechanisms (Manikandan et al. 2023). Functional groups on cell components such as hydroxyl, carboxyl, and amine facilitate the accumulation of heavy metals through chemical and physical interactions. Pesticide bioremediation involves biodegradation and biotransformation. In biodegradation, biological reactions modify the compound's chemical structure, decreasing its toxicity. Several microbial strains such as *Sphingobacterium* sp, *Staphylococcus aureus, Dyadobacter jiangsuensis, Cupriavidus, Micrococcus luteus, Bacillus subtilis Pseudomonas aeruginosa, Pseudomonas putida, Klebsiella, Arthrobacter* and *Streptomyces* etc, have been reported for pesticide bioremediation (Jacob et al. 2020; Mali et al. 2022; Yadav et al. 2021; Yue et al. 2023).

1.5 CHALLENGES IN CONVENTIONAL BIOREMEDIATION APPROACHES

The application of microorganisms in the remediation of contaminated soil and water has demonstrated effective pollutant removal capabilities, however, there are some limitations, which have shown to affect the bioremediation process with time. Poor survival and proliferation of microorganisms in contaminated environments, mainly due to limited availability of nutrients, and competition with native microorganisms pose challenges for sustaining operational stability and achieving efficient recovery and reuse in bioremediation processes (Sun et al., 2020). The survival and reproduction of microorganisms are determined by external factors (e.g., temperature, pH, humidity) and microorganisms can only play a role when the external environmental conditions allow growth activities. To address these limitations of using free cells (bacteria alone), microbial cell immobilization has emerged as an effective approach, exploring various natural and synthetic materials (Manikandan et al.2023). Immobilization provides an ideal habitat for the survival and functioning of bacteria under biotic and abiotic environmental conditions (Sun et al., 2020). Therefore, the development of promising materials for microorganism immobilization holds significant importance. Microbial support material needs to exhibit specific characteristics: cost-effectiveness, environmental friendliness, high mechanical and chemical stability, ample space for immobilized cells, prevention of protein denaturation, and the facilitation of interactions between the substrate and the immobilized cells (Manikandan et al. 2023). Commonly employed materials for microbial immobilization include natural materials such as cellulose,

agar, agarose, chitosan, alginate, and biomasses like wood chips and wheat straw (Mehrotra et al. 2021), as well as synthetic polymers and inorganic materials. Natural materials like chitosan, cellulose, alginate, and carrageenan possess high surface area and uniform pore size, but they are chemically inert, require proper activation, and are susceptible to high contamination rates and limited shelf life. Inorganic polymers like silica and ceramics exhibit good biocompatibility but are limited by mechanical stability and diffusion constraints (Manikandan et al. 2023). Conversely, synthetic matrices like polyurethane offer diverse functional groups and strong binding, though they suffer from relatively low diffusion coefficients, harsh immobilization conditions, and complex, time-consuming synthesis PROCESSES (MEHROTRA ET AL. 2021).

1.6 BIOCHAR AS AN IMMOBILIZATION SUPPORT

Biochar is a carbonaceous material that is produced through the thermal treatment of diverse biomass sources, such as crop residues and biosolids (Noronha et al. 2022). Biochar production can be achieved via various processes, including slow or fast pyrolysis, flash carbonization, gasification, hydrothermal carbonization, torrefaction, etc. (Sahoo and Remya 2022). The key goal when designing the synthesis of biochar is that the final material should possess high porosity, a large specific surface area, and elevated surface chemistry heterogeneity, as with oxygen-containing functional groups and minerals. Such characteristics encourage biochar’s rising application in waste water treatment, soil improvement, and bioremediation highlighting its versatility. In recent years, biochar has garnered significant attention as a promising candidate for use as an immobilization support material in various environmental applications. This rise in interest can be attributed to biochar's exceptional attributes, including its high carbon content, cation exchange capacity, porosity, inherent stability, and abundant surface functional groups.

Various mechanisms are involved in biochar-mediated pollutant removal, such as physisorption, complexation, precipitation, ion exchange, and electrostatic interactions (Zhou et al. 2022). Notably, biochar's high surface area and pore volume confer an enhanced affinity for pollutants heavy metals, and pesticides, physically entrapping them within its surface pores. The negatively charged surfaces of biochar can adsorb positively charged metal ions via electrostatic attraction. When used as a microbial support, biochar offers an ideal substrate for

microbial attachment. Microbial cells anchor themselves to biochar through mechanisms like adhesion, utilizing extracellular appendages and interacting with surface functional groups, including oxygen-containing moieties, which form hydrogen bonds and electrostatic interactions. Furthermore, biochar's porous structure creates a conducive environment for microbial colonization and provides favorable conditions for growth (Mukherjee et al. 2022) Within the biochar matrix, microbial cells have access to essential nutrients, water, and oxygen, enhancing their metabolic activity and overall performance.

1.7 MICROBIAL CELL IMMOBILIZED BIOCHAR

The concept of microbial cell immobilized biochar involves a coordinated approach wherein contaminant-tolerant microorganisms are combined with biochar to enhance environmental remediation processes. This leads to the mass transfer of contaminants from polluted environments to the degrading microbial community, fostering the enrichment of degrading bacteria and facilitating the formation of biofilms. Biochar, recognized for its capacity to improve soil quality and adsorb pollutants in both soil and water, takes on a pivotal role in this synergy. Biochar's multifaceted contributions extend to enhancing soil fertility and biological community composition through physical adsorption, facilitating microbial oxidation and decomposition of pollutants via metabolic processes (Rombel et al. 2022). Its porous structure provides an ideal environment for microbial growth and reproduction, along with a crucial source of nutrients that help counter the adverse effects of external environmental factors (Wahla et al. 2022). Especially, biochar can increase biosorption by alleviating pollutant concentrations and changing environmental conditions to reduce the inhibition of excessive pollutant concentrations on the growth of microorganisms. Therefore, microbial cell immobilized biochar is a promising and innovative remediation strategy for addressing wastewater and soil contamination challenges.

The present study explores the promising potential of microbial cell immobilization using biochar to efficiently remove heavy metals Cd, Ni, and pesticides CP from water and soil environments. Initially, the bacterial strain *P. stutzeri*, known for its heavy metal tolerance, is immobilized on rice husk biochar. The study optimizes the biochar pyrolysis conditions for immobilization and evaluates its efficiency in removing Cd and Ni from water. The characterization of biochar and microbial cells immobilized biochar reveals information about

their structure and functional groups. Furthermore, the study investigates the mechanisms underlying heavy metal removal by *P. stutzeri* immobilized rice husk biochar. The work extends to the remediation of Cd -contaminated soil, evaluating the efficacy of Cd removal and its impact on plant growth using *Spinacia oleracea* are analyzed to assess the overall remediation effectiveness. In addition to *P. stutzeri* immobilized rice husk biochar, other combinations, such as *P. stutzeri* immobilized sawdust biochar, also tested for Cd and Ni removal from water. Similarly, *Bacillus* sp immobilized rice husk biochar and *P. stutzeri* immobilized coconut shell biochar are utilized for Cd removal from soil. Another significant aspect of the research involves exploring the removal of the pesticide, CP from water and soil using *A.veroni* immobilized rice husk biochar. The process is optimized to enhance CP degradation in water. Further soil study is carried out, and soil fertility and remediation efficiencies are assessed through plant growth studies using *Vigna unguiculata*. Finally, the potential degradation pathway of CP by the *A.veronii* immobilized rice husk biochar was elucidated.

CHAPTER 2

LITERATURE REVIEW

2.1 HEAVY METALS AND PESTICIDES AS POLLUTANTS

Soil and water contamination is a pressing issue arising from industrial and agricultural activities, introducing both inorganic (e.g., heavy metals) and organic (e.g., pesticides) pollutants (Manikandan et al. 2022). Heavy metals, encompassing cadmium, lead, mercury, nickel, chromium, arsenic, copper, and zinc, result from natural and human-induced sources, contaminating soil through mining, industrial emissions, and improper waste disposal (Amin and Chetpattananondh 2019). Industrial processes, exhaust gases, and sewage irrigation intensify heavy metal contamination. Additionally, atmospheric deposition from combustion and the use of chemical fertilizers contribute to this environmental concern. These persistent heavy metal contaminants resist natural biodegradation, posing risks to ecosystems and human health, impacting soil productivity, and fertility, and leading to bioaccumulation in the food chain, which raises serious health concerns as depicted in **Figure 2.1**. Certain heavy metals, such as cadmium, arsenic, and mercury, exhibit high toxicity even at low concentrations, adversely affecting soil quality, productivity, and human health (Priyadarshanee and Das 2021). Exposure to these metals can result in severe consequences, including growth abnormalities, carcinogenesis, neuromuscular defects, mental illnesses, and metabolic dysfunction.

In tandem, the escalating use of pesticides, driven by the demand for increased agricultural yields, poses a significant challenge to sustainable agriculture. Runoff and improper waste disposal contribute to long-term contamination, creating sites with high pesticide concentrations. Pesticides, including insecticides, fungicides, and others, play a vital role in pest and disease control, enhancing agricultural productivity. However, their inefficiency in

application, with less than 0.1 % reaching the target, leads to their accumulation in soil (Das and Adhya 2015). Presently, organophosphates (OP) are extensively used in agriculture due to their lower environmental persistence and higher efficiency compared to organochlorine and carbamate pesticides.

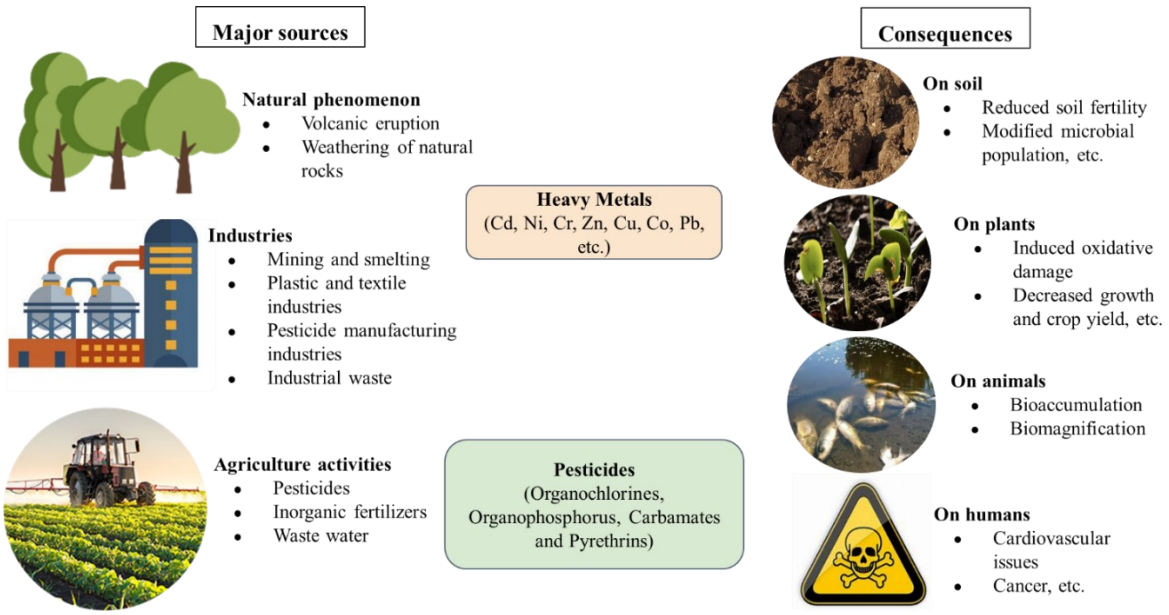

Figure 2.1. Heavy metal and pesticide pollution sources and consequences.

2.1.1 Cadmium

Cd is ranked as the seventh most hazardous metal according to the Agency for Toxic Substances and Disease Registry (Tully et al. 2000). Prolonged exposure to Cd contamination significantly impacts both humans and animals, primarily through inhalation or ingestion from various sources such as metal industries, spoiled food, cigarettes, and Cd-related products in factories and work areas (Beesley and Marmiroli 2011). The indirect oxidative stress caused by Cd is likely associated with its carcinogenic and mutagenic properties, leading to serious health risks like kidney damage, prostate dysfunction, bone diseases, and cancer. Recognized as a highly toxic and nonessential heavy metal, Cd is known for its inhibitory effects on enzymatic reactions, inducing oxidative stress and nutritive deficiencies in plants (Irfan et al. 2013). Its ability to replace calcium in minerals due to similar ionic radius, charge, and chemical behavior adds to its toxic nature. Unlike other toxic elements such as Hg, and As, Cd primarily enters the human diet through terrestrial pathways, notably via vegetables. Chronic

Cd poisoning, known as itai-itai disease and first identified in Japan in the early 20th century, results in renal tubular dysfunction, osteomalacia, and osteoporosis due to competition with calcium and other nutrients. According to WHO (2011), the tolerable monthly Cd intake is set at 25 μg kg^{-1} body weight due to its extended biological half-life in humans, ranging from 10 to 35 years. Previous studies have explored the occurrence and behavior of Cd in soils and groundwater concerning agricultural aspects (bioavailability) and environmental remediation (Khan et al. 2017). Cd typically exists in soil water up to 5 μg L^{-1} and in groundwater up to 1 μg L^{-1} (Naseem et al. 2014).

2.1.2 Nickel

Ni, a potentially harmful element, is commonly present in soil and water systems. It exhibits four oxidation states (+1, +2, +3, and +4), with its primary oxidation state being +2. Ni is more toxic in its cationic form than in its complexes and is released into the environment from both human-made and natural sources (Manikandan and Nair 2022). Examples include emissions from Ni alloy industries, pigment manufacturing processes, and tannery industry wastewater, as well as through weathering and pedogenesis. Inadequate disposal of industrial wastes and airborne deposition of contaminants can result in increased levels of Ni in soil and water. Ni contamination can be directly transferred from air and soil to surface water bodies through deposition and soil runoff, or indirectly to groundwater through leaching (Boros-Lajszner et al. 2018). Excessive amounts of Ni beyond the permissible limits in soil (35 mg kg^{-1}) and water (0.02 mg L^{-1}) pose toxicity risks to all living organisms. Elevated Ni intake can lead to severe health issues in humans, such as allergies, cancer, and reduced lung function (Zambelli et al. 2016). Consequently, the presence of high concentrations of Ni in drinking water, soil, or its entry into the food chain through plant uptake poses significant health threats to both humans and animals, threatening the ecological sustainability of the global system (Rinklebe and Shaheen 2017).

2.1.3 Chlorpyrifos

Chlorpyrifos (O, O-diethyl O-(3,5,6-trichloro-2-pyridyl) phosphorothioate), is a commonly used diethylphosphorothionate organophosphate pesticide (**Figure 2.2)** Dow chemical company introduced CP in 1965 as a foliage pesticide for extensive use in major crops (Sobiecka et al. 2022). CP has been commercially employed in various formulations,

including emulsifiable concentrates, wettable powder, and granules. OP accounts for more than 36 % of the global market share, with millions of kilograms applied annually.

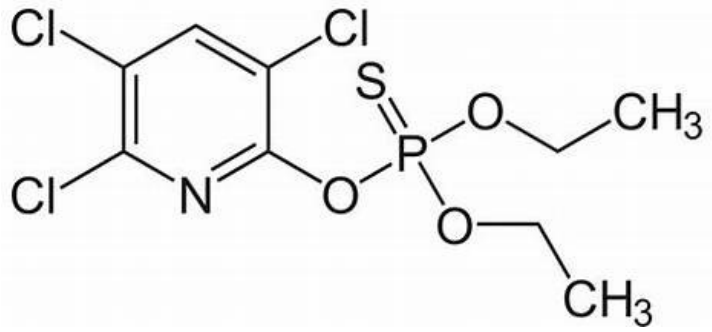

Figure 2.2. Structure of CP.

CP operates by inhibiting the acetylcholinesterase enzyme, leading to overstimulation of the nervous system, paralysis, convulsions, and, ultimately, the death of mammals and insects (Bakshi et al. 2021). CP is employed to control a broad spectrum of insect pests, including leafhoppers, cutworms, leaf folders, corn rootworms, gall midges, cockroaches, flies, grubs, termites, flea beetles, lice, fire ants, and both larval and adult mosquitoes (Hamadeen and Elkhatib 2022; Jacob et al. 2020) The fate of CP is influenced by its water solubility and various environmental conditions. Natural organic matter in soil facilitates the transport of pesticides from soil to water, impacting soil's storage, buffering, filtering, inactivation, and degradation potentials (Aziz et al. 2021). This transport occurs through interflow, leaching, surface overflow, underground drainage, and mineral nutrient transfer from soil to the human food chain. CP undergoes rapid hydrolysis, resulting in the formation of its moderately mobile primary metabolite, 3, 5, 6-trichloropyridinol (TCP) (Rochaddi et al. 2019). Hydrolysis also generates other intermediary derivatives, including diethyl thiophosphoric acid (DETP) and small quantities of chlorpyrifos oxon, desethyl chlorpyrifos, desethyl chlorpyrifos oxon, and 3,5,6-trichloro-2 methoxypyrimidine (Das and Adhya 2015). Chlorpyrifos oxon and TCP byproducts are more hazardous than the parent CP compound.

2.2 DETECTION AND ANALYSIS OF HEAVY METALS AND PESTICIDES

2.2.1 Heavy metal detection and analysis in water and soil

The detection and quantification of heavy metal concentrations in water and soil are imperative before selecting an effective remediation approach. The chosen technique should

fulfill criteria such as cost-effectiveness, environmental friendliness, selectivity, and sensitivity to detect traces precisely (Mali et al. 2022). The advancement and incorporation of various techniques such as electrochemical, optical, and spectroscopic methods for detecting metal ions now facilitate the accurate measurement of heavy metal concentrations.

Electrochemical techniques lie in various approaches such as potentiometric, amperometric, voltammetric, coulometric, impedance, and electrochemiluminescent methods (Malik et al. 2019). An emerging field in this domain involves biosensors, leveraging enzymes and other biological molecules, either independently or in conjunction with nanostructured metallic materials. This innovation has facilitated the identification of a broader range of contaminants in water samples (Gumpu et al. 2015). The procedures associated with these techniques are relatively straightforward and adaptable to portable devices for on-the-spot monitoring (Bansod et al. 2017). Despite their affordability, user-friendliness, reliability, and quick analytical detection times, electrochemical methods exhibit higher detection limits. Notably, their effectiveness diminishes when coexisting with other metal cations in a sample, reducing detection sensitivity (Chen et al. 2018). Consequently, electrochemical methods face challenges in achieving ideal levels of selectivity and sensitivity. Specifically, Voltammetry, a prominent electrochemical method, faces challenges when analyzing heavy metal ions in soil samples due to their complex matrices, which can introduce interferences affecting measurement accuracy (Buledi et al. 2020). In contrast, ICP-OES is less susceptible to such matrix effects as it efficiently atomizes and excites the sample in the plasma, minimizing interference. Additionally, voltammetry is more prone to interference from solution-phase electroactive species, leading to inaccurate determination of analyte concentration compared to ICP-OES (Meng et al. 2023).

A diverse array of optical sensors and test strips has been devised to detect heavy metals in aqueous solutions. Noteworthy techniques include the application of fluorophores or indicator dyes, biosensor tests, or the combination of an ionophore with a pH indicator (Lukyanenko et al. 2019). Another approach involves utilizing nanoparticles and receptor molecules to ascertain the concentration of a single analyte by gauging the light absorbance of the sample (Kurup et al. 2017). Valuable research has been conducted on portable optical enzymatic biosensors, particularly for swiftly identifying pollutants in water samples (Lukyanenko et al.

2019). While several optical molecular detectors promise rapid analyses, many are constrained by poor selectivity (Malik et al. 2019).

Highly sensitive and selective spectroscopic methods, including Atomic Absorption Spectroscopy (AAS), X-ray Fluorescence (XRF), Inductively Coupled Plasma Optical Emission Spectroscopy (ICP-OES) facilitate the detection of heavy metals with low limits of detection in the femtomolar range (Zamora-Ledezma et al. 2021a). For example, AAS exhibits relatively low detection limits, such as 2, 3, and 0.2 µg L^{-1} for Cu, Pb, and Cd ions, respectively (Kurup et al. 2017). While spectroscopic techniques offer advantages in the simultaneous determination of a wide range of heavy metal concentrations, their complexity, cost, and the need for specialized personnel limit their applicability in portable field versions, which often exhibit lower sensitivity and accuracy (Kurup et al. 2017). Portable XRF equipment, for instance, has higher detection limits, making it less useful for trace detection (Kodom et al. 2012). Detection limits of heavy metal Cd and Ni are represented in **Table 2.1.**

Table 2.1. Detection limits of Cd, Ni, and CP as reported by various techniques.

Heavy metal	Technique	Limit of detection	Reference
Cd	ICP-MS	0.01 µg L^{-1}	(Malik et al. 2019; WHO 2017)
	AAS	2 µg L^{-1}	
	ICP-OES	0.0010 µg mL^{-1}	
	Potentiometry	1×10^{-7} mol L^{-1}	
	Amperometric	1.78×10^{-7} mol L^{-1}	
Ni	ICP-MS	0.1 µg L^{-1}	(Malik et al. 2019)
	AAS	0.5 µg L^{-1}	
	ICP-OES	10 µg L^{-1}	
CP	LC-MS	0.4- 13 ngL^{-1}	(Nandhini et al. 2021)
	HPLC-UV	0.3- 0.6 μg^{-1}	
	GC MS	0.2-3.5 ngL^{-1}	

ICP-OES stands out as a powerful analytical technique for the comprehensive analysis of heavy metals in water and soil. This method utilizes a high-temperature inductively coupled plasma to atomize and excite the sample, followed by optical emission spectrometry to quantify the elemental composition (Fu and Wang 2011). ICP-OES is particularly advantageous for heavy metal analysis due to its exceptional sensitivity, allowing for the detection of trace concentrations in both water and soil matrices (Kos et al.1996; Lu et al. 2018). Its broad dynamic range accommodates the measurement of various heavy metals, and the simultaneous multi-element capability enables a comprehensive assessment of metal profiles in environmental samples (Lu et al. 2018).

2.2.2 Detection of pesticides from water and soil

Pesticide analysis in water and soil is commonly conducted through gas chromatography and liquid chromatography, both coupled with various detectors. Multiresidue methods, employing liquid chromatography or gas chromatography-tandem mass spectrometry, are extensively utilized for monitoring environmental contaminants due to their quantification capabilities, even at low concentrations. Recent advancements in sensor-based methods have demonstrated high sensitivity, making them suitable for analyzing specific pesticide groups (Hassani et al. 2017). Sample preparation is a critical step in pesticide analysis, typically involving conventional methods such as liquid-liquid extraction and solid-phase extraction (Khalili-Zanjani et al. 2008).

Gas chromatography (GC) exhibits superior performance for volatile and thermolabile molecules and can be coupled with detectors like electron capture detector (ECD), flame photometric detection, flame ionization detection (FID), or mass spectrometry (GC-MS). For instance, GC-FPD has been applied to water samples for the analysis of organophosphorus pesticides demonstrating rapid and efficient extraction (Khalili-Zanjani et al. 2008). Another study utilized GC-FID after single-drop microextraction for the analysis of pesticides in water, highlighting advantages such as simplicity and minimal solvent and sample volume requirements (de Souza Pinheiro and de Andrade 2009).

In addition to GC methods, liquid chromatography with ultraviolet detection (HPLC-UV) has been applied to detect OP and their metabolites in water samples, showcasing advantages such as reusability and selectivity using molecularly imprinted polymer as a solid-phase

extraction sorbent (Arias et al. 2023). Liquid chromatography (LC) is suitable for polar, nonvolatile, and thermolabile substances and can be coupled with various detectors, including ultraviolet diode array detection, fluorimetric detection, and tandem mass spectrometry (LC-MS/MS). LC-MS/MS has gained popularity for its sensitivity and confirmation capabilities, especially for closely related compound groups like sulfonamides, glyphosate, CP, and its metabolite.

Multiresidue pesticide analysis in water and wastewater samples involves low-resolution mass spectrometers like LC-triple quadrupole MS (TQ-MS) and high-resolution mass spectrometers like LC-QTOF. These are highly selective, and less commonly used due to cost considerations and maintenance issues. Sensor-based methods, employing nanocomposites, and biosensors, represent a promising area of research in pesticide analysis. These methods aim to meet criteria such as user-friendliness, sensitivity, selectivity, reusability, and low cost, although challenges exist, especially in determining multiple pesticides in complex samples like seawater and wastewater (Hassani et al. 2017).

2.2.3 Methods for simultaneous detection of pesticides and metal ions

Electrochemical biosensors have emerged as promising tools for detecting pesticides and heavy metal ions in water due to their portability, low cost, simplicity, selectivity, and sensitivity (Hara and Singh 2021). Chouteau et al. (2005) devised a method involving a bi-enzymatic whole cell conductometric biosensor utilizing immobilized *Chlorella vulgaris* microalgae. It utilizes alkaline phosphatase and acetylcholinesterase enzymes, which are inhibited by heavy metals and pesticides, respectively. The immobilized algae within bovine serum albumin membranes on conductometric electrodes enable the detection of local conductivity variations caused by enzyme activities. The biosensor exhibits sensitivity to specific heavy metal ions like Cd and Zn, with limits of detection of 10 ppb after a 30 min exposure. Another method as described by Tekaya et al. (2014) involves bi-enzymatic conductometric biosensor for detecting heavy metal ions and pesticides in water samples, based on enzymatic inhibition in *Arthrospira platensis*. The biosensor immobilizes Spirulina cells on gold interdigitated transducers, where phosphatase and esterase activities are inhibited by heavy metals and pesticides, respectively. The biosensor exhibits quantification limits for

Cd and Hg at 10^{-20} M in mixtures and pure solutions, and for parathion-methyl, paraoxon-methyl, and triazine at 10^{-20} M, 10^{-18} M, and 10^{-20} M, respectively.

These techniques, while offering significant advantages for detecting pesticides and heavy metals in water, also come with challenges. The complexity of water matrices in environmental samples can lead to interference with electrochemical measurements, compromising the accuracy and reliability of results (Hara and Singh 2021). Additionally, these biosensors are often designed for specific analytes or classes of compounds, limiting their ability to simultaneously detect a wide range of contaminants without customization (Rao et al. 2011). Issues related to durability and stability, such as electrode fouling and degradation of sensing elements, can affect long-term performance (Chouteau et al. 2005). Electrochemical biosensors offer cost advantages over traditional methods, initial setup costs and ongoing maintenance expenses can still be significant, potentially limiting their accessibility for smaller research laboratories or monitoring agencies with limited budgets.

2.3 HEAVY METAL AND PESTICIDE REMEDIATION METHODS

2.3.1 Heavy metal remediation

The removal of heavy metals from wastewater involves various conventional and non-conventional methods. Chemical precipitation is a conventional technique where chemical precipitants react with heavy metals to form insoluble precipitates, facilitating their removal (Chen et al. 2018). Coagulation/flocculation is a physicochemical method that agglomerates fine particles into larger ones, enhancing their removal through settling. Ion exchange involves reversible ion exchange between solid and liquid phases, effectively treating inorganic effluents. Membrane technologies use selective barriers to separate compounds. Electrochemical technologies, including electrocoagulation and electrodeposition, are environmentally friendly but can be capital-intensive. The advantages and disadvantages of conventional technologies for removing heavy metals from wastewater are illustrated in **Table 2.2.**

Table 2.2. Advantages and disadvantages of different technologies for removing heavy metals from wastewater.

Technology	Advantages	Disadvantages	Reference
Chemical precipitation	• Process simplicity • Not metal selective • Inexpensive capital cost	• A large amount of sludge containing metals • Sludge disposal cost	(Azimi et al. 2017; O'Connell et al. 2008)
Ion exchange	• Metal selective • Limited pH tolerance • High regeneration	• High initial capital cost • High maintenance cost	(Kurniawan et al. 2006)
Coagulation–flocculation	• Bacterial inactivation capability • Good sludge settling	• Chemical consumption • High sludge volume	(Azimi et al. 2017)
Membrane filtration	• Low solid waste generation • Low chemical consumption	• High initial capital cost • High maintenance cost	(Bashir et al. 2019)
Electrochemical treatment	• No chemical required • can be engineered to tolerate suspended solids	• High initial capital cost Production of H_2(with some processes)	(Azimi et al. 2017; Bashir et al. 2019)

Non-conventional treatments include adsorption, microbial fuel cell nanotechnology, and Fenton-like reactions. Adsorption, a widely used method, involves materials like activated

carbon, polymeric substances, agricultural residues, and industrial wastes to capture contaminants (Zamora-Ledezma et al. 2021). Microbial fuel cell technology employs microbes to produce electricity while simultaneously removing heavy metals. Nanotechnology-based treatments, using nanomaterials like carbon nanotubes and graphene, leverage their unique properties for efficient heavy metal adsorption. Fenton-like reactions involve the generation of highly reactive hydroxyl radicals for metal removal.

The remediation of heavy metals from soil involves a multi-faceted approach, incorporating physical, chemical, and biological methods. Physical methods, such as soil washing and thermal desorption, exhibit a broad spectrum of applicability but often incur high costs and necessitate further processing (Santos et al. 2015). Electro remediation, leveraging low electric currents, proves effective in confining and recovering pollutants, yet its operational temperatures pose challenges (Bahemmat et al. 2016). Chemical remediation techniques encompass vitrification, chemical leaching, chemical fixation, and electrokinetic methods (Dhaliwal et al. 2020). Vitrification technology, despite its efficiency, is complex and energy-intensive. Chemical leaching transfers heavy metals to the liquid phase, but drawbacks include by-product formation and increased downstream processing (Dhaliwal et al. 2020).

2.3.2 Pesticide remediation

The detection and elimination of pesticides from soil and water are imperative due to their severe threats to human health and the environment. Physical techniques, such as adsorption, oxidation, catalysis, degradation, and membrane filtration, have been employed for pesticide removal in the environment, specifically from soil and water (Nandhini et al. 2021). However, conventional approaches for pesticide degradation often require pre-sample processing, involving mechanical treatments like cleaning, drying, filtering, grinding, and sieving before instrumental analysis. Methods like soil washing, and different adsorbents can reduce organophosphates pesticide levels, but their persistent nature limits the effectiveness of these approaches. Disposal methods such as deep well burial, landfill, and open burning have raised environmental and health concerns. Issues such as land requirements, leaching, slow decomposition, and climatic variations further hinder their application in the removal of pesticides from soil. **Table 2.3.** summarizes the advantages and disadvantages of various techniques used for pesticide removal.

Table 2.3. Advantages and disadvantages of different technologies for removing pesticides from wastewater.

Technology	Advantages	Disadvantages	Reference
Incineration	• Complete degradation of pesticides to ash	• Ash disposal challenge • Generation and release of cyanides into the environment	(Ferguson and Wilkinson 1984)
Zero-valence iron	• Iron is inexpensive	• Action diminishes over time as oxide layer formation obstructs active sites.	(Shoiful et al. 2016)
Electrokinetic combined with Fenton process	• Low concentrations of iron in the solution • Easy recycling of the catalyst	• Optimal pH range is typically narrow, preferably between 3 and 5 in most cases	(Ajiboye et al. 2020)
Fenton oxidation	• Easy to implement • Able to degrade a wide range of contaminants	• High cost • It is pH-sensitive • High organic content soil needs a large amount of oxidant	(Shoiful et al. 2016)
Supercritical oxidation	• Toxic gases and particulates are not released	• Problem associated with construction of super critical oxidation unit	(Xu et al. 2015)
Electrokinetic combined with surfactants	• Decrease the surface tension of the liquid • Improve contaminant solubility.	• Surfactant consumption varies based on type and environmental factors	(Shoiful et al. 2016)
Soil washing	• selectively target and remove specific pesticides	• The process employs chemicals with potential environmental impacts	(Ajiboye et al. 2020)

Advanced Oxidation Processes (AOP), such as photocatalysis, Fenton reactions, electro-Fenton reactions, and radiation, offer a promising avenue for pesticide removal by generating reactive oxygen species that facilitate simultaneous oxidation and destruction of contaminants (M'Arimi et al. 2020). Challenges associated with AOP include the cost of radiation devices and potential material breakdown. Ozonation, coupled with UV irradiation or hydrodynamic cavitation, enhances CP degradation, but concerns about byproducts and cost-effectiveness persist. Electrochemical oxidation technologies, including Sono electrochemical methods and ultrasound-induced acoustic cavitation, present alternative approaches (Joseph et al. 2009). Heterogeneous Fenton processes and nanomaterials, like nanoparticles and nanocomposites, contribute to photocatalysis, albeit with challenges like nanoparticle recovery and potential toxicity.

2.4 ROLE OF BIOCHAR IN THE REMOVAL OF HEAVY METALS AND PESTICIDES

Biochar is a carbon-rich material derived from biomass such as wood, manure, or leaves upon thermal treatment at high temperatures with minimal or in the absence of air (Noronha et al. 2022). Various processes, such as pyrolysis, gasification, and hydrothermal carbonization, are applied in biochar generation (Yaashikaa et al. 2020). Biochar, with its porous structure and diverse surface-functional groups, efficiently adsorbs pollutants through hydrophobic and polar interactions. Its eco-friendly nature and low-cost production, along with simple large-scale synthesis, contribute to economic efficiency in the (bio) economy cycle. Biochar has been well established as a low-cost adsorbent that has adsorption capacities similar to carbon-based adsorbents, such as activated carbon, porous graphitic carbon nitride, graphene oxide, etc

2.4.1 Biochar production

Biochar production usually involves biomass collected from various plant/animal sources or wastewater sludge and thermal treatment using oxygen-deficient conditions, particularly pyrolysis. Pyrolysis in oxygen-free conditions comprises the decomposition of lignocellulosic material, volatile matter release, and the reduction of carbonaceous material for plant biomass (Ogura et al. 2021). The types of pyrolysis include slow, fast, microwave-assisted, hydro- and co-pyrolysis. Slow pyrolysis operates for h in the temperature range of (300–700 °C), whereas fast pyrolysis with lower residence time (< 2–5 s).

Variations in high-temperature processes have also been tested in the context of biochar production. Microwave-assisted pyrolysis for biochar generation has also been demonstrated, with variations in absorbable power observed for biochar property analysis, with the demonstrated advantages of larger surface area and improved porosity characteristics (Kostas et al. 2020). Hydro-pyrolysis is usually conducted within a temperature range of 250–550 °C, with hydrogen gas application, ensuring the hydrocracking of the biomass (Akhil et al. 2021). Co-pyrolysis involves multiple biomass sources for biochar pyrolysis. The resultant physicochemical properties mainly depend on the biomass sources' blending ratios and pyrolysis temperature, improving the biochar sample's pore structure (Ahmed and Hameed 2020). Gasification is another method of generating biochar in the presence of steam/oxygen at 750–900 °C, with the products being syngas and a low biochar yield. Torrefaction is conducted under oxygen-deficient conditions similar to those for biochar, apart from a temperature of 200–300 °C and a residence time of less than 30 min. Another method explored extensively for biochar production is hydrothermal carbonization, with an operating temperature range from 160 to 800 °C (preferably at lower temperatures) in the presence of water. The low-temperature environment results in higher O/C and H/C content, along with the creation of functional groups on the biochar surface; the process yields a low aromaticity level and low-porosity biochar (hydrochar). The conversion of the non-carbonized (amorphous) part of the biomass into a carbonized form can be enhanced by increasing the pyrolysis temperature, which also increases the aromaticity, π electron availability, etc. (Ahmed and Hameed 2020). Both the negative effect of pore-size thermal shrinkage due to the collapse of micropore walls and the positive effect of pore-size increment due to the removal of volatile matter can be observed with increasing temperature conditions. Increasing the pyrolysis temperatures also decreases the biochar's stability in terms of chemical oxidation resistance (Xu et al. 2021).

The biomass source influences the final physicochemical features of biochar. For instance, plant sources include olive pomace and rapeseed straw cereal waste, animal sources include crustacean shells and animal manure, and municipal wastewater sludge has also been used as biomass for biochar production (Kostas et al. 2020; Li et al. 2017; Park et al. 2021; Wang and Wang 2019; Zhang et al. 2021; Ding et al. 2019). Fibrous biomass sources such as wheat/rice

straw generate tubular structures (Igalavithana et al. 2017). In contrast, the usage of sludge biochar prevents the formation of such structures in the biochar matrix (Leng et al. 2021).

2.4.2 Biochar: physicochemical properties and characterization

The properties of biochar play a pivotal role in determining its efficacy as catalyst support, adsorbent for pollutant removal, and soil amendment. Key characteristics such as surface area, pore structure, pH, functional groups, elemental composition, and stability are crucial for assessing biochar's performance in various applications. A larger surface area is generally desirable for effective pollutant removal, and this is influenced by factors such as temperature, time, and feedstock. Functional groups and pore volume are equally important considerations when utilizing biochar as a carrier, emphasizing the role of biochar in enhancing the overall effectiveness.

Several characterization analyses can be conducted to elucidate biochar's physical and chemical properties. The proximate analysis involves the quantification of ash, fixed carbon, volatile matter, and moisture. High ash and fixed carbon contents are good indicators of high adsorbent capacity. Ultimate analysis, i.e., the quantification of C, H, N, and O composition in biochar samples, especially the H/C ratio and O/C and (O + N)/C ratios, is an indicator of the aromaticity and polarity of biochar (Ding et al. 2019). The textural features, with an emphasis on the sizes and the volume of the pores and the specific surface area (S_{BET}), are usually estimated via N_2 sorption tests at 77 K, using the Barrett–Joyner–Halenda (BJH) or density functional theory (DFT) methods for the pore analysis and the Brunauer–Emmett–Teller (BET) theory for the S_{BET}. The definition of pore size category (micro-, meso--, and macropores) decides the interaction ability of biochar with the required moiety. For instance, biochar systems with microporous structures would show a lower adsorption capacity of higher molecular-weight pesticides, although a higher one is needed for metal cations (Yaashikaa et al. 2020).

Surface pH analysis, zeta potential, and electrical conductivity can define the range in which biochar–pesticide and biochar–metal ion interactions are maximized. The graphitization and alkalinity of the produced char increase at higher pyrolysis temperatures (Cuixia et al. 2020). Surface functional group analyses are used to evaluate the biochar's adsorption capacity and microbial support. Fourier transform infrared spectroscopic (FTIR) analysis also provides

insight into the biochar matrix's multiple bond formation, with additional information on post-adsorption studies.

The morphological and structural properties can be explored by scanning electron microscopy (SEM), transmission electron microscopy (TEM), X-ray diffraction (XRD), and atomic force microscopy (AFM). The surface chemistry can be analyzed by IR, Raman spectroscopy, and X-ray photoelectron spectroscopy (XPS). It is always crucial to determine the surface pH and the point of zero charge since they play a key role in the adsorption performance and activity when biochar is used as an adsorbent in aqueous phases. The most important techniques for the physicochemical characterization of biochar are presented in **Figure 2.3.**

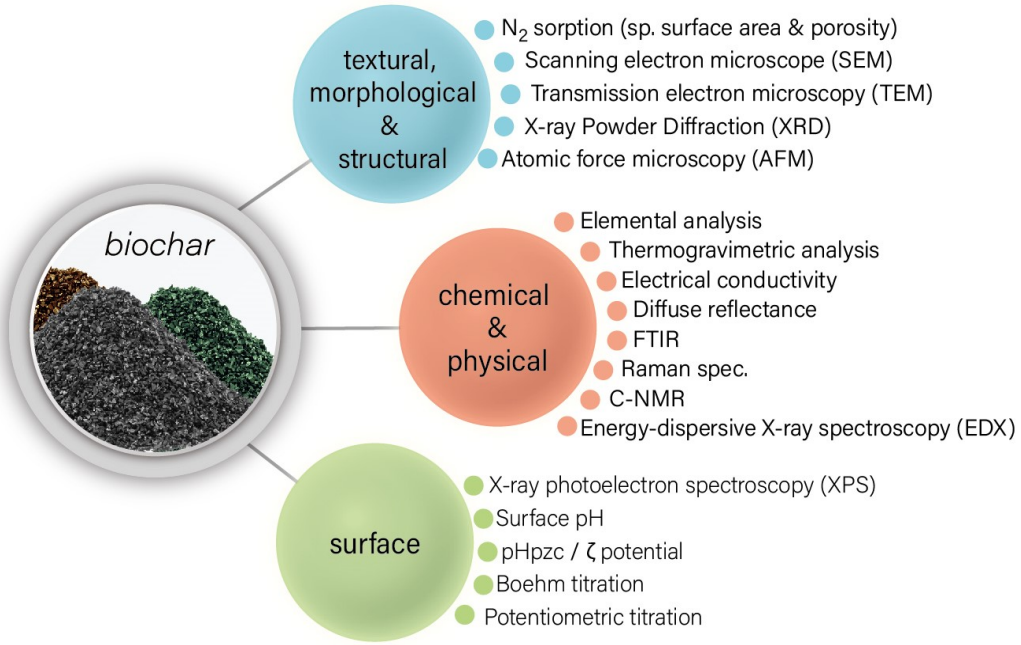

Figure 2.3. The predominant technique for the physicochemical characterization of biochar-based materials (Manikandan et al. 2023).

2.4.3 Application of biochar in remediation of heavy metals and pesticides

Heavy metals and pesticides can be directly adsorbed onto the biochar's surface. Modifying the outer surface of biochar via activation by tuning the chemical heterogeneity can lead to elevated and selective adsorption efficiency, exceptional stability, easy separation efficiency, and better recyclability (Akhil et al. 2021). Modification, including

physical/thermal activation such as steam (for –OH functional group increment) and CO_2 activation, ball milling and sonication/ultrasonication, acid treatment (for deashing and demineralization) and base treatment, functional group activation, such as amine-functionalization, impregnation with metal oxides, doping, electrochemical treatment, plasma treatment, etc., can enhance the properties of biochar as an adsorbent (Vijayaraghavan 2019).

Regarding the analysis of metal ions or pesticide removal using biochar-based materials, Langmuir and Freundlich's isotherm models are the most established ones. In general, a Langmuir versus Freundlich isotherm comparison explains monolayer adsorption vs./multilayer adsorption. Other isotherm models/approaches, such as the Jovanovich, Elovich, and Dubinin–Radushkevich (D–R) models, are also used to present an additional understanding of the role of adsorption conditions (Rahman et al. 2021; Sakulthaew et al. 2021). In addition, pseudo-first-order and pseudo-second-order models are the most widely applied models for kinetic studies for biochar–heavy metal/pesticide systems (Park et al. 2019).

2.4.3.1 Heavy metals

The application of adsorbents for the removal of heavy metal ions involves physical and/or chemical adsorption via electrostatic interactions, ion exchange, complexation, reactions that have taken place on the material's surface, and/or precipitation (Inyang et al. 2016). When interacting with biochar, some metal ions undergo reduction and oxidation reactions, precipitation, and co-precipitation (Imran et al. 2021). Multiple experimental condition parameters can affect the adsorption and removal capacity. The elevated adsorption of metal ions can be due to an increase in the specific surface area of the biochar as a result of optimizing the synthetic protocol, for instance, modifying the pyrolysis temperature (Cuixia et al. 2020). A high pH directly affects the adsorbent's surface due to protonation, thus competing with metal ion adsorption (Zhang et al. 2020). Conversely, in alkaline pH conditions, hydroxy-complex formations can compete with other ions and impede adsorption (Park et al. 2021). Preferably, the point of zero-charge pH should be in the acidic region to efficiently adsorb metal ions and form complexes with a negative surface charge (Fan et al. 2020). Cation-exchanging capacity also plays a crucial role in metal ion adsorption. For instance, Ma et al. (2021) discovered that cation exchange significantly contributed to removing Cu from lobster-

shell-derived (HCl-treated) biochar, with 53–74 % removal contributed by the cation exchange.

Biochar surface modifications are primarily conducted to improve the adsorption efficiency, and some of them are summarized in **Table 2.4**. A zirconium and iron composite with sludge biochar was generated to increase As^{5+} adsorption via complexation. The Zr-Fe biochar composite had a maximum adsorption capacity of 62.5 mg g^{-1} compared to the pristine biochar capacity of 15.2 mg g^{-1}. The probable mechanism was suggested as the inner-sphere complexation of As^{5+} on the Zr-O-Fe surface (Rahman et al. 2021). Khan et al. 2020 studied MoS_2-modified magnetic biochar with a maximum adsorption capacity of 139 mg g^{-1} and hypothesized the presence of complexation, cation exchange, and Cd-π interactions. The deashing of biochar with acid solutions and potassium acetate improved lead adsorption, due to the pore size increment (unblocking SiO_2 particles out of biochar) and complexation of Pb^{2+} and C=C (π-electrons) (Zhang et al. 2020).

The impact of biochar differs in soil versus water concerning metal mobility. Soil pH significantly influences metal movement. Biochar, typically alkaline, alters soil pH, immobilizing metals and mobilizing oxyanions (Almaroai et al. 2013). Higher soil pH due to biochar favors metal sorption; for instance, Pb binds more strongly to kaolinite at elevated pH levels, forming strong inner-sphere bidentate surface complexes (Gräfe et al. 2007). Biochar exhibits potential for mitigating chromium contamination in soil due to its reactivity and ability to donate electrons (Choppala et al. 2012). The presence of various oxygen-containing acidic and basic functional groups in biochar facilitates the supply of protons for Cr(VI) reduction, ultimately leading to the adsorption or surface complexation of Cr(III) with organic amendments (Hsu et al. 2009). However, biochars with high pH values may hinder the dissociation and oxidation of phenolic and hydroxyl groups, limiting proton supply for Cr(VI) reduction (Choppala et al. 2012). Additionally, soil microbes can contribute to Cr(VI) reduction to Cr(III) using biochar-derived carbon as an energy source (Zimmerman, 2010). This reduction leads to the immobilization of Cr, reducing its mobility and transport (Choppala et al. 2012). This higher sorption capacity for organic contaminants can be attributed to the high surface area and microporosity of biochar. In contrast, ion exchange, electrostatic attraction, and precipitation mechanisms prevail in the remediation of inorganic contaminants by biochar. The specific type of contaminant also plays a crucial role in determining biochar's

effectiveness in sorbing contaminants. Polar and non-polar, ionic, and non-ionic organic contaminants have different affinities for biochar compared to cationic and anionic metals.

Table 2.4. Various biochar involved in heavy metal removal.

Biomass Type	Pyrolysis Temperature (°C)	Modification	Metal Ion	System	Adsorption Capacity (mg g^{-1})	Adsorption rate (mg g^{-1} min^{-1})	Reference
Crab shell	350	Fe-La doped	Sb^{3+}	Water	498	1.66	(Zhang et al. 2021)
			SbO_6^{7-}		337	1.12	
Cattle manure	500	Fe-impregnated	Sb^{5+}	Water	58.3	0.91	(Park et al. 2019)
Sesbania bispinosa	450	MnO	AsO_4^{3-}	Water	7.35	0.24	(Imran et al. 2021)
		CuO			12.47	0.41	
Rice straw	500	Thiol-modified	Cd^{2+}	Soil	45.1	0.37	(Fan et al. 2020)
			Pb^{2+}		61.4	0.51	
Lobster shell	600	HCl treatment	Cu^{2+}	Water	71.4	0.17	(Ma et al. 2021)
			Cd^{2+}		126	0.30	
Peanut shell	600	MnO-embedded	Sb^{3+}	Water	248	16.53	(Wan et al. 2020)
Corn straw	600	Fe-impregnated	$HAsO_4^{2-}$	Water	6.80	0.14	(He et al. 2018)

Canola straw	700	Steam activation	Pb^{2+}	Water	195	3.25	(Kwak et al. 2019)
Wood chip	600	Sulfurized	Hg^{2+}	Water	107.5	0.89	(Park et al. 2019)
Rice husk	500	HA/Fe-Mn oxide-loaded	Cd^{2+}	Water	67.11	0.1	(Guo et al. 2019)
			As^{5+}		35.59	0.14	
Rice husk	1 kW (microwave)	Fe_3O_4-magnetic	Cr^{6+}	Water	8.35	0.07	(Liu et al. 2016)
Pomelo peel	300	K_2FeO_4-promoted	Cr^{6+}	Water	209.64	0.14	(Yin et al. 2020)
Sawdust	180	Amino-functionalized (HNO_3, nicotinamide)	Sb^{5+}	Water	241.92	0.33	(Deng et al. 2020)
			Cr^{6+}		132.74	0.22	

Therefore, the suitability of biochar for remediating contaminated soil or water on a large scale should be carefully considered, given the variation in its effectiveness depending on contaminant type, biochar properties, and environmental conditions. A general outline for adsorption and the removal mechanisms for heavy metal biochar systems are shown in **Figure 2.4.**

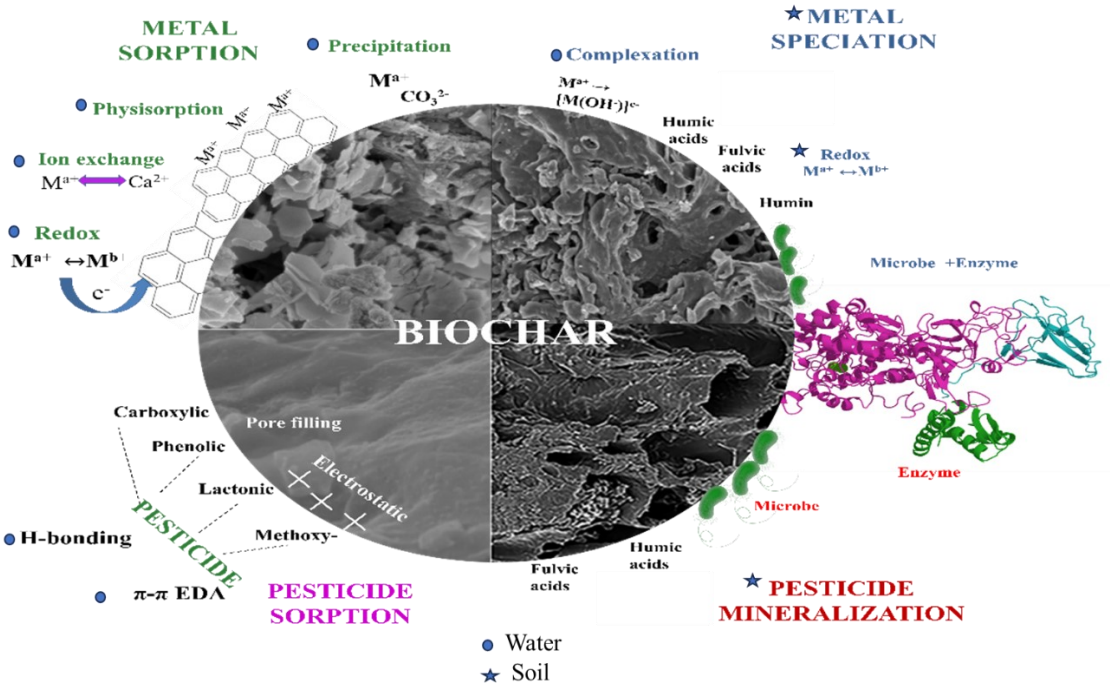

Figure 2.4. The overall involvement of biochar in heavy metal and pesticide remediation (Manikandan et al. 2023).

2.4.3.2 Pesticides

The common mechanisms for pesticide adsorption onto biochar are the hydrophobic effect, π–π electron donor–acceptor interaction, pore filling, electrostatic interactions, ionic bonding, and H-bonding (Binh and Nguyen 2020; Ding et al. 2019). Several studies regarding the adsorption/removal of pesticides by biochar have been evaluated in **Table 2.5**, wherein the parameters of biochar pyrolysis temperature and surface modifications have been compiled, along with the adsorption capacity values. The pyrolysis temperature has a similar effect on biochar-pesticide adsorption as on biochar-heavy metal adsorption. The adsorption of carbendazim on dewatered sludge biochar was at a maximum at 700 °C, owing to the increased surface area and the increment in the partition coefficient (Ding et al. 2019). Pore size governs

the definitive adsorption capacity for pesticide–biochar interaction. Dichlorvos and pymetrozine had molecular sizes that were comparable to pore diameter; thus, adsorption was facile in both cases (Binh et al. 2020). A decrease in the original biochar's H/C and O/C atomic ratios is expected to enhance the π–π electron donor-acceptor interactions, contributing to the sorption of certain pesticides, such as oxytetracycline and carbaryl (Li et al. 2017). Binh and Nguyen 2020 concluded that a pH of 2 is a more favorable condition for the adsorption of 2,4 dichlorophenoxy acetic acid on corn-cob biochar based on the electrostatic interactions. In addition to the inherent functional groups and mechanisms involved in metolachlor adsorption onto biochar, Liu et al. (2021) incorporated fulvic acid and citric acid into walnut-shell biochar that augmented the functional groups with oxygen. The removal capacity was also observed to decrease after 3 cycles in the metolachlor-simulated sewage biochar system.

Application of biochar is reported to increase the sorption and decrease the dissipation of pesticides which can consequently minimize the risk of human exposure to pesticides **(Figure 2.5)**. Jones et al. (2011) evaluated investigated the impact of biochar on soil contaminated with simazine. They found that the strong absorption of simazine into the micropores of biochar inhibited its breakdown and prevented it from leaching into groundwater. Similar studies by Yu et al. (2009) revealed that biochar derived from woodchips and cotton straw, produced at 850°C, significantly reduced the dissipation of CP, carbofuran, and fipronil from the soil. This reduction was attributed to their high absorption capabilities, leading to decreased availability of these compounds. This biochar also showed a marked reduction in the uptake of these pesticides by plants in contaminated soils, unlike biochar produced at temperatures lower than 450 °C, which proved less efficient. A key factor influencing the efficiency of pesticide adsorption in soils is the potential interaction of biochar with dissolved organic matter in the soil. This interaction might coat biochar particles, hindering the pesticides' access to absorption sites (Zhang et al. 2010). Moreover, the absorption of atrazine by the organic carbon content of biochar derived from dairy manure at 450 °C indicates that higher levels of dissolved organic carbon in the soil could impede atrazine absorption by blocking the biochar's pores (Cao et al. 2011). Generally, biochar produced at higher temperatures demonstrates greater efficiency in absorbing organic contaminants from soil and water. Various mechanisms contribute to this absorption, such as the electrostatic attraction between the charged surfaces of biochar and ionic organic compounds. To ensure optimal results, biochar production should adhere to

specific pyrolysis conditions, and the properties of biochar should be thoroughly evaluated before implementing it for the remediation of particular organic contaminants in soil or water.

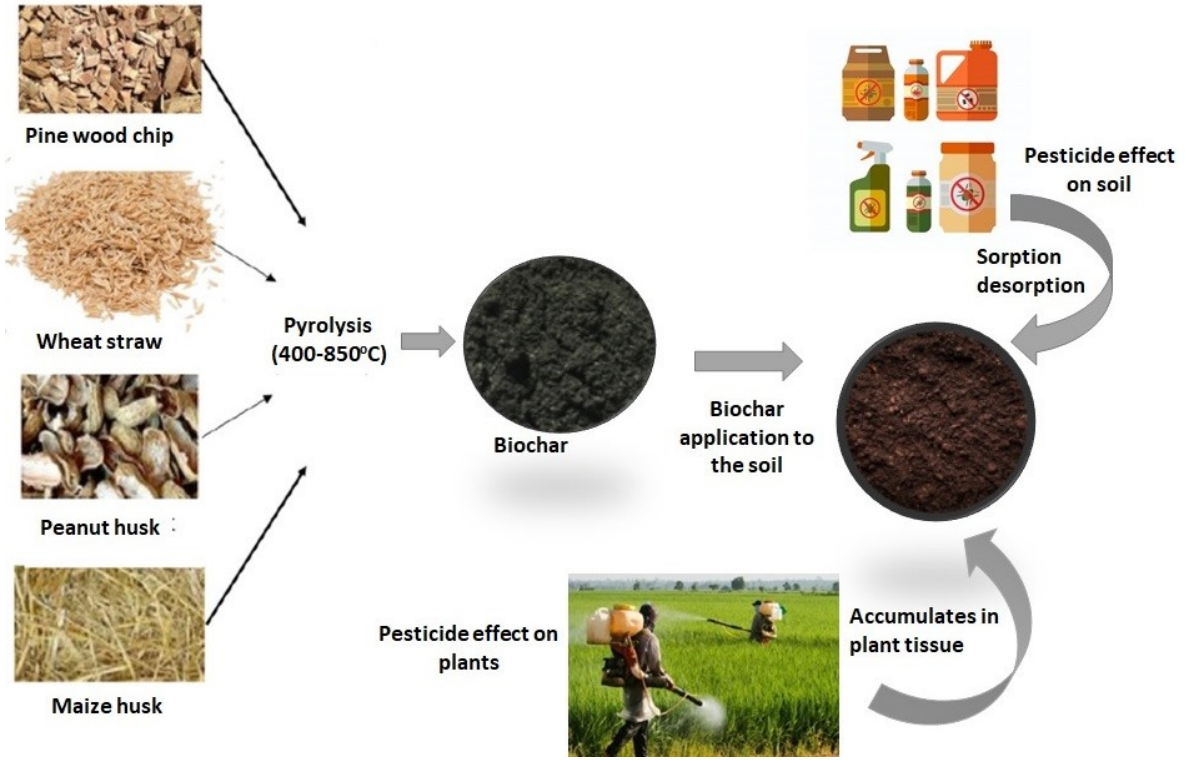

Figure 2.5. Biochar application in soil for pesticide removal (Manikandan et al. 2022).

Biochar usually possesses a greater sorption capacity of pesticides from the soil due to its charge density, large surface area, and negative surface charge. Studies by Yang et al. (2003) showed that the biochar synthesized by burning crop residues had a high sorption capacity of pesticides in the soil. Additionally, modified biochar has shown greater potential to effectively remove a variety of organic contaminants from water as a sorbent. In another work, Zheng et al. (2010) the ability of biochar to adsorb two triazine pesticides, atrazine and simazine was evaluated. A green waste biochar was produced in this study by heating the waste biomass at 450°C under oxygen-limiting conditions. The sorption affinity of the biochar for the pesticides increased with decreasing the pH and solid/solution ratio. It also observed that the aging of biochar can lead to lower sorption capacity with time. This is important for the control of herbicide efficacy in biochar-amended soil (Martin et al.2012).

Table 2.5. Various biochar involved in pesticide removal.

Biomass Type	Pyrolysis Temperature (°C)	Modification	Pesticide	System	Adsorption Capacity (mg g^{-1})	Adsorption rate (mg g^{-1} min^{-1})	Reference
Cow manure	600	HCl/HF	Carbaryl	Water	~55	0.12	(Li et al. 2017)
Sludge	700	-	Carbendazim	Soil	0.144	0.01	(Ding et al. 2019b)
Corn cob	600	HF	2,4-dichloro-phenoxyacetic acid	Water	31.87	0.17	(Binh and Nguyen 2020)
Coconut fiber	600	HCl	Dichlorvos	Water	90.9	1.51	(Binh et al. 2020)
Walnut shell powder	700	Fulvic acid	Metolachlor	Water	99.01	3.30	(Liu et al. 2021)
	700	Citric acid	Metolachlor	Water	74.07	2.46	(Liu et al. 2021)
Bagasse	500	-	Carbofuran	Water	18.9	-	(Vimal et al. 2019)
Switchgrass	425	Fe^{3+}/Fe^{2+} magnetic	Metribuzin	Water	205	0.14	(Essandoh et al. 2017)
		-			223	0.15	

2.4.4 Biochar as soil enhancer

The potential effects of biochar on soil during the remediation process are multifaceted. Biochar has been studied for its ability to bind and mitigate pollutants, which can lead to improved soil quality and reduced environmental risks. Additionally, biochar can enhance soil structure and water retention, promoting better overall soil health. Alterations induced by biochar in soil properties have been extensively explored in numerous studies, examining the biological, chemical, and physical dimensions.

2.4.4.1 Biochar induced modifications in soil

Biochar exhibits unique properties, influencing the physical attributes of soil. Biochar enhances soil porosity, but the effect can differ, with factors like biochar type and application rates influencing the relative contribution of different pores in the soil (Shilli et al. 2023). Biochar's application also affects soil bulk density, showing a negative correlation as higher application rates lead to reduced bulk density (Liu et al. 2016). Additionally, biochar promotes soil aggregation, particularly in sandy soils, contributing to improved stability (Burrell et al. 2016). Biochar application has significant implications for soil chemical properties. The composition of biochar plays a crucial role, with its high pH contributing to increased soil pH (Song et al. 2018). Biochar enhances carbon reserves in the soil, promoting nutrient retention, soil fertility, and carbon sequestration (Ouyang et al. 2014; Song et al. 2018). It also affects the nitrogen and phosphorous cycle, reducing leaching and enhancing retention, ultimately benefiting crop growth (Chan et al. 2008; Major et al. 2012). Biochar application positively influences microbial populations, contributing to soil carbon sinks and reducing CO_2 emissions (Zhang et al. 2014). Enzymatic activity is affected by biochar, with both positive and negative outcomes depending on soil type and biochar application (Ouyang et al. 2014). The influence on mycorrhizal associations is multifaceted, affecting soil nutrient availability, soil organisms, and chemical detoxification (Warnock et al. 2007).

2.4.4.2 Role of biochar on plant growth

The relationship between biochar and crop yield is complex and depends on factors such as biochar quantity, soil type, and the specific crop. Plants require a variety of macro and micronutrients to function properly, and these play a major role in controlling plant growth and development (Mehmood et al. 2021). Biochar helps in accumulating soluble nutrients in the

seedling embryo. Nguyen et al. 2018 reported that improved rice growth after the biochar amendment in loamy soil could be directly attributed to the nutrients P and K in amended biochar. It was suggested to be effective in soil nutrients and enzyme promotion (Noronha et al. 2022). Early seedling growth is a pivotal determinant for the vitality and progression of plant species. Rondon et al. (2007) observed increased biomass production of beans due to enhanced seed germination and early seedling growth facilitated by biochar addition. The positive impact of biochar on crop yield is attributed to factors such as improved water-holding capacity, nutrient availability, and soil microbial and physical properties. In general, biochar is more effective in enhancing crop yield in medium to low-fertility soils compared to fertile soils (El-Naggar et al. 2018). Major et al. (2010) reported that maize yield was not immediately enhanced by biochar addition, but significant improvements were observed in subsequent years. Combining biochar with fertilizers, especially biochar-based fertilizers, has been shown to enhance crop yield in various crops (Shilli et al. 2023). The effects of biochar amendment on various plant growth are listed in **Table 2.6.**

Abd El-Mageed et al. 2021 reported that water content is one of the most commonly reported soil hydraulic parameters and a key indicator of soil quality and productivity. Biochar amendment can affect the hydraulic conductivity of the soil-biochar mixture by influencing soil aggregation and the formation of accommodation pores between biochar and surrounding soil (Das and Ghosh 2022). Biochar amendments are likely to reduce the bulk density of most mineral agricultural soils because the bulk density of most biochar (0.3–0.6 g cm^{-3}) is significantly lower than that of typical agricultural soil (Verheijen et al. 2019). Biochar's high porosity substantially impacts soil water retention. The increase in water retention assists the soil in retaining more water, increasing the available moisture in the root zone and allowing for longer intervals between irrigations (Ghorbani et al. 2023).

Table 2.6. The effects of biochar amendment on plant growth and crop yield.

Biochar	Plant	Crop yield	References
Maize straw	Maize (*Zea mays*)	Increase in maize dry weight up to 62–113 %, dry biomass to 115- 600 %	(Khan et al. 2022)
Poultry waste	Mustard (*Brassica campest*ris)	Improved photosynthetic and accessory pigments production	(Fiaz et al. 2014)
Vine pruning	Tomato (*Solanum lycopersicum*)	50 % increase in plant height, number of leaves, and collar diameter	(Calcan et al. 2022)
Wheat straw	Rice (*Oryza sativa*)	Increased rice yield by 16.6 %	(Bian et al. 2014)
Corn cob	Soybean (*Glycine max*)	Increased seed vigor, germination percentage, shoot length, membrane stability index, and chlorophyll contents	(Hafeez et al. 2017)
Corn	Wheat (*Triticum aestivum)*	Increased grain mass per plant of the wheat by 27.7 %	(Lin et al. 2015)
Bamboo	Rice (*Oryza sativa)*	Increased rice yield by 19.8 % and enhanced nitrogen retention	(Dong et al. 2015)

Wheat straw	Wheat (*Triticum aestivum)*	Enhanced grain yield of 6.61 t ha^{-1} (91%)	(Lashari et al. 2013)
Corn straw	Cotton (*Gossypium arboretum*)	Increased the cotton lint yield by 8.0–15.8 %, Enhanced soil organic carbon and total nitrogen	(Tian et al. 2018)
Cotton stalk	Cotton (*Gossypium arboretum*)	Higher leaf water content, chlorophyll stability index, and seed cotton yield	(Velusamy 2017)
Wood residues	Rice (*Oryza sativa*)	Higher grain yields with low P availability	(Asai et al. 2009)
Acacia	Apple (*Malus domestica*)	Altered plant water status, photosynthetic capacity, and leaf micro-nutrients	(Eyles et al. 2015)
Peanut hull residues	Quinoa (*Chenopodium quinoa*)	Improved growth promotion, soil conditions; increased photosynthetic and accessory pigment production	(Kammann et al. 2011)
Almond shell, pine wood Olive stone wheat straw	Sunflower (*Helianthus annuus*)	Enhanced sunflower seed germination; improved soil properties and crop production	(Alburquerque et al. 2014)

2.4.5 Biochar as a catalyst support

Biochar emerges as a versatile and eco-friendly catalyst support, leveraging its physicochemical properties. The application of biochar photocatalysts in pollutant remediation has gained significant attention due to their promising capabilities (Fito et al. 2022). These nanocomposite materials leverage the combined effects of adsorption and photocatalysis to enhance the removal of pollutants. The biochar-based photocatalyst showcases, enhanced photocatalytic activity, increased mechanical hardness, enhanced thermal stability, chemical inertness, magnetic permeability, reduced energy band gaps, improved reusability, and simplified recovery processes (Fito et al. 2022; Sutar et al 2022). Furthermore, it demonstrates diminished recombination rates of electron-hole pairs, a favorable characteristic for effective photocatalytic applications. Farahbakhsh et al. (2022) demonstrated the degradation of CP through the utilization of a biochar nanocomposite, derived from grapefruit skin and modified with Fe_3O_4 and CdS nanoparticles (biochar/CdS-Fe_3O_4), resulting in an impressive 97 % removal rate. Several studies have been conducted for enzyme-immobilized biochar, particularly with laccase utilized as an enzyme to degrade pollutants (Pandey et al. 2020). The basic biochar–enzyme immobilization techniques are adsorption and covalent bonding. Wang et al. (2021) used laccase-immobilized biochar to degrade 2,4-dichlorophenol and obtained 64.6 % degradation. The immobilized laccase improved the cation exchange capacity, organic matter content, stability, and catalytic degradation effect.

2.5 ROLE OF MICROORGANISMS IN THE REMOVAL OF HEAVY METALS AND PESTICIDES

Microorganisms play a crucial role in eliminating metal ions and pesticides from polluted environments by adapting and thriving in harsh conditions (Castro et al. 2019). These microorganisms employ diverse survival strategies, such as surface adsorption, micro-precipitation, extracellular or intracellular sequestration, reduction, enzymatic degradation, and more.

2.5.1 Factors influencing microbial remediation

Bioremediation is possible only when microbial activity and growth are allowed by environmental conditions. In certain situations, environmental factors can be altered to allow

microbial population growth to eliminate contaminants (Karimi et al. 2021). As shown in **Figure 2.6**, various factors influence microbial remediation:

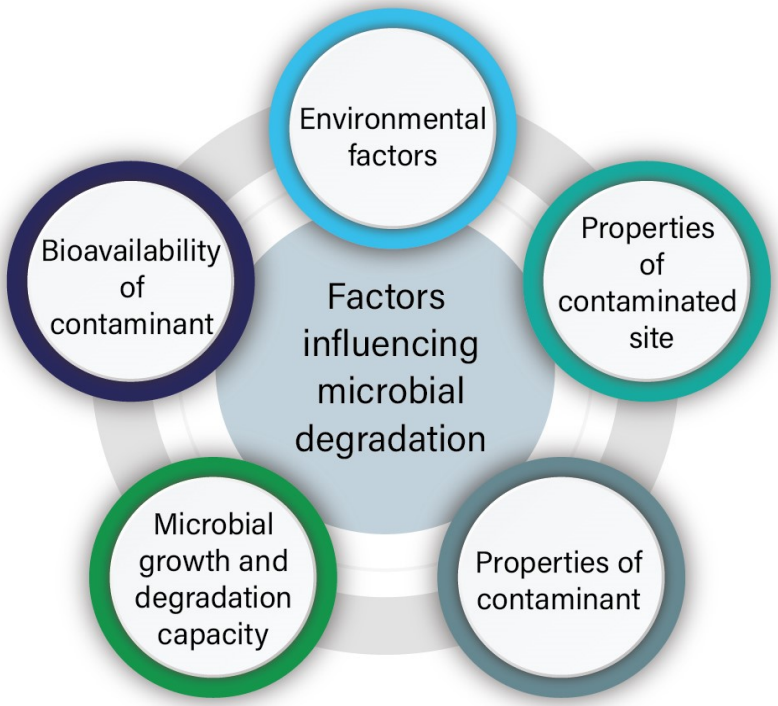

Figure 2.6. Factors influencing microbial degradation (Manikandan et al. 2023).

2.5.1.1 Environmental factors

The pH can affect bioremediation by changing metal bioavailability; for instance, a decrease in soil pH value generally causes an increase in metal bioavailability (Zhang et al. 2020b). This is because, at lower pH, the exchangeable capacity between metal cations and H^+ on the surface of soil particles is more prominent than at higher pH. Additionally, an optimum pH is essential for microbial growth, and some microbial degradation processes can be inhibited at an extreme pH. Temperature is another crucial factor influencing the bioremediation of heavy metals and pesticides (Zhang et al. 2020b). The solubility of these contaminants is increased at higher temperatures, which leads to their increased bioavailability. The physical nature and chemical composition of several organic pollutants and their adsorption-desorption mechanism are governed by temperature. Temperature also influences microbial growth, activity, and degradation potential. Furthermore, the soil moisture content

is another parameter that affects the bioremediation process. A low soil moisture content limits the growth and metabolism of microorganisms, while high values can reduce soil aeration.

2.5.1.2 Type of microorganism and degradation capacity

The microorganism that is selected for biodegradation should be able to survive in a high-contamination environment and should be evaluated first for its degradation capacity before employing it for in situ remediation. The survival of these strains can be ensured by providing favorable growth conditions. It is also important to note that microbial strains selected for pollutant removal may need to meet certain ecological requirements. One such requirement is that the strains should be non-pathogenic. For instance, *Staphylococcus aureus*, as a typical pathogen, was resistant to many antibiotics and showed high bioremediation efficiency for heavy metals such as Cr and U through bioprecipitation (Tariq et al. 2019). However, certain metabolites that formed during the degradation of contaminants can be toxic. Therefore, deeper investigations of ecological security and the metabolic functions of microbial cells are indispensable before their possible application in environmental pollution control.

2.5.1.3 Bioavailability of the contaminants

The bioavailability of the contaminants can be defined as the fraction of a contaminant in a specific environment that is either adsorbed or degraded by the microbial cells within a given time. The control of bioavailability is dependent on the diffusion, uptake, and desorption of the contaminants. The slow mass transfer of contaminants into degrading microbes reduces their bioavailability. The significance of bioavailability depends very much on the properties of the pollutant, microorganism, and characteristics of the contaminated site (Karimi et al. 2021).

2.5.1.4 Aerobic or anaerobic operating conditions

Depending on the type of organism and contaminant, bioremediation can be either aerobic or anaerobic. Most bioremediation systems work under aerobic conditions, but to effectively degrade the recalcitrant molecules, it is better to run the microbial degradation tests under anaerobic conditions. Apart from the abovementioned factors, the properties of the contaminated site (soil type, soil porosity, soil nutrients) and the properties of the contaminants (structure, hydrophobicity, recalcitrance, toxicity, solubility, and leaching ability) are also important in bioremediation.

Table 2.7. Microorganisms involved in heavy metal removal from water and soil.

Heavy Metal	Microorganism	Initial Concentration (mg L^{-1})	Incubation Time	Degradation Efficiency (%)	Reference
Bacteria					
Pb	*Bacillus cereus* BPS-9	-	48 h	77.57	(Sharma and Shukla 2021)
	Oceanobacillus profundus KBZ 3-2	50	24 h	97	(Mwandira et al. 2020)
	Enterobacter sp. FM-1	100	24 h	93.85	(Li et al. 2021)
Cr	*Bacillus subtilis SZMC 6179J*	55	24 h	93.50	(Liu et al. 2020)
	Pseudomonas aeruginosa	20	21 days	89.67	(Oyewole et al. 2019)
	Pseudomonas stutzeri L1	100	24 h	97	(Sathishkumar et al. 2017)
	Bacillus cohnii	100	25 h	94	(Kumaresan Sarankumar et al. 2020)
	Bacillus licheniformis	100	25 h	95	(Kumaresan Sarankumar et al. 2020)

Cd	*Weissella viridescens* ZY-6	NM	2 h	69.45–79.91	(Li et al. 2021a)
Zn	*Oceanobacillus profundus* KBZ 3-2	2	24 h	54	(Mwandira et al. 2020)
Cu	*Pseudomonas aeruginosa*	15	14 days	90.89	(Oyewole et al. 2019)
As	*Bacillus* sp.	100	72 h	53.29	(Dey et al. 2016)
	Aneurinibacillus aneurinilyticus	100	72 h	50.37	(Dey et al. 2016)
Fungi					
Pb	*Trichoderma brevicompactum* QYCD-6	50	5 days	97.5	(Zhang et al. 2020a)
Cr	*Trichoderma brevicompactum* QYCD-6	100	5 days	31.83	(Zhang et al. 2020a)
Cd	*Penicillium notatum*	10	14 days	77.67	(Oyewole et al. 2019)
	Trichoderma brevicompactum QYCD-6	30	5 days	20.13	(Zhang et al. 2020a)
Cu	*Trichoderma brevicompactum* QYCD-6	50	5 days	64.46	(Zhang et al. 2020a)
Ni	*Aspergillus niger*	20	28 days	81.07	(Oyewole et al. 2019)

Microalgae					
Cd	*Desmodesmus* sp. MAS1	5	7 days	>58 %	(Abinandan et al. 2019)
	Heterochlorella sp. MAS3	5	7 days	>58 %	(Abinandan et al. 2019)
	Chlorella vulgaris	100	5–15 min	Live cells—95.2 Dead cells—96.8	(Cheng et al. 2017)
Zn	*Chlorophyceae* spp.	3	3 h	91.9	(Saavedra et al. 2018)
Cu	*Chlorella vulgaris*	1.9–11.9	12 days	39	(Rugnini et al. 2017)
	Chlorophyceae spp.	3	10 min	88	(Saavedra et al. 2018)
As	*Scenedesmus almeriensis*	12	3 h	40.7	(Saavedra et al. 2018)
Ni	*Chlorella vulgaris*	1.9–11.9	12 days	32	(Rugnini et al. 2017)
Mn	*Scenedesmus almeriensis*	3	3 h	99.4	(Saavedra et al. 2018)

2.5.2 Removal of heavy metals using microorganisms

The removal of heavy metals by microorganisms is considered economical and sustainable. Any environmental stress can be withstood by microorganisms through rapid mutation and evolution, leading to toxic heavy metal resistance. They can sequester heavy metal ions, either intracellularly or extracellularly. Additionally, microorganisms can transform and reduce the metal ions to inactive forms. **Table 2.7** summarizes the microorganisms used for various heavy metal remediation conditions in recent years.

2.5.3 The mechanism of heavy metal removal by microorganisms

Microorganisms can adopt several mechanisms to survive in heavy-metal toxicity conditions. These mechanisms are depicted in **Figure 2.7** and include biotransformation, extracellular polymeric substances secretion, metallothionein synthesis, etc. Heavy metal degradation by microorganisms can be described in two ways: biosorption and bioaccumulation. Biosorption is the reversible physicochemical interaction of living (or dead) biomass or biomass-secreted products that act as biosorbents with sorbate molecules (e.g., heavy metals). It was previously categorized as metabolism-dependent and metabolism-independent biosorption. Recently, the former has been widely accepted as bioaccumulation (also called active biosorption), and only the metabolism-independent processes are considered to be biosorption (Ilyas et al. 2020). A metabolism-independent mechanism occurs passively on the dead or the living biomass cell surface. However, the biosorption of metal ions carried out by dead biomass is superior to that carried out by living cells. Cheng et al. (2017) studied the biosorption of Cd^{2+} in the living and dead cells of the microalgae *Chlorella vulgaris*. The dead algal biomass removed 96.8 % of the total Cd while the live algal biomass achieved 95.2 % of Cd adsorption. The steps involved in toxic heavy metal biosorption include binding the metal ions to various extracellular functional groups present on the microbial cell wall, via surface precipitation, chemical bonding (complexation/chelation), adsorption, or ion exchange. Physical adsorption depends on intermolecular or inter-ionic attraction forces. Complexation or chelation occurs due to the dative covalent bonds between metal ions, surface functional groups, and the ligands of biomass. When metal ion concentrations are higher than the solubility limit, surface precipitation or micro-precipitation has been observed. The exchange involves electrostatic interaction between the metal cations and the negatively charged

functional groups on the cell surface; the interchange of the cations resulted in the metal ion being bound to the surface (Escudero et al. 2019; Ilyas et al. 2020). Surface-binding is found to be the principal phenomenon governing the biosorption of metal ions (Hansda et al. 2016).

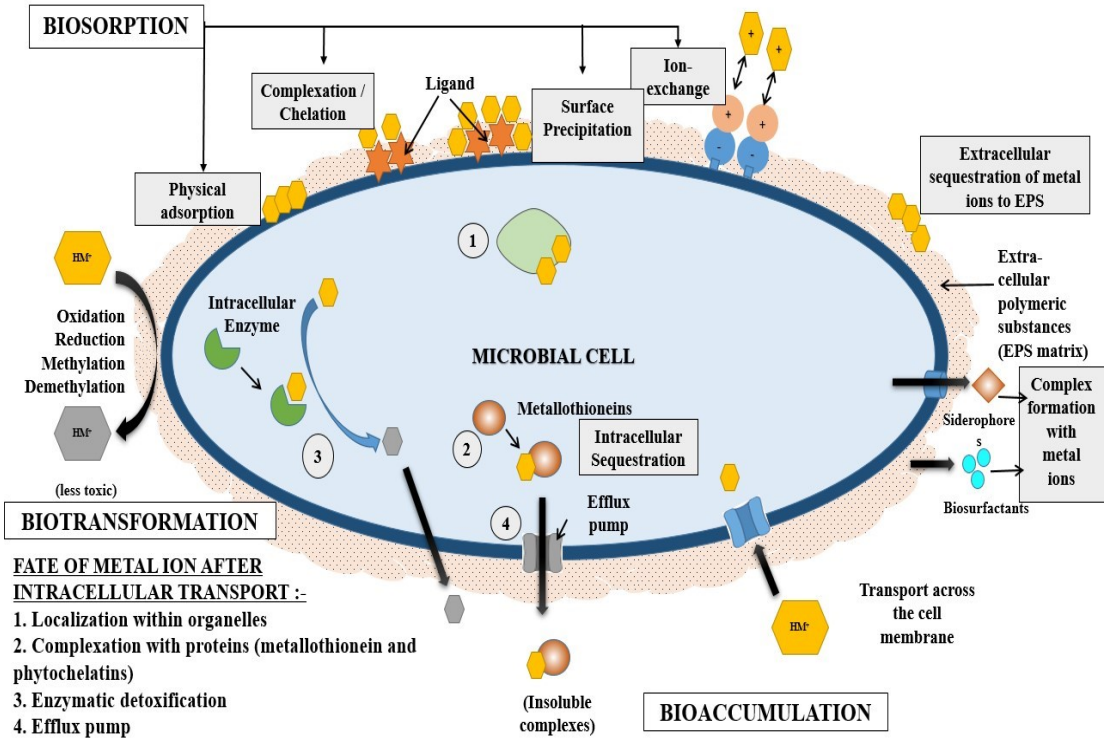

Figure 2.7. Mechanism of the microbial bioremediation of heavy metals (Manikandan et al. 2023).

The extracellular sequestration of metal ions often occurs due to various biological structures produced by microbial cells, including extra-cellular polymeric substances, siderophores, glutathione, and biosurfactants. Under heavy metal stress, microorganisms often secrete extra-cellular polymeric substances or exopolysaccharides (EPS) as a protective response. EPS are constituted of proteins, lipids, complex carbohydrates, nucleic acids, uronic acid, humic acid, etc., which prevent the entrance of heavy metals into the cell (Gupta and Diwan 2017; Mwandira et al. 2020). Generally, EPS contain negatively charged functional groups and can interact electrostatically with heavy metals, resulting in the immobilization of the metal ions within the EPS. Some examples include the accumulation of Pb^{2+} and Zn^{2+} in the soluble EPS secreted by *Oceanobacillus profundus* KBZ 3-2 (Mwandira et al. 2020), and Pb^{2+} adsorption onto EPS of *Enterobacter* sp. FM-1 (Li et al. 2021) and Cd^{2+} adsorption onto

the EPS secreted by living cyanobacteria, *Synechocystis* sp. PCC6803 (Shen et al. 2018). Siderophores are secreted by microbes and act as metal chelators, with an extreme affinity for ferric iron. They can reduce the metal's bioavailability and toxicity by binding metal ions with variable affinities that have a similar chemistry to that of iron (Xie et al. 2021).

Biosurfactants are amphiphilic compounds that are produced extracellularly by microorganisms for the solubilization, desorption, complexation, and mobilization of pollutants in solutions. The induction of biosurfactants in microbe-heavy metal systems facilitates the extracellular sequestration and formation of biosurfactant–metal complex (Mishra et al. 2021). Rhamnolipids produced by *Pseudomonas aeruginosa* showed 53 % As, 90 % Cd, and 80 % Zn extraction capacity from contaminated soil (Lopes et al. 2021). Ayangbenro and Babalola (Ayangbenro and Babalola 2020) observed that a lipopeptide biosurfactant generated by *Bacillus cereus* NWUABO1 could remove 69 % of Pb, 54 % of Cd, and 43 % of Cr from the soil. Several microorganisms, including *Pseudomonas* sp., *Bacillus subtilis*, *Candida tropicalis*, *Candida* sp., *Burkholderia* sp., and *Citrobacter freundii* can produce biosurfactants, demonstrating heavy metal removal capacity (Mishra et al. 2021).

2.5.4 Removal of pesticides using microorganisms

The major types of pesticides and persistent organic pollutants include insecticides, herbicides, and fungicides. As with heavy metals, the microbial remediation of these persistent pesticides is economical and sustainable, compared to physical or chemical removal processes. It involves the degradation of complex pesticide molecules into simpler inorganic chemicals. **Table 2.8** includes the commonly used microorganisms for the removal of pesticides. Indigenous soil microbial consortia have been more effective for the microbial degradation of pesticides than the non-indigenous strains, as non-indigenous strains are exposed to pesticide-contaminated regions exhibiting unfamiliar conditions. Several studies have reported on the degrading ability of indigenous microbes. Some of them show organophosphate degradation by indigenous *Kosakinia oryzae* (Dash and Osborne 2020), herbicide glyphosate degradation by *Providencia rettgeri* (Xu et al. 2019), and herbicide atrazine remediation by indigenous microbial consortia (Kolekar et al. 2019). Individual or mixed microbial cultures can degrade the various sources of pesticides. Single microbial cells abide by their metabolic pathways for pesticide degradation, whereas mixed microbial cultures can achieve the same result through coupled metabolic pathways (Bhatt et al. 2021). Thus, pesticides can rapidly be degraded by

applying the combined microbial consortia isolated from indigenous sites. Certain recalcitrant pesticides have resilience against biodegradation by the indigenous microbial community. In such situations, bio-augmentation and bio-stimulation are considered promising approaches for the remediation of contaminated sites. Bio-augmentation involves the introduction of specific exogenous microbes to improve the degradative capacity of the contaminated sites. The two main strategies of bio-augmentation are autochthonous bio-augmentation, where the microbes are isolated from the same site and then re-injected, and allochthonous bio-augmentation, where the microbes are cultured from another site (Cycoń et al. 2017). In one study, bio-augmentation with *Paenarthrobacter* sp. W11 significantly accelerated the degradation rate of atrazine in soil and dampened its toxic effect on wheat growth (Chen et al. 2021). Bio-stimulation can be performed by providing the necessary nutrients or electron acceptors, such as oxygen or nitrate, to promote the proliferation of indigenous microbes.

Table 2.8. Microorganisms involved in pesticide removal from water and soil.

Pesticide	Microorganism	Initial Pesticide Concentration	Incubation Time	Degradation Efficiency (%)	Reference
Bacteria					
Chlorpyrifos	*Pseudomonas nitroreducens* AR-3	100 mg L^{-1}	8 h	97	(Aswathi et al. 2019a)
Chlorpyrifos	*Lactobacillus plantarum*	0.20–0.80 mg kg^{-1}	-	24.9–34.4	(Zhang et al. 2016)
Malathion	*Escherichia coli* IES-02	50 ppm	4 h	99	(Sirajuddin et al. 2020)
Mesotrione	*Bacillus megaterium* Mes11	1 mM	5 h	99	(Carles et al. 2018)
Carbofuran	*Enterobacter* sp.	4 µg mL^{-1}	7 days	80	(Ekram et al. 2020)
Fungi					
Chlorpyrifos	*Aspergillus sydowii* CBMAI 935	50 mg L^{-1}	30 days	32	(Soares et al. 2021)
Methyl parathion				80	
Profenos				52	

Pyrethroid mixture (cypermethrin, cyfluthrin, cyhalothrin)	*Aspergillus* sp.	500 mg L^{-1}	15 days	≈100	(Kaur and Balomajumder 2020)
Microalgae					
Paraoxon, Malathion and Diazinon	*Coccomyxa subellipsoidea*	0.1 mg mL^{-1}	10 days	-	(Nicodemus et al. 2020)
Atrazine	*Chlorella* sp.	40 µg L^{-1}	8 days	83.0	(Hu et al. 2021)
		80 µg L^{-1}		64.3	

2.5.5 Mechanisms involved in pesticide removal by microorganisms

There are several mechanisms by which microorganisms transform pesticides into their non-toxic forms in a contaminated site. Some include the surface adsorption, enzymatic degradation, or co-metabolism of the pesticide molecules, as depicted in **Figure 2.8.** Adsorption of the pesticide molecules is categorized as a passive process and involves the direct interaction of molecules with the microbial cell surface. As a result, the efficiency of pesticide adsorption by microorganisms is primarily determined by the available surface-active groups. The ultimate result of adsorption is the reduced mobility of the toxic pesticides. The extent of removal and degradation efficiency is influenced by various components, such as the charge, polarity, solubility, volatility, and solubility of the pesticide molecules. Extra-cellular polymeric substances (EPS) and biosurfactants produced by the microorganisms also aid in the removal of pesticides. Gupta et al. (2019) observed 98 % carbofuran degradation within 96 h by *Cupriavidus* sp. with simultaneous EPS production. Satapute and Jogaiah (2022) reported that surfactin, a biosurfactant produced by a bacterial strain, could degrade 91% of difenoconazole.

Microbial enzymes can catalyze the breakdown of pesticides. The enzymatic degradation processes may include an alteration in the structural components, the removal of undesirable pesticide properties, oxidation, and reduction (Kumar et al. 2021). The enzymatic degradation of pesticides can either be performed by intracellular enzymes that are present in the microbial cell or by extracting the enzymes capable of degradation from the cells. Sirajuddin et al. (2020 isolated the *E. coli* IES-02 strain from a site contaminated with the organophosphate malathion, and the strain showed efficient degradation, utilizing it as the sole carbon source. They also purified carboxylesterase enzyme from the IES-02 strain and achieved 81 % malathion degradation under optimized conditions within 20 min, whereas the IES-02 cell degradation was completed from 99.0 % to 95.0 % within 4 h. However, the extracted enzymes can be affected by solution properties, such as pH, temperature, etc. Depending on the environmental factors, enzymes may lose their degradation potential due to varied ambient conditions (Marican and Durán-Lara 2018). Some studies that have reported enzymatic degradation are on cypermethrin by esterase and laccase (Gangola et al. 2018), carbendazim by carbendazim hydrolase (Zhang et al. 2017b), malathion by phosphotriesterase (Bigley et al. 2019), and isoproturon, procymidone, CP, dichlorophos, and monocrotophos by laccase (Chauhan and Jha

2018; Sarker et al. 2020; Zeng et al. 2017). The enzymatic biodegradation mechanism of pesticides is often complex, and this diverse biodegradation pathway needs further investigation to understand enzyme involvement properly.

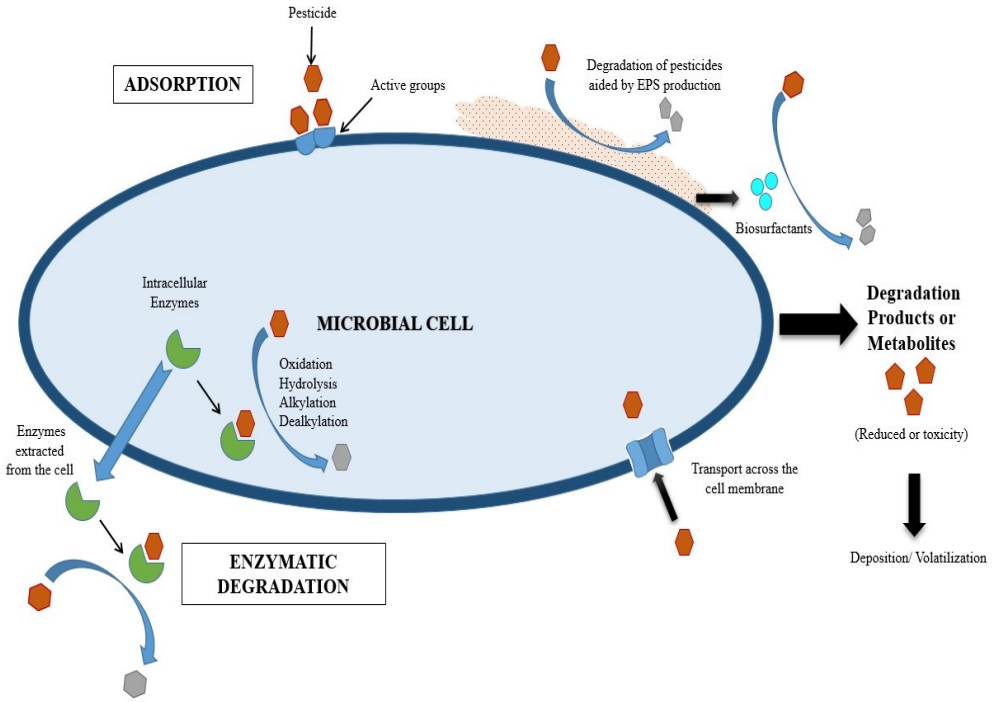

Figure 2.8. The mechanism of the microbial bioremediation of pesticide.

2.6 CHALLENGES OF USING MICROORGANISMS AS A CATALYST

The microbial degradation of metal ions and pesticides tends to be an appealing approach for bioremediation, even though certain challenges hinder their commercial application. These include (i) the loss of microorganisms or reduced microbial survival because of the toxicity to microorganisms at a higher metal ion or pesticide concentration, (ii) reduced microbial proliferation, (iii) uneven microbial growth with high concentrations of the pollutant, (iv) the washing out of the microbial cells during the application, (v) the longer time required for the completion of the process, (vi) the presence of other co-existing metal ions and organics that can positively or negatively affect the remediation process.

Microbial immobilization on a support material can overcome the above drawbacks by fixing the free microbial cells to a specific carrier, either chemically or physically, and keeping them active for longer. An ideal carrier provides operational stability and cell protection from

the toxic external environment, leading to efficient biodegradation. A support material retains the microbes and contributes to the sorption of the pollutants (Sun et al. 2020). Hence, immobilizing the microorganism accelerates the pollutant's biodegradation capacity, enhances the robustness of the immobilized strains, and improves their tolerance to high pollutant concentrations.

2.7 MICROBIAL CELL IMMOBILIZED BIOCHAR FOR REMOVAL OF METAL IONS AND PESTICIDES

Bioremediation with free microbial cells is generally inefficient due to the lesser amount of microbes utilized for degradation, microbial loss, and inhibition of growth and functioning from indigenous microorganisms (Wang et al. 2019). Immobilizing microorganisms creates a safe environment for microbial cells to perform specific functions, such as highly efficient physiochemical sorption and microbial metabolisms. Pollutant adsorption/binding on the carrier material allows degrading cells to outcompete indigenous microbes, overcoming the limitations of using free cells for bioremediation (Yu et al. 2020a). Biochar has been a prominent carrier for microbial cell immobilization due to its minimal toxicity and abundant generation. Immobilized microbes commonly have been observed for better remediation efficiency than pristine biochar or free cells (Zhang and Wang 2021).

2.7.1 Immobilization methods

Microbial immobilization entails placing free microorganisms within restricted spaces through physical or chemical methods. This enhances microbial activity and facilitates their reusability. The application of carriers augments the activity and stability of microorganisms and also ensures the preservation with abundance. The key interaction mechanisms between various carriers with a focus on biochar carriers and microorganisms primarily involve surface adsorption and pore-filling, electrostatic interaction, covalent bonding, and ion grid formation (Zhang et al. 2014: Vasilieva et al., 2021; Liu et al 2020) (**Figure 2.9**)

Surface adsorption is a simple and inexpensive method for immobilizing microorganisms (Ha et al. 2021; Manikandan et al. 2022). Most microorganisms can adhere to the surface of the carrier material by secreting adhesion substances. Microorganisms can grow on the surface and pores of the carrier material during the process of immobilization. Adsorbed cells colonize the biochar after being transferred from a bulk solution to its surface. The adsorption technique

involves physical interactions such as van der Waals forces, ionic interactions, and hydrogen bonding between surface functional groups of microorganisms and functional groups on the surface of carriers, particularly oxygen-containing groups such as carboxylic, phenolic, and sulphonate groups. Microorganisms have a low affinity for carriers; there will be a high rate of desorption of cells from carriers. As a result, appropriate carriers with high cell binding are required for improved remediation. With a relatively weak interaction between the carrier and microbial cells, immobilization does not affect the intrinsic structure of the original microbes if the adsorption method is utilized. Microorganisms with large volumes and faster growth rates are suitable for attachment to pores, which may be related to the physicochemical properties of biochar. As a result, this method is better suited for immobilizing viable cells and biodegrading pollutants in the laboratory.

Electrostatic interaction serves as the key mechanism for immobilizing microbes through adsorption, Microorganisms contain predominantly negatively charged surfaces, and utilizing carrier materials with a positive surface charge expedites the immobilization process (Vasilieva et al. 2021). Microorganisms, adhere to biochar surfaces through electrostatic interaction involving glycoproteins, phospholipids, proteins, and polysaccharides. Electrostatic interaction has gained prominence in microorganism immobilization, while challenges like unstable fixation and limited microbial toxicity resistance still exist.

Surface functional groups of microbial cells, such as sulfhydryl, amino, and hydroxyl, form covalent bonds with carriers This method offers stability and repeatability but is constrained by stringent processing conditions, limiting its practicality except for immobilized enzymes. The complex cell surface structure, encompassing various membrane proteins and lipopolysaccharides, poses challenges to covalent binding between cells and carriers (Ahmad and Khare, 2018).

Ion grid formation, also known as gel embedding, entails incorporating microorganisms into the fine grid of polymer gels. This grid prevents microbial leakage while permitting matrix infiltration and product diffusion (Liu et al. 2020). Certain microorganisms adhere to the surface and pores of biochar through electrostatic adsorption, ultimately becoming embedded in the biochar via entrapment. This loose embedding in biochar fosters microbial development, enhancing tolerance to pollutants and facilitating biodegradation. Alginate gel is effectively

embedded in biochar through a gel microgrid, enhancing porosity and minimizing diffusion resistance (Zhao et al.2020).

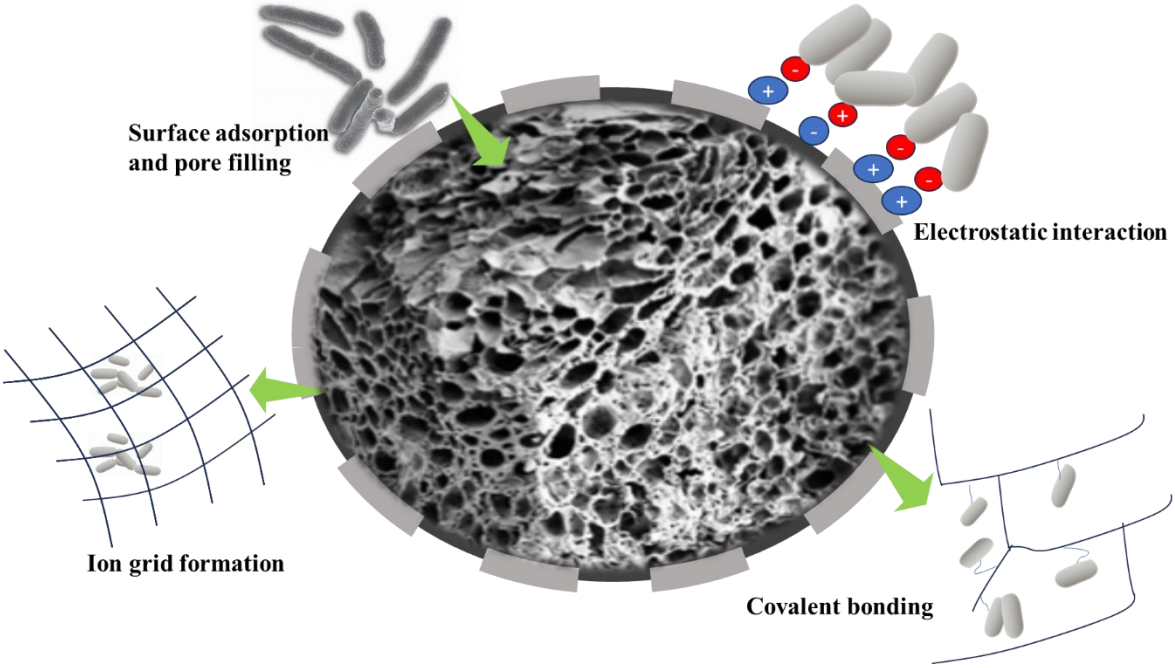

Figure 2.9. Microbial cell immobilization methods on biochar.

2.7.2 Factors that influence bioremediation using immobilized microorganisms

The effective pollutant removal capacity of MCB is affected by pollutant concentration and its bioavailability, incubation time of the cell, and various parameters such as temperature, pH, etc. The microbial cell immobilization technology requires a thorough understanding of the best conditions for maximum contamination removal.

Initial pollutant concentration influences the removal of pollutants, wherein setting initial pollutant concentration until saturation point increases the adsorption capacity of biosorbed pollutants per unit weight of MCB (Shen et al. 2017). The bioavailability of pollutants is defined as the total amount of a contaminant that is either available or may be made available for uptake by microorganisms from its surroundings within a given period. The significance of bioavailability depends on the pollutant's physicochemical properties, microorganisms, and contaminated site characteristics (Karimi et al. 2021). Incubation time is another critical parameter affecting bioremediation because it has been observed to affect the growth pattern of microorganisms directly. *Proteus mirabilis* YC801 immobilized on biochar achieved 42.5 % Cr bioreduction and adsorption capacity after 6 h of incubation (Huang et al. 2020). The

temporal requirement is high for microbial degradation, and the reaction time for complete degradation is higher compared to other methods. The time scale of the microbial degradation process can be reduced by selecting suitable microorganisms with quicker growth phases for pollutant degradation or removal. However, choosing biochar with a high adsorption potential for pollutants is critical for reducing bacterial adaptation time.

The pH value also influences microbial metabolic processes, particularly growth, cell membrane transport, the zeta potential of sorbate, and changes in sorbent surface characteristics (Chojnacka 2010). Huang et al. 2020 observed an increase in Cr^{6+} reduction with a pH increment from 6.0 to 7.0, with a maximum removal of 83.7 % at pH 7.0. However, alkalifying the Cr^{6+} MCB system from pH = 8.0 to 10.0 inhibited the removal capacity of MCB for Cr^{6+}. Similarly, the highest Cr bioreduction was found at 30 ℃, similar to the optimal culture temperature for strain. Bioreduction significantly decreased with a further increase in temperature above 30 ℃, which might be attributed to the loss of cell viability and the inhibition of essential enzymes and proteins responsible for microbial growth and biodegradation at elevated temperatures (Abu Talha et al. 2018; Huang et al. 2020).

Temperature and pH significantly influenced tebuconazole degradation by *Alcaligenes faecalis* WZ2, and degradation efficiency was strongly correlated with bacterial growth (Sun et al. 2020). Tebuconazole degradation efficiency reached 88.5 % under ideal conditions (temperature 30–35 °C and pH 6–8). Because of bacterial growth inhibition and a decrease in catalytic activities of microbial enzymes involved in tebuconazole degradation, efficiency was significantly reduced below the ideal temperature and pH.

2.7.3 Microbial cell immobilized biochar for heavy metal removal

Using biochar and bioremediation in tandem with functional microbial strains is a viable and emerging strategy for the long-term remediation of contaminated water and soil. Numerous microbial strains with strong metal tolerance or adsorption capability have been isolated and used for bioremediation either as free-living cells or by immobilizing microbial cells with a specific carrier substance. Metal-tolerant microorganisms immobilized on biochar have been used as a bio-augmentation method to improve heavy metal remediation, indirectly reducing heavy metal contamination in soil. Incorporating bacteria immobilized on biochar into the soil may indirectly improve Cd removal by promoting plant growth and the phytoremediation effect (Chuaphasuk and Prapagdee 2019). Cd-resistant bacteria immobilized on biochar

improved phytoextraction efficiency by *Chlorophytum laxum* R. Br, via Cd phytoaccumulation in the shoots and roots, and Cd translocation from the roots to the shoots.

Insoluble phosphate solubilization can be achieved through microbial phosphate solubilizers (PSB). Teng et al. 2020 observed that combining PSB and biochar improved Pb^{2+} immobilization by forming a stable crystal texture on its surface. Zhang et al. 2017 used the PSB bacteria *Pseudomonas chlororaphis* for lead removal. However, the organism could not proliferate in indigenous bacteria, whereas the addition of PSB-immobilized biochar (PIB) improved bacterial growth and reduced Pb concentrations to less than 1 mg kg^{-1}. As a result, soil inoculation with PIB can be used as a substitute for Pb immobilization, avoiding secondary pollution caused by phosphorus toxicity.

The microorganism immobilization with biochar carrier was also influential in remediating soil polluted with a combination of heavy metals. Tu et al. 2020 applied *Pseudomonas* sp. NT-2 loaded onto maize straw biochar into Cd-Cu mixed soil. The application of *Pseudomonas* sp. NT-2 loaded biochar effectively reduced the bioavailability of Cd and Cu and increased soil enzymatic activities in the soil system. Qi et al. (2021) used three strains of mixed bacteria, *Bacillus subtilis, Bacillus cereus,* and *Citrobacter* sp. loaded biochar for U and Cd removal. They discovered that MCB promoted growth in celery and reduced U and Cd phytoaccumulation compared to free cell and biochar treatments.

Research on Cr^{6+} removal by immobilized microorganisms with biochar has increased interest recently. The metal ion resistant bacterium *Proteus mirabilis* YC80 was immobilised using biochar derived from the bloom-forming cyanobacterium D. *flos-aquae* (Huang et al. 2020c). The ability of biochar-immobilized *Proteus mirabilis* PC801 to remove Cr^{6+} was superior compared to a free cell. The removal efficiency of Cr^{6+} by PC801-immobilized biochar was 100 %, with 87.7 % total Cr immobilized on the carrier and only 12.3 % Cr^{3+} remaining in the solution. **Table 2.9** includes microbial cell immobilized biochar reported for heavy metal and pesticide abatement.

Physical adsorption, ion exchange, surface complexation, precipitation, and biotransformation are some of the mechanisms involved in MCB-mediated heavy metals removal. Biochar containing oxygen functional groups, mineral components such as carbonates and phosphates, and microbial surface functional groups contribute to the removal of metal cations. Shen et al. (2017) investigated the mechanism of Cd removal using biochar-

immobilized microalgae. They discovered that electrostatic attraction, surface complexation, and ion exchange were responsible for Cd removal (maximum adsorption 217.41 mg g^{-1}) from wastewater. Similarly. Tu et al. (2020) noted that surface complexation with different functional groups on cells, as well as cation exchange and surface complexation on biochar, contributed to the enhanced stability of Cd^{2+} and Cu^{2+} in the contaminated soil. Microorganisms secrete enzymes that mediate redox reactions and surface complexation. These are the mechanisms involved in removing As^{3+}, As^{5+}, Cr^{6+}, $U^{6+,}$ and Mn^{2+}. Youngwilai et al. (2020) examined the mechanism of Mn^{2+} removal by *Streptomyces violarus* strain immobilized on biochar. They found that the two processes, biological oxidation by immobilized strain and adsorption by biochar, work together.

Table 2.9. Microbial cell immobilized biochar for heavy metal and pesticide removal.

Microorganism	Catalyst support	Pollutant type	Mechanism	System water/ soil	Removal Efficiency	Reference
Bacillus sp.TZ5	Coconut shell	Cd^{2+}	Adsorption	Soil	48.49 %	(Ma et al. 2020)
Delftia sp B9	Corn stalk	Cd^{2+}	Adsorption	Soil	81 %	(Liu et al. 2020c)
Chlorella sp.	Water hyacinth	Cd^{2+}	Adsorption	Water	92.5 %	(Shen et al. 2017b)
Leclercia adecarboxylata	Rice hull	Pb^{2+}	Entrapment	Water	93 %	(Teng et al. 2020a)
Bacillus subtilis	Pig manure	Hg^{2+}, Pb^{2+} co-contamination	Adsorption	Water	69 mg g^{-1} Hg 112.3 mg g^{-1} Pb	(Wang et al. 2018c)
Bacillus subtilis	Corn straw	Hg^{2+}, Pb^{2+} co-contamination	Adsorption	Water	53.7 mg g^{-1} Hg; 83.0 mg g^{-1} Pb	(Wang et al. 2018c)
Arthrobacter sp. ZXY-2	Maize straw	Atrazine	Adsorption	Water	59.7 %	(Yu et al. 2020)
P.putida	Corncob	Paraquat	Adsorption	Water	4.21 mg g^{-1}	(Nguyen et al. 2023)
Serratia marcecens N80	Abandoned fungus substrate biochar	Thifensulfuron-methyl	Adsorption	Soil	89.37 %	(Zhu et al. 2021)

2.7.4 Microbial cell immobilized biochar for pesticide removal

Pesticide degradation can be enhanced by providing exogenous free cells to polluted soil. However, this method has several drawbacks, including the growth and survival of microbial cells, inadequate nutrients, lesser adaptability to surroundings, and competition with native microorganisms (de-Bashan and Bashan 2010; Zhang et al. 2017a). Immobilizing exogenous pollutant-degrading bacteria on a support material can be an alternative strategy. This can be an ideal environment for their survival in different soil conditions (Chen et al. 2012). Microorganisms immobilized in biochar have the potential to directly or indirectly reduce environmental pollution while also allowing for the long-term maintenance of catalytic activity. Due to its superior porosity, ample surface area, and functional groups, biochar is an ideal medium and rich nutrient composition for immobilizing and reproducing microbial cells (Sun et al. 2020).

Biochar can improve the soil's pollutant adsorption capacity while providing nutrients for microbial growth and function (Zheng et al. 2019). Adsorption and covalent binding methods were used to immobilize *Pseudomonas putida* onto coconut fiber-derived biochar. The efficacy of MCB in paraquat removal from contaminated water was studied by Ha et al. 2021. After 48 h of incubation, MCB could convert paraquat to 4,4-bipyridyl and malic acid. According to Wahla et al. 2020, immobilization of MB3R consortium on biochar remediated soil contaminated with metribuzin. Immobilization of a microbial consortium on biochar increased the rate of cypermethrin degradation and removal efficiency while lowering the cypermethrin bioavailability to indigenous organisms (Liu et al. 2017a). Sun et al. (2020) isolated and identified *Alcaligenes faecalis* WZ-2 as a tebuconazole-degrading strain and supported on wheat straw biochar as a carrier. The biochar-immobilized WZ-2 reduced the half-life of tebuconazole in soil from 40.8 to 13.3 days and affected microbial population and enzyme activities in polluted soil.

o increase the cell immobilization efficiency, proper physical and chemical modifications are commonly involved in changing the biochar properties, which can facilitate cell adhesion and metabolism through improving surface func tional groups, charge, and porosity of pristine biochar (Chen et al. 2019; Tao et al. 2019). The methods of biochar modi f ication mainly include acid–base modification, oxidation modification, magnetic modification, and doping functional element modification (Ogura et al. 2021). For instance, Youngwilai et al. (2020) revealed that using hydrogen per oxide modified biochar could immobilize twice the amount of Streptomyces violarus strain SBP1 than the raw biochar. Moreover, the immobilized strain provides the highest man ganese

removal efficiency from the wastewater. The reason for this can be attributed to the fact that the modified biochar captures the additional strain SBP1 and creates a better envi ronment or additional nutrients for these cells, resulting in a synergistic manganese biotransformation. While research on the use of modified biochar to immobilize microorganisms for remediation of water and soil contamination has been growing in recent years, only a few studies have reported the use of modified biochar as a carrier to immobilize microor ganisms for efficient pesticide degradation/removal. Among them, Tao et al. (2019) reported that *Acinetobacter lwoffii* DNS32 loaded onto iron-modified corn stalks biochar effec tively accelerated the degradation of herbicide atrazine in culture solution. They stated that the modified biochar facili tates the interaction of the degrading strain and atrazine, which is conducive to atrazine degradation. However, the use of modified biochar to immobilize degrading microor ganisms undoubtedly has some limitations, such as difficulty of manipulation, high cost, reduced vitality of immobilized microorganisms, and risk of secondary contamination. Henceforth, it is highly desirable to develop optimal immo bilization methods for specific functional microorganisms by comparing the modification methods to achieve better pesti cide degradation efficiency and environmental compatibility.

2.7.5 Activated biochar for microbial cell immobilization

Enhancing the efficiency of cell immobilization often involves utilizing physical and chemical activation or modifications to alter the properties of biochar, aimed at boosting cell adhesion and metabolism by enhancing the surface functional groups, charge, and porosity of the original biochar (Han et al. 2023). Methods for modifying biochar typically include treatments such as magnetic modifications, incorporation of functional elements acid-base adjustments and oxidation processes (Pretti Ogura et al. 2021). Youngwilai et al.(2020) demonstrated that biochar modified with hydrogen peroxide could immobilize twice as much *Streptomyces violarus* strain SBP1 compared to unmodified biochar and showed superior efficiency in removing manganese from wastewater. This improvement is due to the modified biochar's ability to capture additional SBP1 strain, thereby creating a more conducive environment or providing extra nutrients for these cells, resulting in enhanced manganese biotransformation. While research into the use of modified biochar for immobilizing microorganisms to address water and soil contamination has grown in recent years, only a limited number of studies have explored the potential of modified biochar as a carrier for efficient pesticide degradation or removal. Tao et al. (2020) demonstrated that *Acinetobacter lwoffii* DNS32 loaded onto iron-modified corn stalk biochar significantly accelerated the degradation of the

herbicide atrazine in culture solution. They suggested that the modified biochar facilitates interaction between the degrading strain and atrazine, thereby promoting its degradation. However, utilizing modified biochar for immobilizing degrading microorganisms poses certain challenges, including difficulties in modification, high costs, reduced vitality of immobilized microorganisms, and the risk of secondary contamination.

2.8 Microbial cell immobilized biochar interaction in soil: enhancing plant growth

The interaction between microbial cell-immobilized biochar and soil holds significant promise in enhancing plant growth and addressing challenges in soil remediation. Biochar, derived from agricultural waste at specific temperatures, has been proven to extend the survival of beneficial strains, promoting crop biomass and yield. This is particularly noteworthy in the context of microbial bioaugmentation, a minimally invasive technique for mitigating the hazardous effects of contaminants in soil without disrupting agricultural activities. Despite the potential limitations of nutrient-deficient contaminated soils, biochar emerges as a solution by releasing essential nutrients to provide carbon and energy sources for microbial growth. Moreover, as a porous material, biochar creates an ideal habitat for microorganisms, offering a conducive micro-environment for their proliferation. Studies indicate that the introduction of microbial inoculants into biochar pores and surfaces allows these microorganisms to effectively colonize plant host roots. Microbial inoculants often employ various nutrient-acquisition strategies, such as nitrogen fixation, phosphorus solubilization, iron uptake, and competitive mechanisms. These strategies not only enhance plant health but also support the growth and reproduction of the introduced bacteria (Chuaphasuk and Prapagdee 2019; Qi et al. 2023). Biochar's ability to support microbial proliferation and abundance further underscores its role in promoting nutrient availability in the soil (Teng et al. 2020). This dual compatibility ensures that beneficial bacteria can thrive alongside native soil microorganisms, creating an environment conducive to plant growth as illustrated in **Figure 2.10**. (Zhu et al. 2017). The dynamic relationship between biochar and bacteria in soil not only promotes soil health and nutrient availability but also enhances plant disease resistance through various mechanisms (Liu et al. 2017).

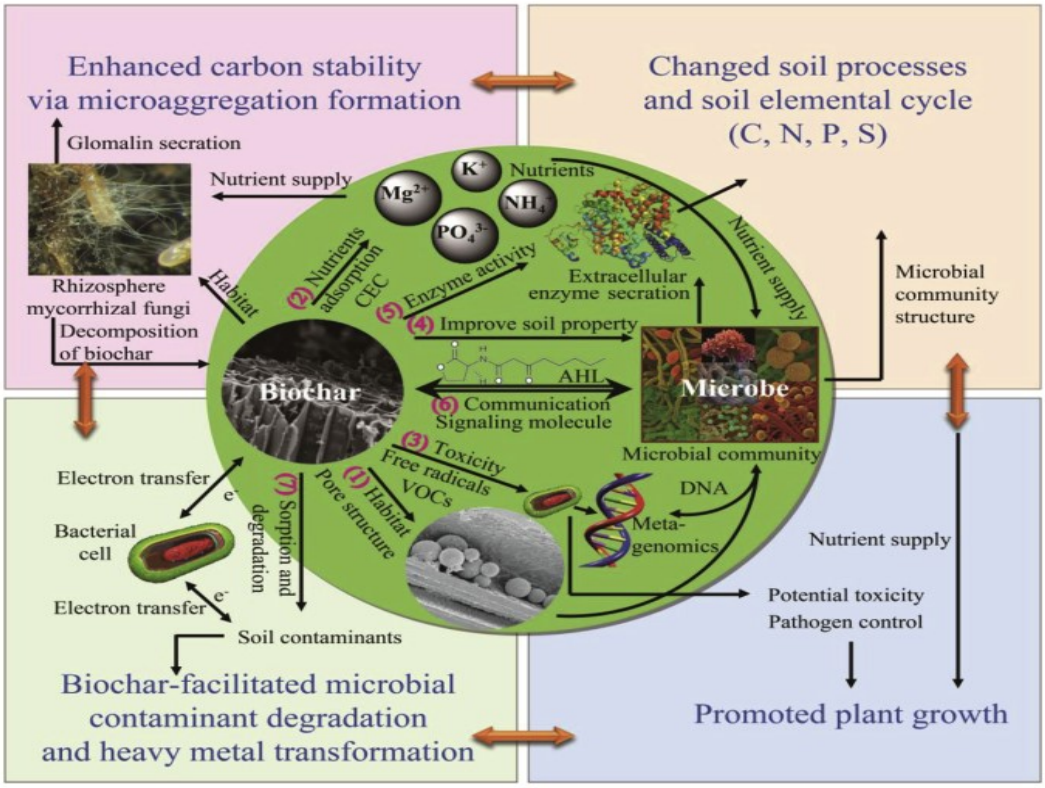

Figure 2.10. Biochar -microbe interaction (Zhu et al. 2017).

2.9 SCOPE & OBJECTIVES

- **Research Gaps**

- Synergistic effect of biochar and functional bacteria on metal ion removal has not been clearly understood.
- Utilization of Box-Behnken studies to optimize chlorpyrifos remediation from water using microbial cell immobilized biochar.
- The mechanism underlying chlorpyrifos remediation through microbial cell-immobilized biochar remains largely unexplored, both in water and soil environments.
- The effectiveness of remediation on plant growth in pollutant-remediated soil has not been adequately analysed.

- **Objectives**

The present study aims to explore the immobilization of microbial cells on biochar and to investigate the mechanism and efficiency of pollutant removal from water and soil.

The specific objectives are as follows:

- Optimization studies for microbial cell immobilization on biochar for heavy metal removal from water.
- Investigating the performance of microbial cell immobilized biochar for heavy metal removal from soil.
- To investigate the application of microbial cell immobilized biochar for removal of pesticide from water and soil.
- To propose the mechanism involved in the bioremediation of different pollutants using microbial cell-immobilized biochar.

CHAPTER 3

MATERIALS AND METHODS

3.1 MATERIALS

Various biomasses, including rice husk (RH), peanut shell (PS), sugarcane bagasse (SC), sawdust (SD), and coconut shell (CS), were collected from Palakkad, Kerala, India. The bacterial strain *Pseudomonas stutzeri* MTCC 101 and *Bacillus* MTCC 3166 were purchased from Microbial Type Culture Collection and Gene Bank, Chandigarh, India. Soil samples were collected from the Palakkad district of Kerala, India (10° 47' 4.9308" N,76° 39' 11.3220" E). *Spinacia oleracea* L. (spinach), *Solanum lycopersicum* L. (tomato), and *Vigna unguiculata* L. (cow pea) seeds were collected from the local market. Farmyard manure (FYM) was collected from a local agriculture farm, in Palakkad, Kerala.

Cadmium nitrate tetrahydrate (Cd $(NO_3)_2.4H_2O$) was obtained from Loba Chemicals Pvt. Ltd. and nickel sulfate heptahydrate ($NiSO_4.7H_2O$) from CDH Chemicals Ltd, India. CP, 3,5,6-trichloro-2-pyridinol (TCP) (99%), dichloromethane, acetonitrile, and Bradford reagent were purchased from Sigma-Aldrich. Luria Bertani (LB) broth and agar from HiMedia Laboratories Pvt. Ltd., Mumbai. Chemicals such as disodium hydrogen phosphate (Na_2HPO_4), dipotassium hydrogen phosphate (K_2HPO_4), glucose, sodium chloride (NaCl), ammonium chloride (NH_4Cl), magnesium sulfate ($MgSO_4$), and calcium chloride ($CaCl_2$) for minimal salt solution preparation were obtained from Merck, India. Deionized water was employed for the preparation of all solutions.

3.2 METHODOLOGY

3.2.1 Microbial cell immobilization and optimization of biochar condition

3.2.1.1 Growth of *P. stutzeri* in the presence of metal ions

Bacterial strain *P. stutzeri* MTCC 101 has been reported for heavy metal tolerance and used for Cd and Ni removal (Deb et al. 2013). Heavy metal tolerance of *P. stutzeri* in different concentrations (10, 50, and 100 mg L^{-1}) of Cd and Ni was tested. 1% of an overnight culture grown in LB medium was used as inoculum. The cultures were incubated at 37 °C, and the growth patterns in the presence and absence of metal ions were monitored by a spectrophotometer at 600 nm at intervals of 4 h for 48 h.

3.2.1.2 Biochar preparation

Various biomasses for biochar preparation were washed twice and oven-dried (80 °C) for 24 h and stored in polythene bags. The pre-processed biomasses were weighed, taken into the ceramic crucible, and kept in a muffle furnace at different temperature. The pyrolysis temperature was set to (300 °C, 500 °C, and 700 °C) for three different periods of 30, 60, and 120 min at a heating rate of 20 °C min^{-1}. After the biochar was cooled to room temperature, sieved through a 0.15 mm sieve. The percentage biochar yield for each biomass at different pyrolyzing and time was calculated using equation (3.1) (Jia et al. 2018)

$$\%\, Biochar\ yield = \frac{Mass\ of\ biochar\ obtained\ (final\ weight)}{Mass\ of\ biomass\ loaded (initial\ weight)} \times 100 \qquad (3.1)$$

3.2.1.3 Optimization of biochar condition based on microbial cell immobilization

Biochar prepared at different temperature and time period were used for immobilization of *P. stutzeri*. The microbial cell biomass was harvested by centrifugation (5,000 g, 5 min). The harvested pellet was resuspended in 10 mL of fresh LB medium. 2 mL of condensed bacterial suspension was inoculated aseptically into a 250 mL conical flask containing sterilized 5 g (dry weight) biochar in 100 mL LB media. The samples were incubated for 24 h at 37 °C on a rotary shaker (160 rpm) until the microbial cells were immobilized onto the biochar surface and pore structure. Following the incubation, microbial cell immobilized biochar culture solution was separated using Whatman filter paper and rinsed with sterile water to remove free cells. 0.1 g (wet weight) biochar was soaked in 10 mL LB medium, and microbial cells immobilized on biochar extracted using a sonication bath (10 min) and vortex mixing (3 min, twice). Serial dilution and plating were performed to determine the number of microbial cells immobilized on the biochar (Huang et al. 2020; Manikandan and Nair 2022).

The number of bacterial colonies was enumerated and expressed as colony-forming units (CFU) per gram of biochar, as depicted in Equation (3.2).

$$CFU\ g^{-1} = [(\text{average colony count}/\ 0.1\ mL)/g\ \text{of biochar}] \times \text{dilution factor} \quad (3.2)$$

Various combinations of microbial cell immobilized biochar are represented in **Table 3.1.** Further, the biochar having maximum immobilization efficiency was selected for metal ion removal.

Table 3.1 Various combinations of microbial cell immobilized biochar.

MCB	Description
PRHB	*P. stutzeri* immobilized rice husk biochar
PSDB	*P. stutzeri* immobilized sawdust biochar
PSCB	*P. stutzeri* immobilized sugarcane bagasse biochar
PPSB	*P. stutzeri* immobilized peanut shell biochar

3.2.1.4 Characterization of biochar and microbial cell immobilized biochar

Biochar having maximum microbial cell immobilization capacity was evaluated for its elemental composition, thermal stability, microstructural morphology, surface functional groups, and mineral composition. The elemental analysis was performed using a CHONS analyzer (LECO Truspec Micro Analyser). Thermogravimetric analysis (TGA) was carried out under a nitrogen (N_2) atmosphere using a TGA 4000 Perkin Elmer analyzer. Extractable mineral concentrations in biochar were determined using Inductively Coupled Plasma – Optical Emission Spectrometry (5100 ICP-OES; Agilent Technologies, USA.) after acid digestion (Kim et al. 2015). Fourier-transform infrared spectroscopy was used to determine the change in functional groups on the biochar. The spectra were recorded using a Spectrum 2 FTIR Spectrometer (PerkinElmer, Singapore) with resolutions ranging from 450 to 4000 cm^{-1}. The functional group involved in microbial cell immobilized biochar was also analyzed and spectra were recorded using a Nicolet IS50 spectrometer. Surface morphology and elemental components analysis was carried out using High Resolution-Field Emission Scanning Electron Microscopy or HR-FESEM (GEMINI 300, Carl Zeiss) with Energy Dispersive X-ray analysis or EDAX (EDAX Octane super EDS System-SDD 70mm) following sputter-coating of the samples with gold. BET-specific surface area, pore volume, and average pore radius of biochar were determined based on nitrogen adsorption at 77.3 K using a surface area analyzer Autosorb-iQ

(Quantachrome, Boynton Beach, USA). The specific surface area was calculated using the Brunauer-Emmett Teller (BET) method. The organic and mineral fractions of RHB samples were analyzed via XRD (Empyrean 3rd Gen, Malvern PANalytical, Netherlands). The diffraction angle was scanned from 10° to 90° (2θ) with Cu Kα radiation (K = 0.15418 nm). The surface states of the biochar were characterized by Thermofisher X-ray photoelectron spectroscopy (XPS).

3.2.2 Cd and Ni removal using PRHB from water

Cd and Ni removal study was carried out using RHB, *P. stutzeri,* and PRHB in a set of 250 mL Erlenmeyer flasks of LB medium containing 50 mg L^{-1} metal ion solution. To ensure the cell count was consistent for all treatments, 1.2 mL free cells of *P. stutzeri* (final density ~ 10^9 CFU mL^{-1}) and 0.1 g PRHB (~10^9 CFU mL^{-1}) were added to 100 mL metal ion-containing LB broth. After incubation, it was sampled from each flask and filtered through a 0.45 μm pore syringe filter. The total Cd and Ni in the solution were analyzed using ICP-OES. The removal percentage of the metal ions was calculated using Equation. (3.3):

$$Removal(\%) = \frac{Ci - Cf}{Ci} \times 100 \qquad (3.3)$$

Here Ci and Cf (mg L^{-1}) are the initial and final concentrations of metal ions in the aqueous solution, respectively.

3.2.2.1 Effect of operating conditions on Cd and Ni removal

Cd and Ni solution were incubated with RHB, *P. stutzeri,* and PRHB for 42 h, and the sample was taken at 0, 1, 3, 6, 12, 18, 24, 30, 36, and 42 h, respectively, to understand the effect of incubation time on metal ion removal. The other reaction conditions were as follows: biocatalyst dosage 1 g L^{-1}, pH 7, the initial concentration of metal ion 50 mg L^{-1}, and temperature 37 °C. The effect of pH on Cd and Ni removal was analyzed by varying pH 5, 6, 7, and 8 by keeping other experimental conditions as follows: incubation time 36 h, biocatalyst dosage 1 g L^{-1}, initial metal ion concentration 50 mg L^{-1} and temperature 37 °C. Under the above optimal conditions of incubation time 36 h, biocatalyst dosage 1 g L^{-1}, initial metal ion concentration 50 mg $L^{-1,}$ and pH 7, the effects of temperature (15, 20, 25, 30, 37, 40 °C) on Cd and Ni removal efficiency was investigated.

The effect of biocatalyst dosage on metal ion removal experiment was carried out in different biocatalyst concentrations ranging from 0.5 to 2 g L^{-1} while other experimental parameters were set

as follows: incubation time 36 h, initial metal ion concentration 50 mg L^{-1}, pH 7, and temperature 37 °C. The effect of initial metal ion concentration on the removal efficiency was checked in different concentrations of Cd and Ni ranging from 10 to 100 mg L^{-1}. The other experimental parameters were performed: incubation time 36 h, temperature 37 °C, pH 7.0 the effects of biocatalyst dosage of 2 g L^{-1}. The removal of Cd and Ni by RHB, *P. stutzeri*, and PRHB were also performed under optimized operating conditions. An overview of the experimental design is presented in **Figure 3.1.**

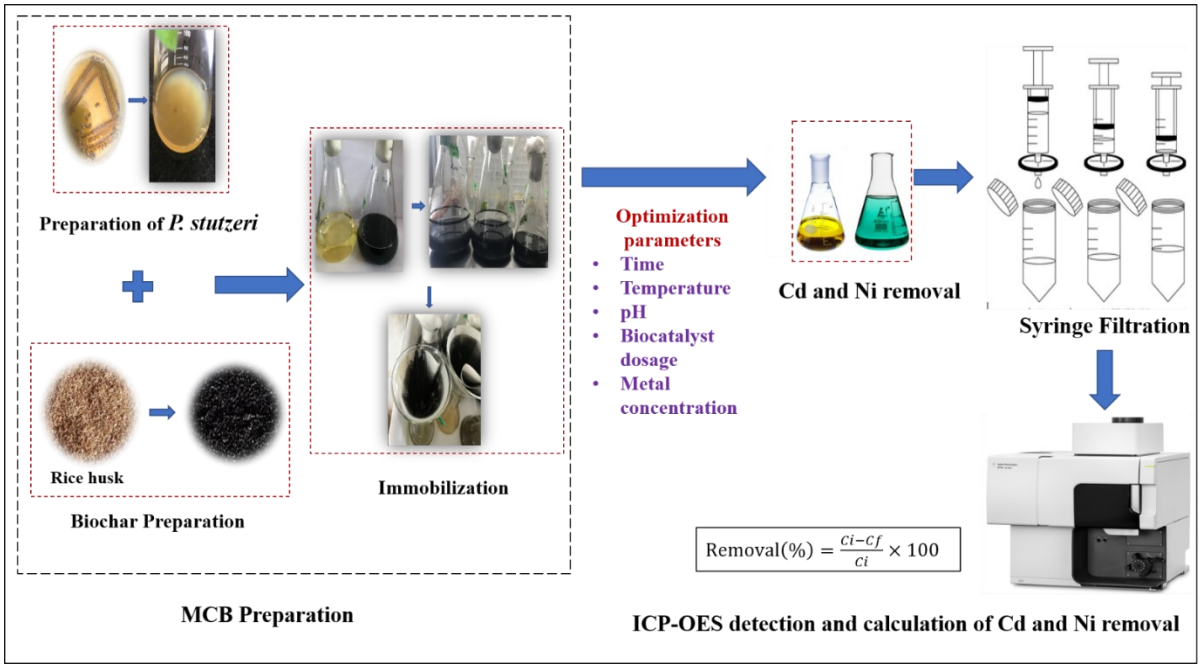

Figure 3.1 Experimental design.

3.2.2.2 Adsorption kinetics and isotherm studies

To evaluate and compare the removal efficiencies of Cd and Ni by microbial cell immobilized biochar, a few well-studied isotherm, and kinetic models were employed to fit the data. 0.1 g of PRHB was added to a 250 mL Erlenmeyer flask containing a 100 mL solution of 50 mg L^{-1} metal ions. The experiments were performed under 37 °C, rotational speed of 160 rpm, and sampled at regular intervals at 0, 1, 3, 6, 12, 18, 24, 30, 36, and 42 h. At the end of each equilibrium time, residual metal ions concentration was determined by ICP-OES, and the quantities of adsorbed metal ions (mg g^{-1}) were evaluated by Equation. (3.4).

$$Q_e = \left[\frac{C_i - C_e}{W}\right] \times V \qquad (3.4)$$

Where C_i and C_e are the initial and final concentrations (mg L^{-1}) of Cd and Ni, respectively, W is the quantity of PRHB (g) used, and V is the volume of the solution (L).

The sorption kinetic data were fitted with the pseudo-first-order (Equation. (3.5)) and pseudo-second-order (Equation. (3.6)) kinetic models (Youngwilai et al. 2020b)

$$\ln(Q_e - Q_t) = \ln Q_e - K_1 t \quad (3.5)$$

$$\frac{t}{Q_t} = \frac{1}{K_2 Q_e^2} + \frac{t}{Q_e} \quad (3.6)$$

Where Q_e (mg g^{-1}) and Q_t (mg g^{-1}) are the amount of Cd and Ni adsorbed at equilibrium and time t (min), K_1 (min^{-1}) and K_2 (g mg^{-1} min^{-1}) are the rate coefficient for pseudo-first order and pseudo-second order equation, respectively.

The adsorption isotherm of metal ions onto PRHB at 37 °C was investigated in a batch experiment. 0.1 g PRHB with different initial concentration metal ion (10, 25, 50, 75, 100) solution in 250 mL Erlenmeyer flask were taken for isotherm studies. The flasks were incubated in the shaker incubator at 160 rpm for 36 h. Langmuir and Freundlich's models were employed to describe the sorption isotherms. The linear forms of the two models are shown in Equations. (3.7), (3.8) (Ali et al. 2022; Fan et al. 2017).

$$\frac{1}{Q_e} = \frac{1}{Q_m} + \frac{1}{K_L Q_m}\frac{1}{C_e} \quad (3.7)$$

$$\ln Q_e = \ln K_F + \frac{1}{n}\ln C_e \quad (3.8)$$

where C_e (mg L^{-1}) and Q_e (mg g^{-1}) are the equilibrium concentrations of Cd and Ni in solution on PRHB. Q_m (mg g^{-1}) and K_L (L mg^{-1}) represent maximum sorption capacity and Langmuir constant, respectively. The parameters K_F and n are Freundlich parameters related to the sorption capacity and sorption intensity, respectively. The fittings of Cd and Ni adsorption kinetics and isotherms data were performed in Origin Pro 2022.

3.2.2.3 Reusability study of microbial cell immobilized biochar

Reusability is one of the desirable factors which are important for the applicability of the immobilized cell in waste water treatment. To investigate the reusability of the immobilized cell, PRHB was continuously used in consecutive Cd and Ni removal processes, and the removal

efficiency (%) was monitored as described in section 3.2.2. Briefly, the immobilized cells were incubated in a 100 mL LB medium with 10 mg L^{-1} metal ion for 36 h as one cycle. After each cycle, the supernatant was taken to analyze residual concentration, and the retrieved biocatalyst by filtration was washed with distilled water and transferred to a fresh batch of LB medium containing metal ions for the next cycle.

3.2.2.4 Experiments for interpreting the mechanism

The differences in surface morphology and surface element composition after the removal of Cd and Ni by PRHB were examined using the scanning electron microscope with energy-dispersive X-ray spectroscopy. The surface functional groups of PRHB after the Cd and Ni removal were determined by FTIR. The role of microbial mineralization was studied through XRD and XPS analysis.

To understand the effect of ion exchange mechanism in the adsorption of Cd and Ni on PRHB, concentrations of K^+ and Mg^{2+} in the liquid before and after metal ions adsorption were analyzed by ICP-OES and then converted into molar equivalents (Wei et al. 2016). Finally, to study the Cd and Ni removal mechanism of PRHB, the cell and protein concentrations in the free cell and PRHB solution were detected. Cell count was analyzed by the standard plate count method, and protein contents of the supernatant were determined through the Bradford assay using bovine serum albumin as a standard (Bradford 1976).

3.2.3 Cd removal using PRHB from soil

3.2.3.1 Soil preparation

Topsoil layer (0-15 cm depth) samples were collected from 10 different soil cores in the Palakkad district of Kerala, India, and these individual samples were then mixed to form a composite. Any residual roots, plant residues, and small stones were removed from the soil. The soil was lateritic loam in nature, air-dried at room temperature, mixed thoroughly, and passed through a 2 mm sieve. To prepare the Cd-contaminated soil, cadmium nitrate tetrahydrate was added to the soil at 10 mg kg^{-1} by following the standard protocol (Chen et al. 2019; Noronha et al. 2022). The soil was mixed thoroughly and aged at room temperature for three weeks (Smith et al. 2010).

3.2.3.2 Experimental design

Five experimental treatments were designed to evaluate the efficiencies of RHB, *P. stutzeri,* and PRHB on the remediation of Cd-contaminated soil. The experiment was conducted in culture dishes containing 500 g of soil. To ensure the cell loading was consistent for all treatments, 1 g RHB, 12 mL *P. stutzeri* (viable cell counts 6×10^9 CFU mL^{-1}), 1 g PRHB (viable cell counts 1×10^9 CFU g^{-1}) were added to 500 g soil. The treated soil in each culture dish was incubated at constant temperature and sampled after seven days intervals up to 80 days. During incubation, the soil moisture was kept at 40 % of water holding capacity to facilitate equilibrium. All treatments and control were performed in triplicate.

3.2.3.3 Soil characterization

The soil pH was measured from the aqueous soil extract in deionized water suspension at 1:2.5 (soil: water) (Choleva et al. 2020). The Walkley-Black chromic acid wet oxidation method was used to determine the organic carbon (C) present in the soil (Kumas et al. 2021). Phosphorus (P) from soil was extracted using Bray- 2 solution and measured colorimetrically based on the reaction with ammonium molybdate. Available potassium (K) and magnesium (Mg) were extracted from the soil sample and measured using a Flame Photometer. For extraction, 0.5 M ammonium acetate solution was added to a soil sample containing a conical flask and shaken for 30 minutes; the resultant sample was filtered and used for analysis (Zhao et al. 2019). Atomic absorption spectrophotometry was used to determine soil micronutrients iron (Fe), copper (Cu), and zinc (Zn) after extraction with 0.1 N HCl. Available sulfur (S) was extracted with calcium chloride and measured using Turbidimetry with barium sulfate. Bioavailable boron (B) extracted by the hot water-soluble method that involves complexing HBO_3 with azomethine-H, which results in the formation of a colored complex that can be measured spectrophotometrically at 420 nm (Javed et al. 2021).

3.2.3.4 Phytoavailability of Cd in soil

Heavy metals in soil extracted by diethylenetriaminepentaacetic acid (DTPA) are considered to be the most available fraction for plant uptake (Fellet et al. 2014). Triethylamine (TEA) functions as part of the buffer solution and masking reagent that forms complexes with aluminum and other interfering elements. Also, TEA burns clearly during atomization of extractant solution while being measured. The presence of 0.01 M $CaCl_2$ enables the extract to attain equilibrium with CaCl2, which

minimizes the dissolution of $CaCO_3$ from calcareous soils. Therefore, the DTPA extraction method determined the effects of RHB, *P. stutzeri*, and PRHB on the phytoavailability of Cd. Soil samples were added into the extract solution of 0.005 mol L^{-1} DTPA, 0.01 mol L^{-1} $CaCl_2$, and 0.1 mol L^{-1} triethanolamine (pH 7.3) at a solid-to-water ratio of 1g soil sample with 25 mL of DTPA solution. The suspensions were agitated in an orbital shaker for 1 h, followed by centrifugation at 5000 rpm for 30 min, and filtered using Whatman No. 1 filter paper (Noronha et al. 2022). The content was analyzed using ICP OES.

3.2.3.5 Cd fractions analysis

Different fractions of soil Cd were extracted using a sequential extraction scheme procedure (BCR) proposed by the European Community Bureau of Reference. The total soil Cd was divided into exchangeable, easily reducible, oxidizable, and residual fractions. Water and acid-soluble forms are most accessible to uptake, whereas residual fractions are mineral matrix forms that are most difficult for plants to absorb (Jayarathne et al., 2018). The present study mainly focused on the dynamic changes of these two fractions when assessing the remediation efficiency of different amendments. Firstly, 1 g of collected soil was extracted for 16 h with 0.11 M CH_3COOH (40 mL) for acetic acid extraction state. The above residues were extracted with a mixture of 0.5 M NH_2OH. HCl and 0.05 M HNO_3 (40 mL) for 16 h, then centrifuged at 5000 rpm for 5 min, and the supernatant was detected for a reducible fraction. Finally, the residual soil was digested with a mixture of HNO_3 and $HClO_4$ to extract the residual fraction (Xiao et al., 2017). The concentrations of different Cd fractions were measured by ICP-OES (Li et al., 2016).

3.2.3.6 Effect of PRHB on the growth of *Spinacia oleracea* L.

To assess remediation efficiency, early and late plant growth studies were conducted. After 80 days of incubation, soil samples collected from each treatment were added to the germination trays. 10 seeds of *Spinacia oleracea* L. were sown in the germination trays with the soil samples and incubated for 10 days. All the trays were watered during the experiment, and a moisture content of 40 % was maintained by supplying distilled water every alternate day (Wang et al. 2020a). The germinated seedlings were uprooted after 10 days, and the germination percentage (GP), seed vigour index (SVI), mean germination time (MGT), mean germination rate (MGR), and germination rate index (GRI) were recorded. Subsequently, the seedling's weight, shoot length, and root length were also measured to study the health of the seedlings. Each treatment was replicated three times.

The GP, SVI, MGT, MGR, and GRI were calculated using the formula reported by (Ranal et al. 2009).

$$\text{GP (\%)} = \frac{Total\ nuber\ of\ seeds\ germinated}{Total\ number\ of\ seeds\ planted} \times 100 \quad (3.9)$$

$$\text{SVI} = standard\ germination\ (\%) \times average\ seedling\ length(cm) \quad (3.10)$$

$$\text{MGT} = \frac{\Sigma\ F.x}{\Sigma\ F}\text{, where F=number of seeds germinated on day x} \quad (3.11)$$

$$\text{GRI} = \frac{G1}{1} + \frac{G2}{2} + \cdots + \frac{Gi}{i}, \quad (3.12)$$

where G1-GP on Day 1, G2-GP on day 2, and so on.

After recording the germination parameters, a sub-sample of plants is chosen to monitor extended plant growth, Cd accumulation, and changes in soil properties. Subsequently, this selected group of plants is replanted in pots containing 500 g of Cd-contaminated soil, which is amended with *P. stutzeri*, RHB, and PRHB. The growth of these plants is monitored for 60 days, during which both biomass and Cd content are recorded.

3.2.3.7 Biomass and Cd content of *Spinacia oleracea* L plants

The harvested plant samples were washed with sterile water to remove the attached soil and dust. The plant roots were immersed in 5 mmol L^{-1} EDTA-Na_2 solutions to remove the bound metal ions on the root surface. Then, plants were dehydrated at 80 ℃ until a constant weight was obtained, and the dry mass of the plants was assessed. The Cd content in plant samples was determined using ICP-OES. The total Cd accumulation in the shoot was determined as follows:

$$\text{Total accumulation} = C_{root} \times DW_{root} + C_{shoot} \times DW_{shoot} \quad (3.13)$$

C_{root}, C_{shoot} represent Cd concentration in root and shoot, DW_{root}, DW_{shoot} represent the dry weight of root and shoot, respectively.

3.2.3.8 Soil enzyme activities and organic matter analysis

Soil phosphatase and β-glucosidase activities in the soil samples from the treatments containing PRHB were determined (Xiao et al. 2019). The activity of soil phosphatase was determined by

incubating 1.0 g of soil with 4 mL of MUB, 0.25 mL of toluene, and 1 mL of disodium 4-nitrophenyl phosphate hexahydrate at 37 ℃ for 1 h. Whereas the activity of β-glucosidase was determined by incubating 0.5 g of moist soil in a test tube with 0.1 mL of toluene, 0.9 mL of distilled water, 1.5 mL of McIlvaine buffer, and 0.6 mL of 4-nitrophenyl β-D-glucoside for 1 h at 30 ℃.

The soil organic matter (SOM) content was determined via potassium dichromate ($K_2Cr_2O_7$) oxidation, followed by measuring the amount of chromic ion (Cr^{3+}) using a colorimetric procedure. UV-spectrophotometer (Cintra 101; GBC Scientific Equipment Ltd, Australia) was used to quantify the concentration of chromic ions.

3.2.4 Other bioremediation studies for the removal of metal ions using microbial cell-immobilized biochar

3.2.4.1 Cd and Ni removal using PSDB from water

3.2.4.1.1 Characterization of SDB

Characterization of SDB encompassed surface area, pore volume, functional groups, elemental composition, and extractable minerals, were carried out following the methodologies detailed in section 3.2.1.4.

3.2.4.1.2 Effect of operating conditions on Cd and Ni removal

Cd and Ni removal experiments were conducted using 50 mg L^{-1} metal ion solution by following section 3.2.2. A consistent cell count was maintained across all experiments, with 0.11 g PSDB (containing ~10^9 CFU mL^{-1} cells) and 1.2 mL free cells of *P. stutzeri* (final density ~10^9 CFU g^{-1}). The study assessed the impact of operating conditions, including incubation time, pH, temperature, biocatalyst dosage, and initial metal ion concentration, similar to section 3.2.2.1. Cd and Ni removal by SDB, *P. stutzeri*, and PSDB at optimized operating conditions were conducted.

3.2.4.1.3 Reusability studies for Cd removal using PSDB

To determine the persistent reusability of immobilized cells, PSDB was repeatedly used in experiments following the same procedure described in 3.2.2.3.

3.2.4.2 Cd removal using BRHB from soil

In this study, the bacterial strain *Bacillus* sp MTCC 3166 was used to remove heavy metal from soil, purchased from Microbial Type Culture Collection and Gene Bank, Chandigarh, India. The soil used in this study was the same soil samples collected from the agricultural plot in Palakkad, Kerala, India. Five experimental treatments, including control soil, were established to evaluate the efficiency of RHB, *Bacillus* sp*,* and BRHB cells for remediation. The experiment was conducted in culture dishes containing 500g of soil. To ensure the cell loading was consistent for all treatments 1 g RHB, 15 mL *Bacillus* sp (viable cell counts 4 $\times 10^7$ CFU mL^{-1}), 1 g BRHB (viable cell counts 1×10^7 CFU g^{-1}) were added to 500 g soil. Soil incubation was carried out based on section 3.2.3.2.

3.2.4.2.1 Phyto availability and Cd fraction analysis in soil

Phytoavailability of Cd was assessed using the DTPA extraction method, following the same procedure described in section 3.2.3.4 Cd fractions analysis was conducted using the same BCR sequential extraction scheme procedure, as detailed in section 3.2.3.5.

3.2.4.2.2 Effect of BRHB on the growth of *Spinacia oleracea* L

Plant growth studies were performed following the methodology as outlined in 3.2.3.6. section, including the calculation of GP, SVI, MGT, MGR, GRI, and the assessment of various growth parameters. The determination of biomass and Cd content in *Spinacia oleracea* L plants followed the procedure described in section 3.2.3.7. Soil enzyme activities and soil organic matter analysis were carried out according to section 3.2.3.8.

3.2.4.3 Cd removal using PCSB from soil

3.2.4.3.1 Preparation and characterization of CSB

For the preparation of biochar, coconut shells were dried under sunlight for two days and pyrolyzed at 450 °C in a conventional pit stove. The coconut shell biochar (CSB) was then dried, crushed, and sieved through mesh of different sizes (<1 mm, 1-2 mm, and 2-5 mm). The pH and the electrical conductivity of the CSB were determined for the solutions resulting from shaking for 30 minutes of biochar in deionized water at a ratio of 1:20 (w/v)(Xia et al. 2021). Extractable nutrient concentrations in CSB were determined using Inductively Coupled Plasma – Optical Emission Spectrometry (5100 ICP-OES; Agilent Technologies, USA). Microscopic observations and

elemental components of CSB were analyzed using a Scanning Electron Microscope (SEM; FEI-Quanta F.E.G. 200F, USA) and Energy Dispersive X-ray Spectrometry (EDX) (FEI-Quanta F.E.G. 200F)**.** The specific surface area was calculated according to the Brunauer-Emmett-Teller method. The elemental analysis of CSB was performed using a CHONS analyzer (Flash 2000, Thermo Scientific, Cambridge, UK). The functional groups of the CSB were determined by Fourier Transform Infrared Spectroscopy (FT-IR; PerkinElmer Spectrum One FT-IR, USA). The Thermo Gravimetric Analysis (TGA) of CSB was carried out under a nitrogen (N_2) atmosphere using Perkin Elmer STA 600 TGA analyzer.

3.2.4.3.2 Water holding capacity studies using CSB

The water-holding capacity of soil with and without CSB was determined using the modified soil column method (Gebre and Earl 2020; Menzies Pluer et al. 2020). The experiment was carried out in polyvinyl chloride (PVC) columns of 17 cm in height and 3 cm in diameter. The soil-biochar mixtures were prepared by adding 5 % (w/w) CSB of different particle sizes, i.e., <1 mm, 1-2 mm, and 2-5 mm, with three replicates per treatment to determine the effect of particle size.

The total mass of dry soil in the column was 144 g. For the 5% CSB treatment, columns contained 7.2 g of CSB and 136.8 g of soil. Treated soil was filled into the columns as they were tapped on a bench to obtain an initial bulk density of 1.25 g cm^{-1} and placed in water. After removing it from the water, this soil column was allowed to saturate for 1 h and sealed with cellophane tape. Further, it was placed in humidified plastic containers for 3 h, thus preventing evaporation. Then, the wet weight of the soil from the columns was measured. The samples were then dried under sunlight until no further water loss occurred and reweighed to record the dried sample. The water holding capacity was determined from equation 3.14.

$$\text{Water holding capacity (\%)} = \frac{wet\ weight - dry\ weight}{dry\ weight} \times 100 \qquad (3.14)$$

Based on the above results, the effect of different concentrations of CSB was studied for the optimized biochar size in soil.

3.2.4.3.3 Effect of CSB on the growth of *Solanum lycopersicum* L

The seed germination study was conducted to evaluate the effect of CSB and FYM amendment on initial plant growth. The experiment was carried out using a 14 x 7 cell protray. The treatment combinations are shown in Table 3.2.

Table 3.2 Treatment description of CSB and FYM.

Treatment	**Amendment details**
Control	No amendment
FYM	1 % Farmyard manure
1 % CSB	1 % of coconut shell biochar application
1 % CSB + FYM	1 % of coconut shell biochar and 1 % farmyard manure in equal proportion
5 % CSB	5 % coconut shell biochar application
5 % CSB + FYM	5 % of coconut shell biochar and 5 % farmyard manure in equal proportion
10 % CSB	10 % coconut shell biochar application
10 % CSB + FYM	10 % of coconut shell biochar and 10 % farmyard manure in equal proportion

Plant growth studies were performed following the same methodology as outlined in 3.2.3.6. section, including the calculation of GP, SVI, MGT, MGR, and GRI, and the assessment of various growth parameters. Soil enzyme activities and soil organic matter analysis were carried out by following the methodology of section 3.2.3.8.

3.2.4.3.4 PSCB preparation and experimental design

PCSB was prepared by following the procedure outlined in section 3.2.1.3. The soil was artificially contaminated with Cd to obtain a final concentration of 2 mg kg^{-1} by following the standard protocol (Noronha et al. 2022). Four experimental treatments were designed to evaluate the efficiencies of CSB, PCSB, and *P.stutzeri* in the remediation of Cd-contaminated soils. The contaminated soil, without any amendment, served as the control. Different materials were added as 5 % CSB, 10 mL of *P.stutzeri* suspension with viable cell count 10^6 CFU mL^{-1}, and 5 % PCSB with

viable cell count 10^6 CFU g^{-1}. The treated soil in each culture dish was incubated at constant temperature and sampled after 7-day intervals up to 21 days. During incubation, the soil moisture was kept at 40 % water-holding capacity to facilitate equilibrium. All treatments and control were performed in triplicate.

3.2.4.3.5 Phytoavailability of Cd in soil

Heavy metals in soil extracted by diethylenetriaminepentaacetic acid (DTPA) are considered the most available fraction for plant uptake. Therefore, the effects of biochar, microbial cell, and microbial cell immobilized biochar treatments on the phytoavailability of Cd were determined by the DTPA extraction method. Soil samples were added into the extract solution of 0.005 mol L^{-1} DTPA, 0.01 mol L^{-1} $CaCl_2$, and 0.1 mol L^{-1} triethanolamine (pH 7.3) at a solid-to-water ratio of 1g soil sample with 25 mL of DTPA solution. The suspensions were agitated in an orbital shaker for 1 h followed by centrifugation at 5100 rpm for 30 min, and filtered using Whatman No. 1 filter paper (Noronha et al. 2022). The content was analyzed using ICP OES.

3.2.5 Removal of CP using ARHB

3.2.5.1 Enrichment and isolation of CP degrading bacteria

The present study employed a selective enrichment method to isolate and enrich CP-degrading bacteria. Soil samples were collected from a pesticide-contaminated crop field in Palakkad district, Kerala, India. The samples were obtained from a depth of approximately 20 cm and immediately stored in a plastic container for transportation to the laboratory, where isolation studies were conducted. For enrichment, 1 g of the soil sample was added to a 250 ml Erlenmeyer flask containing 100 ml of MSM supplemented with CP as the sole carbon source at 10 mg L^{-1} concentration. The flask was then placed on a rotary shaker set at 30°C and 180 rpm for 7 days. This allowed for the growth and proliferation of bacteria which is capable of utilizing CP as a carbon source. Following the incubation period, 2 ml of the enrichment culture was subcultured four times into fresh MSM containing 50 mg L^{-1} of CP every 7 days. This process ensured the enrichment and selection of CP-degrading bacteria, A serial dilution method was employed to isolate the CP-degrading bacteria. The diluted samples were then cultured on MSM agar plates supplemented with the CP using the spread plate technique (Saravanan et al. 2022). Subsequently, the plates were incubated overnight at 30°C, allowing for the growth and formation of visible colonies. Following incubation, the resulting

colonies were carefully observed, and CP-resistant colonies were selected and purified for further analysis. These purified colonies were subsequently employed in degradation assays to assess their ability to degrade CP.

3.2.5.2 16S rRNA analysis and construction of phylogenetic-tree

The analysis of CP degrading bacterial species in this study involved the extraction of bacterial DNA using a DNA isolation kit obtained from QIAGEN (USA). The quality assessment of the extracted DNA was carried out using 1 % agarose gel electrophoresis. Subsequently, the 16S rRNA gene sequences were amplified utilizing the 27F (5′-AGAGTTTGATCCTGGCTCAG-3′) and 1492R (5′-CCCCGTCAATTCATTTGAGTTT-3′) primers (Koippully et al. 2018). The amplified products were purified using a PCR purification kit and subjected to sequencing using the BDT v3.1 cycle sequencing kit on an automated ABI 3730xl Genetic Analyzer. A consensus sequence was generated by aligning the forward and reverse sequence data to obtain a representative 16S rRNA gene sequence. This sequence was compared against the 'nr' database available in the NCBI GenBank database, which employs the Basic Local Alignment Search Tool (BLAST). The top seven sequences exhibiting the highest identity scores were selected for further analysis. The selected sequences were aligned using the Clustal W multiple alignment software program to ensure accurate comparisons. Finally, phylogenetic analysis was conducted using these aligned sequences, employing the Mega X software.

3.2.5.3 Growth kinetics and CP degradation experiments using the isolate

Based on phylogenetic analysis, CP-degrading bacteria are identified as *A.veronii.* The growth kinetics of *A.veronii* and its CP degradation ability were investigated using batch experiments conducted in MSM (Shabbir et al. 2018a). Initially, a pre-grown culture of the selected bacteria was transferred into a 250 mL flask containing 100 mL of MSM supplemented with CP at a 50 mg L^{-1} concentration. The flasks were placed in a shaking incubator at 160 rpm and maintained at 30 °C for 3 days. The optical absorbance at 600 nm was measured at different intervals to monitor bacterial growth. The strain cultivated without CP served as the control against which the growth in the presence of CP was compared. For the degradation study, Overnight grown bacterial cells were collected and suspended (OD=600 nm, (0.9)) in MSM. Briefly, bacterial suspension of 1 ml was transferred into 100 ml of MSM supplemented with CP (50 mg L^{-1}), and the culture flasks were incubated in a rotary shaking incubator (160 rpm) at 30 °C for 60 h. At different periods, 2 mL of sample was pipetted out from the flasks to which acetonitrile was added in the ratio of 1:1, then centrifuged with a rate of 1000

rpm for about 20 min. The supernatant which is procured is subjected to UV-Vis analysis. The residual pesticide was determined at 290 nm (Shabbir et al. 2018a; Y. Makino et al. 2009) and the removal (%) was calculated as follows.

$$\text{Removal (\%)} = [(A-B) / A] \times 100 \quad (3.17)$$

where A= absorbance of CP at 290 nm, B=absorbance of the *A.veronii* /RHB/ARHB amended with CP

3.2.5.4 Immobilization of *A.veronii on rice husk biochar*

The immobilization study was conducted following the procedure outlined in section 3.2.1.3. The quantification of immobilized cells on each biochar was determined using serial dilution and plating techniques. The CP removal efficiency of ARHB, prepared under various pyrolysis temperature conditions, was evaluated by incubating 1g of ARHB in CP-containing MSM. The culture flasks were placed in a rotary shaking incubator (160 rpm) at 30°C for 48 h. After the incubation period, the percentage removal of CP was calculated according to section 3.2.5.3.

3.2.5.5 Characterization of ARHB

ARHB characterization encompassed FTIR, TGA, and FESEM following the methodologies detailed in Section 3.2.1.4.

3.2.5.6 Optimization of CP removal by ARHB using RSM methodology

Statistical analysis and parameter optimization for pesticide remediation using ARHB were performed using the State-ease Design Expert software, which generated 17 experiments with varying combinations of parameters. The study employed a Box-Behnken statistical design (BBD) to explore the conditions for enhanced CP removal. Three levels of treatments were applied to CP concentration (10, 30, and 50 mg L^{-1}), ARHB dosage (0.5, 1.25, and 2), and incubation time (12, 24, and 36 h) based on the requirements of the design. The degradation ability of ARHB was then investigated in Erlenmeyer flasks (250 mL) containing MSM (100 mL) pH 6.5 under the optimized conditions mentioned earlier. CP residues after biodegradation were determined according to section 3.2.5.3. The percentage degradation was studied through spectroscopic analysis. RSM was consistently applied to narrow the parameter gap until an optimized value was obtained, with the highest pesticide

concentration treated against the lowest ARHB concentration. The model results were evaluated using R^2, ANOVA, and 3D plots.

3.2.5.7 Reusability studies for CP removal using ARHB

To determine the persistent reusability of immobilized cells, ARHB was repeatedly used in experiments following the same procedure described in 3.2.2.3.

3.2.5.8 CP removal using ARHB from soil

The soil was collected from the top layer (0-15 cm depth) of an agricultural field in the Palakkad district of Kerala, India, where there has been no history of pesticide application in the past five years. The soil samples were air-dried at room temperature, mixed thoroughly, and passed through a 2 mm sieve. Different concentrations of CP (10 mg kg^{-1}, 30 mg kg^{-1}, and 50 mg kg^{-1}) were tested with a dosage of 1g ARHB to analyze the effect of ARHB in the remediation of CP-contaminated soil along with RHB and *A.veronii*. Additionally, the impact of different ARHB concentrations (0.5 g, 1 g, and 2 g) on CP remediation in soil was investigated. Four treatment groups were established: soil spiked with CP, soil spiked with CP and RHB, soil spiked with CP and free strain *A.veronii*, and soil spiked with CP and ARHB. All the experiments were conducted in triplicate. Afterward, the soil samples were incubated at 30 °C for 45 days in the dark, and soil moisture was always kept at 60 % of water holding capacity by periodically adding deionized water. Soil samples (5 g) were withdrawn at different time intervals (7, 21, and 30 days) to quantify the removal of CP from the experimental soil samples. CP was extracted from the soil particles according to the methods described in Silambarasan and Abraham, 2013. The concentration of CP was quantified by UV–vis spectrophotometer

3.2.5.9 Effect of ARHB on the growth of *Vigna unguiculata* L.

A plant growth study was conducted to evaluate the effect of CP on the growth and development of *Vigna unguiculata* (cowpea) plants. *Vigna unguiculata* L., also known as the long bean, is an important economic vegetable of high nutritional value widely used in India and China (Herniter et al. 2020a). Plant growth studies were performed following the same methodology as outlined in 3.2.3.6. section, including the calculation of GP, SVI, MGT, MGR, and GRI, and the assessment of various growth parameters. Soil enzyme activities were carried out by following section 3.2.3.8.

3.2.5.10 Analysis of metabolite products of CP degradation

The metabolic products of CP in water and soil samples after remediation were analyzed using high-resolution liquid chromatography-mass spectrometry (HR-LCMS). For water samples, 10 ml of the culture filtrate after treatment was recovered and centrifuged at 8000 rpm for 10 min. The resulting supernatant was extracted with an equal volume of dichloromethane, and the organic layer was dried at room temperature (Silambarasan and Abraham 2013a). The residue was then dissolved in HPLC-grade acetonitrile and subjected to LC-MS analysis. In the case of soil samples, 10 g of soil was mixed with 20 ml of HPLC-grade acetonitrile on a rotary shaker at 120 rpm for 30 min. After settling, the clear supernatant was collected for pesticide concentration determination. The LC-MS analysis of CP and its metabolites in water and soil samples was performed on an XEVO QTOF model instrument (Waters, USA) equipped with an ACQUITY UPLC® BEH C18 column (1.7 μm, Waters, USA). The column temperature was maintained at 30 °C, and the injection volume was set to 10 μL. A gradient elution method employing a mixture of water (A, 20 %) and acetonitrile (B, 80 %) with 0.1 % formic acid was used for 10 min. The column temperature was set at 30 °C. CP and its degraded products were detected using electrospray ionization (ESI) in both positive and negative ionization modes. The source parameters were optimized: capillary voltage 2.5 kV, sampling cone 40 V, source temperature 150 °C, source offset 80 V, desolvation temperature 450 °C, cone gas flow 80 L h^{-1}, desolvation gas flow 500 L h^{-1}. Mass spectrometric data were acquired in the m/z range of 50-750, enabling the detection and characterization of CP and its metabolites.

3.2.6 Statistical analysis

Statistical analysis employed one-way analysis of variance to evaluate differences among various treatments. Tukey's test was utilized to determine the significance of variation among treatments, considering a significance level of $p < 0.05$. All experiments were carried out in triplicate, and the error bars are the mean ± SD.

CHAPTER 4

MICROBIAL CELL IMMOBILIZATION AND OPTIMIZATION OF BIOCHAR CONDITIONS

4.1 GROWTH AND HEAVY METAL ION TOLERANCE OF *P. stutzeri*

Heavy metal tolerance of *P. stutzeri* was initially assessed through agar plate assays, utilizing various heavy metals such as Cr, Hg, As, Cd, Ni etc. (**Figure A1** Appendix I). *P. stutzeri* exhibited exceptional tolerance to Cd and Ni during these preliminary experiments and was selected for further study in a LB medium with varying concentrations. The growth curve of *P. stutzeri* was determined by measuring optical density (OD 600) for 48 h. Growth of *P. stutzeri* showed varied results in LB broth with Cd and Ni compared to the growth curve without Cd and Ni (control), as depicted in **Figure 4.1**. The maximum growth of *P. stutzeri* without Cd and Ni was obtained at 32 h, followed by a stationary phase from 32- 40 h. The growth curve demonstrated that *P. stutzeri* grew in Cd concentrations of 10 and 50 mg L^{-1} for 36 h and then declined, whereas, in 100 mg L^{-1} concentration, growth of *P. stutzeri* declined after 44 h. The presence of Cd resulted in a prolonged lag phase i.e., for Cd concentration of 10 mg L^{-1}, the lag phase duration was 10 h, which varied with concentrations showing 18 h and 24 h for 50 and 100 mg L^{-1}, respectively. It was observed that the *P. stutzeri* showed maximum growth at 36 h when the initial Cd concentration was 10 mg L^{-1} and decreased to 0.94 (50 mg L^{-1}), further showing comparatively less growth of 0.5 at 100 mg L^{-1} concentration. Choińska-Pulit et al. (2018) reported a reduction in the growth of *P.azotoformans* with increasing Cd, Cu and Pb concentrations. Reduced growth at higher concentrations was attributed to bacteria utilizing energy for cellular function rather than growth to resist metal toxicity (Bautista-Hernández et al. 2012).

A similar growth pattern was observed for *P. stutzeri* in the presence of Ni. 10 mg L^{-1} Ni addition to LB medium showed an increase in cell growth up to 36 h and then declined, whereas 50 and 100 mg L^{-1} concentration cell growth declined after 44 h. The presence of Ni affected the duration of

lag phase, which increased from 10 h (10 mg L^{-1}) to 24 h (100 mg L^{-1}). Addition of 10 mg L^{-1} Ni showed OD of 1.3, which decreased to 1 and 0.62 at 50 and 100 mg L^{-1}, respectively. Better growth of *P. stutzeri* was observed in LB containing Ni than Cd because Ni plays an important role in the metabolic process of the microorganism (Alboghobeish et al. 2014). Our results are supported by other studies where metal ions may influence the growth of microorganisms (Sandaa et al. 2001; Tsai et al. 2006). Lo and Su (2016) reported similar observations on the decrease in bacterial growth rate with increasing concentrations of Cd and Ni using different bacterial cultures. Hence, it can be concluded that the *P. stutzeri* exhibited tolerance to Cd and Ni up to 50 mg L^{-1} concentration and was able to grow well in heavy metal stressed conditions. This particular concentration was chosen for Cd and Ni removal analysis.

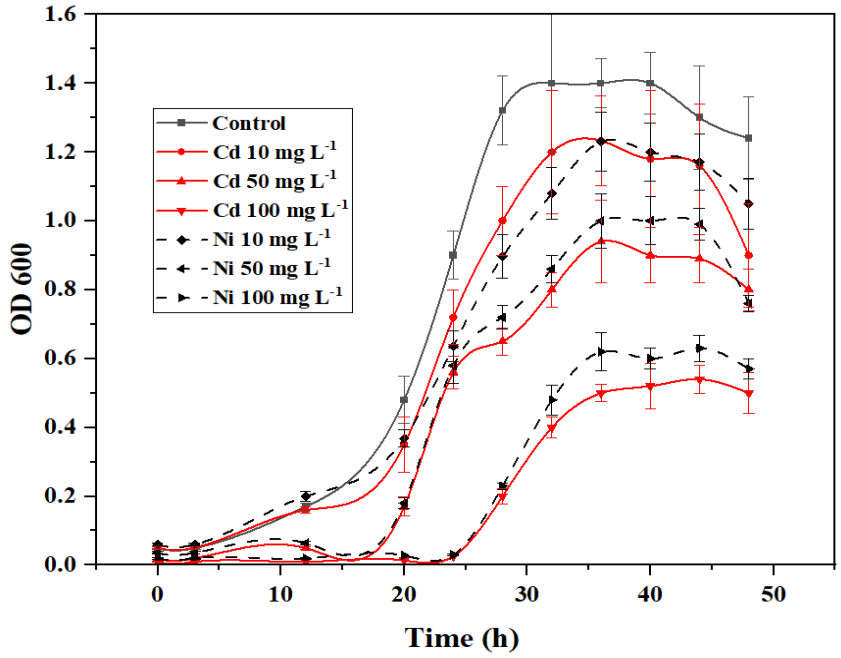

Figure 4.1. Cd and Ni tolerance of *P. stutzeri* at concentration of 10, 50 and 100 mg L^{-1}.

4.2 BIOCHAR YIELD

The percentage of biochar yield produced at different conditions is depicted in **Figure 4.2**. The biochar yield decreases as the pyrolysis temperature increases. This trend is evident for all types of biochar (RHB, SDB, SCB, and PSB). Different feedstock types influence the biochar yield percentage mainly due to the variation in lignocellulosic content (Shariff et al. 2016; Zhang et al. 2015b). A maximum of 45.65 % yield was observed for RHB-300 ℃-30 min, and the yield subsequently decreased to 17.36 % for RHB-700 ℃-120 min as more ash content was observed at

higher temperature (**Figure A2**, Appendix I). RHB consistently showed the highest biochar yield among the four types at all temperature and time intervals, making it the most efficient feedstock for biochar production under these conditions. A maximum yield of 38.17 % was observed for SDB prepared under 300 ℃ for 30 min, and the yield subsequently decreased with increasing temperature and time, reaching a minimum of 10.4 % for SDB pyrolyzed at 700 ℃ for 120 min. A maximum of 43.06 % yield was achieved for SCB at 300 ℃ for 30 min, which eventually decreased with pyrolysis temperature and time and reached a minimum value of 0.8 % for SCB pyrolyzed at 700 ℃ for 120 min. PSB also showed the same trend and biochar yield of 47.62 % at PSB pyrolyzed at 300 ℃ for 30 min and reduced to 7.31 % for PSB prepared under 700 ℃ for 120 min. This reduction in the yield can be because an excessive release of water and volatile compounds from the biomass is promoted at high pyrolysis temperatures (Mašek et al. 2013). A sharp reduction in yield occurred at 700 °C, implying that high-molecular-weight structures such as lignin and cellulose were completely degraded at higher production temperatures (Shariff et al. 2016).

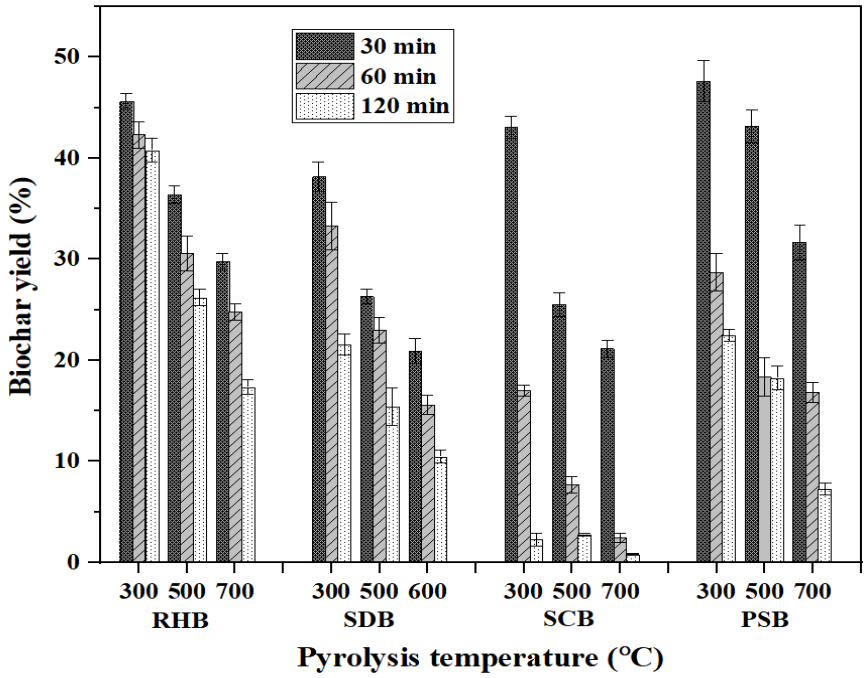

Figure 4.2. Biochar yield (%) at various temperatures (300 ℃, 500 ℃, and 700 ℃) and time (30 min, 60 min, 120 min) for RHB, SDB, SCB, and PSB.

Higher temperatures lead to more extensive decomposition of biomass, resulting in the production of gases and volatiles, leaving less solid biochar (Thangalazhy-Gopakumar et al. 2010).

Increasing the pyrolysis time from 30 min to 120 min generally leads to a slight decrease in biochar yield. However, shorter pyrolysis times may not provide adequate duration for the complete decomposition of biomass components such as cellulose, hemicellulose, and lignin, leading to an increase in biochar yield compared to longer pyrolysis times. Thangalazhy-Gopakumar et al. (2010) reported that thermal volatiles were further broken down at higher temperatures into low molecular weight liquid and gas instead of char.

4.3 MICROBIAL CELL IMMOBILIZATION

Pyrolysis temperature is an essential factor affecting biochar properties during production. Surface area, pore size, and functional groups are important criteria for choosing biochar as a carrier or material support for immobilizing bacteria. Different combinations of MCB based on biochar production temperature were prepared, and the immobilized cell number in terms of Log_{10} cells g^{-1} of *P. stutzeri* was calculated. The number of cells immobilized on all prepared biochar samples is represented in **Figure 4.3.** The results showed that the ability of different biochar types to immobilize cells varied significantly, with RHB demonstrating the highest cell immobilization capacity, followed by SDB, SCB, and PSB.

According to the graph, the maximum number of *P. stutzeri* cells was immobilized onto RHB-500-30 and SDB-500-60 biochar samples. However, a subsequent decrease in the number of immobilized cells was observed for RHB and SDB produced at higher temperatures of 700 ℃. Conversely, biochar produced at lower temperatures with extended time periods showed better immobilization of cells. For example, RHB and SDB pyrolyzed at 300 ℃ for 120 min showed 10 and 9.6 Log_{10} cells g^{-1}, respectively, whereas RHB and SDB pyrolyzed at 300 ℃ for 30 min could immobilize only 6.9 and 7 Log_{10} cells g^{-1}. Moreover, comparing the results at different pyrolysis times (30 min, 60 min, and 120 min), it can be seen that there was no consistent trend in cell immobilization. For some biochar types, longer pyrolysis times led to higher cell immobilization (e.g., RHB at 120 min), while for others, it led to lower immobilization (e.g., SCB at 120 min). This variability suggests that the relationship between pyrolysis time and cell immobilization is complex and may be influenced by other factors such as biochar properties and bacterial cell interactions.

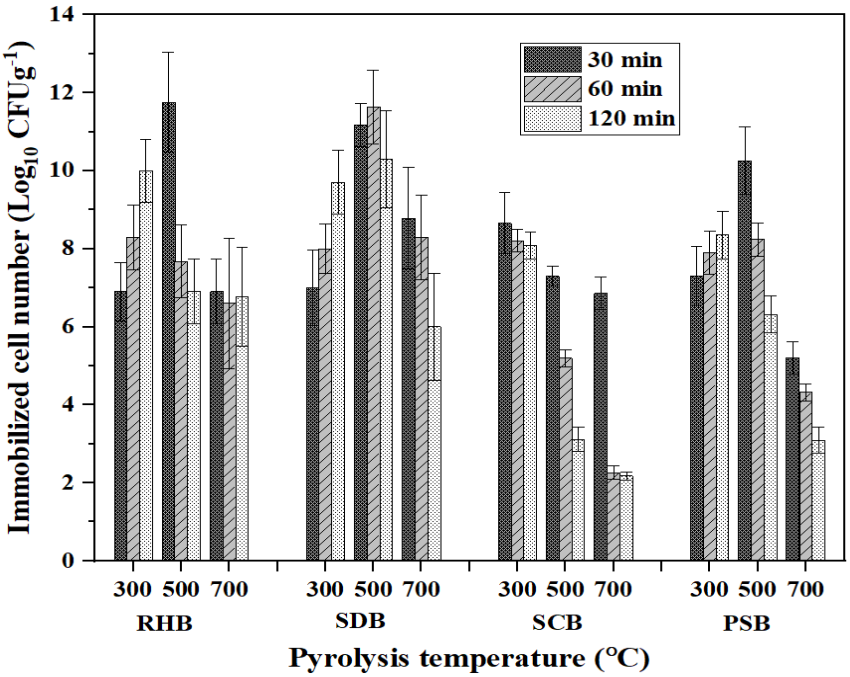

Figure 4.3. Number of cells immobilized on different biochar at various temperature (300 °C, 500 °C, and 700 °C) and time periods (30 min, 60 min, 120 min).

This suggests that the physical and chemical properties of biochar play a crucial role in determining its ability to incorporate bacterial cells. Pyrolysis temperature was found to be a crucial factor affecting biochar properties during production. As the pyrolysis temperature increased from 300 °C to 700 °C, the number of immobilized cells decreased (**Figure A3**, Appendix I). This observation can be attributed to changes in biochar porosity, surface area, and functional groups as a result of higher pyrolysis temperatures.

The presence of potentially harmful substances in biochar, such as polycyclic aromatic hydrocarbons, dioxins, furans, volatile organic compounds, and free radicals, which can lead to microbial cytotoxicity and inhibit microbial activity during immobilization on biochar (Odinga et al. 2021). To assess the toxicity of biochar on microbial cell immobilization, immobilization studies were conducted with RHB 500°C-30 min and bacterial colonies were enumerated after 6, 12, and 24 h to evaluate the survival of cells. The results showed that the number of cells increased with each subsequent incubation period. Specifically, cell counts increased from 7.9 7.9 Log_{10} cells g^{-1} after 6 h to 8.26 Log_{10} cells g^{-1} after 12 h, and peaked at 11.5 Log_{10} cells g^{-1} after 24 h (**Figure A4,** Appendix I). This indicates a significant increase in cell numbers over the incubation period, suggesting that

the biochar immobilization did not exert toxic effects on the *P. stutzeri* cells and even support their growth and proliferation.

4.4 CHARACTERIZATION OF RHB AND PRHB

Temperature-dependent variations significantly influence the efficacy of biochar as a carrier material for immobilized microorganisms. Therefore, characterizing biochar produced under different temperatures is imperative to elucidate the correlation between biochar properties and its potential for microbial cell immobilization. RHB demonstrated the highest biochar yield among various feedstock types, highlighted its efficiency for biochar production under the studied conditions. Moreover, RHB produced at 500 °C for 30 min showed exceptional performance in terms of immobilizing bacterial cells compared to other biochar types. The ability of RHB to effectively immobilize bacterial cells is significant as it directly influences the efficiency and effectiveness of biochar applications in water and soil. The higher number of immobilized cells on RHB suggests its superior surface area, pore size, availability of functional groups, and nutrient composition, which are critical factors for successful microbial cell immobilization. Furthermore, the abundance of rice husk as an agricultural waste in many rice-producing countries, including India, provides a substantial and readily available source for biochar production, making it an attractive option for sustainable waste management and resource utilization initiatives.

4.4.1 Characterization of RHB

The SEM images of biochar produced at three distinct temperatures (300 °C, 500 °C, and 700 °C) reveal distinctive surface characteristics. RHB 300 exhibits underdeveloped pore structures, limiting bacterial entry (**Figure 4.4a**). At 500 °C, the biochar displays well-defined pores (**Figure 4.4b**), while at 700 °C, a channel-like structure emerges due to aromatic structure development and this indicates a collapse of macropores or a reduction in number at higher temperature (**Figure 4.4c**).

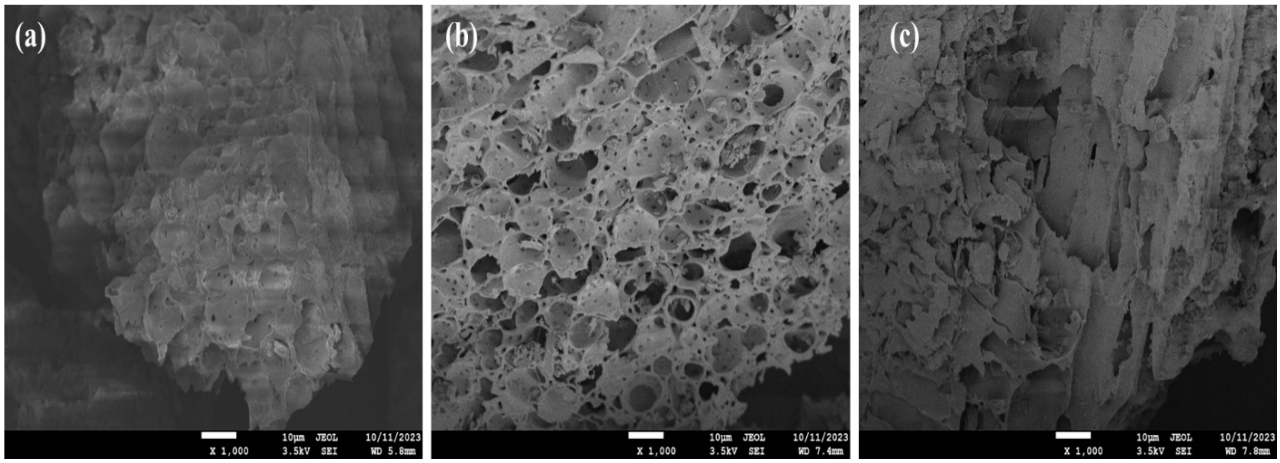

Figure 4.4. SEM images of RHB prepared at various temperatures (300 ℃, 500 ℃, and 700 ℃) for 30 min **(a)** RHB 300 ℃, **(b)** RHB 500 ℃ **(c)** RHB 700 ℃.

Another critical parameter influencing immobilization potential is the total pore volume, with RHB 500 showing 0.65 cm^3 g^{-1}, whereas it was lower for RHB 700 at 0.11 cm^3 g^{-1} (Table 4.1). These results align with the findings of Zhao et al. (2017), they found that biochar produced at temperatures above 400 ℃ exhibited larger surface areas and pore volumes, facilitating the accommodation and immobilization of more bacterial cells within the biochar. In another study carried out by Leng et al. (2021) found that pore volumes and surface area of biochar produced at 700 ℃ were smaller than those produced at 500 ℃. Biochar particle size influences the surface area-to-volume ratio, pore structure, reactivity of biochar and immobilization capacity. Finer biochar particles, such as those with a size of <1 mm, offer a larger surface area, which facilitates extensive contact with contaminants. This increased surface area enhances adsorption or chemical reactions, leading to improved pollutant removal efficiency. Biochar particles with a size of 0.15 mm, chosen for their suitability in microbial cell immobilization and pollutant removal. Han et al. (2016) suggested that the adsorptivity of chromium on biochar differs significantly with particle size. Smaller biochar particles (0.15-0.50 mm) exhibit higher reaction rates and removal capacities compared to larger particles (0.50-1.00 mm). This is attributed to the larger surface area of smaller particles, which provides more active sites for pollutant adsorption.

Table 4.1 Surface area, pore volume and pore size of RHB prepared at various temperatures (300 ℃, 500 ℃, and 700 ℃) for 30 min.

Biochar	Surface area	Total pore volume	Average pore size
RHB 300 °C	85.92 m^2 g^{-1}	0.51 cc g^{-1}	1.16 nm
RHB 500 °C	149.87 m^2 g^{-1}	0.65 cc g^{-1}	1.26 nm
RHB 700 °C	151.80 m^2 g^{-1}	0.11 cc g^{-1}	1.16 nm

Surface functional groups on biochar provide insights into its immobilization potential. Analyzing functional groups in RHB at varying pyrolysis temperatures revealed distinctive peaks. The band at 1600 cm^{-1} was indicative of a stretching vibration of C=O bonds associated with carboxylic acids or esters present in the biochar. The functional groups observed at 1441 cm^{-1}, were related to aromatic C=C ring stretching, indicating the dehydration of cellulosic compounds. The wavelength range of 1000–1300 cm^{-1} identifies various functional groups including ethers, alcohols (primary and secondary), sugars, sulfur, phosphorus, and inorganic compounds like silica. Bond types typically found in this range are C-O-C, C-OH, S=O, P=O, and Si-O-Si. Broad peaks observed at 1070 cm^{-1} is attributed to the presence of aliphatic ethers (C-O-C) and alcohols (C-OH) stretching or phenols groups. The peaks at 795 cm^{-1}, and 443 cm^{-1} were assigned to the Si-O-Si groups (Zhen-Yu et al. 2012). RHB 500 °C showed dominance in silica functional groups, including Si–O–Si (1103 cm^{-1}) and Si–H (792 cm^{-1}). However, at 700 °C, the intensity of active surface groups decreased and some peaks disappeared at 300 °C. RHB 300 °C notably lacked C=C ring stretching at 1440 cm^{-1} (**Figure 4.5a**). Loss of functional group is one of the reasons for the reduction in number (Tu et al. 2020). The biochar produced at higher temperatures of 700 ℃ showed fewer immobilized cells because some macropores collapsed at these temperatures, and the pore volumes and surface area decreased compared to biochar produced at 500 ℃.

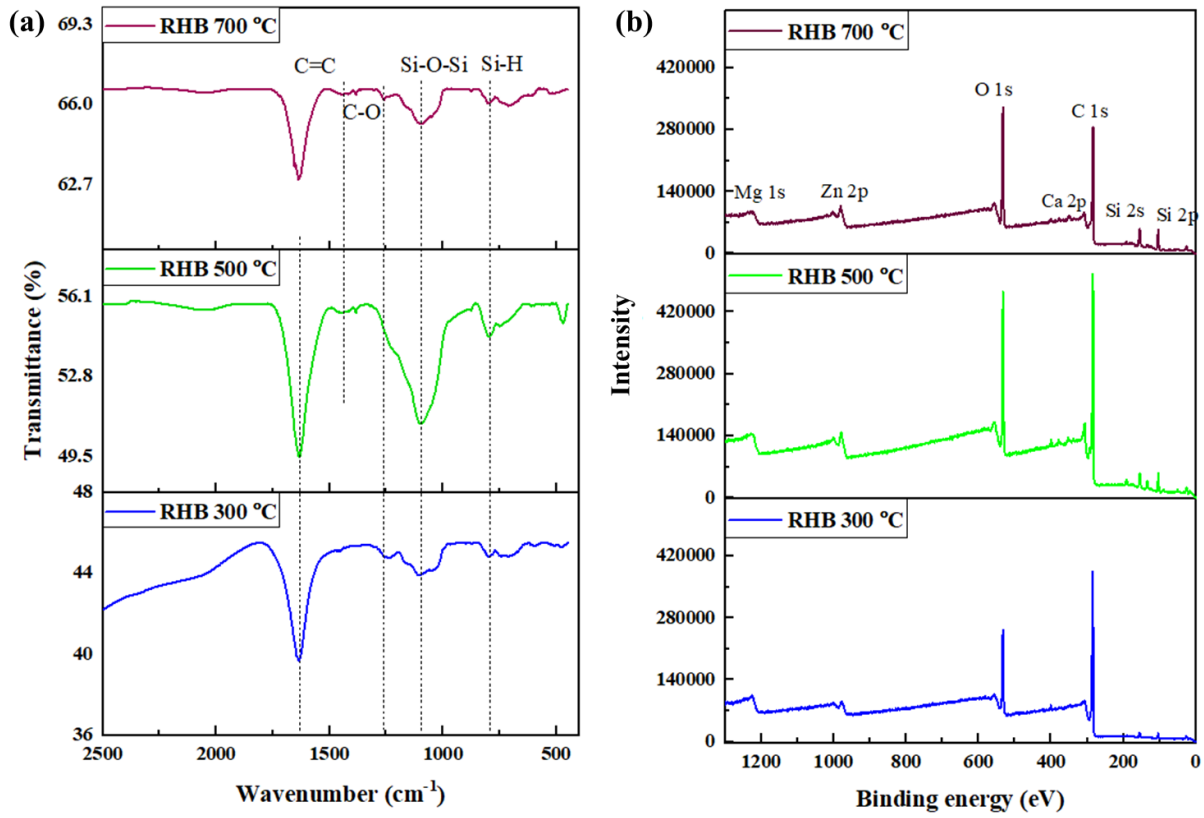

Figure 4.5. Characterization of RHB prepared at various temperatures (300 ℃, 500 ℃, and 700 ℃) for 30 min **(a)** FTIR and **(b)** XPS.

Further analysis of biochar samples involved determining the XPS spectra (**Figure 4.5b**). The photoelectron lines revealed the presence of O, C, N, Si, Ca, and Mg in the biochar. The O (O 1s) spectral lines for RHB indicated a binding energy of 530 eV, corresponding to C=O type bonds. Ca (Ca 2p) spectral lines exhibited a binding energy of 347 eV. C (C 1s) spectral lines, with a binding energy of 290 eV. The Si spectral lines occurred at two binding energies of Si 2s and Si 2p, indicating Si in the inorganic form of SiO_2 (Wang et al. 2018; Zhang et al. 2018). XPS characterization revealed that biochar produced under different conditions contained varying minerals, with abundant presence in RHB 500 °C. The mineral composition, crucial for microbial cell growth in biochar, also facilitates bacteria adherence to the mineral-enriched region (Huang et al. 2020). Additionally, the oxidation states of carbon (C 1s) were analyzed, indicating that RHB 300 exhibited a peak at 284.88 eV, RHB 500 at 284.29 eV, and RHB 700 at 284.46 eV, respectively (**Figure A5,** Appendix I). The deconvolution spectra of C1s at 284 eV suggest the presence of C−H carbons. Based on this

characterization and immobilization studies, the biochar produced at RHB 500 °C-30 min was chosen as the carrier for further studies

4.4.2 Characterization of PRHB

FTIR analysis was carried out to determine the surface functionalities of RHB, PRHB, and *P. stutzeri*. The FTIR results demonstrate differences in the surface functional groups of biochar due to differences in the feedstock and the pyrolysis conditions. The main functional groups of RHB include 3189 cm^{-1} attributed to hydroxyl stretching (–OH). The peaks at 2325 cm^{-1}, 1600 $cm^{-1,}$ and 1441 cm^{-1} were assigned to $–CH_2$ groups and aromatic C=O ring stretching (**Figure 4.6)**. The peaks at 1060 cm^{-1}, 795 cm^{-1}, and 443 cm^{-1} were assigned to the Si-O-Si groups (Zhen-Yu et al. 2012). The spectral peaks of *P. stutzeri* at 3268 cm^{-1} are assigned to the stretching vibrations of O-H and N-H bonds (Filip and Hermann 2001). The bands at 2850 cm^{-1} represent C-H bending vibrations of fatty acids and lipids on the bacterial surface.

The intense band at 1639 cm^{-1} and 1541 cm^{-1} represent the protein amide band caused by C=O stretching vibrations and N-H bond stretching vibrations, respectively. A peak at 1259 cm^{-1} was attributed to the P=O stretching of the phosphate group (Liu et al. 2015). FTIR analysis of PRHB showed significant alteration of surface chemistry of biochar and changes of certain bands compared to biochar. Increased band intensity was more pronounced after *P. stutzeri* immobilization for the peak 1600 cm^{-1}. A shift in C=C stretching bands to lower frequencies 1441 to 1428 cm^{-1} was observed after immobilization. The peak at 1743 cm^{-1} in bacteria and 1698 cm^{-1} in biochar disappeared after cell immobilization. These peaks are related to the structure of the carboxyl groups. These changes in bands may account for the functional group responsible for the immobilization of *P. stutzeri* onto the RHB.

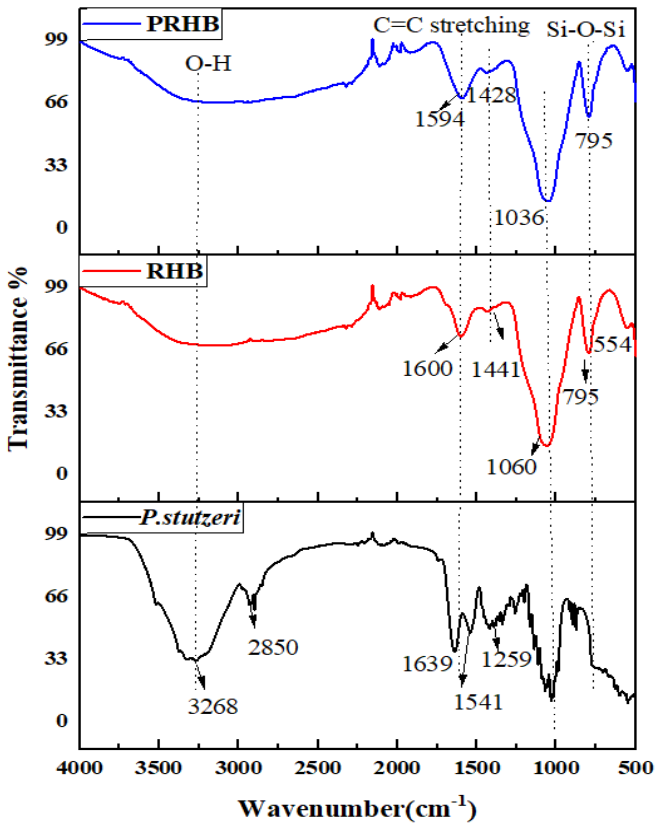

Figure 4.6. FTIR spectra of *P. stutzeri*, RHB and PRHB.

The elemental composition and mineral components of RHB are shown in **Table 4.1**. RHB showed a carbon content of 41.93 % and 55.21 % oxygen content. This suggests the abundance of oxygen-containing surface functional groups in RHB, which are the main metal adsorption sites (Zuo et al. 2016). Biochar can obtain more effective adsorption sites during the adsorption process due to its loose and porous structure, high porosity, large total pore volume, and surface area (Song et al. 2014). Based on the ICP analysis results, RHB comprises various mineral constituents such as Fe, Mg, Mn, Zn, K, Cu, Pb, etc., that could support nutrients for the growth of *P. stutzeri*. A study by Ye et al. (2017) suggested that bacteria could adhere to the mineral-enriched region of biochar. The pH_{zpc} values of RHB and PRHB are 6.0 and 6.4, (**Figure A6,** Appendix I). pH_{zpc} indicates the solution pH in which the surface charge of the biochar is neutral. When the pH of the nutrient broth is lower than the pH_{zpc}, the surface of the biochar is protonated and positively charged. When the pH is above the pH_{zpc}, the surface is negatively charged, which favors the attraction of positively charged metal ions (Inyang et al. 2015).

Table 4.2 Elemental composition and extractable minerals present in RHB.

Elemental composition (% mass-based)					**Extractable minerals (mg kg^{-1})**							
C	H	N	S	O	Ca	Fe	Mg	Mn	Zn	K	Cu	Pb
41.93	2.12	0.37	0.35	55.21	0.42	9.51	74.18	3.59	1.62	19	0.17	0.04

The surface morphology of RHB revealed a porous surface texture (**Figure 4.4b**), which could be due to the evaporation of volatile matter from rice husk biomass during pyrolysis. Rough surface with well-developed and relatively regular pore structures, which facilitates the adsorption of microorganisms and heavy metals. During the metabolic process of microorganisms, the biochar pore structure can act as a transport channel for oxygen, micronutrients, and pollutants, making it an excellent carrier for microbial cell immobilization (Zhen-Yu et al. 2012). The surface morphology of PRHB showed the presence of rod-shaped *P. stutzeri* (**Figure 4.7a**). The presence of microorganisms on the surface and in the pores of PRHB is due to its large specific surface area and a high number of micropores, which have a high adsorption capacity for microorganisms. It was also found that the morphology of the colonies of bacteria distributed on the surface of the biochar was different, partly aggregated, and partly dispersed. This suggests that there may be two ways of microbial immobilization by biochar: physical adsorption between microorganisms and electrostatic attraction between the microorganism and the carrier biochar.

The X-ray diffraction patterns of RHB and PRHB are depicted in **Figure 4.7b**. In RHB, a broad hump in the 18.84°–28.15° region corresponds to the crystal plane index C (002). The presence of amorphous silica, a predominant component in rice husk biochar, contributes to a broad XRD peak cantered at $2\theta \sim 22.5°$, indicative of disordered cristobalite. Sharp peaks at 35° in RHB suggest SiO_2 (quartz) presence (JCPDS card no. 46-1045) (Mohan et al. 2018). In the case of PRHB, a small peak at 38.42° is attributed to CaO (JCPDS Card no. 011-1160), while the peak at 50.54° is linked to Ca $(OH)_2$ (JCPDS card no. 01-073-5492). Peaks at 44.67° indicate the presence of $CaCO_3$ (calcite) in PRHB (JCPDS card no. 05-0586). Small peaks at 65.14° in both RHB and PRHB indicate the presence of MnO_2 (JCPDS Card no. 44-0141)(Kim et al. 2019; Nabieh et al. 2021; Severo et al. 2020; Xu et al. 2017).

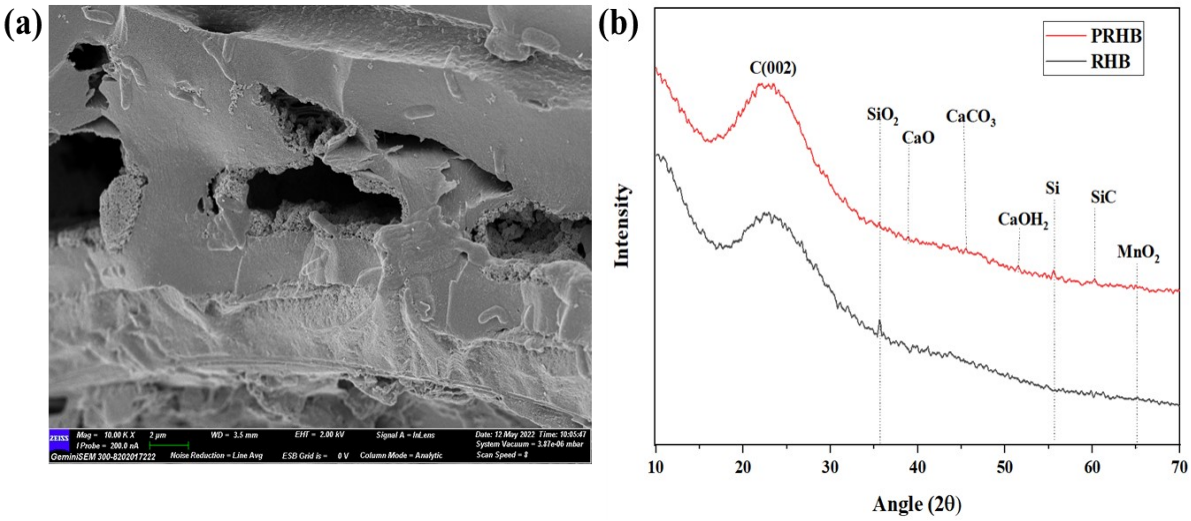

Figure 4.7. **(a)** SEM image of PRHB **(b)** XRD spectra of RHB and PRHB.

CHAPTER 5

Cd AND Ni REMOVAL USING *P.stutzeri* IMMOBILIZED RICE HUSK BIOCHAR FROM WATER

5.1 EFFECT OF OPERATING CONDITIONS ON Cd AND Ni REMOVAL USING PRHB

5.1.1 Effect of incubation time

The influence of incubation time on Cd and Ni removal efficiency by *P.stutzeri* and PRHB is depicted in **Figure 5.1a.** Cd removal efficiency increased with incubation time, from 6.38 % to 48 % for *P. stutzeri* and 42.26 to 78.6 % for PRHB from 3 to 42 h**.** A steep increase in Cd removal efficiency was seen till 36 h for PRHB, whereas *P. stutzeri* showed a significant increase till 30 h. Maximum Cd removal of 78.60 % was observed at 36 h for PRHB, whereas *P. stutzeri* showed only 48 %. Ni removal efficiency increased from 8.58 to 44.6 % for *P. stutzeri* and 40.8 to 69.4 % for PRHB, with an increase in incubation time from 1 to 42 h at an initial Ni concentration of 50 mg L^{-1}. This increase in removal with incubation time may be because Cd and Ni were gradually adsorbed into the immobilized system as the incubation time was extended, which increased the contact area between the PRHB and heavy metals and thus accelerated the removal. Metal adsorption by RHB typically reaches equilibrium when all available binding sites on the adsorbent surface are occupied by metal ions in solution. In the early contact period, PRHB might exhibit rapid metal adsorption compared to *P. stutzeri* due to the abundant binding sites mediated by RHB.

The maximum removal of Cd and Ni ensued when most cells had reached the stationary phase and cell density was the highest **(Figure 4.1)**. Hossan et al. (2020) reported that during the initial phase, the cells experience slow division or remain in a lag phase, resulting in fewer available binding sites, thus leading to insignificant metal uptake by the isolates. Subsequently, metal uptake and cell growth intensify, depending upon the presence of active binding sites. Similarly, Sinha and

Mukherjee (2009) reported 75 % of Cd removal from the culture medium during the stationary phase of 96 h. PRHB showed a delay in maximum removal capacity compared to *P. stutzeri* (30 h), with a maximum removal time of 36-42 h. This is primarily due to the increased complexity of the immobilized cell. It was evident that RHB used as the immobilized carrier would be favorable for bacterial growth, since it increased the adaptability of the cells to stressful environments such as Cd and Ni, thereby increasing removal efficiency.

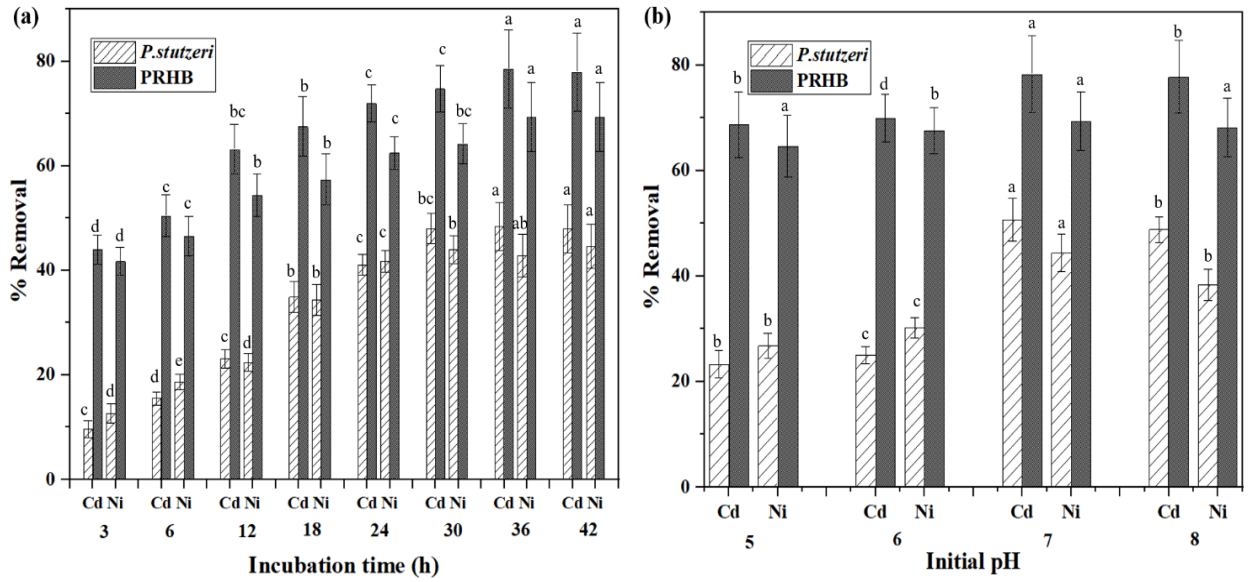

Figure 5.1. Cd and Ni removal by *P. stutzeri* and PRHB **(a)** Effect of incubation time **(b)** Effect of initial pH.

5.1.2 Effect of initial pH on Cd and Ni removal

Metal ion removal capacity depends on the initial pH of the solution (Qiu et al. 2021). It is crucial to comprehend the effect of pH on the removal of Cd and Ni because changes in solution pH affect microbial physiology, the charge on the surface of PRHB, and the speciation of heavy metals (Esfandiar et al. 2022). Cd and Ni removal increased with pH and was found to be maximum at a neutral pH of 7.0 for immobilized cells and *P. stutzeri* (**Figure 5.1b**). The cd removal capacity of *P. stutzeri* increased from 5.0 to 7.0 and displayed the highest removal efficiency of 50.68 % at pH 7.0 after 36 h of incubation. The percentage removal of Cd increased from 68.72 % to 78.28 % when the pH was increased to 7.0 using PRHB. The capacity of immobilized cells and *P. stutzeri* to remove Ni also varied with pH similar to Cd removal. PRHB had a Ni removal efficiency of 69.36 % at pH 7.0. However, the removal of Ni was more pronounced in the *P. stutzeri,* increasing from 26.76 -

44.38 % with an increase in pH compared to PRHB. pH serves as a critical factor influencing the activity of microorganisms involved in metal ion remediation. Microbial activity is particularly sensitive to changes in pH, with optimal growth typically occurring within a range of pH 6.0 to 8.0. Neutral pH conditions (pH = 7) are commonly optimal for microbial degradation or removal of pollutants, facilitating the efficient functioning of microorganisms such as *P. stutzeri* and PRHB in removing Cd and Ni ions.

PRHB and RHB exhibit zero-point charges of 6.6 and 6.2, respectively (Figure A4, Appendix I). Below this pH, the surface of the material becomes positively charged, indicating an increase in the number of positively charged surface sites. This condition may not favor the adsorption of Cd and Ni ions, which are also positively charged, due to repulsive electrostatic forces. Conversely, higher uptake values observed at higher pH levels can be attributed to electrostatic attractions between the positively charged Cd ions and the negatively charged RHB and PRHB. However, the presence of both RHB and *P. stutzeri* in PRHB complicates the clear connection between surface charge and removal efficiency. The observed higher removal efficiency at lower pH with PRHB compared to free cells suggests that RHB acting as a carrier, mitigating the harmful effects caused by changes in pH that affect microbial physiology. This is further supported by the lower removal efficiency at lower pH observed with free cells.

5.1.3 Effect of temperature

Metal ion removal is an energy-dependent mechanism involving its binding onto microbial cell walls, so temperature plays an important role (Congeevaram et al. 2007; Das et al. 2007). It alters the functional groups on the cell wall surface and parallelly affects heavy metal binding sites. The Cd and Ni removal efficiency of PRHB and *P. stutzeri* was investigated at 25, 30, 35, 37 and 40 °C. The removal of Cd by PRHB was 52.28 % at 25 °C and increased with temperature (**Figure 5.2a**). Maximum removal efficiency of 78.6 % was obtained at 37 °C, with a further increase in temperature to 40 °C, Cd removal decreased using PRHB. This aligns with Coelho da Costa Waite et al. (2020) who also reported a maximum temperature of 37 °C for *P. stutzeri* growth in a study on Cu and Pb removal. Bacterial strains normally remove maximum metal at 37 °C like *Acromobacter* sp. and *P. stutzeri* could uptake 82% copper effectively (Ölmezoğlu et al. 2012). On contrary to this, higher temperatures generally lead to increase in metabolic activity along with an increase in energy of the

system that would result in active uptake of metals. For instance, the rate of Cr (VI) removal by *S.cerevisiae* was very high at 45 °C (Goyal et al. 2003).

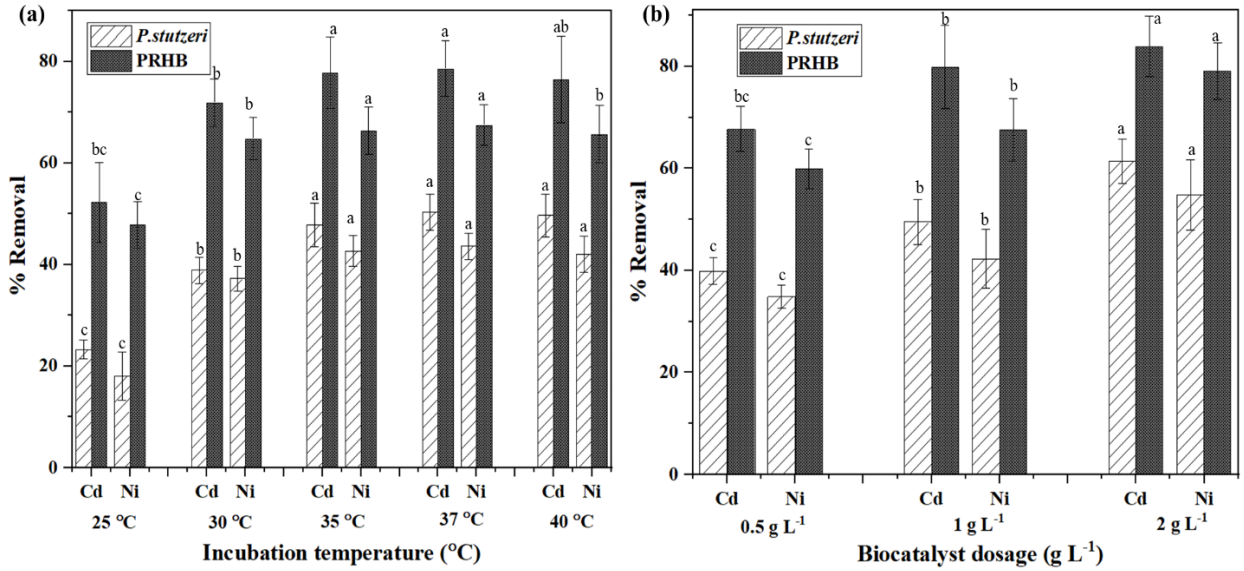

Figure 5.2. Cd and Ni removal by *P. stutzeri* and PRHB **(a)** Effect of incubation temperature **(b)** Effect of biocatalyst dosage.

The percentage of Ni removal increased from 18 to 43.6 % with an increase in temperature from 25 to 37 °C by employing free cells. PRHB showed a 47.82 % Ni removal capacity at 25 °C, which increased to 67.52 % at 37 °C. An increase in temperature significantly affected the metal removal efficiency of the free cell, whereas no significant change in removal capacity was observed at 30 - 40 °C in PRHB. When the temperature rises, the pores enlarge; thereby, more surfaces will be available for sorption, diffusion, and penetration of metal ions, favoring adsorption, and hence there is an increase in the removal of Cd and Ni (Saleem et al. 2007). A slight decrease in metal ion removal capacity was observed with the rise in temperature from 37 to 40 °C for free cells and PRHB.

At higher temperatures, the thermal energy can disrupt the hydrogen bonds and other weak interactions holding the cell wall components together. This disruption can lead to changes in the conformation of molecules within the cell wall, potentially altering the accessibility of functional groups such as hydroxyl (-OH), carboxyl (-COOH), and amino ($-NH_2$) groups. These functional groups are essential for metal ion binding through complexation mechanisms. Moreover, temperature influences the kinetics of reactions involved in metal ion adsorption onto cell walls.

Higher temperatures typically accelerate these reactions by increasing the rate of molecular motion and collision frequency, thereby enhancing the removal efficiency of metal ions from aqueous solutions. Saleh et al. (2016) indicated that the elevated adsorption of copper ions capacity of sunflower seed husk biochar at higher temperatures may be due to the enlargement of the pore size and/or activation of the adsorbent surfaces and an increase in the mobility of metal ions.

5.1.4 Effect of biocatalyst dosage

The effect of *P. stutzeri* and PRHB dosage was evaluated with experiments conducted at initial metal concentrations of 50 mg L^{-1}, pH 7.0, temperature 37 °C, and contact time 36 h. The removal efficiency of Cd and Ni increases with an increase in biocatalyst dosage (**Figure 5.2b**). As *P. stutzeri* dosage increases from 0.5 g L^{-1} to 2 g L^{-1}, the percentage removal increased from 39.8 % to 61.4 % for Cd and 34.8 to 55 % for Ni. 84 % Cd and 79 % Ni removal were achieved using a PRHB dosage of 2 g $L^{-1.}$ These data also show that *P. stutzeri* and PRHB had a higher affinity towards Cd than Ni. An increase in biocatalyst dosage leads to enhanced removal efficiency due to the availability of more biochar adsorption sites and an increase in the functional group for metal removal.

5.1.5 Effect of initial Cd and Ni concentration

The influence of initial Cd and Ni concentration on removal efficiency by *P. stutzeri* and PRHB was investigated. PRHB showed the highest removal efficiency of 95.4 % Cd and 92 % Ni at the initial Cd concentration of 10 mg L^{-1}. Further decreased the removal with an increase in Cd and Ni concentration. The removal efficiency has decreased from 69.3 % to 41.43 %, with an increase in Cd concentration from 10 to 100 mg L^{-1} using *P. stutzeri* (**Figure 5.3a**). A similar trend was observed with Ni, where the removal efficiency decreased from 67 % to 40 % with increased concentration (**Figure 5.3b**). The percentage removal by free cell and immobilized cell was high at lower concentrations because all heavy metal ions in the solutions interacted with the cell's binding sites. The significantly reduced removal capacity of *P. stutzeri* at higher concentrations could be attributed to the inhibition of bacterial cell activity and proliferation (Ren et al. 2018).

PRHB showed 9.7 and 8.3 Log_{10} cells after treating with 10 mg L^{-1} Cd and Ni solution, respectively, which decreased to 6.4 and 5.3 Log_{10} cells when the concentration increased to 100 mg L^{-1}. The number of cells decreased as the Cd and Ni concentrations increased, indicating that removal efficiency depended on cell viability and activity. The rapid adsorption of contaminant mixtures by

PRHB reduced the pollutant levels in the initial stage, which reduced cell damage. Additionally, the biochar carrier ensured bacterial growth and prolonged cell survival under pollutant stress (Ouyang et al. 2014). It was evident that using RHB as an immobilized carrier would benefit bacterial growth because it increased the cells adaptability to stressful environments like Cd and Ni, thereby increasing removal efficiency.

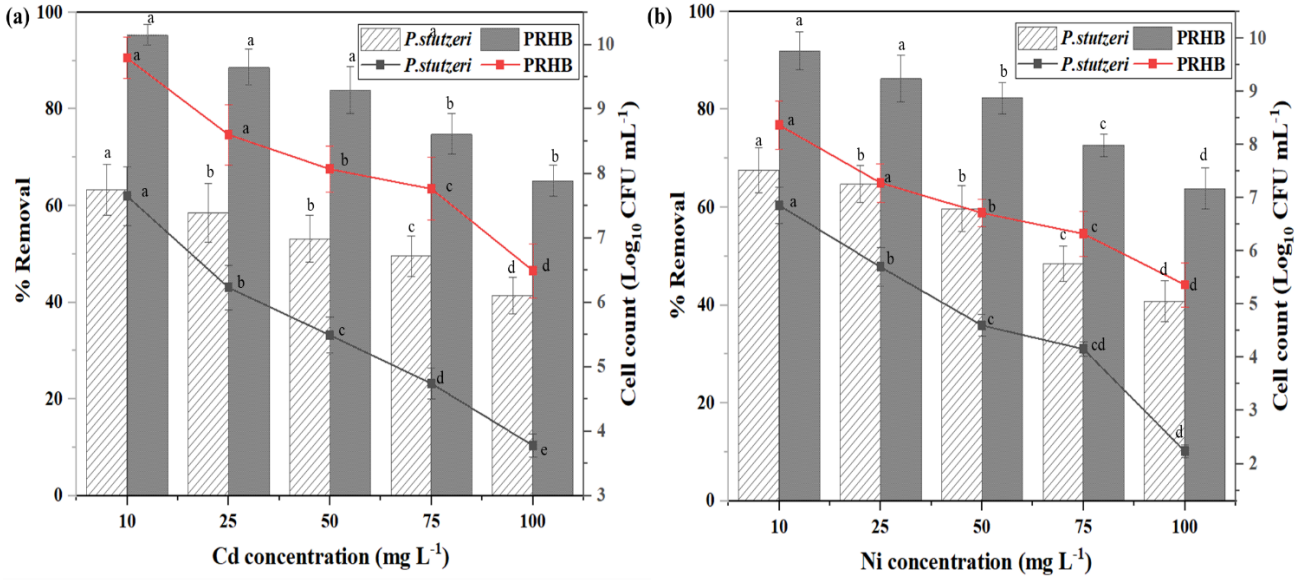

Figure 5.3. Effect of initial Cd and Ni concentration on removal efficiency by *P. stutzeri* and PRHB **(a)** Cd **(b)** Ni.

5.2 Cd AND Ni REMOVAL BY RHB, *P. stutzeri*, AND PRHB AT OPTIMIZED OPERATING CONDITIONS

Experiments were conducted to assess the removal of Cd and Ni by RHB, *P. stutzeri*, and PRHB under optimized conditions of incubation temperature of 37 °C, initial solution pH of 7.0, PRHB dosage of 2 g L^{-1}, 36 h of incubation time, and 10 mg L^{-1} initial Cd and Ni concentration (**Figure 5.4**). The results demonstrated that RHB achieved 48.67 % Cd removal and 45.35 % Ni removal. *P. stutzeri* exhibited the capability to eliminate 63.3 % of Cd and 67.6 % of Ni from the solution. This metal ion-resistant bacterium demonstrated resistance to Hg and Cr in our preliminary microbial tolerance study, suggesting its potential for removing these heavy metals. Furthermore, studies by Coelho da Costa Waite et al. (2021) employed *P. stutzeri* strain W228 to target Cu and Pb removal, while Sathish Kumar et al. (2017) utilized *P. stutzeri* L1, and Kumari et al**.** (2020) employed *P. stutzeri* Cr8 for chromium removal. The immobilization of cells on PRHB resulted in a substantial

improvement in the removal of both Cd and Ni. This enhancement is attributed to the higher number of cells attached to the biochar due to immobilization. The increased cell immobilization, coupled with the enhanced biochar adsorption capacity, likely accounts for the superior Cd and Ni removal observed with PRHB.

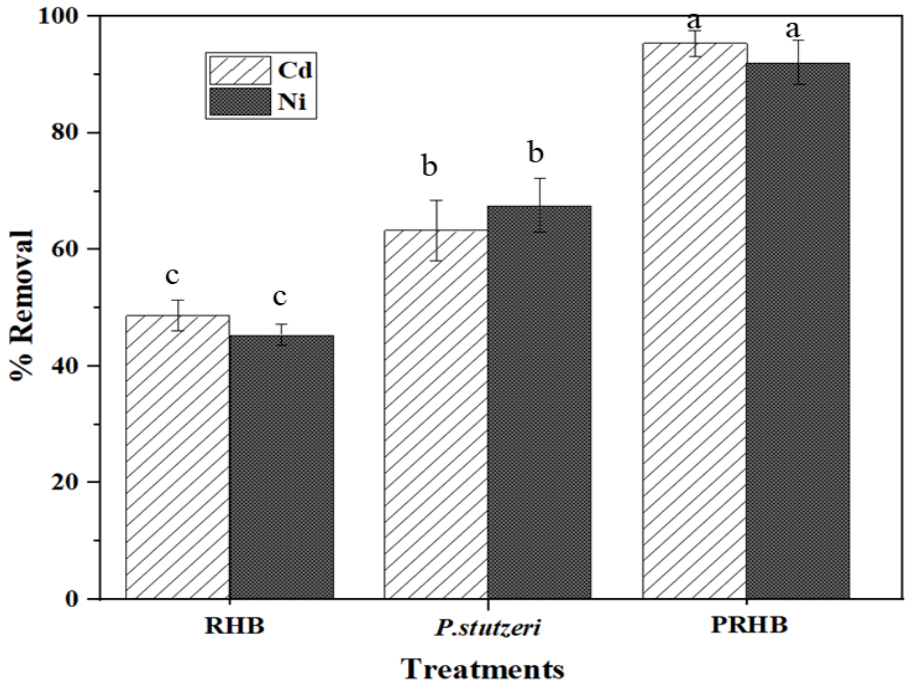

Figure 5.4. Comparative plot of Cd and Ni removal efficiency by RHB, *P. stutzeri*, and PRHB.

5.3 ADSORPTION STUDY

5.3.1 Adsorption kinetics

The adsorption kinetics of RHB and PRHB were investigated using an initial Cd and Ni concentration of 50 mg/L. To elucidate the adsorption mechanism and potential rate-limiting steps, the experimental data were fitted to pseudo-first-order (PFO) and pseudo-second-order (PSO) models, commonly employed in such studies. The majority of Cd and Ni ion sorption is followed by a slower rate attributed to metal ion penetration into pores and interaction with internal active sites until equilibrium is achieved, typically within 36 hours. Compared with the PFO model, the PSO model fits the Cd and Ni adsorption kinetics data well for PRHB, with an R^2 value of 0.99 **(Figure 5.5).** The PSO model confirms chemisorption as the rate-limiting step by providing a more thorough and accurate reflection of the adsorption mechanism of Cd and Ni onto the PRHB.

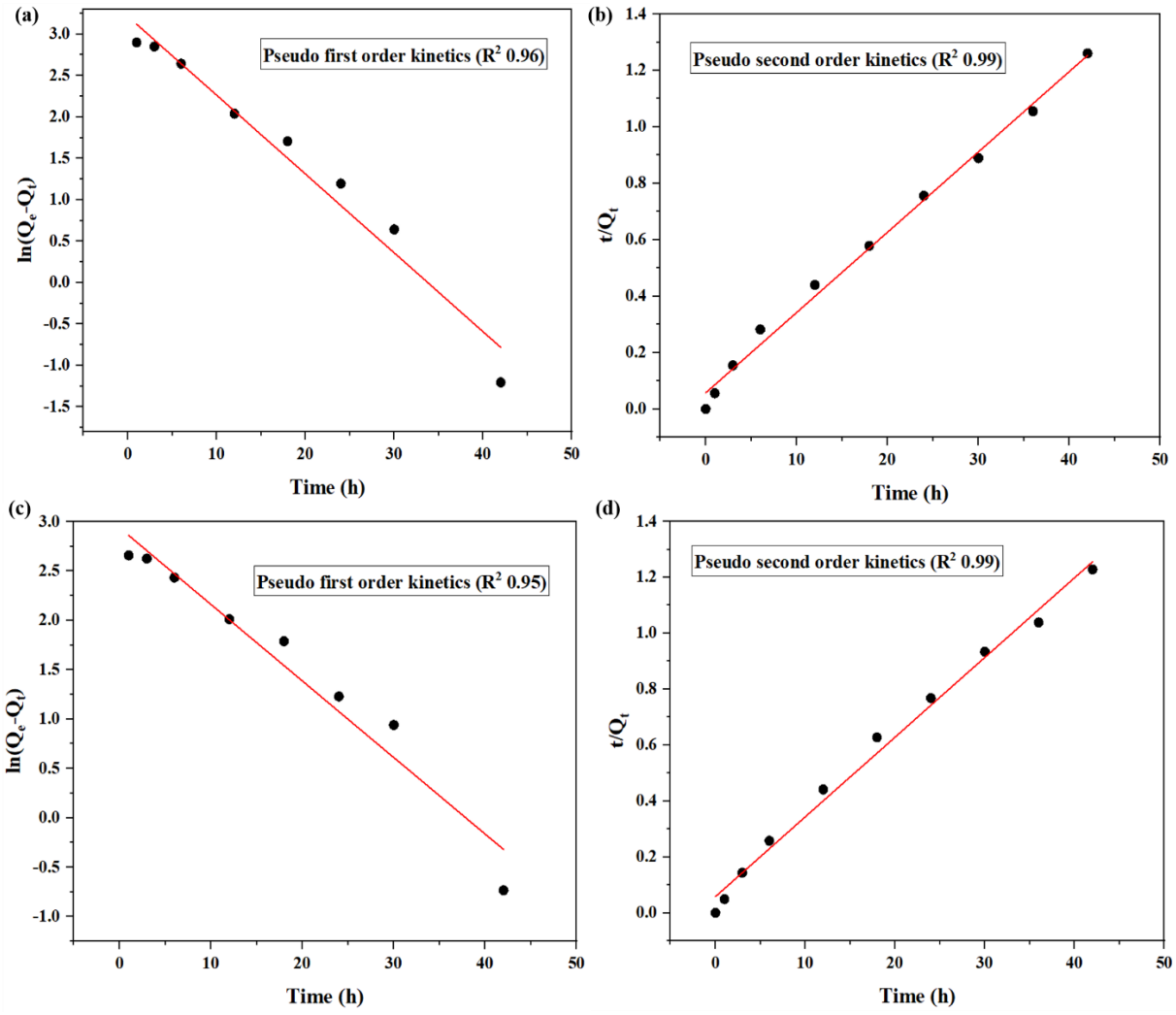

Figure 5.5. Kinetic models for Cd and Ni adsorption by PRHB (a) pseudo-first-order and (b) pseudo-second-order model of Cd adsorption (c) pseudo-first-order and (d) pseudo-second-order model of Ni adsorption.

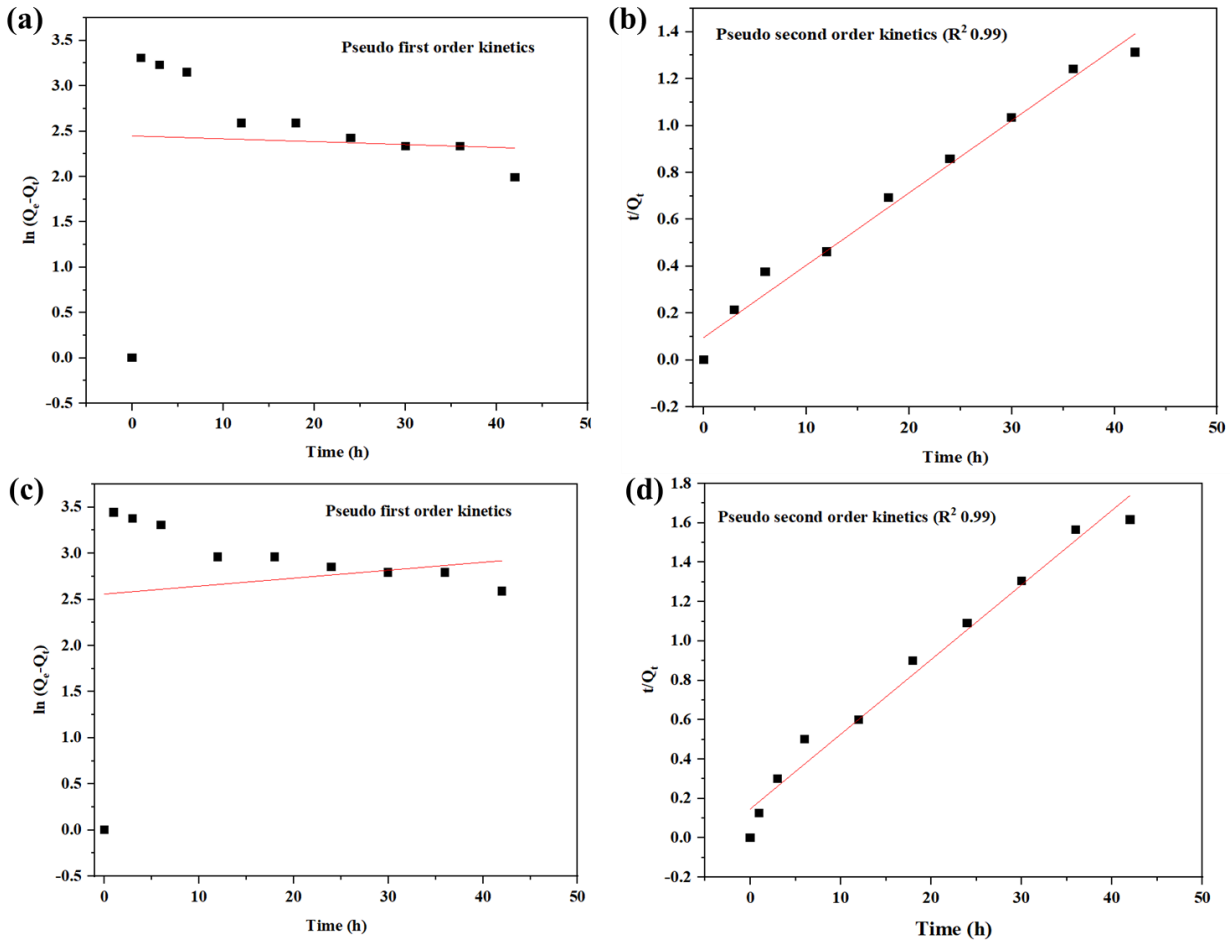

Figure 5.6. Kinetic models for Cd and Ni adsorption by RHB (a) pseudo-first-order and (b) pseudo-second-order model of Cd adsorption (c) pseudo-first-order and (d) pseudo-second-order model of Ni adsorption

5.3.2 Adsorption isotherm

The Langmuir and Freundlich isotherm models are commonly used and were fitted to the adsorption data. The Langmuir isotherm model assumes that every molecule has a constant adsorption activation energy and enthalpy and represents homogeneous adsorption. The Freundlich isotherm model is empirical and considers the surface to be heterogeneous. As depicted in **Figure 5.7**, the correlation coefficients indicated that the Langmuir model provided a better fit to the experimental data compared to the Freundlich model for the Cd and Ni adsorption isotherms of RHB and PRHB with various initial metal ion concentrations (ranging from 10 to 50 mg L^{-1}) at pH 7. According to the Langmuir parameters, PRHB exhibited the highest Cd adsorption ability (Table 2).

This might be attributed to its large number of active sites, extensive surface area, strong affinity towards Cd, and the presence of *P. stutzeri* cells. The Langmuir parameter Qm, with a value of 55.71 mg g^{-1}, indicates the monolayer adsorption capacity.

Table 5.1. Adsorption kinetics and isotherm parameter values for adsorption of Cd and Ni by PRHB.

Models	Model Parameter	PRHB Cd	PRHB Ni
Pseudo-second order kinetics	Q_e (mg g^{-1})	35.71	35.06
	K_2 (g mg^{-1} h^{-1})	0.013	0.014
	R^2	0.99	0.99
Langmuir isotherm	Q_m (mg g^{-1})	55.71	50
	K_L (L mg^{-1})	0.25	0.16
	R^2	0.99	0.99

Langmuir and Freundlich models represented monolayer and multi-layer adsorption on the surface of biomaterials, respectively. From Langmuir's fitting parameters, the maximum adsorption capacities (Q_m) values for Cd and Ni on PRHB were 55.71 mg g^{-1} and 50 mg g^{-1}, respectively. On Cd and Ni adsorption, the correlation coefficient (R^2) fitted by the Langmuir model was greater than that of the Freundlich model. These results indicated that Cd and Ni adsorption was monolayer chemisorption and may occur on the surface of PRHB.

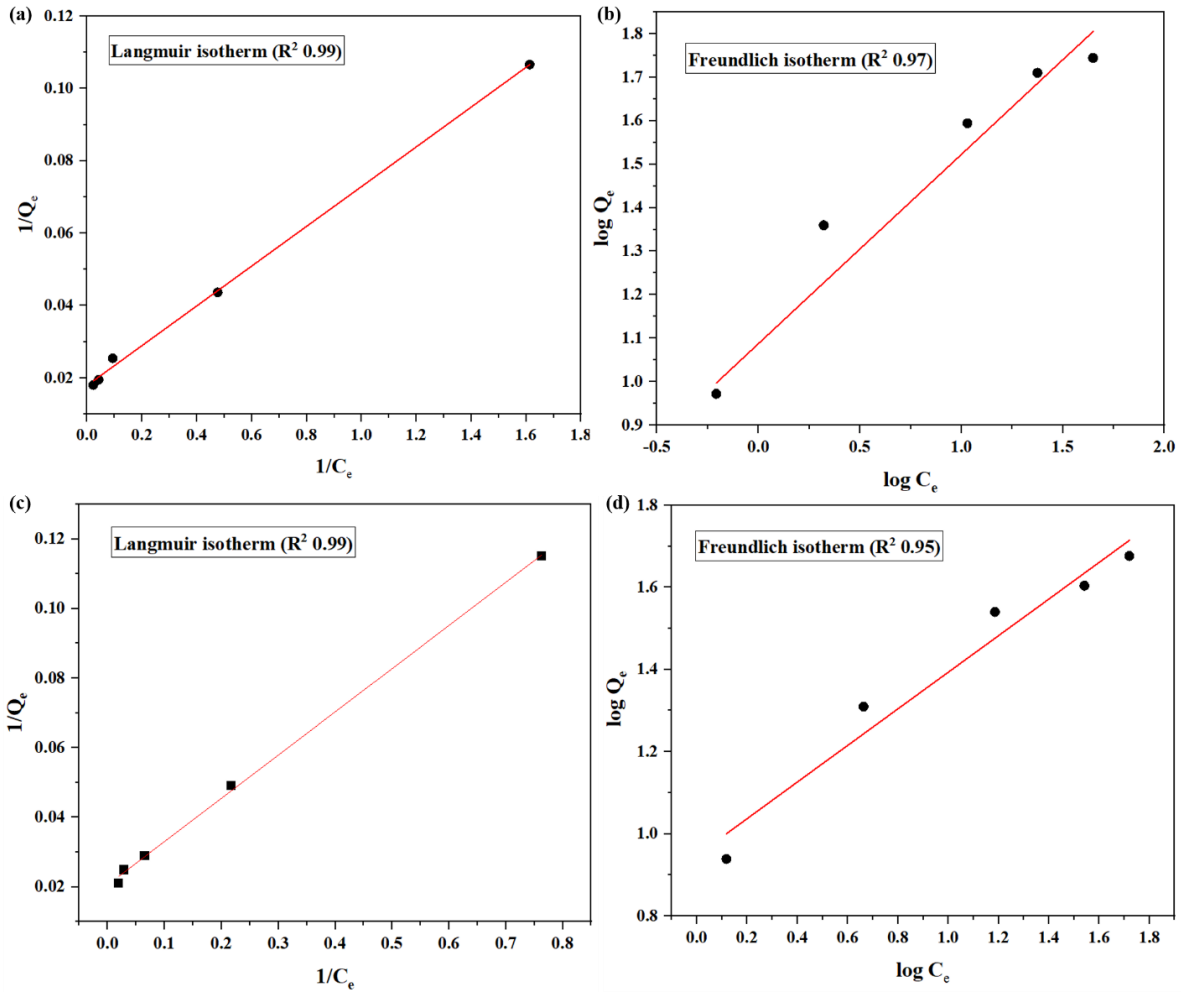

Figure 5.7. Isotherm models for Cd and Ni adsorption by PRHB; (a) Langmuir and (b) Freundlich isotherm models for Cd adsorption (c) Langmuir and (d) Freundlich isotherm models for Ni adsorption.

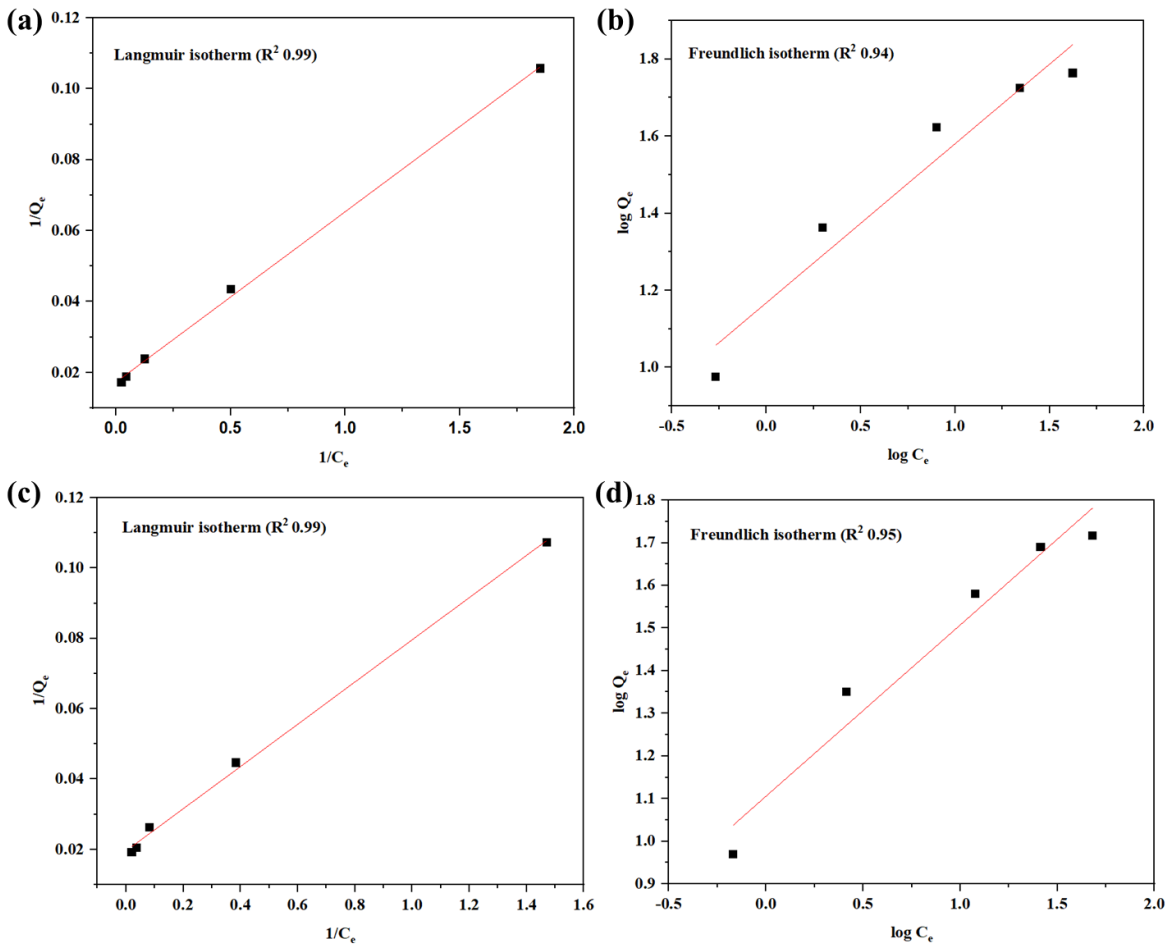

Figure 5.8. Isotherm models for Cd and Ni adsorption by RHB; (a) Langmuir and (b) Freundlich isotherm models for Cd adsorption (c) Langmuir and (d) Freundlich isotherm models for Ni adsorption.

5.4 REUSABILITY STUDIES

Five consecutive Cd and Ni removal experiments were carried out under optimized conditions to investigate the continuous application of *P. stutzeri* and PRHB. The result showed that the initial Cd removal efficiency of PRHB was 95 %. In contrast, the second and third cycles showed 91 % and 89 %, revealing their steady removal efficiency up to 3 cycles (**Figure 5.9a**). Whereas, free cells demonstrated a reduction in Cd removal efficiency from 69.3 % to 8.7 % within the fifth cycle.

Figure 5.9b shows the reusability study of PRHB in Ni removal. The Ni removal rates for PRHB and free cells were 92 % and 67.6 % after the first cycle and decreased to 72.1 % and 18.5 % within the fifth cycle, respectively. After the third cycle, PRHB had an 88 % removal rate, indicating that the immobilized cell was more reusable than the free cell. PRHB could be reused in successive removal experiments and had a high steady efficiency of Cd and Ni removal. 80 % of Cd and 72 % of the Ni removal capacity was obtained for the 5th cycle, which demonstrated *P. stutzeri* immobilized on rice husk biochar could sustain their heavy metal removal ability under several cycles of reuse. Microbial cell counts also varied with each cycle; a decrease in cell number was more pronounced with free cells. Cell number decreased from 7.6 to 3.2 Log_{10} cells after five cycles with 10 mg L^{-1} Cd and 6.8 to 3 Log_{10} cells with Ni. PRHB showed 9.7 cells in the first cycle, which decreased to 6.7 Log_{10} cells after five consecutive experiments. The substantial decline in removal efficiencies with *P. stutzeri* over each cycle may be caused by the inhibition of bacterial growth and enzyme activity attributed to direct contact with Cd and Ni. On the contrary, when PRHB was reused, some of the Cd and Ni were adsorbed by the carrier, reducing their toxic effects on the *P. stutzeri* and promoting better bacterial activity.

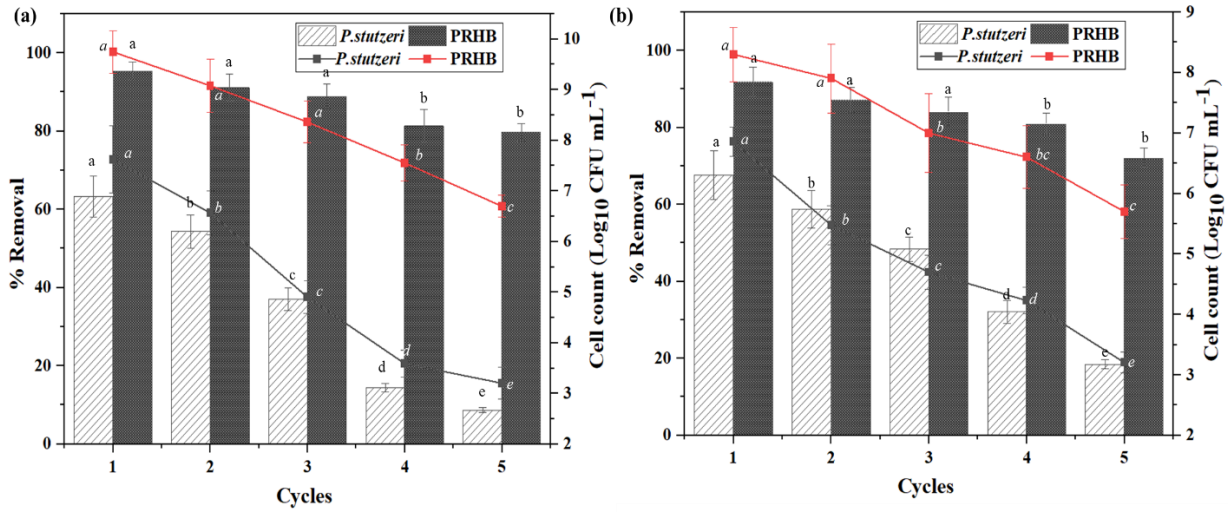

Figure 5.9. Reusability study of *P. stutzeri* and PRHB for **(a)** Cd and **(b)** Ni removal.

5.5 MECHANISM OF Cd AND Ni REMOVAL BY PRHB

The mechanism underlying the removal of Cd and Ni by PRHB is multifaceted. In comparison to RHB and *P. stutzeri*, the Cd removal rate by PRHB escalated by 48.56 % and 33.64 %, respectively. Similarly, PRHB-mediated Ni treatment exhibited a substantial increase of 50.77 %

and 26 % compared to RHB and *P. stutzeri*. PRHB, achieved a maximum removal rate of 95.4 % for Cd and 92 % for Ni, underscoring the synergistic efficacy of metal ion removal.

The mechanism involved in Cd and Ni removal by PRHB is analyzed through various characterization techniques. The differences in functional groups of PRHB were analyzed using FTIR spectroscopy to understand the role of PRHB-mediated Cd and Ni removal. As shown in **Figure 5.10**, several significant changes were observed in the PRHB samples after incubation with Cd and Ni, implying that various functional groups of PRHB participated in the removal process. Prominent peaks in PRHB at 3054 cm^{-1}, 1594 cm^{-1}, 1435 $cm^{-1,}$ and 1053 cm^{-1} were caused by the vibrations of O-H, C=C, and -COOH, respectively. After the removal of Cd, the stretching vibration peak of -OH shifted towards 3211 cm^{-1} due to the substitution of some of the hydrogen in -OH. The functional group at 1594 cm^{-1} and 1428 cm^{-1} indicates that C=C shifted to 1631 cm^{-1} and 1445 cm^{-1}, respectively, and -COOH shifted from 1053 cm^{-1} to 1044 cm^{-1}. The peak near 2325 cm^{-1} can be accredited to the C–N vibration that disappeared after Cd treatment, indicating the involvement of the amine group in Cd removal emphasizing the synergistic interaction between the microorganism and biochar. The extra peak observed at 1399 cm^{-1} indicated the presence of carbonate may be due to the precipitation of Cd (Liu et al. 2020). Peak Si-O-Si at 557 cm^{-1} changed to 549 after Cd treatment, suggesting $CdSiO_3$ precipitation due to SiO_2 (Zhang et al. 2022). Similarly, PRHB after Ni removal also showed C=C and -COOH peak shifts, such as a peak at 1428 cm^{-1} shifted to 1445 cm^{-1}, 1053-1061 cm^{-1}, and the emergence of a new peak at 1399 cm^{-1}, attributed to carbonate formation. This new peak at 1399 cm^{-1} is indicative of the involvement of carbonate ions in a reaction with Ni ions, resulting in the precipitation of nickel carbonate. This observation aligns with Wu et al. (2021) (Wu et al. 2021) and Zhang et al. (2019) (Zhang et al. 2019) wherein the formation of insoluble metal carbonate compounds signifies the removal of the metal from the solution. In conclusion, PRHB treatment with Cd and Ni altered surface chemistry by modifying surface functional groups. Notably, significant changes in FTIR spectra of -OH, C=O, -CN, and C=C highlight the role of complexation in effectively removing Cd and Ni, giving insights into the detailed changes in surface properties.

FE-SEM-EDS and elemental mapping were used to characterize the morphology and element distribution in PRHB after treatment with Cd and Ni, as shown in **Figure 5.11.** It is assumed that Cd does not affect *P. stutzeri* ability to grow inside the pore structure of biochar.

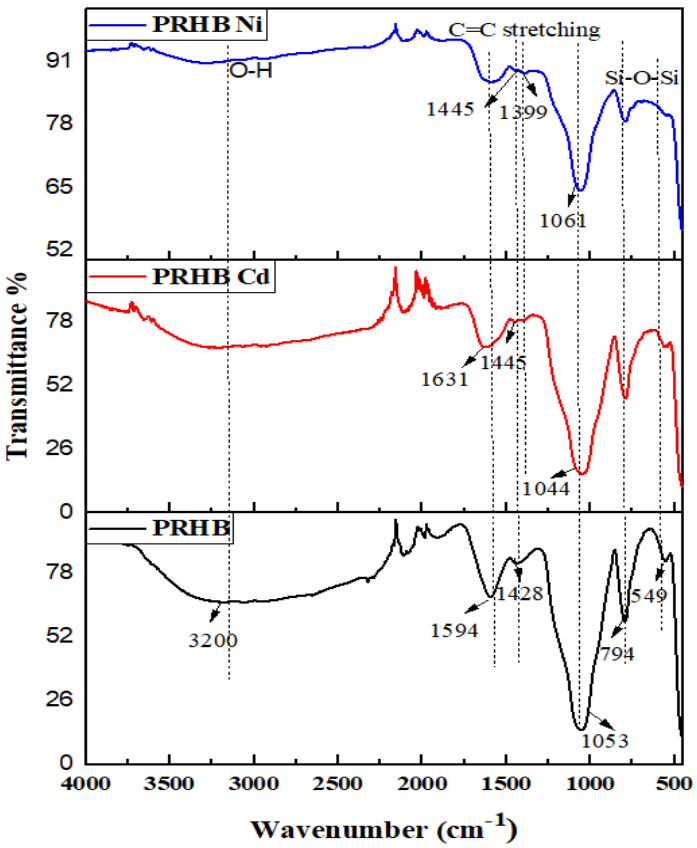

Figure 5.10. FTIR spectra of PRHB before and after Cd and Ni removal.

The presence of *P. stutzeri* inside biochar pores despite Cd exposure suggests synergistic interaction, reinforcing the biochar's role as a carrier and providing nutrients for cell growth. Observing **Figure 5.11a,** minor alterations in the appearance and shape of surface-attached cells were noted, marked by a red arrow. This observation indicates the response of *P. stutzeri* to Cd treatment, emphasizing the adaptability of microorganisms to Cd stress. Notably, these surface-attached cells exhibited a tendency to aggregate, forming clusters as a protective measure against metal toxicity. This collective behavior underscores the synergetic interaction between microorganisms and biochar, where the biochar matrix provides a conducive environment for microbial growth, and the microorganisms, in turn, contribute to the efficacy of metal removal through bioaccumulation. The element mapping revealed that *P. stutzeri* had a good tolerance to Cd, and PRHB could adsorb and retain Cd on the surfaces. Thus, the slight morphological changes of *P. stutzeri* appeared to be associated with Cd bioaccumulation, which may play an essential role in the interaction of Cd with the bacterial surface (Huang et al. 2014a). **Figure 5.11b** and **d** depict the SEM

images and EDS spectra of PRHB after Ni removal. Despite biochar structure disruption, *P. stutzeri* inside RHB had intact cell structures protected inside the pore (**Figure A1**, Appendix II).

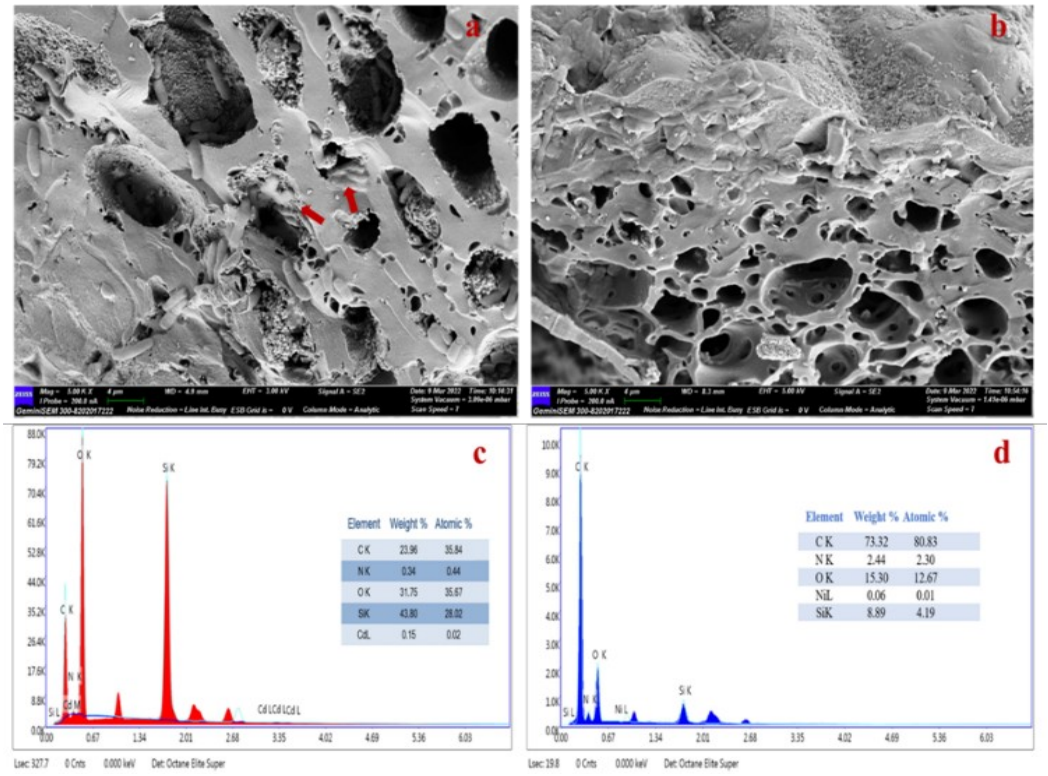

Figure 5.11. FE-SEM image and corresponding EDS spectra of PRHB **(a)** and **(c)** after Cd removal **(b)** and **(d)** after Ni removal.

Many granular materials were also observed in the inner pores of PRHB after Cd removal (**Figure A2a,** Appendix II). EDS and elemental mapping were performed to further analyze those substances on the surface and inside the biochar. Silica was found to be the most abundant element on the surface and inner pores of biochar (**Figure A2,** Appendix II). The oxygen distribution indicated silica oxide formation, which is consistent with the FTIR and XRD results. To verify the occurrence of microbial mineralization, XRD analysis was performed. The XRD patterns for RHB indicated the presence of SiO_2, CaO, $Ca(OH)_2$, $CaCO_3$, and MnO_2 (**Figure 4.7b**). This observation was further confirmed through ICP-OES analysis, which revealed the presence of various minerals, including Ca, Zn, Mn, Fe, K, etc., as outlined in **Table 4.1**. The formation of $CaCO_3$ and $Ca(OH)_2$ was attributed to the microbial mineralization process, a clear indication of the active involvement of microorganisms in metal ion precipitation. The XRD results also demonstrated the presence of

heavy metal minerals on the biochar surface (**Figure A3,** Appendix II). Three distinct mineral peaks corresponding to Cd precipitate, $CdCO_3$, $CdSiO_3$, and Cd $(OH)_2$ (JCPDS card 72-1939, 72-0969) (Lai et al. 2022; Liu et al. 2023; Nie et al. 2023; Xu et al. 2013) were evident, suggesting that the observed granular material was a result of Cd precipitation. Similarly, after Ni removal, XRD analysis showed the peaks of NiO and $Ni(OH)_2$, confirming the successful removal of Ni (Nie et al. 2023; Talebi et al. 2021; Xu et al. 2013; Zhang et al. 2019).

Microbial cell-mediated precipitation in PRHB was further studied using XPS. The photoelectron lines revealed the presence of Cd and Ni in the PRHB after treatment (**Figure 5.12a**). Two distinct peaks at 406.12 eV and 412.82 eV, corresponding to Cd 3d 5/2 and Cd 3d 3/2 were observed after the deconvolution using Gaussian fitting. As per previous reports, the binding energy of 404.87 eV was associated with CdO, while 411.66 eV was ascribed to $CdCO_3$ (**Figure 5.12b**) (Chen et al. 2019b; Hossain et al. 2020; Shi et al. 2021; Yin et al. 2018). In the Ni 2p spectra, three primary peaks at 848.21 eV, 851.06 eV, and 855.78 eV were identified as Ni $(OH)_2$, NiO, and $NiCO_3$, respectively (Prieto et al. 2012; Shi et al. 2021; Zhou et al. 2014) (**Figure 5.12c**). This strengthens the understanding of the remediation mechanism and also highlights the synergistic interaction between *P. stutzeri* and RHB. The pronounced outcomes in mineral transformations, particularly the precipitation of heavy metal compounds, highlight the cooperative influence of microbial activity and biochar characteristics in the effective removal of Cd and Ni.

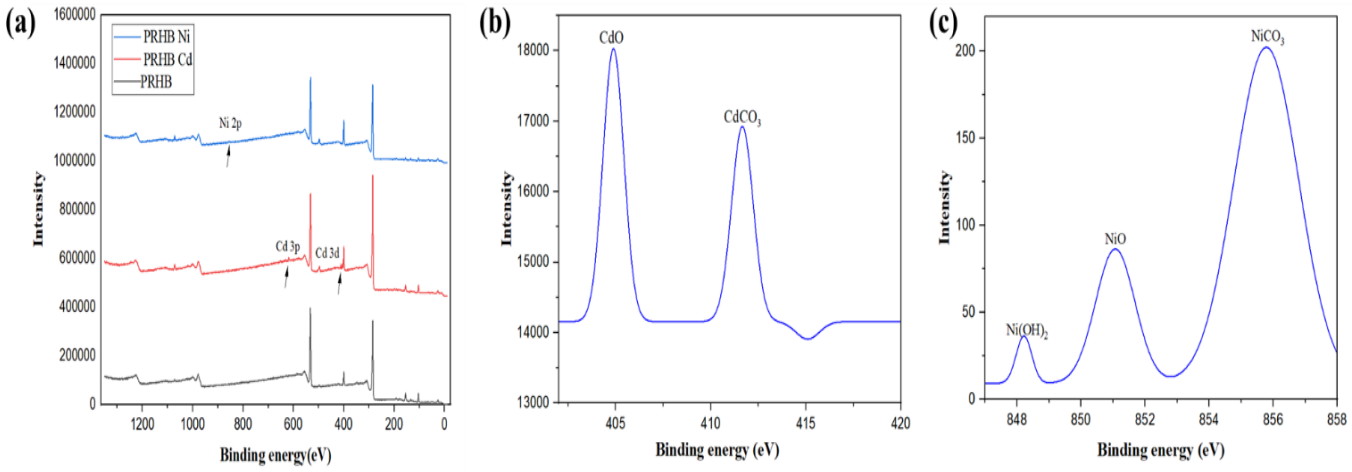

Figure 5.12. (a) XPS survey spectra of PRHB before and after Cd and Ni treatment **(b)** XPS spectra of Cd 3d and **(c)** Ni 2p.

The role of the ion exchange process in Cd and Ni removal was investigated. The amount of exchanged metal cations (K^+ and Mg^{2+}) released from PRHB in the solution was determined before and after sorption. **Table 5.2** shows the number of released cations (mequiv g^{-1}). More Mg^{2+} ions were released into the supernatant during adsorption than K^+ ions. The increased amount of released Mg^{2+} and K^+ ions after Cd and Ni adsorption indicated that these cations were released to the supernatant, which participated in the ion exchange process.

Table 5.2. Molar equivalents of Mg^{2+} and K^+ detected in the medium before and after Cd and Ni removal.

Ions	**PRHB Cd**		**PRHB Ni**	
	$mequiv._{before}$	$mequiv._{after}$	$mequiv._{before}$	$mequiv._{after}$
Mg^{2+}	0.01251	0.01382	0.01251	0.01300
K^+	0.00097	0.00115	0.00097	0.001025

To ascertain the Cd and Ni removal mechanism of PRHB at the microbial level and to confirm the protective properties of biochar, the total protein concentration of cells in metal ion -treated solution was measured. Protein count decreased in the order of PRHB Ni >PRHB Cd > *P. stutzeri* Ni > *P. stutzeri* Cd. PRHB showed a protein concentration of 16 µg mL^{-1} for the Ni-treated solution and 12 µg mL^{-1} for Cd-treated solution. *P. stutzeri* showed less protein concentration of 3.8 µg mL^{-1} after Cd treatment and 5.2 µg mL^{-1} after Ni treatment. These findings suggest the efficacy of PRHB in mediating the response to metal ion stress, indicating a potential protective role of biochar in the context of microbial activity (Manikandan et al. 2023). In summary, the current study proposes a mechanism (**Figure 5.13)** that involves

- Initial adsorption of Cd and Ni onto a biochar surface with the oxygen-containing functional group
- Binding of Cd and Ni to the biochar via ion exchange, complexation, and precipitation.

• Transportation and sequestration of Cd and Ni into the cell cytoplasm causing intracellular accumulation and cell death

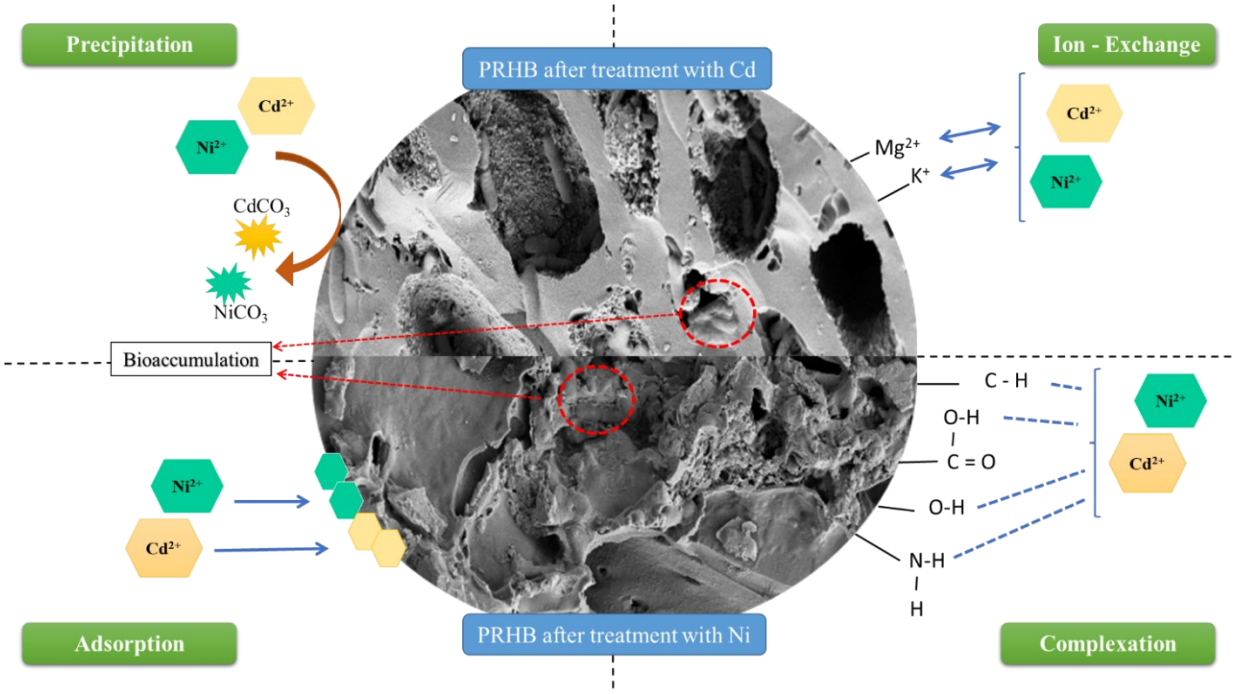

Figure 5.13. Schematic representation of Cd and Ni removal by PRHB.

CHAPTER 6

Cd AND Ni REMOVAL USING *P.stutzeri* IMMOBILIZED RICE HUSK BIOCHAR FROM SOIL

6.1 SOIL CHARACTERIZATION

The preliminary study demonstrated the efficacy of PRHB in removing heavy metals from water. Further studies were employed to assess the effectiveness of PRHB in soil remediation. The physicochemical properties of the soil utilized in the study are presented in **Table 6.1.** Textural analysis showed that the soil was laterite loam with a pH of 6.30 and contained a high concentration of Mn, Fe, and an optimal concentration of other soil micronutrients. Such laterite soil characteristics have previously been reported and Mn and Fe toxicity is common in the laterite soils of Kerala (Geetha and Sureshkumar 2018).

Table 6.1. Physicochemical properties of soil.

Soil parameter	**Value**
pH	6.30
Soil organic carbon (%)	0.70
Available P (kg ha^{-1})	35
Available K (kg ha^{-1})	400
Zinc (mg kg^{-1})	1.96
Manganese (mg kg^{-1})	51.20
Iron (mg kg^{-1})	74.50
Copper (mg kg^{-1})	4.70
Sulphur (mg kg^{-1})	3.97
Boron (mg kg^{-1})	0.40

6.2 PHYTOAVAILABILITY OF Cd IN SOIL

The DTPA-extraction is usually employed to predict the mobility and bioavailability of heavy metals (Qi et al. 2021). RHB, *P. stutzeri,* and PRHB were added to the Cd-contaminated soil and their heavy metal immobilization abilities were analyzed by determining the DTPA-extractable Cd (**Figure 6.1**). The soil was incubated and analyzed for 80 days to account for various factors influencing changes in Cd concentration such as soil type, initial cadmium concentration, soil pH buffering capacity, and microbial activity. Soil properties like, organic matter content, clay content, and cation exchange capacity influence heavy metal solubility, mobility, and bioavailability, while biochar properties like pH, organic carbon content, and surface area affect metal immobilization (Qi et al. 2023; Shen et al. 2016). Considering the complex interactions involved, an 80-day duration was chosen to ensure sufficient interaction between soil, biochar, and microbial communities, given the slow microbial processes. Continuous monitoring was crucial due to uncertainty about the exact duration needed for remediation. In previous studies, Tu et al. 2020 investigated cadmium and copper removal from soil using *Pseudomonas* sp. NT-2 immobilized maize straw biochar with a 75-day incubation period, while Chuaphasuk and Prapagdee (2019) analyzed remediation over a duration of 60 days.

DTPA-extractable Cd was 6.80 mg kg^{-1} in the soil initially. After incorporating *P. stutzeri*, RHB, and PRHB in soil, the amount of Cd decreased significantly at all tested time points (7 to 80 days). RHB amendment resulted in a decrease in Cd concentration to 3.20 mg kg^{-1}, while the PRHB amendment further lowered the Cd concentration to 2.20 mg kg^{-1}. This led to a total reduction of 68.58 % compared to the control soil. Changes in soil properties induced by these amendments play a pivotal role in altering the forms of metal ions (Hamid et al. 2020). PRHB demonstrated remarkable efficacy in Cd removal from the soil. This effectiveness can be attributed to the characteristics of RHB, such as its surface area and functional groups, which facilitate adsorption mechanisms and bioaccumulation by *P. stutzeri* cells.

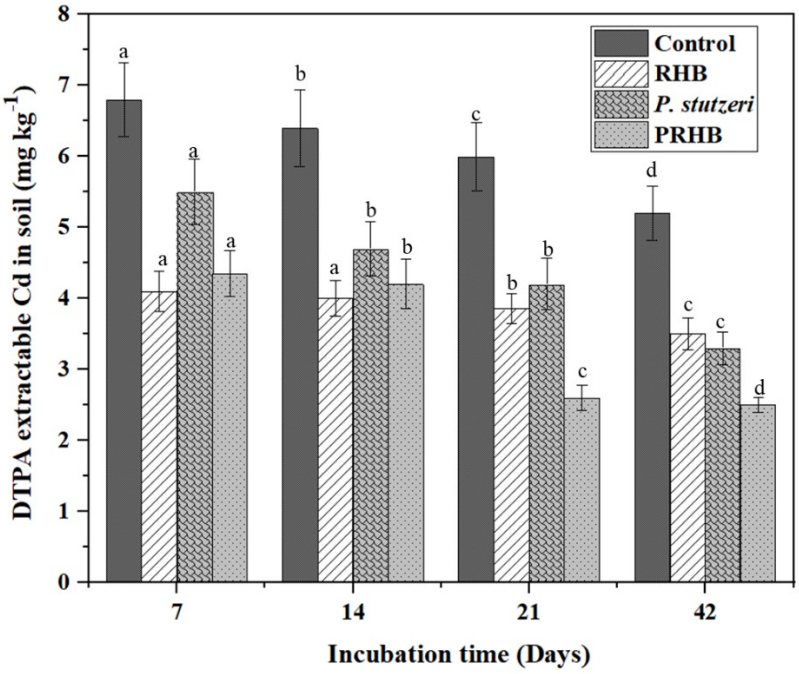

Figure 6.1. DTPA extractable Cd concentration in the soil during incubation.

6.3 FRACTIONATION OF Cd IN SOIL

The assessment of heavy metal toxicity in soil relies on both the total quantity and chemical speciation of these metals. Heavy metals exhibit distinct migration, transformation, and toxicity patterns, with the following order: acid-soluble fraction > reducible fraction > oxidizable fraction > residual fraction (Liu et al. 2018). Among these, the acid-soluble and reducible fractions are identified as particularly harmful to organisms. The oxidizable fraction carries potential toxicity, whereas the residual fraction, characterized by stability, poses lesser harm compared to other speciation. In contaminated soil on the 0^{th} day, Cd mainly existed in the acid-soluble fraction (60.8 %), followed by the reducible fraction (28 %) while the oxidizable and residual Cd accounted for less (3.6 % and 0.4 %, respectively), After 80 days of incubation, the proportion of exchangeable Cd in soil dropped to varying degrees, suggesting the exchangeable Cd fraction transformed into other fractions. Application of RHB, *P. stutzeri*, and PRHB, reduced the acid-soluble fraction of Cd by 16.30 %, 17.5 %, and 27.6 % respectively (**Figure 6.2**).

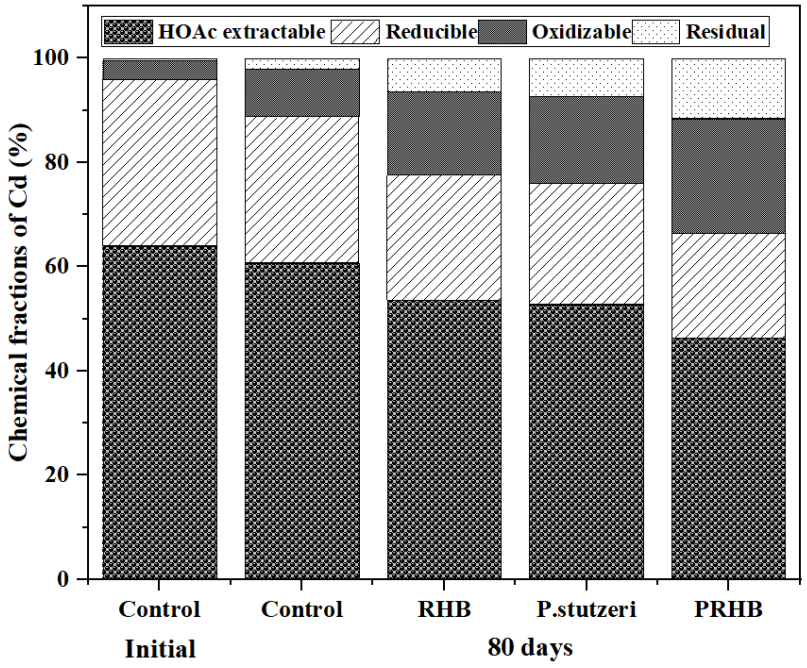

Figure 6.2. Percentage fraction distribution of Cd in soil with different treatments.

Enhancements in both residual and oxidizable forms were observed across all treatments. Changes in chemical speciation indicated a transformation of acid-soluble Cd into oxidizable and residual fractions. Consequently, the introduction of these materials led to a significant reduction in Cd toxicity in the soil, with more pronounced effects noted when PRHB absorbents were added. This trend aligns with the findings reported by Ma et al. (2020). Both acid-soluble and residual fractions serve as indicators for assessing the efficacy of in-situ immobilization (Rinklebe et al. 2016). Recent work by Nie et al. (2018) revealed a decrease in the labile fractions of Cd and Cu in soil with increased biochar addition, accompanied by an increase in their recalcitrant fractions. In our study, a parallel observation was made, wherein acid-extractable Cd concentrations in the PRHB treatment were significantly lower than those in the control treatment.

6.4 CHANGES IN SOIL pH DURING THE INCUBATION

The impact of various treatments on Cd-contaminated soil revealed distinctive pH variations over 80 days. Notably, within the initial 7 days of incubation, both RHB and PRHB effectively elevated the soil pH **(Figure 6.3**). In contrast, the control group demonstrated minimal fluctuations, maintaining an initial pH of 5.6.

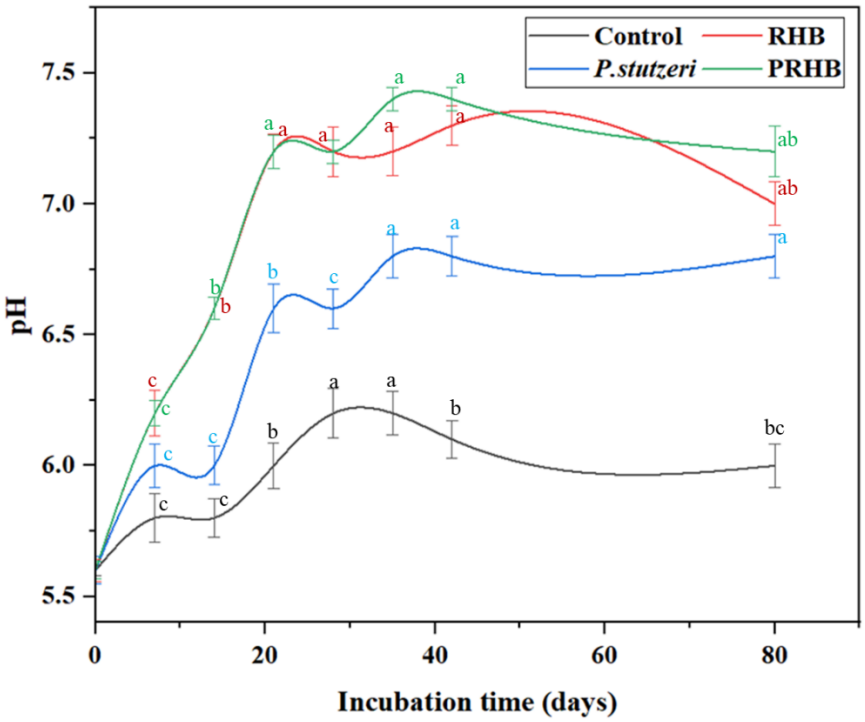

Figure 6.3. Changes in soil pH during remediation.

The rapid increase in soil pH observed with the biochar amendments can be attributed to the dissolution of alkaline substances, such as inorganic carbonate in the biochar. Significantly, the PRHB treatment exhibited a more pronounced increase in pH, similar to the effect observed with RHB alone. Specifically, PRHB demonstrated the highest pH increase, reaching 7.4, closely followed by the RHB treatment, which showed a pH of 7.3. Rice husk biochar play a significant role in correcting soil acidity due to their alkaline nature and high pH buffering capacity. During the pyrolysis process, various cations present in feedstocks, such as Ca, K, Mg, Na, and Si, undergo transformations into carbonates or oxides. These compounds then interact with H^+ ions and monomeric Al and Fe species in soils, consequently elevating soil pH and reducing exchangeable acidity(Novak et al. 2009). Yuan et al. (2011) emphasized that while carbonates and oxides contribute significantly to alkalinity, functional groups within biochar, such as COO− and O− also play a substantial role, especially when pyrolyzed at lower temperatures (500 °C). These functional groups are capable of reacting with H^+ ions present in the soil solution, further influencing pH levels (Dai et al. 2017). The treatment involving *P. stutzeri* resulted in a pH increase after the 20-day incubation period. The fluctuation in soil pH associated with the *P. stutzeri* amendment signifies survival and activity. The observed rise in soil pH following PRHB treatment can be attributed to

the alkaline properties of rice husk biochar, including both its inherent alkalinity and the alkaline substances released during its application, along with metabolites secreted by bacteria contain low molecular weight compounds, contributing to the observed rise in soil pH.

6.5 SOIL ENZYME ACTIVITIES AND ORGANIC MATTER ANALYSIS

Soil enzyme activity is sensitive to various environmental stresses and is closely associated with physicochemical properties, organic matter content, and biomass of microorganisms in the soil (Das et al. 2021). Thus, it is well-recognized as an integrative bioindicator of soil health, soil fertility, and soil quality (Gao et al. 2010). Soil phosphatase activity plays an important role in organic phosphorous mineralization potential in soils (Wang et al. 2018a). Whereas β – glucosidase enzymes are considered good soil quality indicators, and their activities are mainly associated with the carbon cycle (Ferraz De Almeida et al. 2015). In the current study, all treatments increased the soil phosphatase, β – glucosidase, and organic matter content although the extent varies (**Figure 6.4**). Soil phosphatase activity increased from 23.42 to 35.4 µg p-Nitrophenol g^{-1} of dry soil under PRHB treatment, which was higher than RHB treatment (29.6 µg p-Nitrophenol g^{-1} of dry soil). The maximum β – glucosidase activities were observed in PRHB-treated soil, which was 47.3 % higher than those of the control soil.

The soil organic matter is the organic component of the soil that serves as a reservoir of nutrients (Voltr et al. 2021). The application of biochar and PRHB significantly increased the soil organic matter in all treatments compared to the controls. RHB may elevate the carbon availability in soil and provide nutrient sources for microorganisms. They could also immobilize heavy metals and reduce the toxicity to soil microorganisms thus increasing the microbial biomass and diversity, which in turn promoted the soil enzymes activities. The porous structures of RHB provide habitats for immobilized bacteria (Nie et al. 2018), which would be helpful for the proliferation of the microbes and the improvement of soil enzyme activities.

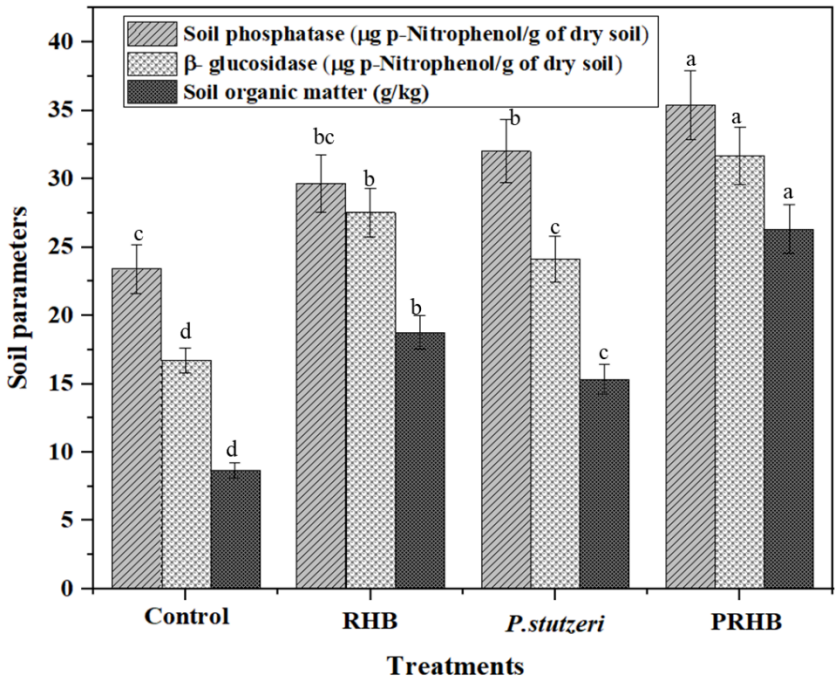

Figure 6.4. Effects of different treatments on soil enzyme and organic matter content.

6.6 INITIAL PLANT GROWTH STUDY

One of the indicators of soil heavy metal detoxification is the assessment of plant growth in remediated soil. To study the effect of various amendments such as RHB and PRHB in soil on the growth of *Spinacia oleracea* L., various parameters such as GP (%), SVI, MGT (days), MGR, GRI (days), shoot length (cm) and root length (cm), has been measured. The Initial plant growth of *Spinacia oleracea* L. is depicted in (**Figure A1**, Appendix III), showcasing the early seedling development under various treatments. This protray (seed tray) study results provide a visual representation of the comparative effects of different amendments on seed germination parameters.

GP is the number of seeds germinated divided by the total number of seeds sown. From **Figure 6.5a**, contaminated soil showed the lowest GP, i.e., 66.67 %, compared to other treatments. This can be due to the toxic effect of Cd in the contaminated soil on the germination of seeds. Bautista et al. (2013) showed that the GP of *Spinacia oleracea* L. is affected by Cd due to the toxic effects of metals in direct contact with the tissues of the developing seedlings (Bautista et al. 2013). Ahmad et al. (2012) reported that the Cd drastically affected spinach seed germination rate. 90 % GP was obtained in treatment with PRHB. Application of RHB showed a GP of 86.6 %. The treatment with PRHB showed better germination rates and SVI than individual free cell amendments (**Figure 6.5b**).

The increase in the GP was due to the removal of Cd from contaminated soil by biochar and microbial cells, the improvement of soil properties, and an increase in soil fertility.

MGT, as shown in **Figure 6.5c,** is the measure of time the seeds spend to germinate. The lower the MGT, the faster a population of seeds has germinated. MGT decreased in the order of Control > *P. stutzeri* > RHB > PRHB indicates PRHB shows a lower value of MGT, which denotes faster germination of *Spinacia oleracea* L. seeds. Similarly, the GRI indicates the percentage of seeds germinated per day of the germination period. Control soil without Cd showed the highest GRI of 4.25 days, followed by PRHB treatment.

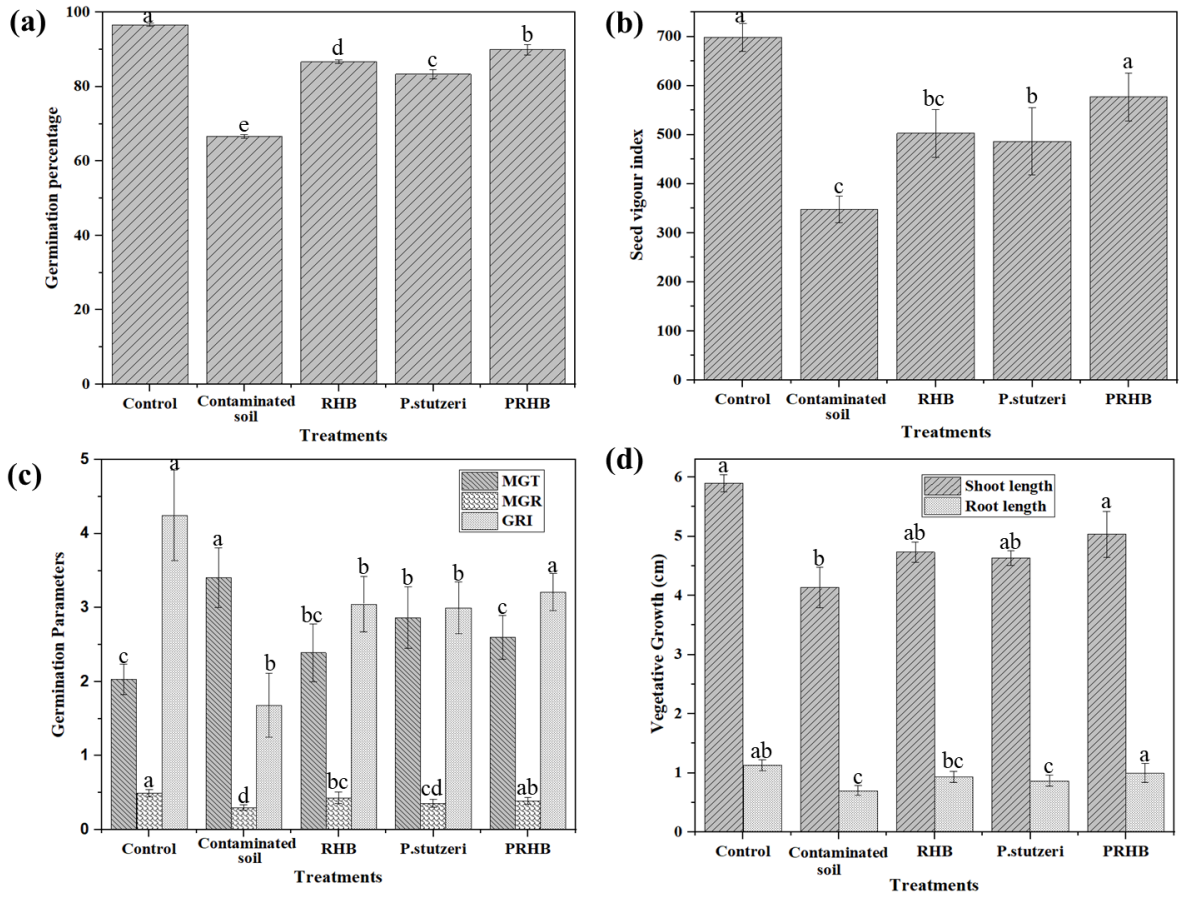

Figure 6.5. Germination and growth Parameters of *Spinacia oleracea* L. under different Treatments **(a)** GP **(b)** SVI **(c)** MGT, MGR, and GRI **(d)** vegetative growth.

Plant growth parameters such as shoot length and root length indicate the overall health of the plant and changes in the soil qualities. After 10 days of germination, the seedlings were carefully removed from the tray and cleaned with distilled water. The shoot length was measured from the

soil contact point to the tip of the plant, and the root length was measured similarly (Mwenye et al. 2019). The measured shoot length and root length of the seedings from various treatments are shown in **Figure 6.5d**. The results showed that the minimum shoot length (4.13 cm) and root length (0.67 cm) were found in contaminated soil **(Figure A1**, Appendix III). This was due to the negative impact of Cd ions on plant growth. The maximum shoot length was found in treatments that contained PRHB, followed by RHB. Similarly, maximum root length was found in treatments PRHB. These results show that biochar influences the growth of the plants and PRHB compared to free cells. It can be due to the biochar's increased pH and organic matter. Furthermore, the application of the PRHB alleviated the Cd toxicity to plants and positively impacted the metabolism of root exudates (e.g., amino compounds, sugars, organic acids). These substances act as nutrients for microbes (Wu et al. 2016) and thus indirectly enhance the soil enzyme activities.

6.7 BIOMASS AND Cd CONTENT OF *Spinacia oleracea* L PLANTS

A significant enhancement in plant growth was observed in spinach plants cultivated in Cd-contaminated soil supplemented with RHB, PRHB, and *P. stutzeri* in contrast to the control soil with spiked Cd **(Figure 6.6).** This observation suggests a positive impact of these treatments on the growth of spinach plants under Cd-induced stress. Pot study results, depicted in (**Figure A2**, Appendix III), further corroborate these findings by showcasing spinach growth under various treatments in triplicate. Enhancement in dry biomass was noted in *Spinacia oleracea* L plants cultivated in contaminated soil supplemented with RHB, *P. stutzeri*, and PRHB compared to the control. This indicates a positive impact of these treatments on plant growth under Cd stress, with PRHB treatment showing the most significant effect of a 94 % increase in dry-weight biomass. PRHB exerted a better effect than RHB, *P. stutzeri* alone, indicating that the combination of *P. stutzeri* and RHB had a synergistic effect in alleviating Cd-induced growth inhibition of spinach plants. These treatments likely improved the physicochemical properties of the contaminated soil, enhancing nutrient utilization by the plants (Ma et al. 2020). Moreover, the biochar used in the study demonstrated Cd immobilization capacity, reducing the bioavailability and toxicity of heavy metals in the soil (Wu et al. 2021).

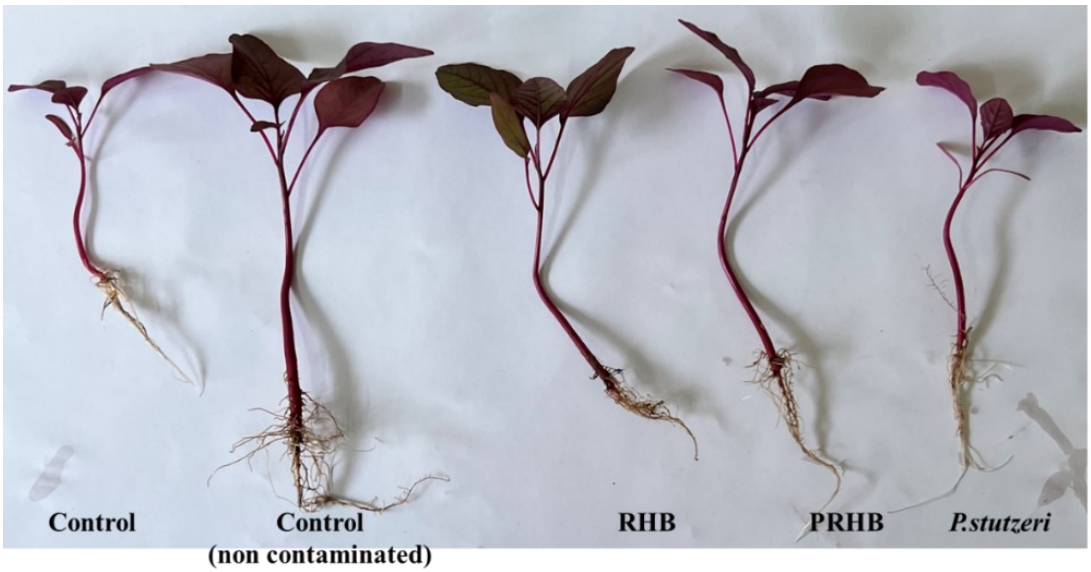

Figure 6.6. Growth of *Spinacia oleracea* L. under different treatments.

Heavy metals in soil could be readily uptake by various plants. Some heavy metal-tolerant bacteria could change the speciation and mobility of heavy metal via bioaccumulation and biosorption and relieve the heavy metal toxicity to plants. The application of RHB, *P. stutzeri,* and PRHB resulted in decreased Cd content in *Spinacia oleracea* L plant shoots, with PRHB being the most effective with 87.5 % reduction **(Figure 6.7)**, followed by *P. stutzeri*. The decrease in Cd content in *Spinacia oleracea* L. plant shoots treated with PRHB can be attributed to a combination of factors. The RHB utilized in the treatment is rich in functional groups capable of binding and adsorbing heavy metals. These functional groups may release anions that combine with Cd ions to form carbonate and precipitation, thereby reducing the availability of metals for uptake by spinach plants. Additionally, the application of PRHB enhanced soil properties conducive to Cd retention, such as increased pH or enhanced cation exchange capacity, thereby reducing Cd mobility and limiting uptake by plant roots. The presence of *P. stutzeri* immobilized within PRHB could further contribute to the decrease in Cd content in plant shoots. These bacteria may facilitate the conversion of Cd to less bioavailable forms or enhance the plant's tolerance to Cd stress through various mechanisms, including interactions with bacterial cell walls, cell secretions such as phytochelatin production or induction of antioxidant enzymes, and plant root exudates, further diminishing the accumulation of Cd in plants. Some studies also suggest that bacterial inoculation can modulate the expression of metal transporter genes in plants, reducing heavy metal accumulation (Xu et al. 2018). Additionally, the carbon source released by biochar, along with its pore structure, may provide

nutrients and habitat for heavy metal-immobilizing *P. stutzeri*, indirectly restricting Cd transfer to plants by promoting microbial activity that aids in Cd immobilization in the soil. The combined effects of RHB's metal-binding properties, microbial interactions facilitated by *P. stutzeri*, and biochemical processes in the soil contribute to the decrease in Cd content in *Spinacia oleracea* L. plant shoots.

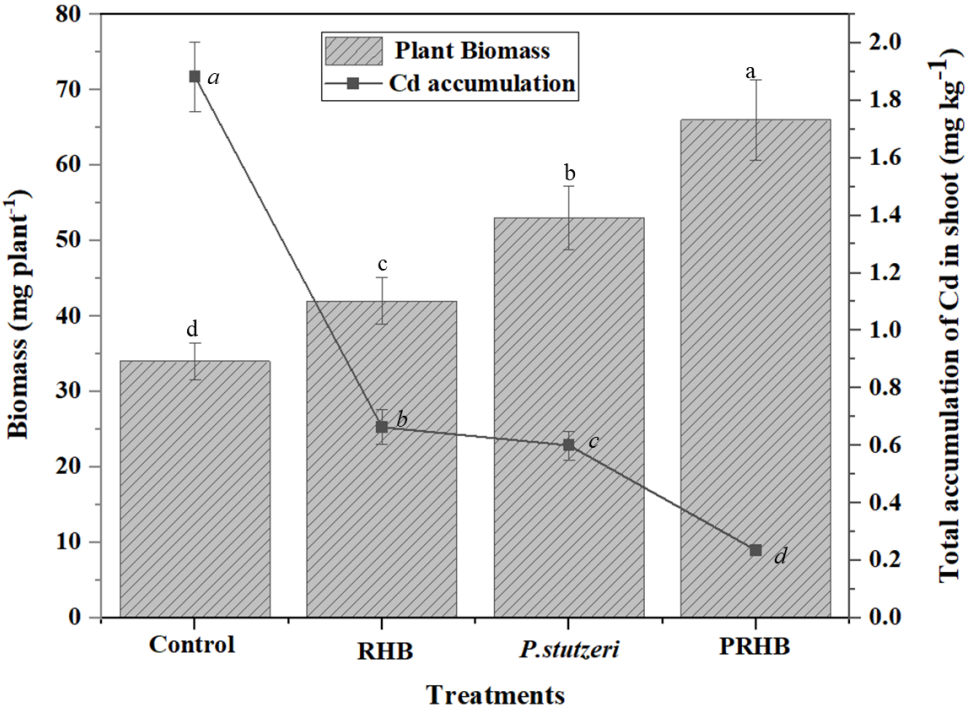

Figure 6.7. Effects of different treatments on growth of *Spinacia oleracia* L. plants and Cd accumulation.

The present study indicated the efficacy of PRHB, RHB, and *P. stutzeri* in mitigating Cd contamination in soil. However, it's crucial to analyze the restrictions or limitations of these findings in real-world situations. The experimental setup was conducted under controlled laboratory conditions, which may not fully reflect the complexities of natural soil environments, including variations in environmental factors and microbial interactions. Additionally, the study's duration was limited to 80 days, providing only a short-term perspective on the long-term effectiveness and sustainability of the applied treatments. Longer-term studies spanning multiple growing seasons would offer a more comprehensive understanding of the persistence and durability of these remediation approaches. Moreover, variations in soil characteristics such as texture, pH, and organic matter content across different geographical regions may impact the applicability and effectiveness

of the proposed remediation methods in diverse soil types. Therefore, while our findings show promise, further research under broader environmental conditions and extended durations is necessary to fully assess the practical applicability and scalability of these soil remediation strategies.

CHAPTER 7

OTHER BIOREMEDIATION STUDIES FOR THE REMOVAL OF METAL IONS USING MICROBIAL CELL-IMMOBILIZED BIOCHAR

7.1 Cd AND Ni REMOVAL USING *P. stutzeri* IMMOBILIZED SAWDUST BIOCHAR FROM WATER

7.1.1 Characterization of SDB and PSDB

Immobilization studies in section 4.3 indicated that SDB 500 ℃ 60 min immobilized the maximum number of *P. stutzeri* cells. They were utilized for Cd and Ni removal from water. The SEM result of SDB is depicted in **Figure 7.1a**. The surface morphology of biochar under 500X revealed a porous surface texture, possibly due to the evaporation of volatile matter from sawdust biomass during pyrolysis. Generally, the pore volume of the biochar is closely related to its bacterial and heavy metal adsorption potential. It was observed that the distribution of honeycomb-like pores on the surface of the SDB could facilitate the immobilization of *P. stutzeri* and metal ions. These pores provide a large surface area, which enhances the contact between the biochar material and the surrounding environment, including the bacteria and metal ions. This increased surface area allows for more sites for bacterial attachment and colonization, enabling the biochar to act as a suitable habitat for microorganisms like *P. stutzeri.* Moreover, the porous structure of the biochar also promotes the adsorption of metal ions onto its surface. The intricate network of pores creates binding sites where metal ions can adhere through various mechanisms such as chemical complexation and physical adsorption. During the metabolic process of *P. stutzeri*, the SDB pore structure can act as a transport channel for oxygen, micronutrients, and pollutants, making it an excellent carrier for microbial cell immobilization (Huang et al. 2020a). Rashad et al. (2022) utilized pinewood sawdust biochar as an effective biosorbent for PAH removal

FESEM analysis of PSDB after lyophilization showed the presence of rod-shaped *P. stutzeri*, as depicted in **Figure 7.1b**. The presence of bacterial cells on the surface and in the pores of biochar is due to its large specific surface area and a high number of micropores, which have a high immobilization capacity for microorganisms (Zhang and Wang 2021b).

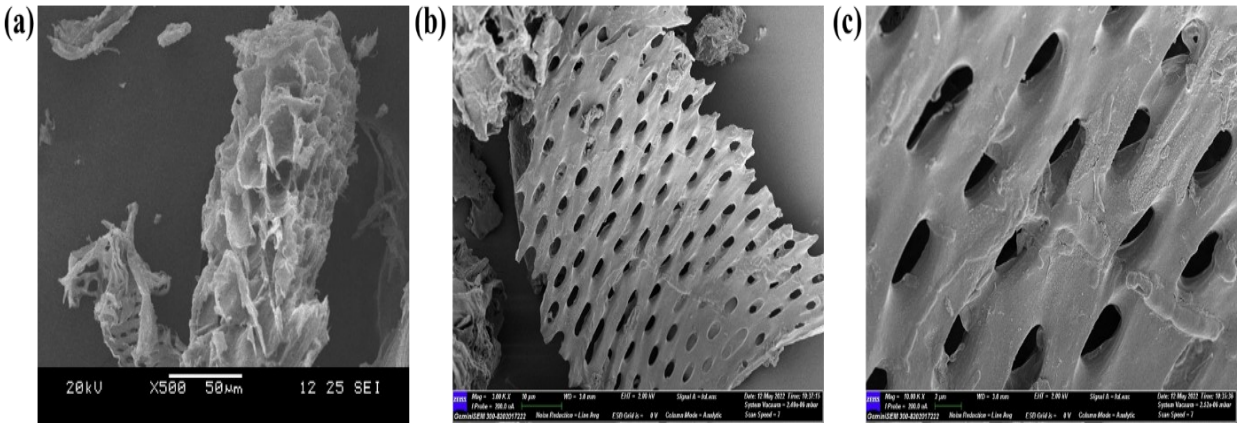

Figure 7.1. (a) SEM image of SDB, (a) PSDB at 3 KX, and (c) PSDB at a 10 KX magnification.

The elemental composition of SDB showed carbon (64.01 %) and oxygen (34.21 %). This suggests the abundance of oxygen-containing surface functional groups in SDB, the primary metal adsorption sites (Chi et al. 2017). The specific surface area of 195.68 m^2g^{-1} and total pore volume of 0.99 cm^3g^{-1} and average pore diameter obtained is 0.9 nm, indicate significant porosity within the biochar matrix. A larger specific surface area correlates with a stronger adsorption capacity of biochar towards heavy metals. This is because a higher specific surface area provides more adsorption sites for metal ions to attach to the biochar surface. Additionally, the porosity of biochar enhances its adsorption capacity by providing additional space for metal ions to interact with the biochar matrix. the pore size of biochar is a critical factor in the adsorption process. Biochar with smaller pore sizes may be limited in its ability to capture larger adsorbates, regardless of their charge or polarity. Present study indicated that the number of micropores formed by pyrolysis and the pore structure developed fairly. SEM analysis of SDB revealed abundant pore distribution. This structural property provides a suitable habitat for microbial colonization and proliferation, with numerous micropores offering a high adsorption capacity for bacteria. This provides space for the growth and reproduction of microorganisms and is more favorable for increasing cell density. Biochar can obtain more effective adsorption sites during removal due to its loose and porous structure, large total pore

volume, and surface areas (Song et al. 2014). BET surface area, total pore volume, and average pore size of the SDB after immobilization with *P. stutzeri* were much less compared to pristine SDB, confirming the immobilization and colonization of *P. stutzeri* on biochar.

Table 7.1. Elemental composition and extractable minerals present in SDB.

Elemental composition (% mass-based)				**Extractable minerals (mg kg^{-1})**							
C	H	N	O	Ba	Fe	Mg	Mn	Zn	K	Cu	Pb
64.02	0.5	0.98	34.4	2.2	673.97	61.4	8.69	11.5	12	40	2.7

Table 7.1 indicates the extractable nutrients and minerals in SDB. Based on the ICP analysis results, SDB comprises various mineral constituents, such as Fe, Mg, Mn, Zn, K, Cu, Pb, etc., that could support nutrients for the growth of *P. stutzeri.* Heavy metal removal can be accompanied by releasing metal cations such as K^+ and Mg^{2+} in the biochar as exchangeable cations to increase efficiency (Zhang et al. 2015a). A study by Ye et al. (2017) suggested that bacteria could adhere to the mineral-enriched region of biochar.

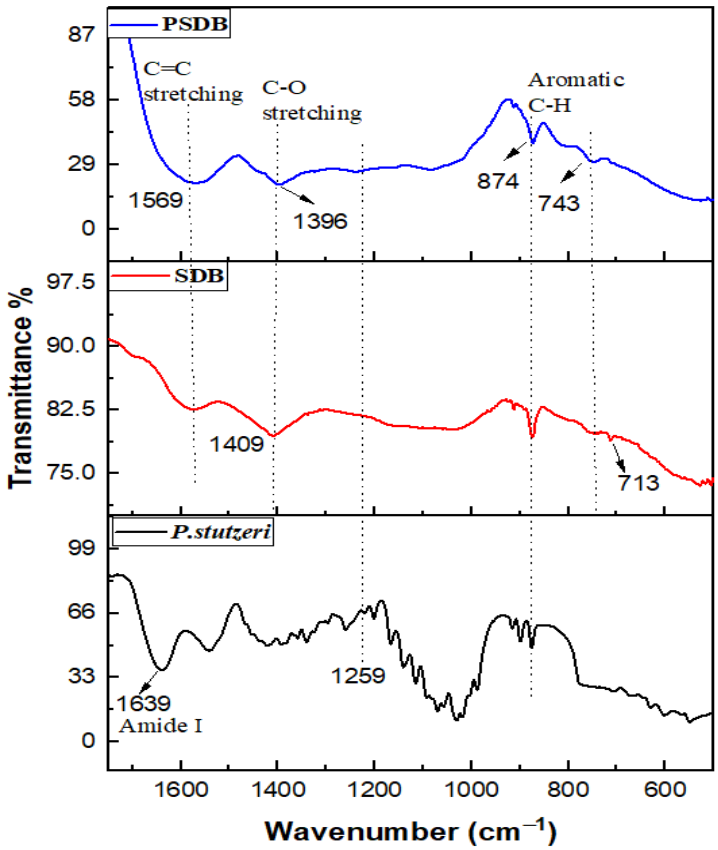

Figure 7.2. FTIR spectra of *P. stutzeri,* SDB and PSDB.

Surface functional groups can provide information about SDB properties, *P. stutzeri* immobilization, and their interactions with the metal ion. **Figure 7.2.** represents the FTIR analysis of *P. stutzeri,* SDB and PSDB. The main functional groups of SDB involve a broad transmittance band of 3337 cm^{-1} (–OH); the bands at 1569 and 1409 cm^{-1} represent the C=C stretching vibration of the biochar and $–CH_2$ groups (Pua et al. 2013). An intense band occurring at 1036 cm^{-1} is due to C–O stretching and is associated with oxygenated functional groups of cellulose, hemicellulose, and lignin. PSDB displayed O-H stretching vibration of the hydroxyl group, mainly responsible for the peak at 3251 cm^{-1}. *P. stutzeri* spectral peaks at 2850 cm^{-1} for C-H bending vibrations were introduced in PSDB, which were absent in SDB **(Figure 7.2).** Some bands in SDB shifted to a lower frequency from 1409 to 1396 cm^{-1}. Increases in peak intensity were more pronounced after the immobilization of *P. stutzeri* for the peak at 1569 cm^{-1}, representing C–H bending vibrations of fatty acids and lipids on the bacteria surface. The FT-IR spectrogram indicates that the microorganisms

are successfully loaded onto the SDB and that the complex integrates biochar and microbial functional groups, improving the stability and removal capacity of the PSDB.

7.1.2 Effect of Operating Conditions on Ni Removal

7.1.2.1 Effect of incubation time

The influence of incubation time on Cd and Ni removal efficiency by *P. stutzeri* and PSDB is depicted in **Figure 7.3a**. Cd removal efficiency increased with incubation time, from 15.5 % to 48 % for *P. stutzeri* and from 42.56 % to 65.6 % for PSDB from 6 to 42 h. A steep increase in Cd removal efficiency was seen until 30 h for PSDB, whereas *P. stutzeri* showed a significant increase until 36 h. Ni removal efficiency increased from 18.6 % to 44.6 % for *P. stutzeri* and 38.52 % to 63.6 % for PSDB, with an increase in incubation time from 1 to 42 h at an initial Ni concentration of 50 mg L^{-1}. Maximum Ni removal of 63.6 % was observed at 36 h for PSDB, whereas *P. stutzeri* showed only 43 % at an initial Ni concentration of 50 mg L^{-1}. Maximum removal efficiency occurred when most cells had reached the stationary phase, and cell density was the highest. Huang et al. (2014) reported that higher cell densities in the stationary phase caused a higher metal accumulation.

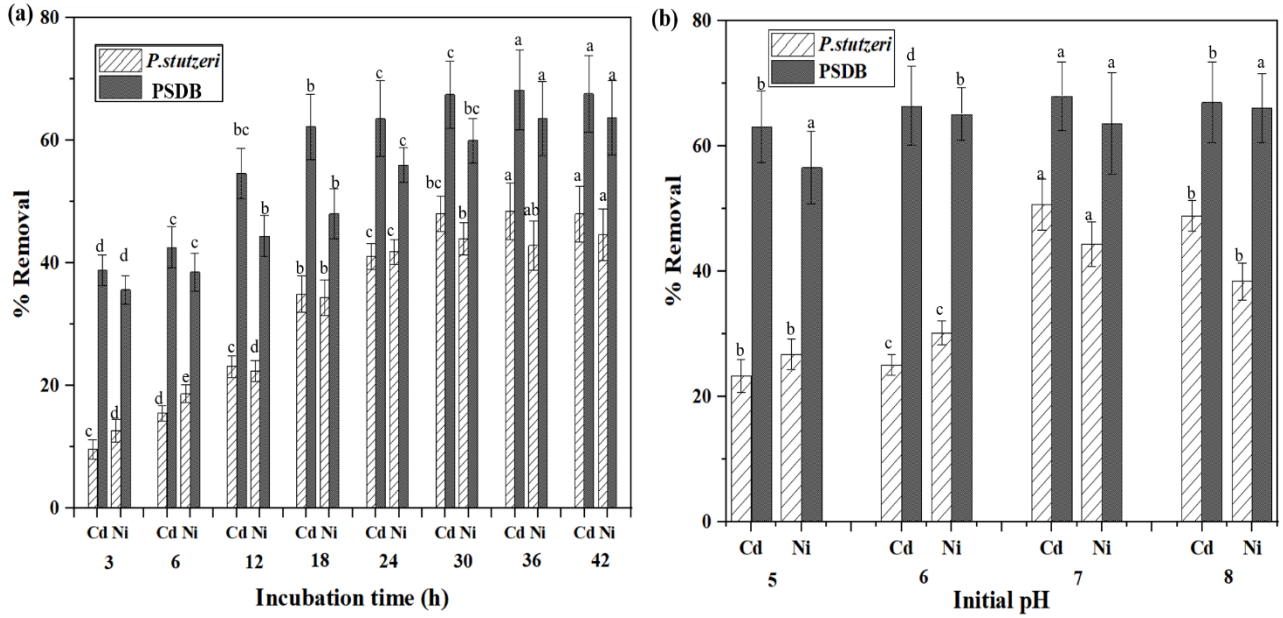

Figure 7.3. Cd and Ni removal by *P. stutzeri* and PSDB **(a)** Effect of incubation time **(b)** Effect of initial pH.

The delay in PSDB reaching maximum capacity compared to *P. stutzeri* was attributed to PSDB's high complexity of Cd and Ni removal. During this process, Cd and Ni were first attached to the

biochar surface and then slowly adsorbed into the internal pores of the biochar and transferred into the *P. stutzeri* cell wall, causing a delay in equilibrium.

7.1.2.2 Effect of initial pH on Cd and Ni removal

PH is a primary factor influencing microbial growth and enzyme activity (Zhao et al. 2020). The effect of initial pH on metal ion removal efficiency was evaluated with experiments conducted at Cd and Ni concentrations of 50 mg L^{-1}, temperature of 37 °C, and contact time of 36 h. Metal ion removal efficiency of PSDB increased from 5.0 to 7.0 and displayed 68.02 % for Cd and 63.6 % for Ni at pH 7.0 **(Figure 7.3b).** In the same condition, free cells showed an increase in removal from 23.32 to 50.68 % and 26.72 % to 44.38 % for Cd and Ni, respectively. The metal ion removal capacity of PSDB and *P. stutzeri* varied with the change in pH. However, the removal efficiency was more pronounced in the case of the free cell with an increase in pH compared to PSDB. That was mainly attributed to the outer surface of PSDB loaded with various functional groups and a certain number of bacteria. This compact outer layer and inner space offered great buffering capacity for Cd and Ni removal due to the unaffected metabolism in PSDB rather than in free cells. Additionally, microbial cells are prone to modify their protein folding in unfavorable pH conditions, thereby reducing metal removal efficiency. The present result was similar to the findings of (Argun 2008) and showed the maximum Ni removal activity under the optimized conditions of pH ~7.0 using clinoptilolite.

The decrease in heavy metal ion removal at lower pH is due to the protonation of surface groups by H^+ ions, which competed with heavy metal ions (Aslam et al. 2020). The surface groups became deprotonated with the increase in pH, and heavy metals were bound to the surface of the biochar. A study carried out by (Bogusz et al. 2017) indicated that when pH was strongly acidic, the Ni was present in the form of Ni ion in the solution, while in the medium acidic pH, Ni was present in the form of Ni $(OH)^+$. The second form of ions was adsorbed more quickly due to lower electrostatic repulsion between the ion and the surface. Based on these findings, Ni removal by PSDB may be followed by precipitation. The removal efficiency in the immobilized system was higher than that of the free cells in the above-tested pH conditions, suggesting that SDB can act as a barrier and carrier for bacteria and ensure the viability of cells, thus improving the total metal ion removal efficiency.

7.1.2.3 Effect of temperature

Temperature affects the stability and configuration of the cell wall by changing the surface functional groups and the binding sites for metal ions. PSDB–mediated Cd and Ni removal was investigated at 25, 30, 35, 37, and 40 °C to study the effect of temperature. PSDB showed a Cd removal efficiency of 43.82 % at 25 °C, increasing with temperature rise **(Figure 7.4a).** The maximum removal efficiency of 67.86 % Cd and 64.54 % of Ni was obtained at 37 °. *P. stutzeri* also demonstrated the same trend of increase in metal ion removal with an increase in temperature from 25 to 37 °C because the temperature is a critical factor that regulates the bacterial metabolism and growth rate by affecting the stability of the cell wall. *P. stutzeri* strains are more active at temperatures between 30 and 40 °C. Thus, the metabolism could be enhanced under optimal temperature, thereby increasing the metal ion removal efficiency. Bacterial-mediated metal ion removal mainly occurs through bioaccumulation and appears to be temperature-dependent. Metal solubility and membrane-binding affinity of metal ions to the bacterial cell wall can be increased at an optimum temperature, accounting for increased removal efficiency. In PSDB, the pore structure enlarges when the temperature increases, creating more surfaces for metal ion adsorption (Saleem et al. 2007).

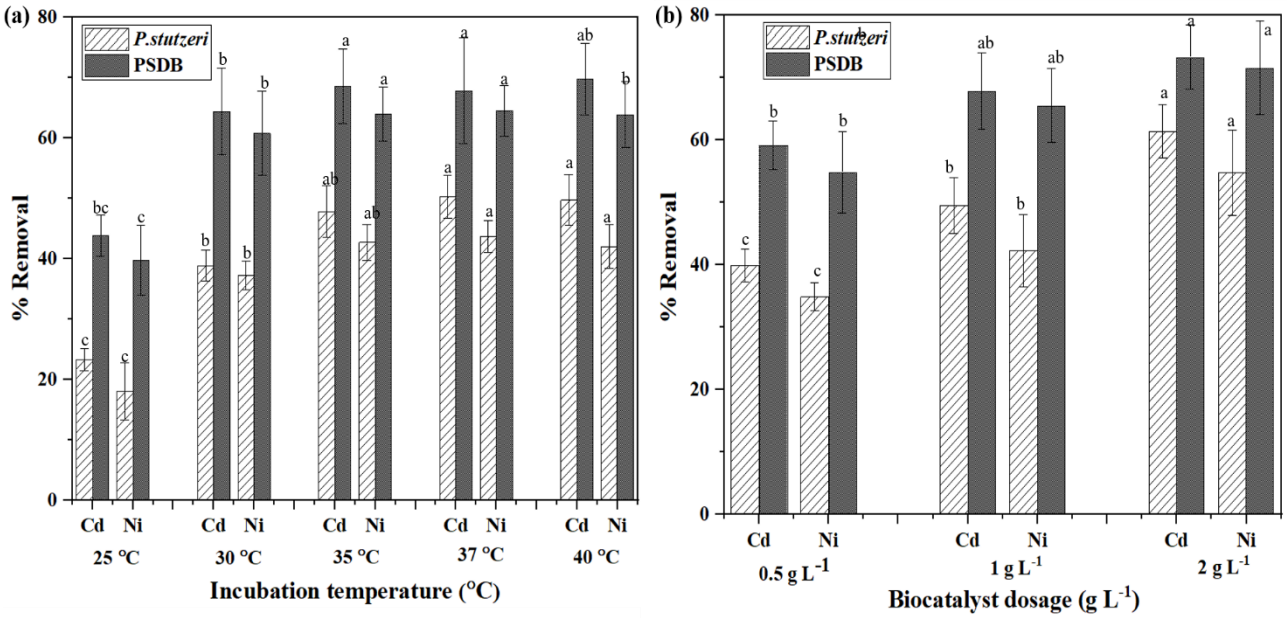

Figure 7.4. Cd and Ni removal by *P. stutzeri* and PSDB (**a)** Effect of incubation temperature **(b)** biocatalyst dosage.

A decrease in Cd and Ni removal at higher temperatures could be due to cell wall disruption or a weak interaction between the active site and metal ions. Finally, the incubation temperature on the removal efficiency of Cd and Ni showed that both PSDB and free cells possessed the highest activity at 37 °C. Similar results have been reported in the bioaccumulation of Ni by *Desulfovibrio desulfuricans*, where maximum Ni removal was obtained at 37 °C (Joo et al. 2015).

7.1.2.4 Effect of biocatalyst dosage

PSDB with various dosages (0.5, 1, and 2 g L−1) were employed in the Cd and Ni solution with an initial concentration of 50 mg L^{-1} at pH 7.0 to enhance metal ion removal. As shown in **Figure 7.4b**, increasing the dosage of the biocatalyst enhanced the removal efficiency. The maximum removal efficiency of 73.3 % Cd and 71.6 % Ni was achieved with a PSDB dosage of 2 g L^{-1}. The free cell-mediated Cd removal efficiency was 61.4 %, and Ni was 54 % under the same conditions. An increase in removal efficiency with biocatalyst dosage can be attributed to increased biochar surface area, availability of more adsorption sites, and a functional group for metal removal.

7.1.2.5 Effect of initial metal ion concentration

The effect of initial metal ion concentration on the removal of Cd and Ni by PSDB is shown in **Figure 7.5**. The removal efficiency decreased from 86.19 % to 61.77 % and 82.87 % to 58.3 %, increasing Cd and Ni concentration from 10 to 100 mg L^{-1}. At lower concentrations, all metal ions in the solutions could interact with the cell's binding sites; thus, the percentage removal was high initially. The decrease in the percentage of removal efficiency with concentration was due to the exhaustion of the adsorption sites available on the biochar for a given dosage. With the increase in Cd and Ni concentration, cell number decreased from 8.7 to 5.6 Log_{10} cells and 8 to 4.6 Log_{10} cells, respectively, suggesting that total removal was critically linked to cell viability and activity. During metal removal, adsorption sites on the PSDB surface were more easily occupied when the initial metal ion concentration was low, and the bioaccumulation by growing bacteria was inhibited insignificantly, resulting in a significant increase in metal ion removal, while at higher concentrations, adsorption sites gradually achieved saturation, and bacterial growth was significantly inhibited. Moreover, SDB provided shelter for the free cells due to its pore structures, thereby prolonging the survival of immobilized bacteria in a stressful environment.

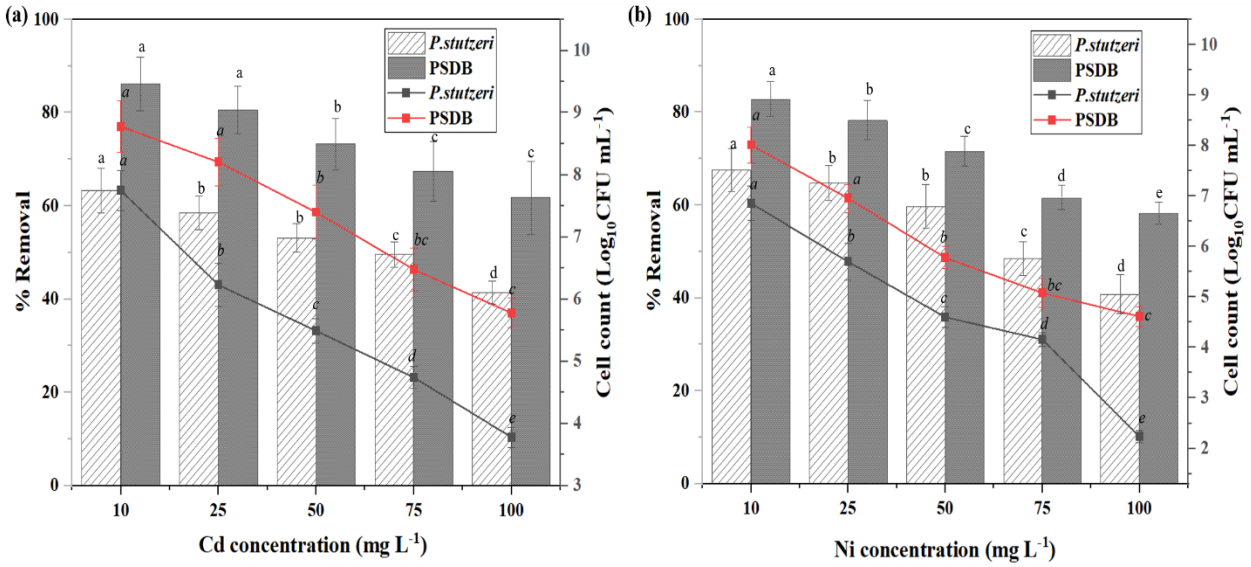

Figure 7.5. Effect of initial metal ion concentration on removal efficiency by *P. stutzeri* and PSDB **a)** Cd **b)** Ni.

7.1.3 Cd and Ni removal by SDB, *P. stutzeri*, and PSDB at optimized operating conditions

Cd and Ni removal experiments by SDB, *P. stutzeri*, and PSDB were performed at an optimized incubation temperature of 37 °C, initial solution pH of 7, PSDB dosage of 2 g L^{-1}, 36 h of incubation time, and 10 mg L^{-1} initial metal ion concentration (**Figure 7.6**). Results indicated that the free cells removed Cd and Ni by 63.3 % and 67.6 %, respectively. Typically, Ni removal by free cells could be from bioaccumulation by the bacterial cells. SDB showed 42 % Cd and 38 % Ni removal through adsorption, whereas cell immobilization on SDB exhibited a significant enhancement of metal ion removal performance of 86.2 % and 82.87 %. Immobilization can cause a higher number of cells attached to biochar. A more significant number of immobilized cells and biochar adsorption capacity could be the reason for the highest metal ion removal by PSDB. It is suggested that the pore structure of the SDB provides a relatively stable growth environment for *P. stutzeri* and protects them from the toxicity of metal ions.

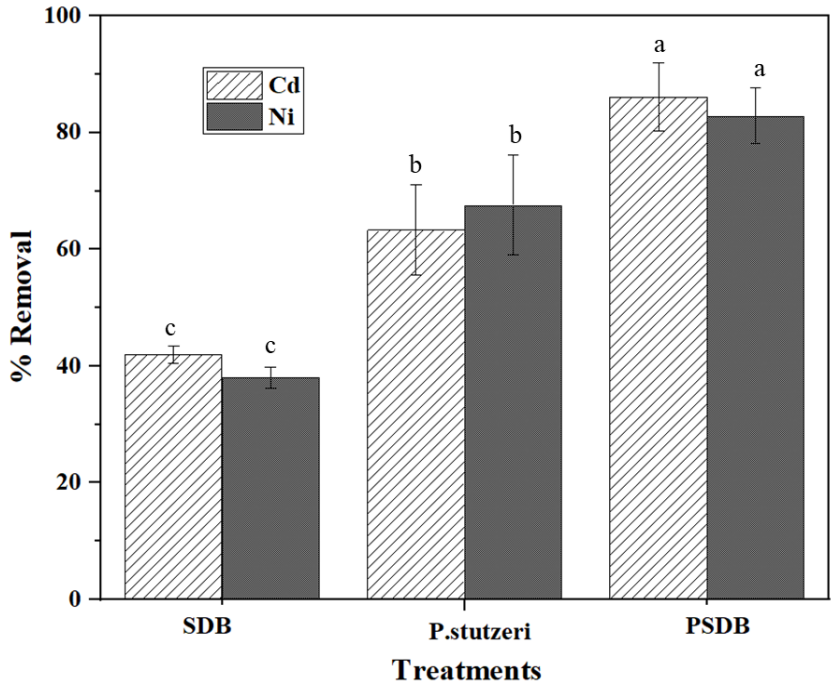

Figure 7.6. Comparative plot of Cd and Ni removal efficiency by SDB, *P. stutzeri*, and PSDB.

7.1.4 Reusability of immobilized cell

Regeneration of material is a crucial factor for their use in water treatment. To investigate the continuous application of PSDB, five consecutive experiments were carried out. The results showed that the initial Cd and Ni removal efficiency of PSDB was 86.2 % and 83%, respectively. In comparison, the second and third cycles showed 83 % and 76 % of Cd and 80 % and 75% of Ni, revealing its steady removal efficiency (**Figure 7.7**). PSDB maintained a 75 % Ni removal rate after the third cycle, indicating the reusability of the immobilized cell. Huang et al. (2020) used algae biochar to immobilize *Proteus mirabilis* PC801 to maintain the chromium removal rate and observed stability until the third cycle.

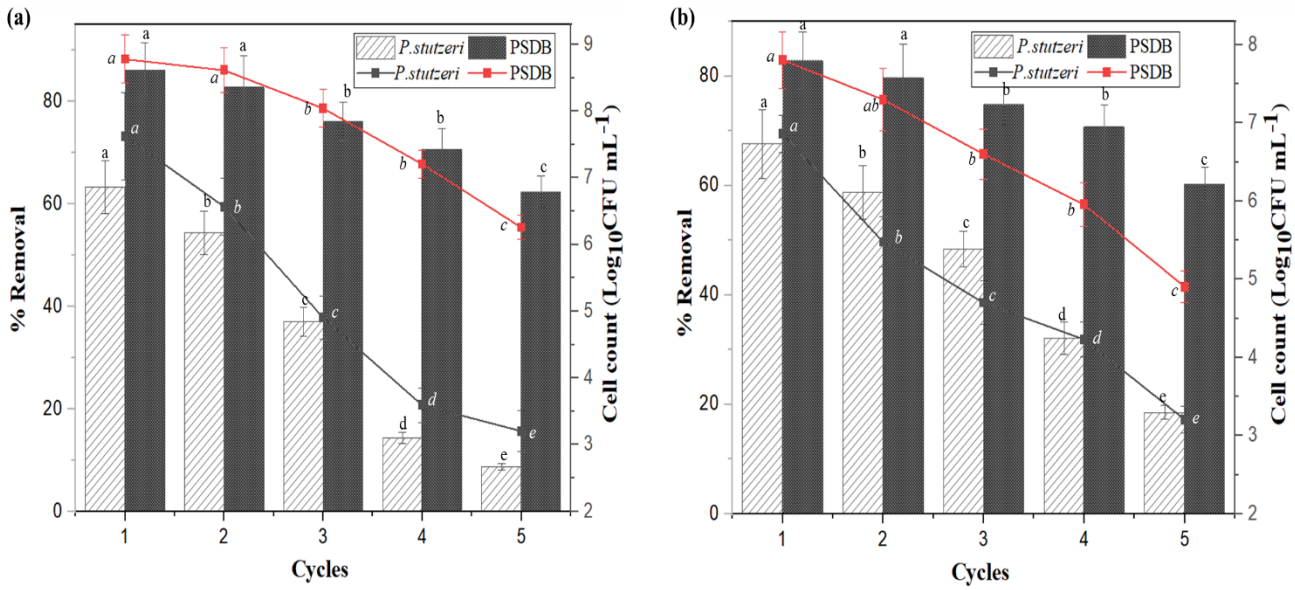

Figure 7.7. Reusability study of *P. stutzeri* and PSDB for **(a)** Cd and **(b)** Ni removal.

Microbial cell count varied from 7.8 to 4.9 Log_{10} cells after five cycles with 10 mg L^{-1} Ni and 8.7 to 6.25 Log_{10} cells after Cd (**Figure 7.7**). This gradually decreases over each cycle due to cell washout or cell death of surface-immobilized cells from direct contact with metal ions during experiments. A constant number of cells was retained after two cycles of treatment with PSDB. This might be because biochar served as a carrier with multiple porosities and offered enough space and a stable microenvironment for the growth of bacteria. Immobilization facilitated its repeated use, cutting costs and making biocatalysts more viable.

7.1.5 FTIR analysis of PSDB after Cd and Ni removal

FTIR absorption peaks of PSDB before and after treatment with Cd and Ni^{2+} are represented in **Figure 7.8**. The changes in peak indicate the attachment of metal ions with various functional groups existing on the SDB and *P. stutzeri* cell membrane. FTIR spectrum produced by PSDB after Ni^{2+} removal showed significant changes at 3273, 2962, and 1575 cm^{-1}, regions representing the stretching of O–H, C–H, C=C, respectively. The peaks representing hydroxyl groups at 3251 and 1020 cm^{-1} in SDB were changed significantly. After the removal of Cd and Ni, the stretching vibration peak of O−H shifted from 3251 to 3308 cm^{-1} and 3273 cm^{-1} respectively due to the substitution of some of the hydrogen in O−H, which indicated that the adsorption could occur through the interaction between surface hydroxyl groups and metal ions. Moreover, the intensity of

peaks at 1396 and 1241 cm^{-1} regions represented the bending of CH_3 and deformation of the C–H group, respectively, reducing to 1377 and 1243 cm^{-1} for Cd and 1384 and 1230 cm^{-1} for Ni after treatment.

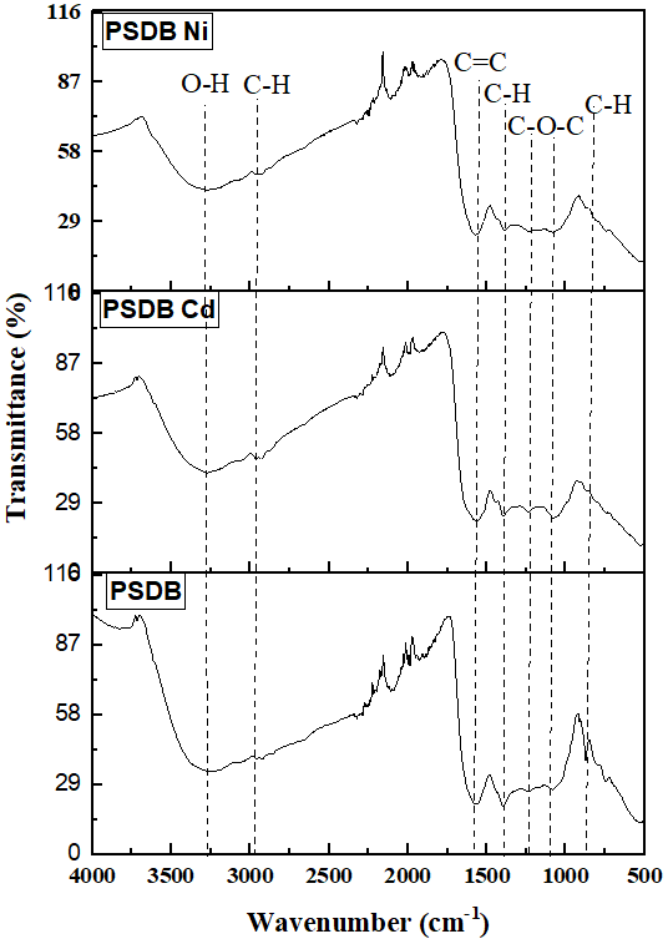

Figure 7.8. FTIR spectra of PSDB before and after Cd and Ni removal.

7.2 *Bacillus* sp IMMOBILIZED RICE HUSK BIOCHAR TO REMEDIATE Cd CONTAMINATED SOIL

7.2.1 Phytoavailability of Cd

In this study, we investigated the remediation of DTPA phytoavailable Cd in soil using three distinct treatments: rice husk biochar, *Bacillus* sp, and BRHB. The DTPA phytoavailable Cd concentrations were monitored over 80 days to assess the efficacy of each treatment. In the control soil spiked with Cd, the concentrations exhibited a gradual decrease from 6.8 mg kg^{-1} at 7 days to 5.2 mg kg^{-1} at 42 days due to the indigenous microorganisms present in the soil. Treatment with

RHB showed consistent reductions in Cd concentrations, with values decreasing from 4.1 mg kg^{-1} to 3.5 mg kg^{-1} over the same period (**Figure 7.9**). *Bacillus* sp treatment demonstrated notable efficacy, leading to a decrease from 6 mg kg^{-1} to 4.2 mg kg^{-1}, while the BRHB treatment outperformed all, with concentrations reduced from 5.2 mg kg^{-1} to 3 mg kg^{-1} within 42 days and further reduced to 2.6 mg kg^{-1} after 80 days of remediation. These findings highlight the potential of BRHB as an effective remediation strategy for DTPA phytoavailable Cd. As revealed by SEM characterization, RHB has a high specific surface area and porous structure, which could strongly adsorb metal ions. Moreover, our results and previous studies demonstrated that heavy metal-tolerant bacteria could immobilize metal ions, thus inducing the decline of DTPA-extractable Cd in soil.

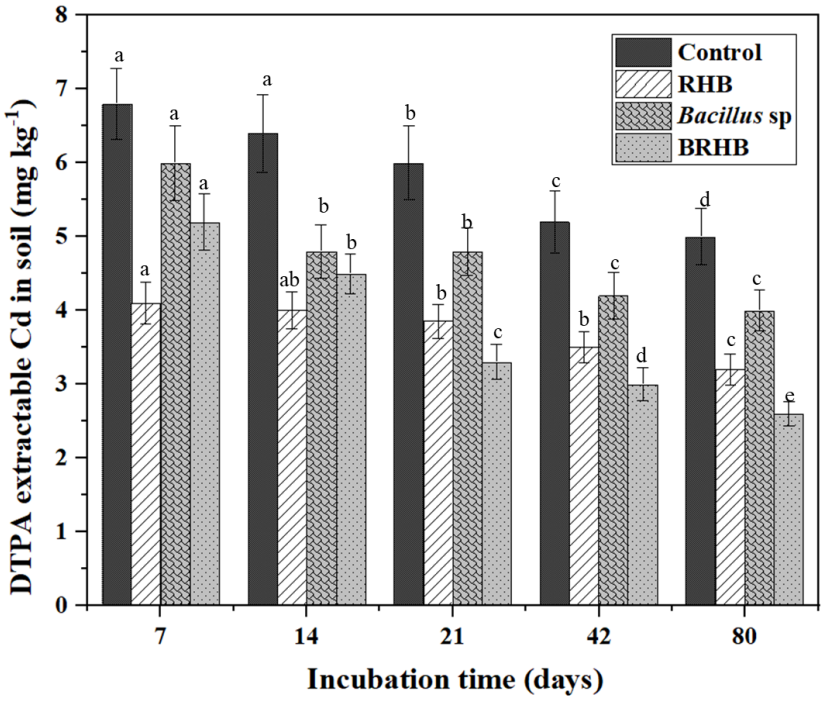

Figure 7.9. DTPA extractable Cd concentration in the soil during incubation.

7.2.2 Fractionation of Cd in soil

The investigation into Cd remediation strategies employing RHB, *Bacillus* sp cells, and BRHB, yielded significant alterations in Cd fractions. The acid-soluble fraction, indicative of Cd bioavailability and potential toxicity, exhibited a consistent decrease across all treatments compared to the control soil spiked with Cd. Application of RHB, *Bacillus* sp, and BRHB reduced the acid-soluble fraction of Cd by 16.3 %, 12.5 %, and 21.3 %, respectively, compared to the control soil

(**Figure 7.10**). In terms of reducible fraction, reductions were observed in all treatments: RHB (25 % decrease), *Bacillus* sp (20 % decrease), and BRHB (32.5 % decrease) compared to the control soil. Similarly, the residual fraction showed a notable increase in all treated samples. BRHB exhibited the highest percentage increase, implying a 19 % augmentation in the stable and less toxic form of Cd, suggesting a synergistic impact of combining *Bacillus* sp with rice husk biochar. These findings underscore the effectiveness of the applied remediation strategies, with BRHB demonstrating the most pronounced shift in Cd fractions, emphasizing the remediation processes' efficiency in influencing Cd speciation.

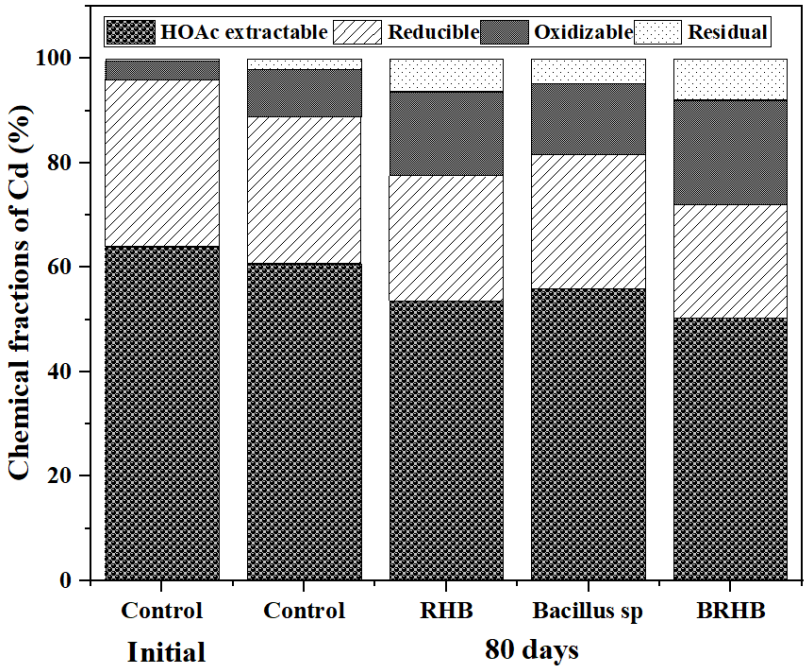

Figure 7.10. Percentage fraction distribution of Cd in soil with different treatments.

7.2.3 Changes in soil pH during the incubation

The application of RHB and BRHB both elevated the soil pH during remediation. The control group exhibited minimal fluctuations, maintaining an initial pH of 5.6. A quick increase in soil pH was observed with the biochar amendments due to the dissolution of alkaline substances (such as inorganic carbonate) in the biochar. The BRHB treatment exhibited a more pronounced increase in pH, similar to rice husk biochar. In particular, the treatment with microbial cells increased the pH in the soil after the 20-day incubation. The fluctuation in soil pH seen with *Bacillus* sp amendment shows the survival of microorganisms. The substances secreted by bacteria might contain some low

molecular weight compounds, which increase the soil pH. BRHB increased pH to 7.4, followed by RHB treatment, which showed 7.3. The pH buffering ability of microbial cell immobilized biochar influences the speciation and bioavailability of Cd, especially in acidic soil. The observed pH changes suggest a promising potential for the remediation of Cd-contaminated soil. The application of biochar, particularly in combination with microbial activity, appears to impact soil pH positively.

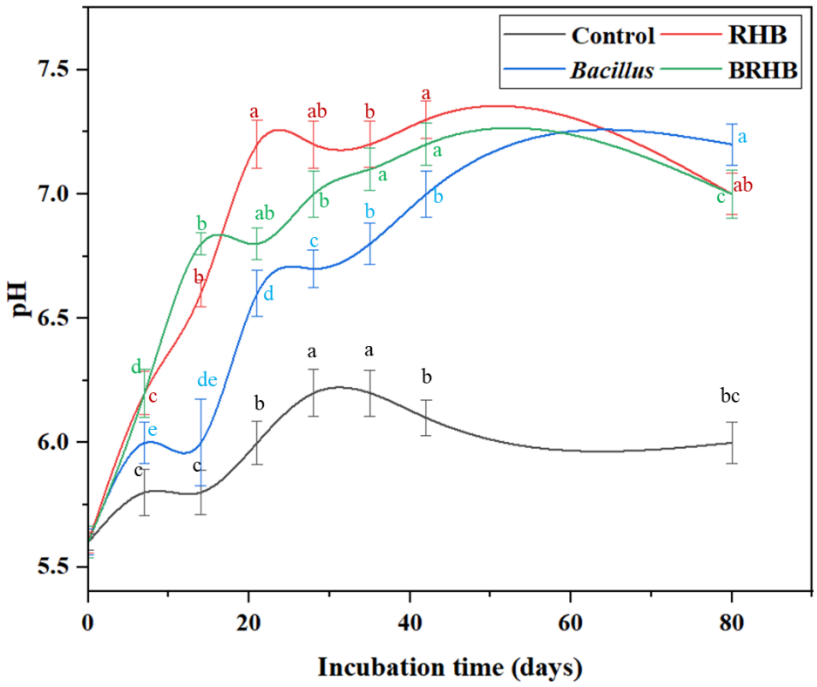

Figure 7.11. Change in soil pH during the incubation time.

7.2.4 Soil enzyme activities and organic matter analysis

Soil enzyme activity is a comprehensive bioindicator for assessing soil health, fertility, and quality (Gao et al. 2010). Soil phosphatase activity plays a pivotal role in the potential mineralization of organic phosphorus in soil ecosystems (Wang et al. 2018). Similarly, β-glucosidase enzymes serve as robust indicators of soil quality, mainly reflecting the carbon cycling processes within the soil (Ferraz de Almeida et al. 2015). In the present study, all treatments exhibited a discernible increase in soil phosphatase, β-glucosidase activities, and organic matter content, albeit with variations in their magnitudes (**Figure 7.12**). Under the influence of BRHB treatment, soil phosphatase activity notably rose from 23.42 to 37.84 µg p-Nitrophenol g^{-1} of dry soil, surpassing the effects observed in the RHB treatment (29.6 µg p- Nitrophenol g^{-1} of dry soil). Concurrently, BRHB-treated soil

displayed the highest β-glucosidase activities, registering a 43 % increase compared to the control soil. Furthermore, applying both biochar and BRHB significantly elevated soil organic matter content across all treatments, exceeding levels observed in control groups.

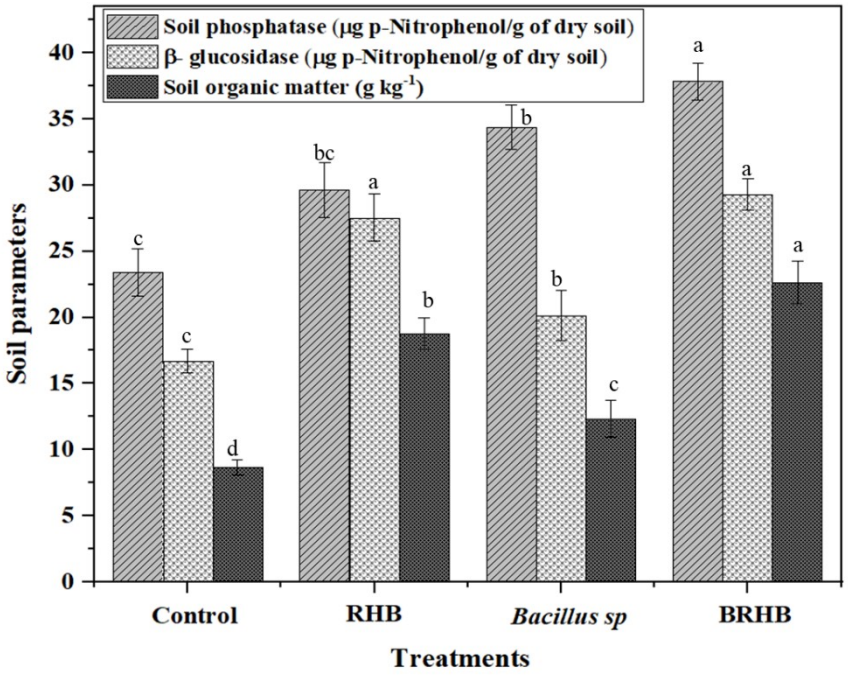

Figure 7.12. Effects of different treatments on soil enzyme and organic matter content.

RHB may augment carbon availability in the soil, providing nutrient sources for microorganisms. This action could potentially immobilize metal ions, mitigating heavy metal toxicity to soil microorganisms and subsequently promoting microbial biomass and diversity, thereby influencing soil enzyme activities positively. Additionally, the porous structures of BRHB were found to create conducive habitats for immobilized bacteria, thereby promoting microbe proliferation and enhancing soil enzyme activities. Furthermore, applying BRHB alleviates heavy metal toxicity in plants, positively influencing the metabolism of root exudates, such as amino compounds, sugars, and organic acids. These substances, acting as nutrients for microbes (Wu et al. 2016), indirectly enhance soil enzyme activities.

7.2.5 Initial plant growth study

The impact of various amendments, such as RHB, *Bacillus,* and BRHB, on the growth of *Spinacia oleracea* L. was investigated. **Figure 7.13**. illustrates the comparative effects of various amendments

on seed germination parameters. The GP was lowest in contaminated soil at 66.67 %, attributed to the toxic effects of Cd on seed germination (**Figure 7.13a**). BRHB demonstrated the highest GP at 90 %, outperforming RHB at 86.6 %. The application of BRHB and RHB exhibited superior germination rates and SVI compared to control soil spiked with Cd (**Figure 7.13b**), with the increased percentage attributed to Cd removal, soil property improvement, and enhanced soil fertility.

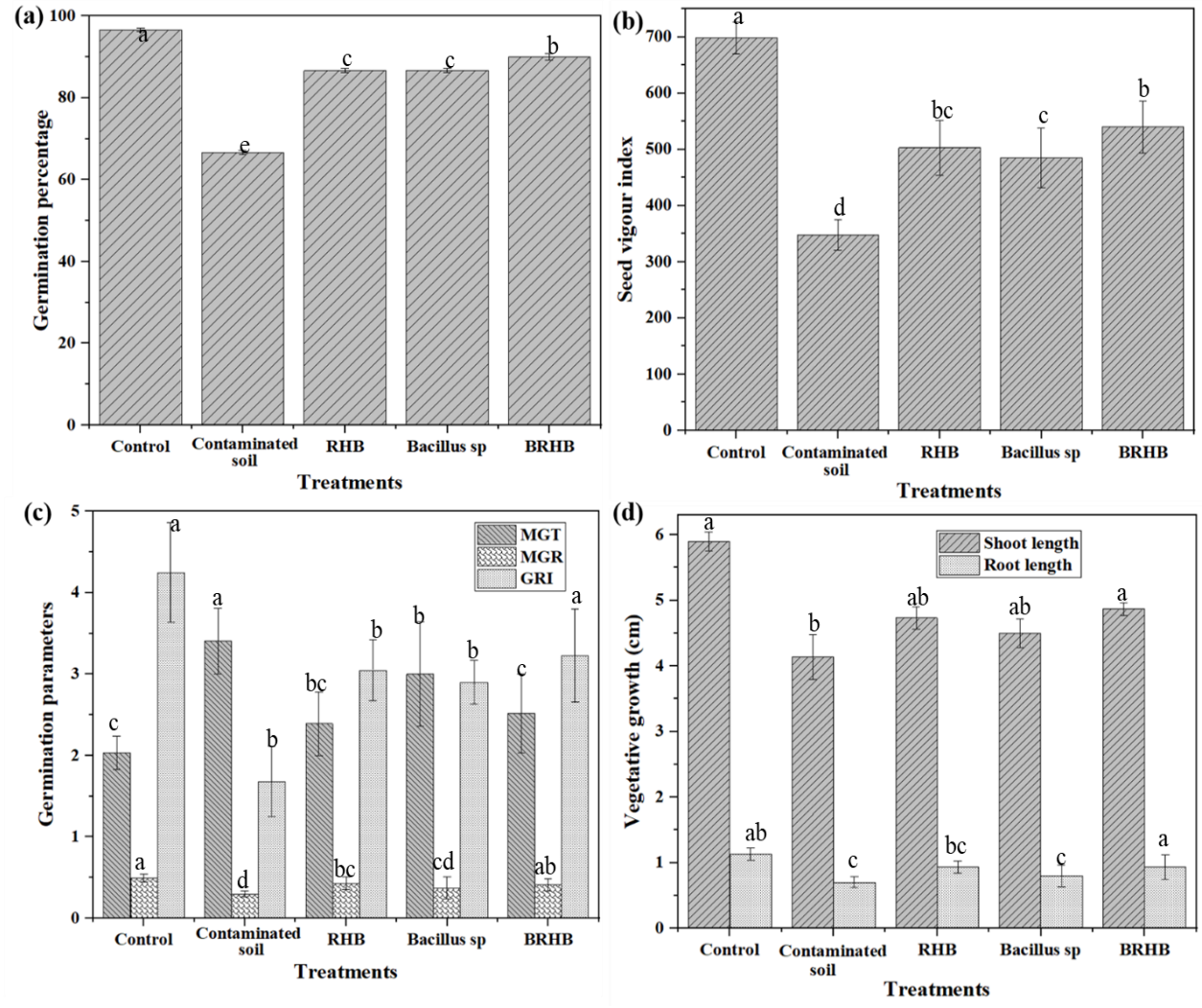

Figure 7.13. Germination and growth parameters of *Spinacia oleracea* L. under different treatments **(**MGT, MGR and GRI **(d)** vegetative growth.

MGT, representing the time seeds take to germinate, decreased in the order of Control > *Bacillus* sp > BRHB > RHB, indicating that RHB led to faster germination of *Spinacia oleracea* L. seeds

(**Figure 7.13c**). Similarly, the GRI, indicating the percentage of seeds germinated daily, was highest in control soil without Cd, followed by BRHB treatment. Plant growth parameters, such as shoot and root length, provide insights into overall plant health and environmental changes. Results after 10 days of germination showed that contaminated soil exhibited the minimum shoot length (4.13 cm) and root length (0.67 cm) due to the negative impact of Cd ions (**Figure 7.13d**). Treatments with BRHB and RHB showed the maximum shoot length, indicating a positive influence on plant growth (**Figure A1**, Appendix IV).

7.2.6 Biomass and Cd content of *Spinacia oleracea* L plants

The remediation efficacy of Cd spiked soil was assessed using various treatments, including rice husk biochar (RHB), *Bacillus* sp, and BRHB, focusing on their impact on biomass content and Cd accumulation in spinach plants. In contrast to the control group, where soil was spiked with Cd, a substantial enhancement in plant growth was evident in spinach plants cultivated in Cd-contaminated soil supplemented with RHB and BRHB **(Figure 7.14)**. Pot study results, illustrated in (**Figure A2,** Appendix IV), further support these findings, showcasing spinach growth under various treatments in triplicate. Enhancement in growth might be attributed to the improvement of soil physio-chemical properties in the presence of biochar, thereby promoting nutrient uptake and utilization by vegetables (Ma et al. 2020).

Figure 7.14. Growth of *Spinacia oleracea* L under different treatments.

The control group, representing Cd-stressed plants without remediation, exhibited less biomass and a high Cd content of 1.88 mg kg^{-1}, highlighting the detrimental effect of Cd stress on plant growth. The application of RHB significantly improved biomass to 42 mg plant $^{-1}$ and reduced Cd content of 0.66 mg kg^{-1}, emphasizing the potential of rice husk biochar in mitigating Cd uptake by spinach plants. *Bacillus* sp contributed to increased biomass but demonstrated a less pronounced effect on Cd reduction 0.86 mg kg^{-1}. In contrast, BRHB treatment synergistically enhanced both biomass 58 mg plant $^{-1}$ and reduced Cd content to 0.35 mg kg^{-1}, showcasing the combined efficacy of *Bacillus* sp and rice husk biochar in alleviating Cd-induced stress on spinach plants **(Figure 7.15)**. RHB, rich in functional groups capable of binding metal ions, can release anions that combine with Cd ions, forming carbonates and precipitates (Tu et al. 2020; Wu et al. 2021). This reduces the availability of metal for spinach plants.

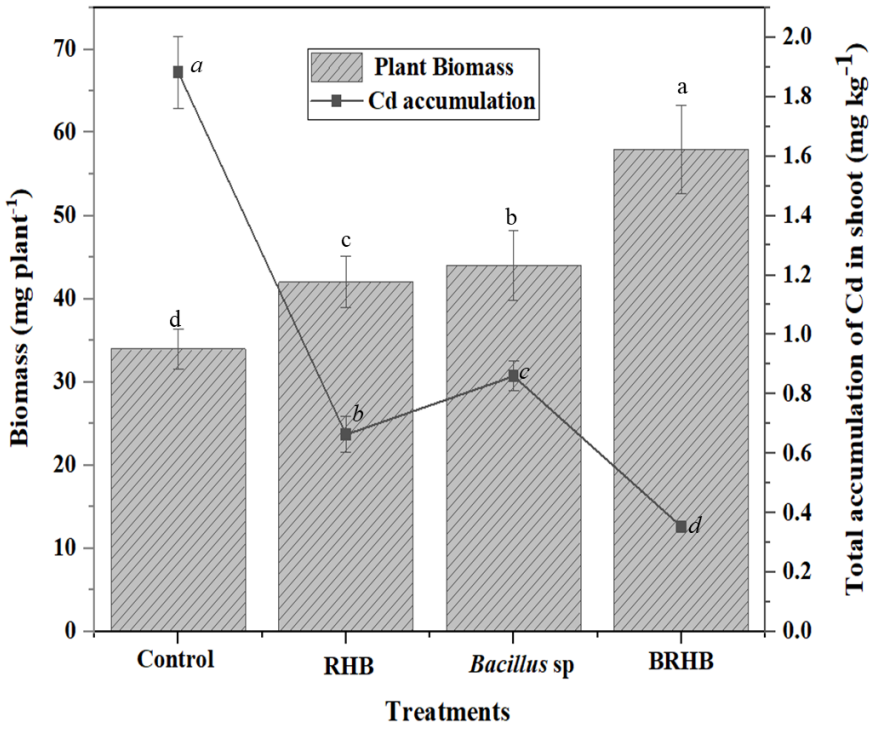

Figure 7.15. Effects of different treatments on growth of *Spinacia oleracia* L. plants and Cd accumulation.

Additionally, bacterial cell walls, cell secretions, and plant root secretions can bind with Cd in the soil, thereby decreasing its accumulation in plants. The carbon source released by biochar and their pore structure provides nutrients and habitat for heavy metal immobilizing microorganisms, extending their life cycle and indirectly impeding Cd transfer to plants. Some studies also suggest

that bacterial inoculation can modulate the expression of metal transporter genes in plants, reducing heavy metal accumulation (Xu et al. 2018).

7.3 *P. stutzeri* IMMOBILIZED COCONUT SHELL BIOCHAR TO REMEDIATE Cd CONTAMINATED SOIL

7.3.1 Characterization of CSB

Biochar pH and electrical conductivity are important variables because biochar additions significantly impact soil properties (Noronha et al. 2022). Electrical conductivity represents salinity, a key limiting factor for seed emergence, germination, and plant growth (Ren et al. 2022). The CSB samples had a pH of 7.6 and high levels of electrical conductivity (221 µS cm^{-1}). SEM, BET, CHNS, ICP, FTIR, and TGA spectrum analyses were carried out to characterize the microstructure, functional groups, presence of extractable minerals, and thermal stability of CSB. **Figure 7.16** shows the surface morphology and EDS analysis of CSB. The SEM results showed a porous surface. One of the most important factors influencing biochar functionality is surface area, as greater surface area results in more porous structures within the biochar, while the EDX analysis showed C and K in CSB, which are essential for plant growth (**Figure 7.16b**).

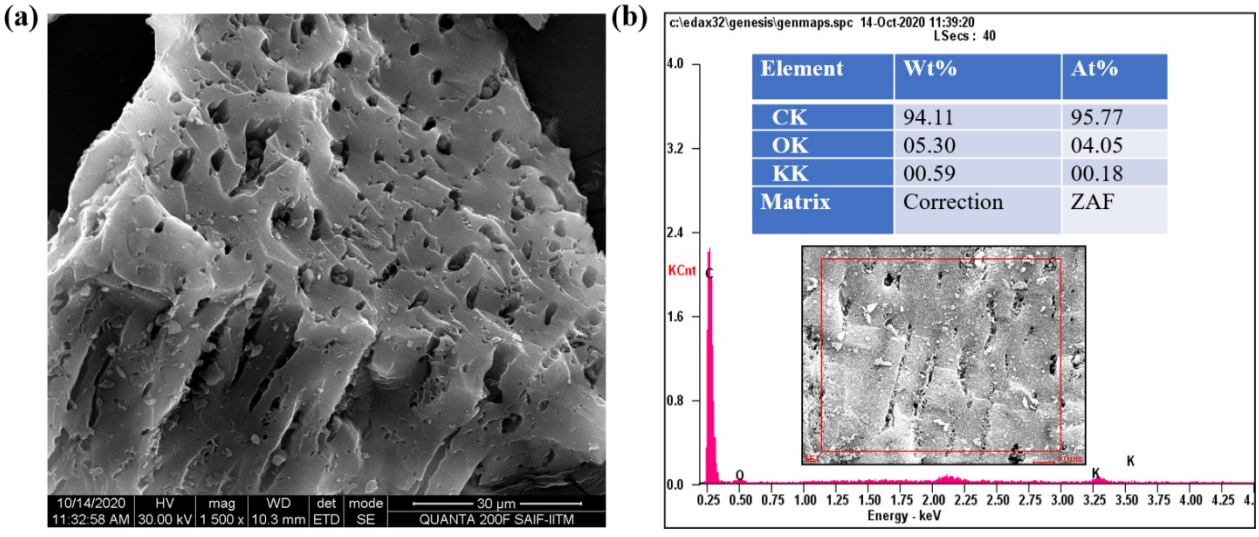

Figure 7.16. Surface morphology of CSB **(a)** SEM images and **(b)** EDS analysis.

The BET surface area and total pore volume of the CSB were 1.46 m^2g^{-1} and 5.16 x 10^{-4} cc g^{-1}, respectively. These pores play an essential role when applied to the soil; CHONS analysis showed biochar contains 76.6 % C, 2.04 % H, 21.07 % O, and 0.29 % N. ICP-OES analysis indicated that

the produced CSB contains large amounts of K (1300 mg kg^{-1}) and also other essential plant nutrients in required quantity such as 3.5 mg kg^{-1} Mn and 6.5 mg kg^{-1} of B (**Table 7.2**).

Table 7.2. Elemental and nutrient composition of CSB.

Element	Mg	K	Mn	Zn	Cu	Co	B
Concentrations (mg kg^{-1})	120	1300	3.5	43	7.5	0.5	6.5

Figure 7.17a shows the FTIR spectra for CSB. The peaks around 1375 cm^{-1} and 1600 cm^{-1} are due to C=C stretching of aromatic rings. The peaks at 1230 cm^{-1} and 1030 cm^{-1} can be attributed to the C–O stretching in carboxyl, phenols, alcohols, or ethers. The existence of ethers, carbonyl groups, phenols, and aromatic compounds confirms the coconut shell's lignocellulosic structure (Castilla-Caballero et al. 2020; Yağmur and Kaya 2021). Hydrophilic functional groups like carboxyl and hydroxyl confirm the hydrophilic nature of CSB (González-Delgado et al. 2022). The TGA curves are given in **Figure 7.17b**. The initial weight of coconut shell biomass used to prepare biochar was 50 g, which resulted in a final weight of 14 g CSB, and the yield was 28 % during the pyrolysis process.

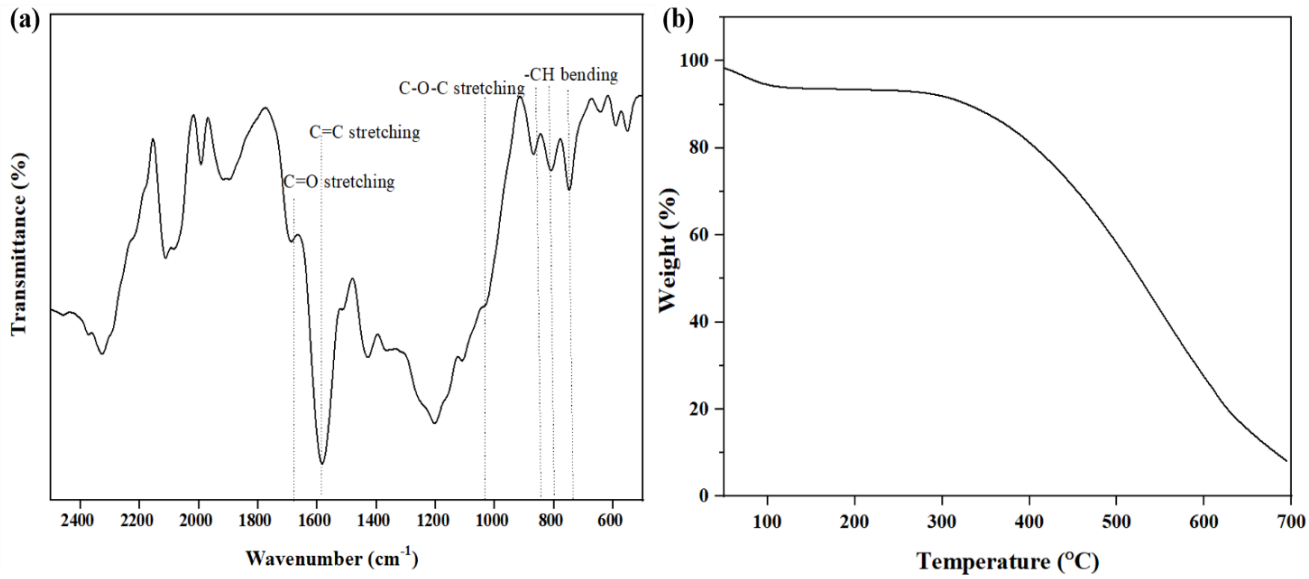

Figure 7.17. (a) FT-IR spectra of CSB **(b)** Thermogravimetric analysis of CSB.

The weight of the coconut shell biomass was significantly reduced during pyrolysis at 450 °C. The coconut shells consist of lignin, cellulose, and hemicellulose. At temperatures around 110°C,

weight loss can be attributed to the loss of adsorbed water and partial dehydration of the cellulose structural units (Das and Ghosh 2022). The weight loss at 250–300 °C corresponds to the degradation of hemicellulose and cellulose (Shangdiar et al. 2021). The weight loss observed at temperatures above 400 °C could be attributed to the decomposition/degradation of the remaining cellulose and lignin (Kazimierski et al. 2022).

7.3.2 CSB as a soil enhancer

7.3.2.1 Effect of CSB particle size on soil water holding capacity

Water holding capacity is one of the most commonly reported soil hydraulic parameters (Ghorbani et al. 2023) and a key indicator of soil quality and productivity (Guo et al. 2022). **Figure 7.18a** depicts the water-holding capacity of soil modified with 5 % CSB of varied particle sizes.

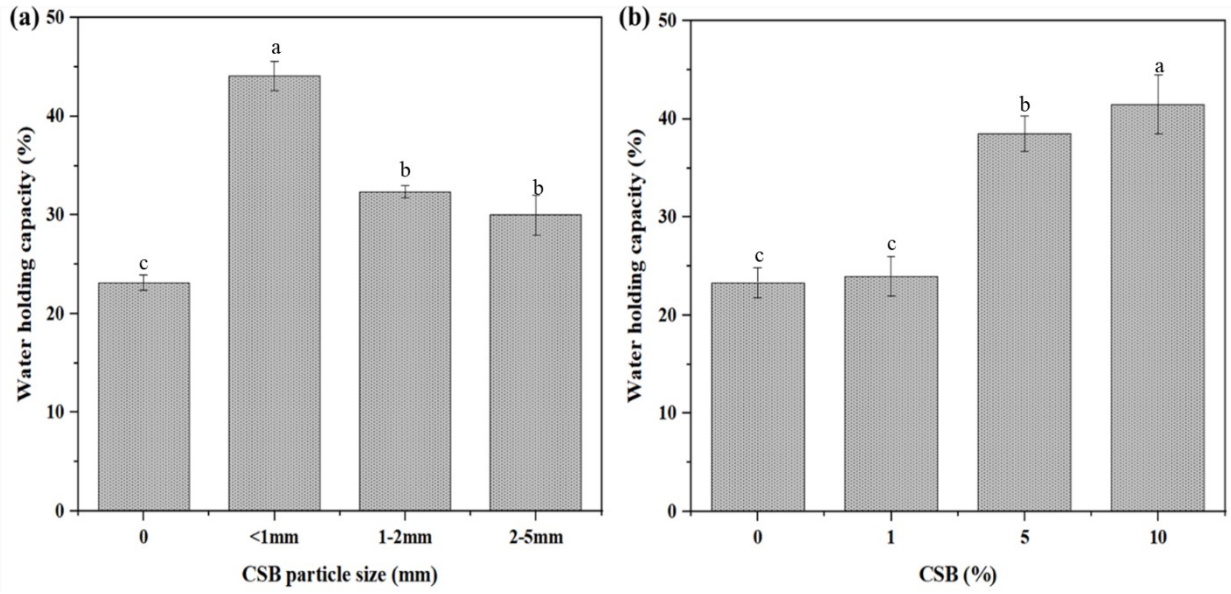

Figure 7.18. Effect of CSB on soil water holding capacity **(a)** CSB particle size **(b)** CSB concentration.

Laterite loam soil had a water-holding capacity of 23.16 %. With the addition of CSB, particle size < 1mm showed the highest water-holding capacity of 44.13 %, followed by 1-2 mm (32.36 %) and 2-5 mm (30 %). Smaller-sized biochar particles can mix or interact with soil particles more efficiently than large ones, forming aggregates (Verheijen et al. 2019b). CSB particle size of <1 mm can fill porous structures in loam soils, increasing water flow. This rise can be attributed to a high specific surface area, which changes inversely with particles. The significant increase in water

retention due to particle size reduction assists the soil in retaining more water, increasing the available moisture in the root zone and allowing longer intervals between irrigations (Das and Ghosh 2022). The effects of biochar amendment are determined by soil conditions, specifically soil texture and mineralogy (Farooque et al. 2020).

7.3.2.2 Effect of CSB concentration on soil water holding capacity

Biochar amendment can influence the hydraulic properties of the soil-biochar mixture by affecting soil aggregation and the creation of accommodation pores between biochar and surrounding soil (Verheijen et al. 2019). The porosity and biochar concentration substantially impact soil water holding capacity (Ghorbani et al. 2023). **Figure 7.19b** depicts the effect of CSB (< 1 mm) on the soil's water-holding capacity with increasing biochar concentration. As the CSB concentration increases, the water-holding capacity of the soil increases. At the lowest application rate (1 %), water holding capacity increased from 23 % to 24 %, and higher concentrations of 5 % and 10 % resulted in an increase of 33.8 % and 41.7%, respectively. The increase in water holding capacity caused by the CSB amendment could be attributed to water accommodation in its inner pores. The study confirmed the presence of numerous pores in CSB (**Figure 7.16a**) that can retain plant-available water. In addition, the presence of hydrophilic functional groups in CSB (**Figure 7.17a**) also contributed to water holding capacity. The results imply that CSB is a good amendment for improving soil hydraulic characteristics. Because biochar increases the volume of stored water in the soil, it may reduce irrigation frequency, positively affecting plant growth during water scarcity. However, the variation in water-holding capacity depends on soil condition, biochar type, particle size, and application rate (Ghorbani et al. 2023; Rabbi et al. 2021).

7.3.2.3 Effect of CSB and FYM amendment on seed germination

Three different concentrations (1 %, 5 %, and 10 %) of <1 mm - sized CSB, in combination with FYM, were employed in the germination parameter study. The GP and SVI of FYM-supplemented soil (57.14 % and 171.64) increased compared to the control (50 % and 158.33). On the contrary, the application of CSB with FYM (1 %, 5 %, and 10 %) in the soil slightly decreased GP and SVI compared to the sole application of CSB, as shown in **Figure 7.19a**. The GP of *Solanum lycopersicum* L. varied from 78.57 % to 90.47 % with increasing CSB dosage, and SVI varied from 330.67 to 464.25 **(Figure 7.19b)**. The increase in GP and SVI with 10 % CSB was marginal

compared to 5% CSB (90.47 % vs. 85.71 % for GP and 464.25 vs. 445.72 for SVI), necessitating the selection of 5 % CSB from an economic perspective.

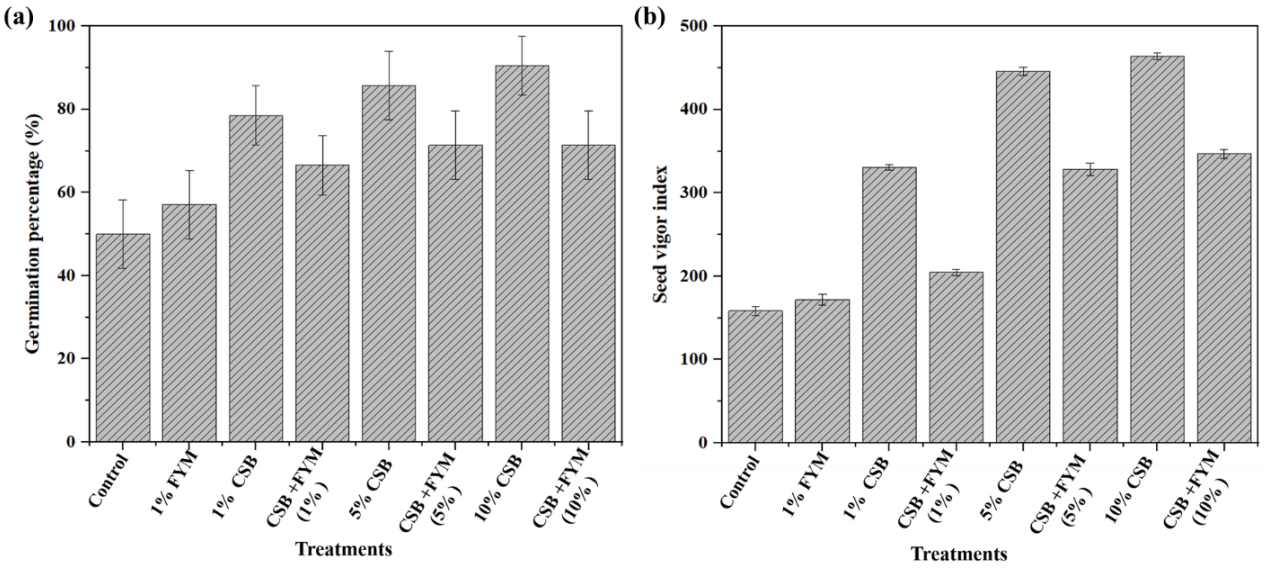

Figure 7.19. Germination parameters of *Solanum lycopersicum* L under different treatments **(a** GP **(b)** SVI.

Increased soil porosity, water holding capacity, and presence of nutrients following CSB application could explain the improved *Solanum lycopersicum* L. seed germination in soil (Farooque et al. 2020). Incorporating plant biomass-derived biochar into the soil system could have resulted in a significant increase in mass during the early stages of development (Saletnik et al. 2019). GP and SVI decreased with the combined application of CSB and FYM because nitrogen is one of the prominent elements required for plants structural development and physiological metabolism. The supply of N after mineralizing soil organic matter under FYM-applied treatments is a vital plant nutrition process that the high C/N ratio of biochar may hinder. FYM contains nutrients like C, N, P, and K and is commonly considered a good nitrogen source (Apori et al. 2021; Rehman et al. 2021). A study found that combined rice husk ash and FYM treatments resulted in higher soil N content but lower microbial biomass N content. These observations revealed that most of the nutrients available for plant growth might become tightly bound to the surfaces of high C/N ratio biochar and remain unavailable to the plant roots, resulting in poor plant growth and crop performance. In contrast, in another study conducted in silty loam soil with FYM application,

nutrient immobilization caused by increased microbial activity resulted in poor nutrient availability to crop plants and lower crop yield (Singh et al.2020).

7.3.2.4 Effect of CSB and FYM amendment on plant growth parameters

Effects of CSB and FYM on early seedling growth parameters such as shoot length, fresh weight, and dry weight are represented in **Table 7.3.** Results showed that the amendment of CSB increased the plant growth parameters more effectively than the control, FYM, and CSB with FYM combination. *Solanum lycopersicum* L. showed a higher shoot length in FYM-treated soil (7.02 cm) than in control (6.34 cm). The FYM with CSB combinations (1,5 and 10 %) displayed a slightly lesser shoot length than the CSB alone treatment i.e., 1% CSB addition resulted in 8.14 cm, and combined application of 1 % CSB with FYM showed 7.96 cm in shoot length. The highest shoot length of 9.16 cm was obtained with 10% CSB, almost equal to 5 % CSB addition (9.14 cm), whereas 1 % CSB resulted in 8.14 cm of shoot length. A similar pattern of results for fresh weight was observed for 5 % and 10 % CSB (0.94 and 0.90 g respectively vs 0.62 g for control). The dry weight of *Solanum lycopersicum* L. in control and FYM treatment were equal (0.11 g). However, CSB and CSB with FYM combinations (1, 5 and 10 %) displayed a similar pattern as that of shoot length and fresh weight. However, the difference was marginal i.e., dry weight of 0.18 g was observed for 10 % CSB application, whereas a similar concentration of CSB with FYM showed 0.16 g. Application of CSB improved soil porosity and water-holding capacity, resulting in increased plant root development and nutrient uptake. It also aided in enhancing plant biomass. The increase in plant growth parameters in response to the application of FYM is adduced to the fact that FYM contains nutrients like C, N, P, and K, which are released to the soil for plants compared with control.

Improvements in plant growth after the CSB amendment in soil could be directly attributed to the organic carbon content in amended biochar (Farooque et al. 2020), and it was demonstrated to be effective in enzyme synthesis, seed germination, and nutrient promotion (Rehman et al. 2020). The application of CSB with FYM showed an increase in the plant growth parameters, but their effect was less than treatments with CSB. The increase in plant growth has been attributed to nutrients present in the CSB, which highly influenced seedling growth (Rehman et al. 2020).

Table 7.3. Effect of biochar on shoot length, plant fresh weight, and plant dry weight in different soil samples.

Treatments	Shoot length (cm)	Fresh weight (g)	Dry weight (g)
Control	6.34±0.35	0.62±0.02	0.11±0.01
FYM	7.02±0.21	0.72±0.02	0.11±0.01
1 % CSB	8.14±0.48	0.80±0.02	0.15±0.01
1 % CSB + FYM	7.96±0.48	0.74±0.03	0.12±0.01
5 % CSB	9.14±0.36	0.94±0.02	0.20±0.03
5 % CSB +FYM	8.16±0.55	0.78±0.03	0.16±0.02
10 % CSB	9.16±0.29	0.90±0.04	0.18±0.01
10 % CSB+FYM	7.5±0.26	0.71±0.04	0.16±0.03

7.3.2.5 Changes in soil properties after enhancement

The changes in soil properties were determined to verify the influences and enhancement effect of CSB in the soil. *Solanum lycopersicum* L. plants grown in control soil displayed less growth than those with a 5 % CSB application rate (**Figure A3,** Appendix I). **Table 7.4** indicates the changes in soil parameters after enhancement. The pH increased in soil with 5 % CSB (6.6) compared to the control (6.3) due to the alkaline composition of CSB because the carbonate component of alkaline biochar helps liming in soils and can raise the pH (Sun et al. 2023). Soil organic carbon strongly impacts soil quality and functionality (Rehman et al. 2020). The application of 5 % CSB increased soil organic carbon from 0.70 to 0.82 %. A combination of macronutrients and micronutrients gives the soil its optimum health (Singh et al. 2019). Zn content increased in soil modified with 5 % CSB. The increase in Zn availability could be attributed to CSB containing Zn (**Table 7.4**) and the subsequent release of Zn into the soil. The impact of biochar on soil pH can affect the concentrations of micronutrients in the soil and their availability (Manikandan et al. 2022). Decreased soil available Mn, Fe, and Cu with 5 % CSB addition may be due to increased soil pH. Biochar application can also reduce soil micronutrient availability (Karimi et al. 2020). However, other studies observed contrasting findings and reported adding biochar increased soil micronutrient availability (Das et al.

2021). The decrease in available S and B from 3.97 to 0.79 and 0.40 to 0.04 (mg kg^{-1}) could be attributed to *Solanum lycopersicum* L. uptake, reducing their soil concentrations.

Table 7.4. Soil properties after enhancement.

pH	Soil organic carbon	P	K	Zn	Mn	Fe	Cu	S	B
	(%)	(kg ha^{-1})		(mg kg^{-1})					
6.60	0.82	35	301	2.27	18.90	67.20	3.30	0.79	0.04

7.3.2.6 Soil enzyme activity after enhancement

Enzymatic activity in agricultural soils has long been used as a fertility and productivity indicator (Muniswami et al. 2021; Noronha et al. 2022). High enzymatic activity rates are often used to indicate good soil quality (Yang et al. 2020). The activity of β-glucosidase in the soil is essential for catalyzing the hydrolysis of various β-glucosides (Yadav et al. 2022). Phosphatase is an enzyme that catalyzes the hydrolysis of anhydrous phosphoric acid in soil and indicates organic phosphorous mineralization potential (Ouallal et al. 2022).

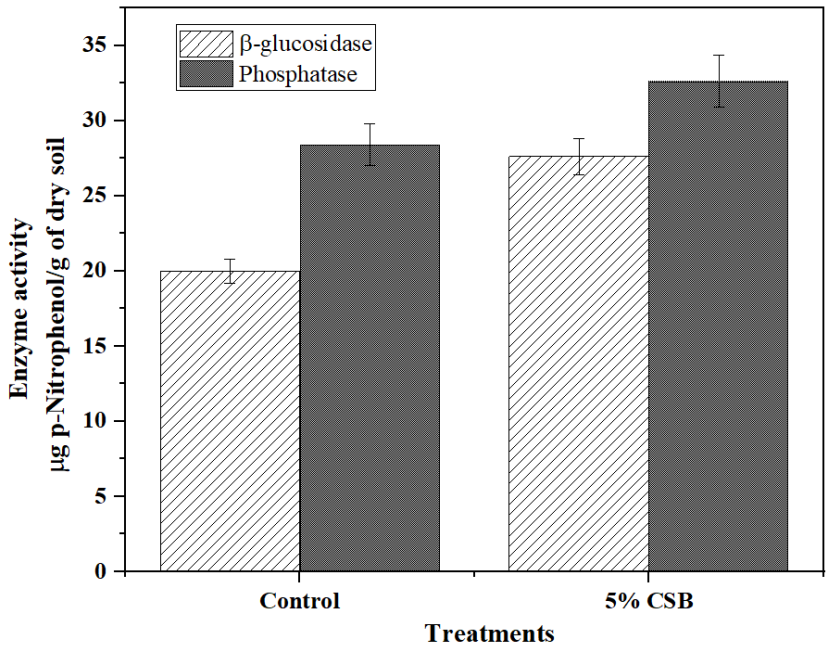

Figure 7.20. ß-glucosidase and phosphatase activity of soil treated with 5 % CSB.

Variations in phosphatase activity are a reliable indicator of soil fertility because they show changes in the quantity and quality of phosphorated substrates (Ouallal et al. 2022). **Figure 7.20**. depicts the soil β – glucosidase and phosphatase activities in the soil. When the soil was amended with a 5 % CSB dosage, glucosidase activity increased from 20 to 27.63 µg of p- Nitrophenol g^{-1} of soil, and phosphatase activity increased from 28.4 to 32.64 µg of p- Nitrophenol g^{-1} of soil. CSB application positively affected soil enzyme activity in terms of its increment. Due to the presence of organic carbon, amended CSB quickly decomposed, resulting in high enzyme activities (Noronha et al. 2022).

7.3.2.7 Phyto availability of Cd

Heavy metal mobility and bioavailability are frequently predicted using DTPA extraction. The DTPA-extractable Cd in the control soil was 1.3 mg kg^{-1}, and the values decreased as the incubation time increased **(Figure 7.21).**

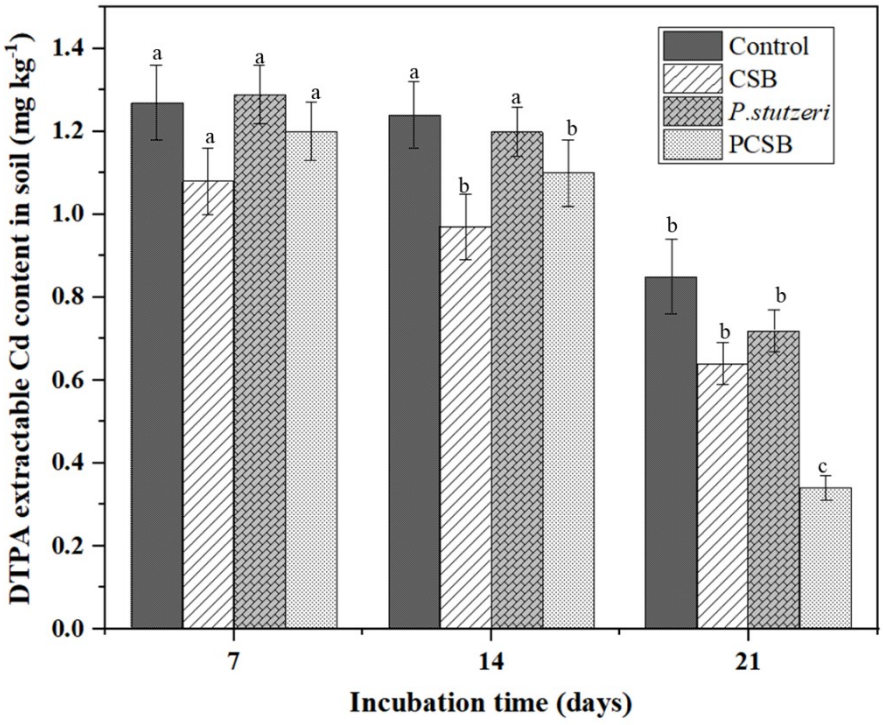

Figure 7.21. Changes of DTPA-Cd in the soil during remediation.

All the amendments showed a gradual decrease in DTPA-Cd with increased incubation time. The addition of 5 % CSB reduced bioavailable Cd to 0.64 mg kg^{-1} after 21 days of incubation. In contrast,

the PCSB amendment reduced DTPA-Cd to 0.34 mg kg^{-1}. Compared to the CSB amendment, PCSB with the same dosage was more effective in reducing DTPA-Cd. It revealed a synergistic effect of biochar and *P. stutzeri* on Cd immobilization. The variations in soil properties induced by amendments are responsible for decreasing bioavailable metal concentration (Tu et al. 2020). SEM and FTIR analysis revealed that the surface area and porous structure of CSB **(Figure 7.16)** could adsorb metal ions, and functional groups on the biochar and bacterial cell surface could participate in heavy metal biosorption. Furthermore, biochar could provide a safe habitat for *P. stutzeri* and nutrient elements C, N, and P to *P. stutzeri* and indigenous microorganisms for growth (Wahla et al. 2020). Our findings also showed that CSB could significantly improve soil properties and enzyme activities in sections 3.5 and 3.6. In addition, combining functional microbes and a biochar amendment could be a promising technology for the sustainable remediation of polluted soil.

CHAPTER 8

CP REMOVAL FROM WATER AND SOIL USING MICROBIAL CELL-IMMOBILIZED BIOCHAR

8.1 ISOLATION OF CP- TOLERANT BACTERIA

CP- tolerant bacteria were isolated by enrichment and domestication techniques. This screening process yielded eight morphologically diverse bacterial colonies (**Figure 8.1**), each subjected to analysis for their tolerance to CP. Among these species, only three exhibited visible CP tolerance, with one strain demonstrating superior growth at elevated CP concentrations (50 mg L^{-1}). Consequently, the bacterial strain displaying enhanced tolerance at higher CP concentrations was isolated, and its broth culture was prepared using MSM.

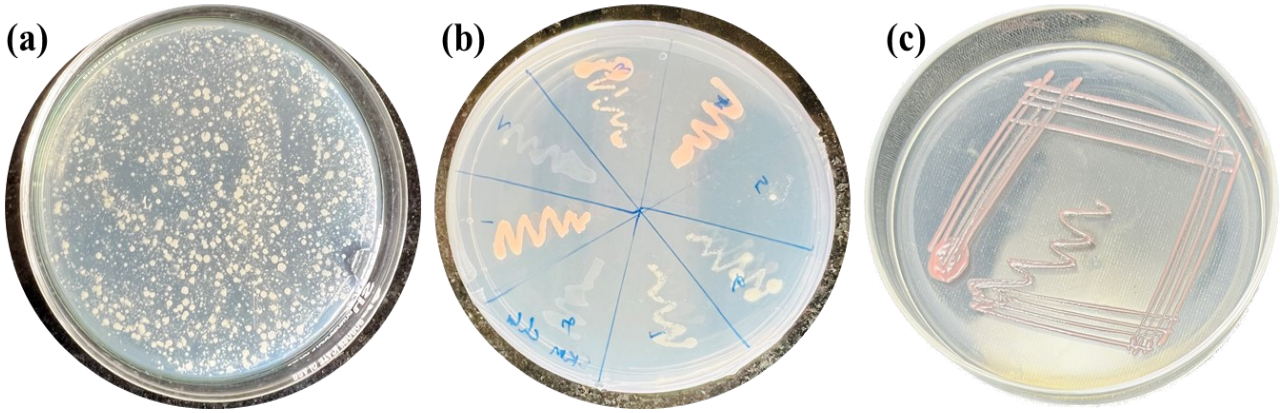

Figure 8.1. Isolation of CP tolerant strain **(a)** Different colonies of bacteria grown in MSM+CP plate **(b)** Purified CP tolerant isolates **(c)** Selected isolate grown at 50 mg L^{-1} CP.

8.2 IDENTIFICATION OF CP DEGRADING BACTERIA

The isolated bacteria were first identified based on the morphological, and cultural characteristics of individual colonies. The individual isolated colony was re-streaked on minimal salt agar plates for identification. Selected strain showed gram negative rods and grown well in temperature range

of 30-40 °C. 16 S rRNA gene sequencing for identification of bacterial phylogeny and taxonomy, the isolated strain was identified as *Aeromonas veronii* (*A.veronii*). BLAST analysis indicated that the sequence exhibited 100 % homology with *Aeromonas veronii* strain LPD2SHD2. The partial 16S rDNA nucleotide sequence was deposited to NCBI with the accession number OQ102239. The phylogenetic tree was constructed using the partial 16S rDNA sequences of the isolate *A. veronii* SVNITK with NCBI database sequences (**Figure 8.2).** Aeromonads are gram-negative facultative anaerobes, commonly found in fresh surface waters (Szewzyk et al., 2000), which possess a wide variety of exoenzymes, active in the biodegradation of organic compounds (amylases, proteases, lipases, nucleases, etc.).

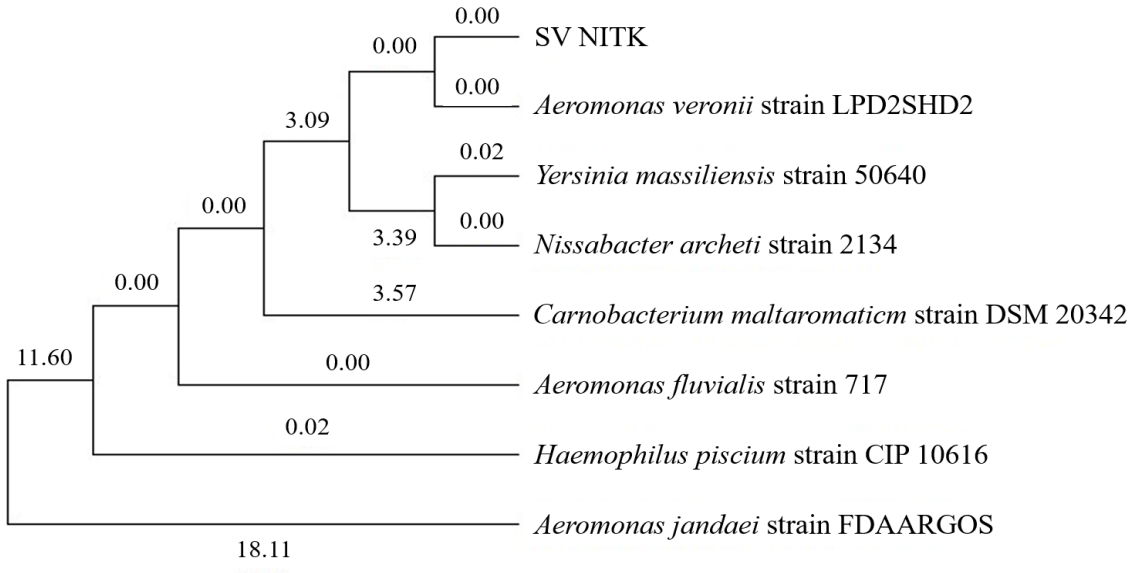

Figure 8.2. Phylogenetic tree of *A.veronii* SV NITK.

8.3 GROWTH RESPONSE AND CP REMOVAL BY *A. veronii*

A time-dependent decrease in CP concentration by the *A.veronii* strain is depicted in **Figure 8.3.** At the beginning of the experiment, the bacteria exhibited less CP removal capacity in both 10 and 50 mg L^{-1} concentrations, indicating an initial adaptation to this pesticide. However, after 12 h, a remarkable CP removal rate of 52.3 % (10 mg L^{-1}) and 27.38 % (50 mg L^{-1}) was observed. This value increased further; at 60 h, the removal efficiency reached 92.12 % and 54.76 % for 10 mg L^{-1} and 50 mg L^{-1} CP, respectively. The progressive increase in CP removal percentage suggests the ability of *A.veronii* to adapt and enhance its degradation capabilities, possibly through activating

specific metabolic pathways or the induction of hydrolytic enzymes responsible for CP breakdown (Chishti et al. 2013).

Growth response and CP removal by *A. veronii* were conducted at an incubation temperature of 30 °C and an initial solution pH of 6.5. *A. veronii* exhibited maximum growth in the samples incubated at 25-30 °C and declined at higher temperatures (**Figure 8.3**). Chen et al. (2019) and Ormanci and Yucel (2017) reported optimal growth at 30 °C. Additionally, studies by Silambarasan et al. Silambarasan and Abraham (2013) reported efficient CP degradation at 30 °C. The microbial degradation of CP has been widely studied under a pH of 6.5 (Das and Adhya 2015b; Singh et al. 2006).

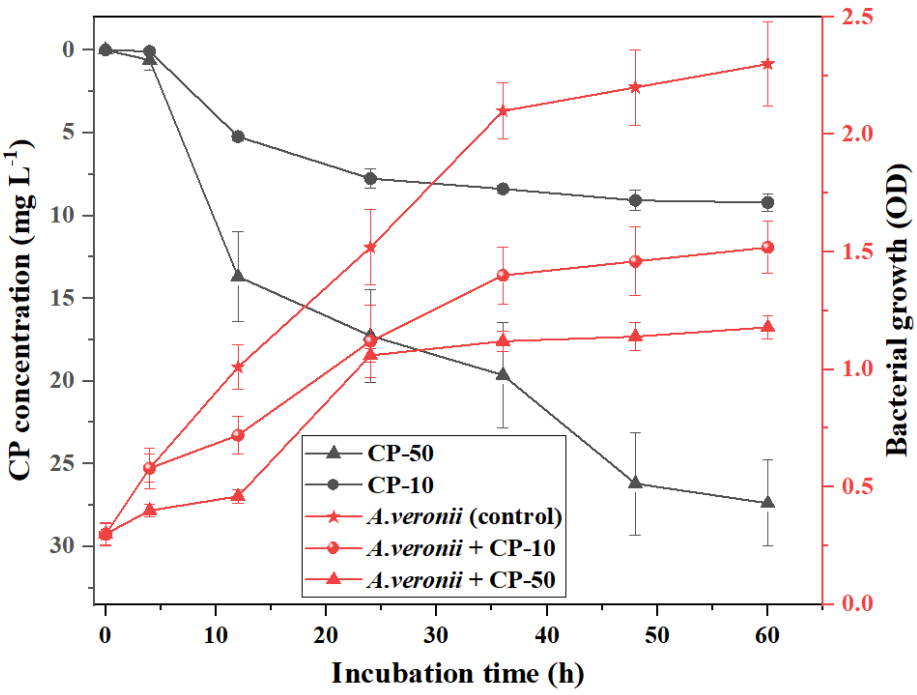

Figure 8.3. Growth curve and CP removal efficiency of *A.veronii.*

The growth curve of *A.veronii* exhibited a time-dependent decrease in CP concentration (**Figure 8.3**), indicating an initial adaptation to the pesticide. After 12 h, CP removal rates reached 52.3 % (10 mg L^{-1}) and 27.38 % (50 mg L^{-1}), which further increased to 54.76 % (50 mg L^{-1}) and 92.12 % (10 mg L^{-1}) at 60 h. This indicates the strain's ability to adapt and enhance its degradation capabilities, possibly through activating specific metabolic pathways or hydrolytic enzymes.

Enzymes like hydrolases are pivotal in CP degradation, hydrolyzing its ester bond (Gao et al. 2012). Specific enzymes such as organophosphorus hydrolase, phosphotriesterase, and organophosphorus acid anhydrolase play key roles in catalyzing various organophosphorus pesticides. These enzymes, present in diverse microorganisms, target specific bonds in pesticides, revealing varied pathways for degradation. The growth of *A.veronii* in the presence of CP showed a lag phase at the onset, but at 4 h, the growth rate notably increased, peaking at 36 h (**Figure 8.3**). This suggests that the bacterial strain can utilize CP as a carbon source for enhanced growth (Govarthanan et al. 2020; Shabbir et al. 2018b). Studies on *Cladosporium cladosporioides* Hu-01 and *Pseudomonas nitroreducens* AR-3, have demonstrated CP degradation (Aswathi et al. 2019b; Gao et al. 2012). The growth of *A.veronii* in the presence of CP showed a lag phase at the onset, but at 4 h, the growth rate notably increased, peaking at 36 h. This suggests that the bacterial strain can utilize CP as a carbon source for enhanced growth (Govarthanan et al. 2020; Shabbir et al. 2018).

8.4 IMMOBILIZATION OF *A.veronii*

Pyrolysis temperature is essential to biochar properties during production (Manikandan et al. 2022). Surface area, pore size, and functional groups are important criteria for choosing biochar as a carrier for immobilizing bacteria (Ajeng et al. 2020). **Figure 8.4** depicts the impact of different pyrolysis temperatures on CP removal and the immobilization of *A.veronii* on biochar. Biochar samples were produced at three different temperatures: 300 °C, 500 °C, and 700 °C, and the immobilized cell number in terms of Log_{10} cells g^{-1} of RHB and respective removal rates were calculated. The results indicated significant variations in CP removal and immobilized cell numbers among the different pyrolysis temperatures. At a pyrolysis temperature of 300 °C, the CP removal percentage was 66.2 % with 5.2 Log_{10} cells g^{-1} RHB of immobilized cells. As the pyrolysis temperature increased to 500 °C, the CP removal percentage significantly improved to 95.6 %, and the number of immobilized cells increased to 9.61 Log_{10} cells g^{-1}. Interestingly, at a pyrolysis temperature of 700 °C, the CP removal percentage decreased slightly to 88.46 %, while the number of immobilized cells remained relatively high at 8.90 Log_{10} cells g^{-1} RHB.

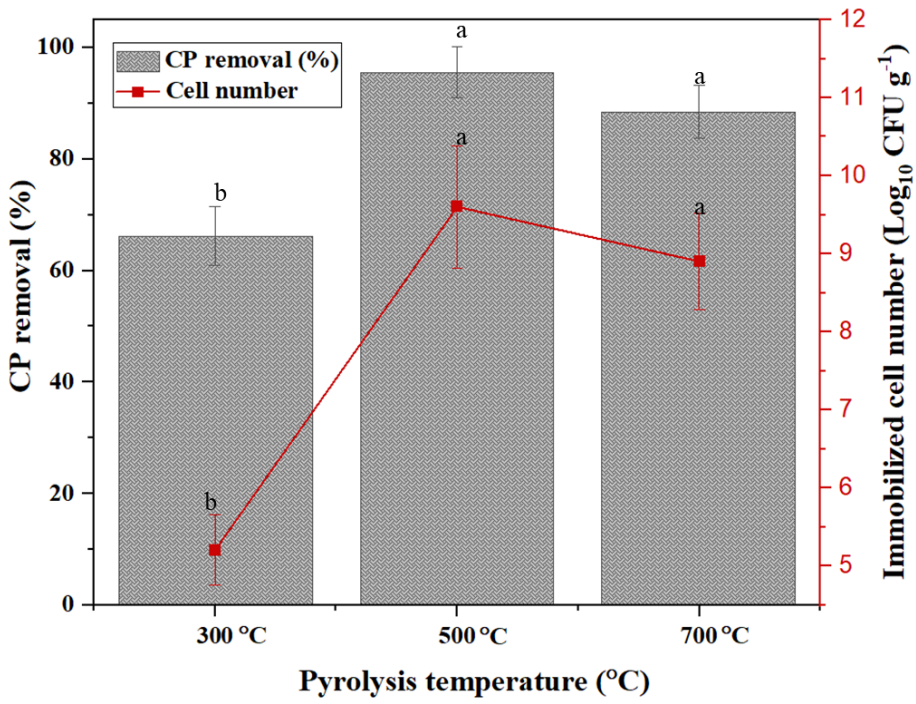

Figure 8.4. Immobilization and removal efficiency of ARHB prepared at various temperatures (300, 500, and 700 °C) and time 30 min.

The observed trend in CP removal percentage suggests that an increase in pyrolysis temperature positively influences the sorption capacity of biochar. Higher temperatures during pyrolysis increase carbonization, pore volume and surface area, enhancing the biochar's ability to effectively adsorb CP molecules (Wang et al. 2015). The higher number of immobilized cells observed at 500 °C compared to 300 °C suggests that the surface properties of biochar produced at higher temperatures are more conducive to microbial colonization and growth (**Figure 4.4**). The increased porosity and surface area of biochar produced at higher temperatures likely provide favorable microhabitats for microbial attachment and subsequent metabolic activity (Ajeng et al. 2020; Liu et al. 2019). The slight decrease in CP removal percentage observed at 700 °C compared to 500 °C may be attributed to the thermal degradation of biochar's surface functional groups (**Figure 4.5a**.) (Zhao et al. 2017). At higher pyrolysis temperatures, the loss of oxygen-containing functional groups on biochar surfaces can reduce the adsorption capacity of CP molecules (**Figure 4.5a**) (Liu et al. 2019). Nevertheless, the substantial presence of immobilized cells at 700 °C indicates that the biochar maintains a favourable environment for microbial activity, even with a potential decline in sorption capacity. The findings indicate that

biochar produced at 500 °C immobilized cells exhibited the highest CP removal and a greater number of cells was selected as the carrier for further investigation.

8.5 CHARACTERISATION OF BIOCHAR AND ARHB

Surface functional groups can provide important insight into the characteristics of biochar and microbial cells and the immobilized cells on biochar. Immobilization of *A. veronii* on rice husk biochar was investigated using FTIR studies to analyze the functional groups involved. The height of each FTIR peak can reflect the changes occurring after immobilization in RHB. A comparison between RHB and ARHB revealed sharper peaks in ARHB, suggesting an increase in functional groups due to the incorporation of *A.veronii* by biochar. Conversely, a comparison of *A.veronii* before and after immobilization onto RHB indicated that the peaks of ARHB were comparatively less sharp, possibly indicating the entrapment of some bacteria within RHB pores, thus demonstrating successful immobilization.

The intense peaks observed at 3435 cm^{-1} in the FTIR spectrum can be attributed to O-H and NH- stretching vibrations (Filip and Hermann 2001). These peaks were more prominent in *A. veronii* than RHB and ARHB due to NH- groups in the bacterial cells (**Figure 8.5a**). In addition, peaks at 2925 cm^{-1} were observed in three materials, which are associated with the C-H group vibrations of alkane ($-CH_2$). In the case of bacteria adjacent to this peak, other peaks were observed at approximately 2850 cm^{-1}, indicating the presence of methyl ($-CH_3$) groups. The peaks at around 1638 cm^{-1} and 1441 cm^{-1} corresponded to the C=O stretching vibration mode of the carboxyl group in RHB and ARHB, while in *A. veronii*, it indicated the presence of the amide group (NH_2CO). Interestingly, the same peak was sharper in ARHB compared to RHB, suggesting changes due to the immobilization process. Peaks at 1259 cm^{-1} may be attributed to the presence of the -NH group, which is unique to bacteria and absent in both RHB and ARHB. Broad peaks in RHB and ARHB at 1070 cm^{-1} indicates C-O-C stretch of the ethers present in lignin or Si-O-Si (Pattnaik et al. 2018) and the peak at 808 cm^{-1} indicate Si-O-Si (Zhen-Yu et al. 2012), the main component of rice husk, but absent in *A. veronii*. Moreover, the sharp peaks observed at 1079 cm^{-1} and 880 cm^{-1} in *A. veronii* indicate the presence of phosphate functional groups (Liu et al. 2015b). However, in ARHB, the peak at 880 cm^{-1} disappeared after immobilization. These findings provide insights into the immobilization process.

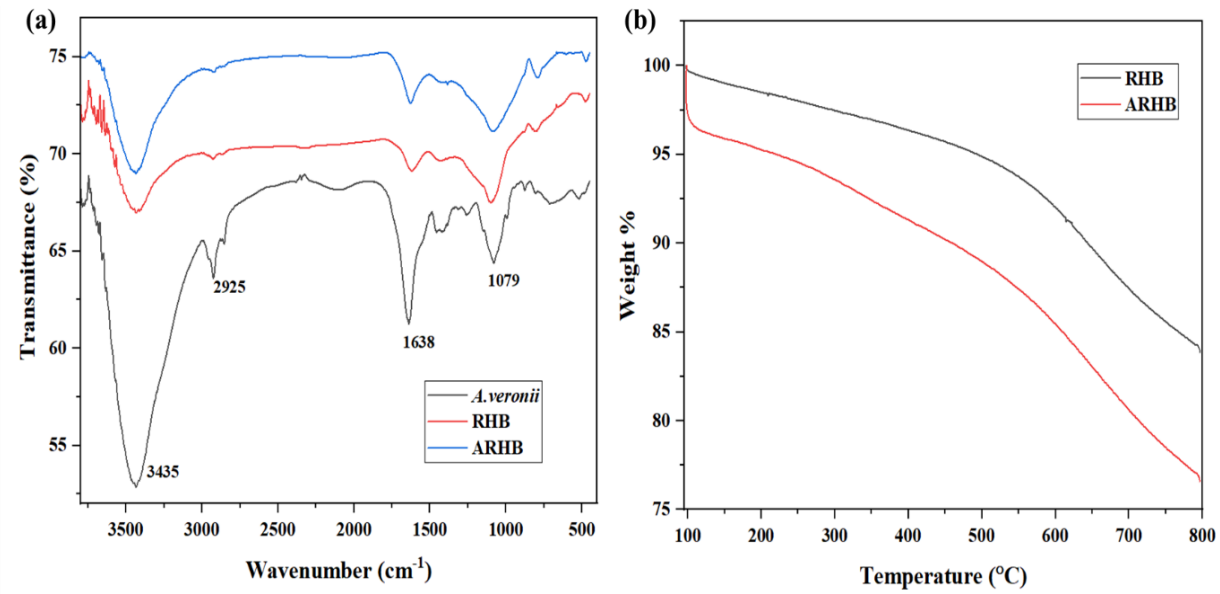

Figure 8.5. (a) FTIR spectra of A.*veronii*, RHB, and ARHB **(b)** TGA of RHB and ARHB.

Figure 8.5b presents the TGA analysis of RHB and ARHB. As the temperature increases, both RHB and ARHB show a gradual decrease in weight. RHB and ARHB showed that heating the sample at 100 °C removed hygroscopic water, sorbed gases, and various volatile low-molecular-weight organic compounds from the surface (Burachevskaya et al. 2023). The comparative analysis during TGA indicated a lower decomposition rate for ARHB in contrast to RHB. Both samples were initially equal in quantity, highlighting that the variance in weight loss is due to the degradation of bacteria immobilized on ARHB.

The SEM image of RHB and ARHB is shown in **Figure 8.6**. RHB displayed abundant pore distribution and large pore size higher than 6 µm. This structural property provided a suitable habitat for microbial colonization and proliferation with several micropores, which have a high adsorption capacity for microorganisms. The *A.veronii* strain exhibited a short and rod-shaped morphology, approximately 1.74 µm in length. ARHB showed the presence of immobilized *A.veronii,* indicating RHB provided sufficient space for bacteria to enter the pore channel. The abundant pores on RHB facilitate mass transfer and pollutant degradation and provide sufficient space for bacterial attachment, proliferation, and nutrient exchange (Tu et al. 2020; Wahla et al. 2020).

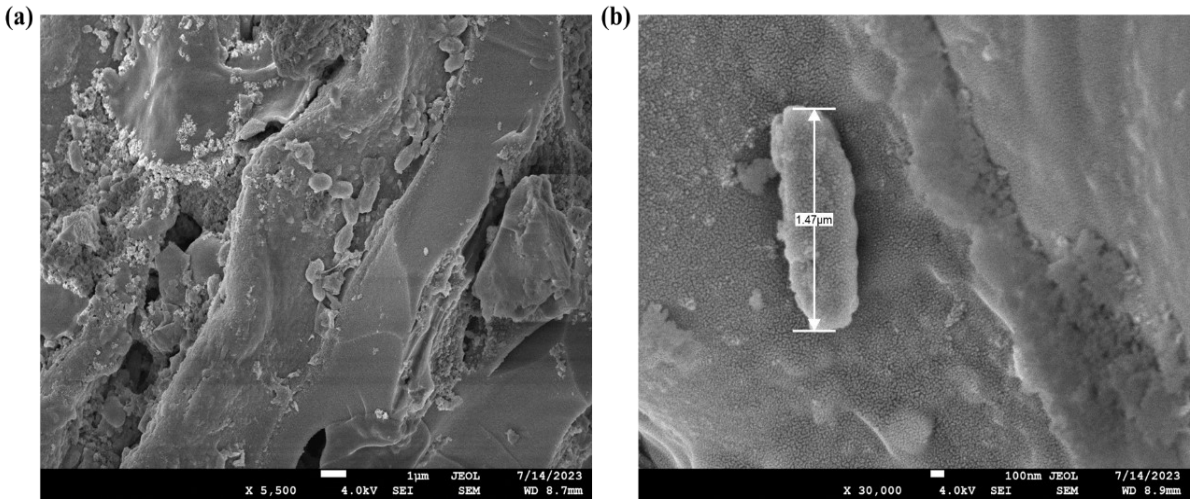

Figure 8.6. FE-SEM image of ARHB at different magnifications **(a)** 5500 X **(b)** 30kX.

8.6 OPTIMIZATION OF CP REMOVAL BY ARHB

Response Surface Methodology, employing the Box-Behnken design, aims to assess the interactive effects of chosen parameters on CP removal by ARHB. This methodology involves using quantitative data from experiments and employing multiple regression analysis (Khatoon and Rai 2020; Shilli et al. 2023). The Box-Behnken design is recognized for its robustness in efficiently exploring the response surface while minimizing the number of experimental runs, thereby saving time and resources (Nam et al. 2018). It is often regarded as a more efficient and practical alternative to CCD, which demands more experiments, time, and costs to construct the model equation (Nam et al. 2018; Oza et al. 2022). This established method within Response Surface Methodology facilitates evaluating factors and their interactions within a quadratic model, avoiding extreme combinations of variables and ensuring the model's effectiveness.

A total of 17 experiments were conducted, including five central runs, which involved three independent parameters, with the response being the percentage of CP removal. **Table 8.1** presents the actual and predicted values of the CP removal capacity of ARHB. The close relationship between the actual and predicted values is confirmed by regression analysis, with an R^2 value close to 1 indicating less deviation, as illustrated in **Figure 8.7**. The actual values represent the measured response data for each specific run, while the predicted values are determined using the approximating functions generated by the models.

Table 8.1 Box Behnken experimental design of independent variables and the response of dependent variable CP degradation.

Run	Factors			% Removal	
	A: CP concentration	B: ARHB dosage	C: Incubation time	Actual	Predicted
1	30	1.25	24	96.12	95.37
2	50	0.5	24	12.8	12.95
3	30	1.25	24	96.61	95.37
4	30	1.25	24	94.58	95.37
5	50	1.25	12	22.18	23.19
6	30	2	12	14.32	13.47
7	10	1.25	12	27.41	28.41
8	50	1.25	36	53.6	52.60
9	30	1.25	24	95.27	95.37
10	30	0.5	36	40.28	41.13
11	30	2	36	87.3	88.46
12	30	1.25	24	94.28	95.37
13	10	0.5	24	45.32	45.48
14	10	2	24	58.4	58.25
15	30	0.5	12	20.11	18.95
16	10	1.25	36	97.15	96.14
17	50	2	24	42.18	42.02

The empirical relationship between the coded parameters and the removal percentage was determined using regression analysis. The developed quadratic model for pesticide remediation is presented in Equation 8.1.

$$\% \text{ Removal} = 95.37 - 12.19 * A + 10.46 * B + 24.29 * C + 4.07 * AB - 9.58 * AC + 13.20 * BC - 23.06 * A^2 - 32.64 * B^2 - 22.23 * C^2 \quad (8.1)$$

The coefficients in the equation represent the effects of the factors A (CP concentration), B (ARHB dosage), and C (incubation time), as well as their interactions (AB, AC, and BC) and the quadratic terms (A^2, B^2, and C^2).

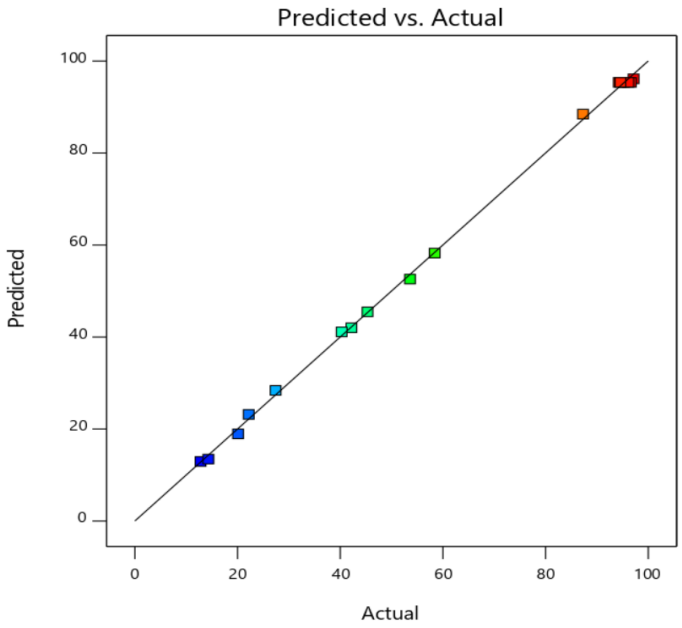

Figure 8.7. Validation of Predicted vs. Actual values for CP removal by ARHB.

The developed quadratic model for pesticide remediation was evaluated using ANOVA analysis, and the findings are presented in (**Table A1,** Appendix V). The significant F-value of the model (1135.29) indicates its relevance to the pesticide remediation process. Moreover, the Lack of Fit F-value (2.79) suggests a 17.34 % chance that a Lack of Fit F-value this large could occur due to noise. The R^2 Pred (0.99) further supports the model's performance and R^2 Adj. (0.99) values indicate a satisfactory fit for CP remediation capacity with ARHB. The graphical representation of the response surface illustrated the effects of two variables on CP removal, keeping the other variable at a fixed level. The 3D plots and contour plots are displayed in **Figure 8.8 (a-c).**

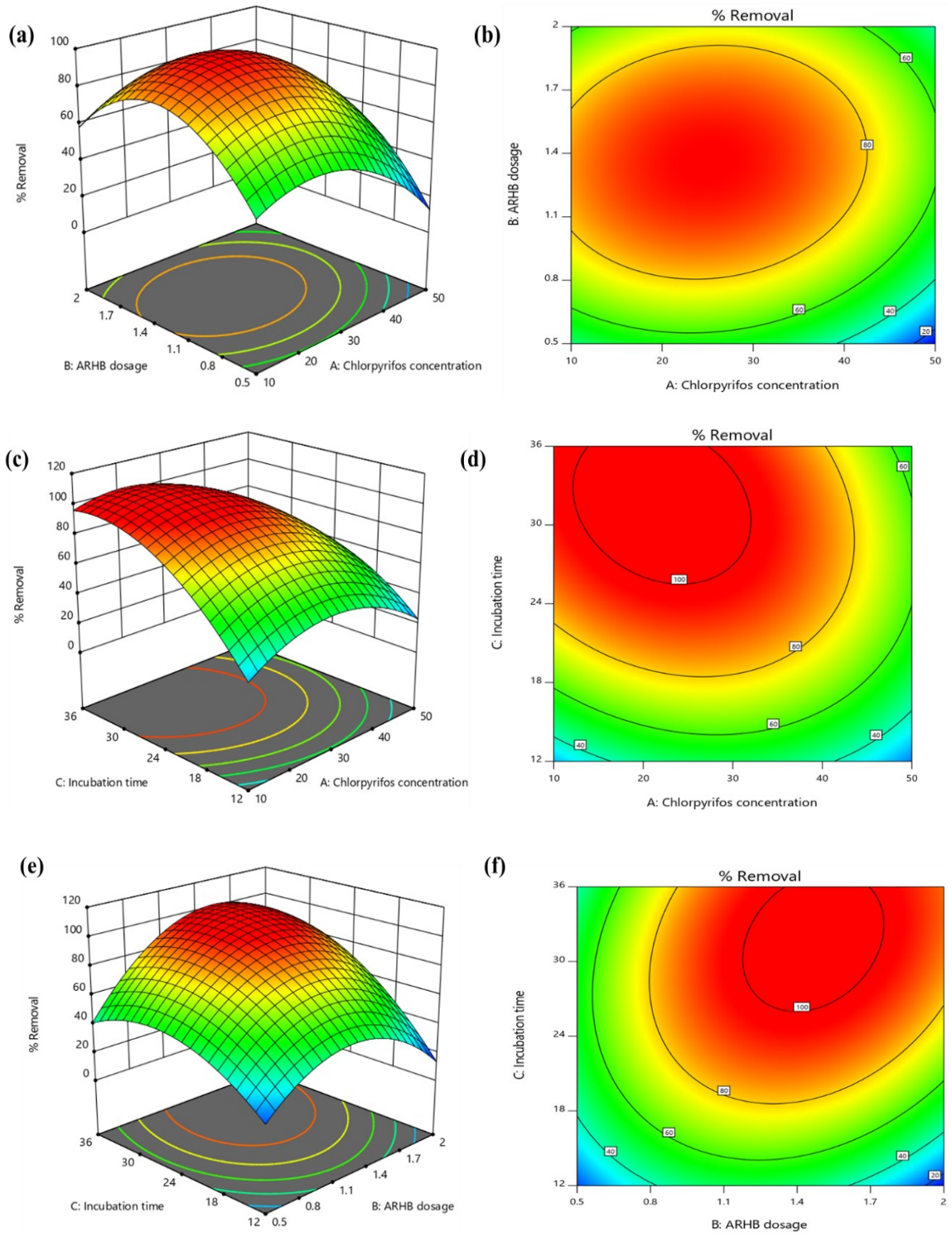

Figure 8.8. The 3D plots and contour plots showing the effect of (a). CP concentration and ARHB dosage (b). CP concentration and incubation time (c). ARHB dosage and incubation time on CP removal.

8.6.1 Effect of CP concentration and ARHB dosage

The interactive effect of CP concentration and ARHB dosage on CP remediation using ARHB was investigated in this study. **Figure 8.8a** presents a 3D and contour plot illustrating the interactive effect of ARHB dose and pesticide concentration at 24 h of incubation. At an initial CP concentration of 10 mg L^{-1} and an ARHB dosage of 0.5 g L^{-1}, the removal efficiency was 53 %. However, as the initial CP concentration increased to 30 mg L^{-1} and the biomass dosage increased to 1.5 g L^{-1}, the removal efficiency improved to 92 %. This finding is consistent with previous research that has highlighted the importance of pesticide concentration and biocatalyst dosage in the biodegradation of CP (Jacob et al. 2020b; Malla et al. 2023). The removal efficiency started to decline beyond 30 mg L^{-1} CP concentration, potentially due to the negative impact of higher concentrations on the bacterial cells. The initial study on bacterial tolerance underscored the ability of *A.veronii* to tolerate up to 50 mg L^{-1}, suggesting a threshold beyond which elevated concentrations negatively impact bacterial survival. The diminished microbial growth at higher CP concentrations may result in a slower degradation rate of CP (Malla et al. 2023). The removal efficiency of CP involves the combined action of *A.veronii* and RHB. The properties of RHB significantly influence the remediation efficiency. As CP concentrations increase, the ability of ARHB to adsorb CP decreases due to saturation, leading to a reduction in the percentage of CP removal. Consequently, a higher dosage of ARHB was necessary for the removal of higher concentrations of CP.

8.6.2 CP concentration and incubation time

The 3D surface plots and contour plots presenting the interaction effect of CP concentration and incubation time for its remediation are shown in **Figure 8.8b** at a fixed ARHB dose of 1.25 g L^{-1}. At an initial CP concentration of 10 mg L^{-1} and an incubation time of 24 h, the removal efficiency was found to be 45.32 %. However, as the initial CP concentration increased to 50 mg L^{-1}, the removal efficiency decreased to 12.8 %. The observed decrease in remediation with increasing CP concentration suggests that the surface area and active sites of ARHB become saturated, reducing CP removal. This saturation effect can limit the adsorption capacity of the ARHB resulting in a decrease in overall remediation efficiency (Manikandan and Nair 2022). A study conducted by Shirzad Siboni et al. 2015 on CTAB-modified nanoclay for herbicide adsorption in aqueous solutions indicated that adsorbents possess a finite number of active sites, which can reach saturation beyond a specific concentration threshold of bentazon herbicide. This limitation in active sites

impacting adsorption efficiency has also been reported in various studies exploring diverse pesticides and utilizing different adsorbents adsorbents (Ayranci and Hoda 2005). The efficiency of CP removal exhibits an increase over incubation time, reaching an adsorption equilibrium, where extending beyond 24 h demonstrates minimal impact on removal efficiency. This is attributed to the reduced growth of *A. veronii* at higher concentrations for the free cell. However, in ARHB, the RHB supported the cells, thus maintaining removal efficiency.

8.6.3 Effect of ARHB dosage and incubation time

The results presented in **Figure 8.8c** demonstrate the combined effects of ARHB dosage and incubation time on the removal of CP. As the ARHB dosage increased, there was a corresponding increase in CP removal up to optimum level; further, it decreased. The removal efficiency of CP concentration of 10 mg L^{-1} was 45.32 % when ARHB dosage was 0.5 g L^{-1} and incubation time was 24 h. The CP removal efficiency increased to 58.4 % when the ARHB dosage was 2 g L^{-1} at the same incubation time. This finding suggests that increasing the ARHB dosage enhances the adsorption capacity and effectiveness of the biochar in removing CP from the solution. However, it is noteworthy that further increases in the ARHB dosage resulted in a decrease in CP remediation. At C concentration of 30 mg L^{-1}, increasing the dosage to 2 g L^{-1} reduced CP removal to 88 %. It's worth noting that a specific dosage was crucial for effective remediation. Notably, lower ARHB concentrations and extended incubation periods didn't lead to CP removal. Conversely, a minimum concentration of 1.375 g L^{-1} resulted in optimal CP removal. This could be due to biochar particle agglomeration, potentially restricting CP to active adsorption sites on the biochar surface.

The optimal conditions for CP remediation using biochar were determined as a pesticide concentration of 30 mg L^{-1}, an ARHB dose of 1.375 g L^{-1}, and an incubation time of 24 h. Validation of the statistical model and regression equation was performed based on the optimal conditions suggested by the model. The predicted response for CP removal was 96.25 %, and the experimental result was 98.18 %, thus proving the validity of the model.

8.7 CP REMOVAL BY RHB, *A.veronii* AND ARHB

CP removal by *A.veronii*, RHB, and ARHB was performed at an optimized incubation temperature of 30 °C, initial solution pH 6.5, ARHB dosage of 1.375 g L^{-1}, 24 h of incubation time, and 30 mg L^{-1} initial CP concentration (**Figure 8.9a**). As shown, the CP removal efficiency was

highest when ARHB was employed, with a removal rate of 96.45 %. *A. veronii* alone exhibited a CP removal efficiency of 66.81 %, indicating its inherent capability to degrade CP. However, the lower efficiency compared to ARHB suggests that the immobilization onto RHB enhances the bacterium's performance. Similarly, RHB alone achieved a removal efficiency of 50.76 %, indicating its adsorption capacity for CP due to the high surface area and porous structure of RHB facilitating the adsorption of CP, contributing to its removal. However, the lower efficiency compared to both *A. veronii* and ARHB highlights the importance of microbial degradation in enhancing CP removal. The higher efficiency of ARHB compared to free cells implies that pore structure of the biochar provides a relatively stable growth environment for the bacteria and protects them from the toxicity of pesticides (Sun et al. 2020; Wahla et al. 2020). Jacob et al. (2021) conducted experiments assessing the removal of chlorpyrifos from aqueous systems using sugarcane bagasse biochar, achieving an impressive 89% removal from an initial concentration of 10 ppm. Singh et al. (2020) treated chlorpyrifos against potato peel biochar and observed a pesticide removal efficiency of 72.06%, further demonstrating the effectiveness of biochar-based approaches for chlorpyrifos remediation.

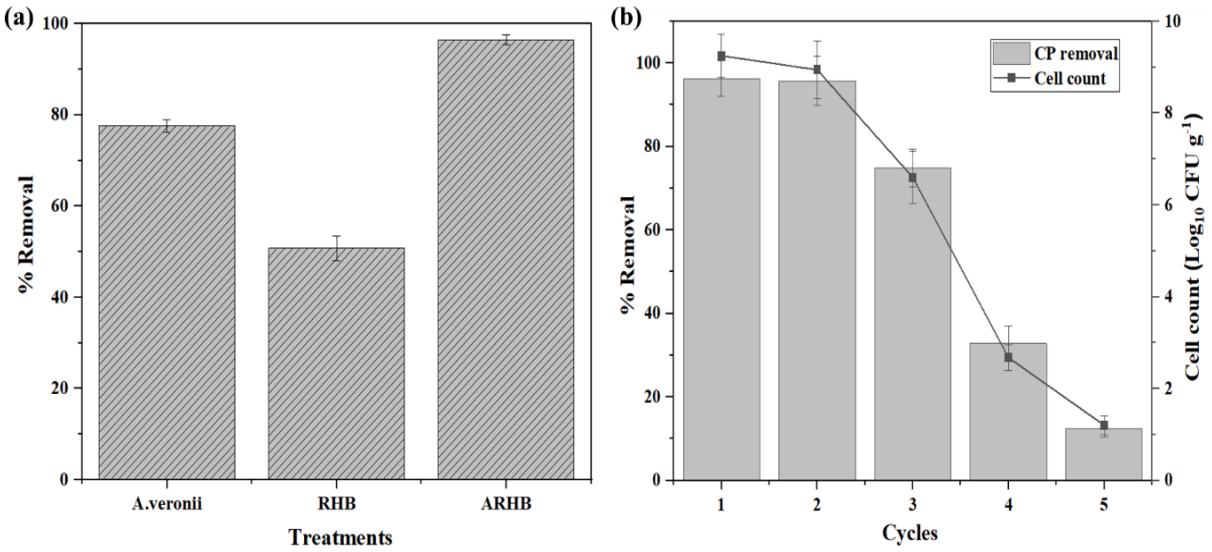

Figure 8.9. (a) Comparison of CP removal by *A.veronii*, RHB, and ARHB at optimized operating conditions **(b)** Reusability study of ARHB for CP removal (conditions-temperature of 30 °C, initial solution pH 6.5, ARHB dosage of 1.375 g L^{-1}, 24 h of incubation time, and 30 mg L^{-1} initial CP concentration).

8.8 REUSABILITY STUDY OF ARHB

The stability and reusability of ARHB for removing CP were investigated through reutilization experiments conducted over five cycles. The results are presented in **Figure 8.9b**, including the CP removal percentage and cell counts for each cycle. The initial cycle demonstrated a notable CP removal efficiency of 96.3 % by ARHB. The CP removal percentage remained relatively high as the cycles progressed, with 95.8 % and 74.9 % observed in the second and third cycles, respectively. However, a prominent decrease in CP removal was observed in the fourth and fifth cycles, with 32.8 % and 12.3 % values, respectively. This decline could be attributed to the saturation of the biocatalyst surface (Othmani et al. 2021). The cell count remained relatively stable during the subsequent cycles, indicating the viability and resilience of the immobilized cells where biochar served as a carrier with multiple porosities and offered enough space and a stable microenvironment for the growth of *A.veronii* (Zhen-Yu et al. 2012b). However, a gradual decrease in cell count was observed, in the fourth and fifth cycles, respectively. This decrease could be attributed to cell detachment or cell death of surface-immobilized cells due to prolonged exposure to CP (Manikandan and Nair 2022). Manikandan and Nair (2023) demonstrated that *P.stutzeri* immobilized on rice husk biochar exhibited higher reusability for cadmium and nickel removal compared to free cells even after five cycles. While free cells showed a prominent decrease in cell number over cycles, this was attributed to metal ion-induced inhibition of bacterial growth and enzyme activity.

8.9 CP REMOVAL FROM SOIL

CP degradation in soil was studied by analyzing the removal efficiency of *A. veronii*, RHB, and ARHB over 42 days with varying concentrations of CP at 10, 30, and 50 mg L^{-1}. All treatments, including RHB, *A.veronii*, and ARHB, significantly reduced CP levels compared to the control group at different initial concentrations **(Figure 8.10a)**. For instance, when the initial CP concentration was 10 mg L^{-1}, the application of ARHB reduced CP to 2.35 mg L^{-1} (76.5 %) at day 42. *A.veronii* showed slightly lower efficiency due to its vulnerability to environmental stress and limited survival in the soil. Whereas in ARHB, RHB and *A.veronii* combination provided adsorption sites for the enrichment of CP from soil aggregates, served as a suitable habitat and nutrient source for bacterial growth, and positively affected soil microbes, further contributing to enhanced microbial degradation (Manikandan and Nair 2022).

The effect of ARHB dosage on CP remediation was studied using RHB, *A. veronii*, and ARHB at 10 mg L^{-1} CP with dosages of 0.5, 1, and 2 g kg^{-1}. Increasing the ARHB dosage improved remediation efficiency for all treatments (**Figure 8.10b)**. The highest dosage of 2 g showed 92.4 % removal in 42 days, with ARHB consistently exhibiting the highest remediation efficiency at each dosage (**Figure 8.10c**). These findings align with previous studies showing that combining bacteria and biochar significantly increases the dissipation rates of pesticides and emphasizes the potential of biochar-immobilized strains in efficiently remediating contaminated soil (Tu et al. 2020; Wahla et al. 2020).

Microbial enzymes are commonly used as soil health indicators and are crucial in nutrient cycling (Manikandan and Nair 2023). The present study focused on the activities of two key enzymes, glucosidase and phosphatase, to assess changes in soil microbial functions under different treatments (Shilli et al. 2023; Tu et al. 2020). The enzyme activities in control soil were considerably higher than in the CP-contaminated soils, indicating that CP exerted a toxic effect on soil microbial activity (**Figure 8.10d**). The glucosidase activity was lower in the bacteria-treated soil despite the presence of CP-tolerant *A.veronii.* This could be due to the time required for the degrading bacteria to colonize and adapt to the new conditions in the soil before metabolizing CP to non-toxic levels (Sasikala et al. 2012). The biochar treatments RHB and ARHB showed higher glucosidase activities than the contaminated soil, and *A.veronii* treatments indicate that adding RHB or ARHB to the soil can rapidly restore the inhibited soil enzyme activities caused by CP. The improved enzymatic activities in ARHB treatments can be attributed to increased substrate availability and reduced toxic effects of CP on soil microbes (Govarthanan et al. 2020).

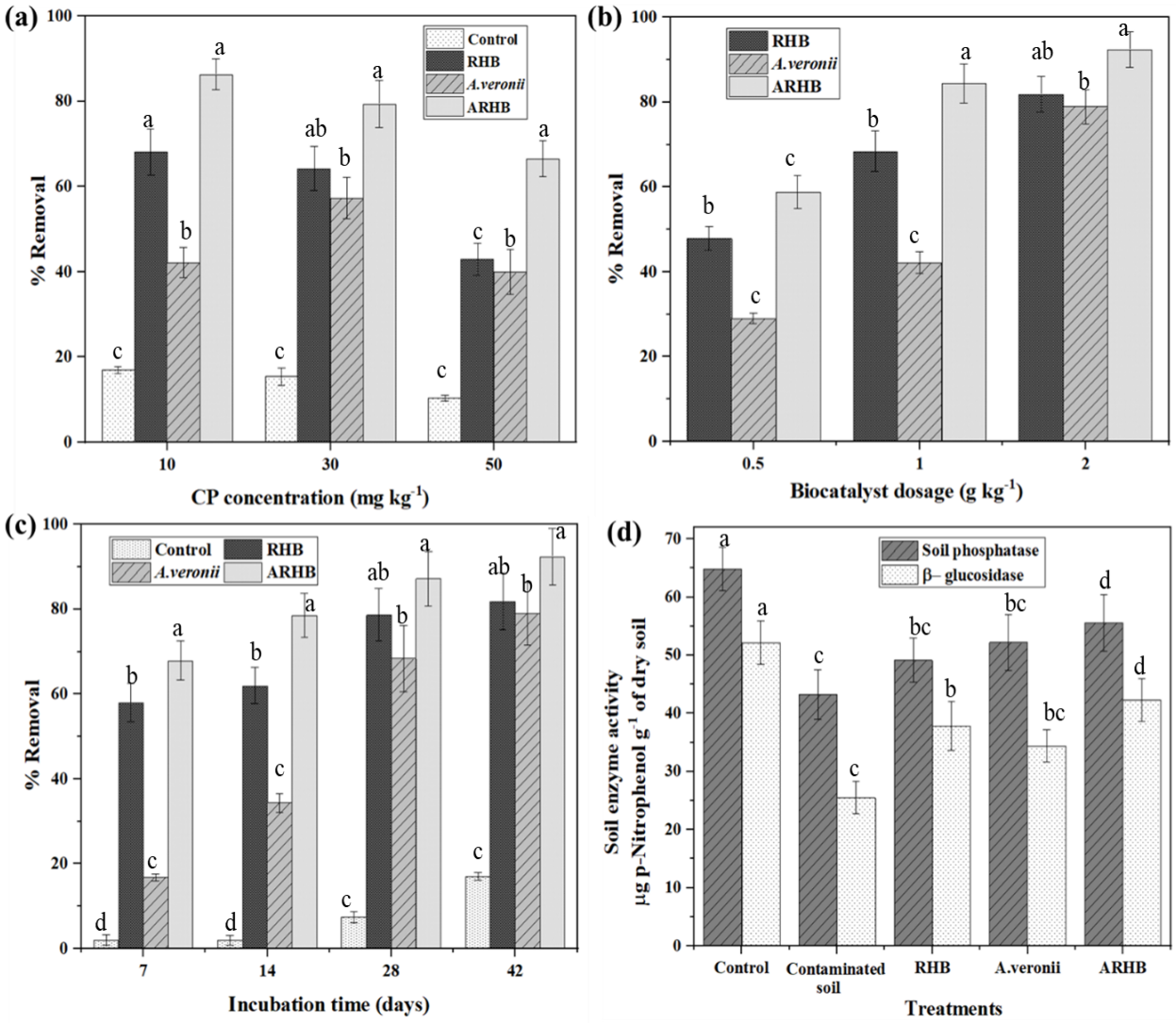

Figure 8.10. (a) Percentage removal at different concentrations of CP in various treatments after 42 h incubation **(b)** Percentage removal of CP in various treatments at different dosages of *A.veronii*, RHB, and ARHB **(c)** Percentage removal of CP at 10 mg kg^{-1} concentration and 2 g kg^{-1} catalyst dosage over a different time interval. **(d)** Changes in soil phosphatase and β – glucosidase enzyme activities after remediation.

8.10 PLANT GROWTH STUDIES

CP hinders plant growth and development by inhibiting DNA and protein synthesis, reducing seed germination and seedling growth. Consequently, a plant growth study using *Vigna unguiculata* (cowpea) was conducted to investigate the effects of CP and the efficacy of different remediation methods. Cowpea holds substantial economic importance as a highly nutritious vegetable,

particularly in countries like India and China (Herniter et al. 2020b). It is susceptible to various stressors such as weeds, pests, and diseases during field growth. This vulnerability often leads farmers to use pesticides extensively to enhance cowpea quality and quantity, inadvertently resulting in pesticide residues that pose potential hazards to human health., A study by Han et al. (2016) monitored 171 pesticides in cowpea samples, emphasizing the crop's susceptibility to pesticide accumulation. Analyzing the effects of CP and the efficiency of remediation on cowpea serves as a representative model for crop growth and soil properties.

Control soil without CP showed 100 % germination, indicating favorable conditions for seed germination. In contrast, CP-spiked soil exhibited a significantly lower GP of 33.3 ± 0.47 %, suggesting the inhibitory effect of CP on seed germination. Reduction in seed germination was attributed to different types of impairment in the cell division apparatus induced by CP. Reports indicate that organophosphate pesticides can have detrimental impacts on the seeds of various plants by inhibiting the synthesis or activity of hydrolytic enzymes that are typically essential for metabolic processes during germination. The GP in RHB, *A.veronii,* and ARHB increased to 58.3 ± 0.47 %, 66.67 ± 0.47 %, and 91.67 ± 0.47 %, respectively (**Figure 8.11a**). The SVI reflects the overall seed quality. Control soil exhibited an SVI of 1394.6, indicating healthy and vigorous seedlings. In comparison, contaminated soil showed a comparatively less SVI of 312.2, suggesting an inhibitory effect of the pesticide on seedling growth. However, remediation with *A.veronii* and ARHB improved seed vigour, making ARHB more effective (**Figure 8.11b**).

MGT represents the average time required for seed germination. Control soil displayed a MGT of 4 ± 0.2, reflecting optimal conditions for germination. CP spiked soil had a significantly prolonged MGT of 6.5 ± 0.4, indicating the negative impact of the pesticide on germination speed. However, RHB, *A.veronii,* and ARHB showed reduced MGT values (4.88 ± 0.43, 5.16 ± 0.23, and 4.11 ± 0.15, respectively), implying that the remediation techniques positively influenced the germination process. GRI and MGR are indicators of seedling growth and development. Control soil demonstrated a GRI of 1.04 ± 0.05 and an MGR of 0.25 ± 0.01, signifying healthy growth. In contrast, contaminated soil exhibited a lower GRI (0.2 ± 0.07) and MGR (0.15 ± 0.01), indicating reduced growth due to the presence of the pesticide (**Figure 8.11c**).

Inoculation of *A.veronii* appeared to help plants grow better because bacteria alleviate stress by mineralizing the contaminants and improving plant growth. The cowpea plants grown in

paraquat-contaminated soil with *B.arybhattai* showed longer root and shoot lengths than those grown in soil without bacterial inoculation (Inthama et al. 2021) . The use of ARHB enhanced plant growth due to its positive effects on soil properties and plant-microbe interactions. RHB is reported to improve soil physio-chemical properties, leading to increased nutrient availability and uptake by plants, and enhancing plant biomass. The porous nature of biochar provides a safe habitat for bacteria and promotes their survival and activity with enhanced nutrient availability in ARHB (Manikandan and Nair 2023; Noronha et al. 2022).

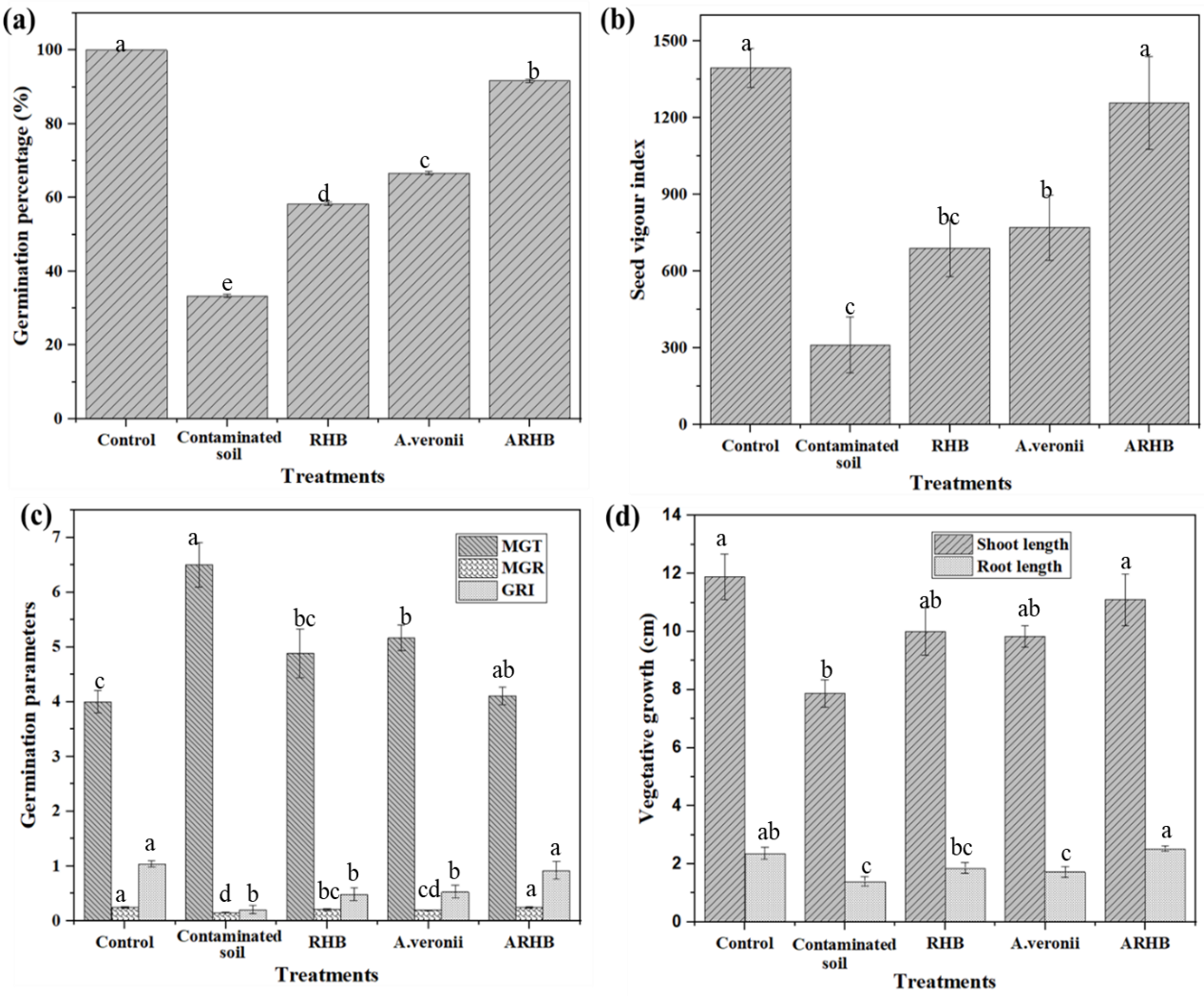

Figure 8.11. Germination and growth parameters of *Vigna unguiculata* under different treatments **(a)** GP **(b)** SVI **(c)** MGT, MGR, and GRI **(d)** vegetative growth.

The soil study showed promising results in CP removal, but several limitations exist in this research. Firstly, laboratory-scale experiments may not entirely capture the complexities and variability present in real-world contaminated environments. Soil is a complex system that can significantly influence mass transfer related to pollutant degradation, as well as the survival of microbes within the soil matrix. The study's duration of 42 days may not sufficiently account for the long-term effects of ARHB application on soil health and CP degradation efficiency over prolonged periods. Environmental variability, including differences in temperature, pH, and microbial interactions, could also impact the performance of ARHB in practical applications.

8.11 LC-MS ANALYSIS OF CP BIODEGRADATION BY ARHB

LC-MS analysis was conducted to identify CP and its metabolic products of biodegradation by ARHB. The culture medium containing 30 mg L^{-1} CP was incubated with the ARHB in MSM and samples were collected on 0, 12, 24, 36 and 48 h of incubation. Non-inoculated samples containing the same amount of CP served as the control. The identification of degraded products was performed by comparing the mass spectra of the peaks with standard and through subsequent library search. CP was detected in positive ion mode, while its metabolites were determined in negative ion mode. The mass spectra of standard CP showed three major peaks at m/z values of 352, 354, and 356 (Fig. 8a). In the initial stages of degradation at 0 h, the extracted sample showed a prominent molecular ion peak of standard CP. However, after 12 h, a major metabolite, di-ethyl-thio-phosphoric acid (DETP), was identified at m/z 169 (Fig. S5). Other metabolite peaks were discerned after 24 h of incubation, with significant peaks observed only in the inoculated sample, indicating CP degradation. The deprotonated molecular ions of TCP were identified at m/z = 195.9 (M-H)–, 197.9 (M-H)–, 199.9 (M-H)–, and 201.9 (M-H)– (Fig. 8b). TCP and DETP are considered the major degradation products of CP(Huang et al. 2021). It has been reported that CP undergoes hydrolysis to transform into TCP and DETP (Shi et al. 2019). However, these metabolites were found to be unstable and further metabolized into other products which are also detected in sample extracted after 24 h of incubation. DETP was converted into di-ethyl-acid-phosphate (DEAP), identified by the standard molecular ion peak at m/z 153.9. DEAP could further undergo metabolism to form H_3PO_4(Shi et al. 2019b) . Regarding TCP degradation, the deprotonated molecular ion at m/z 162.2 (M-H)– was identified as 5,6-dichloro-2-pyridinol, which is believed to be a reductive dechlorination product of TCP generated by *Cupriavidus* DT-1(Lu et al. 2013). The deprotonated molecular ions

at m/z = 182 (M-H)– identified as 3,6-dichloro-2,5-dihydroxypyridine observed at 36 h of incubation (Fig. S5). This metabolite also reported as hydrolytic products of TCP by *Cupriavidus nantongensis* X1T (Shi et al. 2019b). TCP can further metabolize into simple compounds like maleic acid with m/z 116.9 detected after 48 h (Fig.S5) which can enter the tri-carboxylic acid cycle and ultimately be completely metabolized into CO_2 and H_2O (Hamadeen and Elkhatib 2022; Malla et al. 2023).

Comparison of CP degradation by *A.veronii* and RHB, the *A.veronii* exhibited multiple intermediates, signifying complete mineralization, RHB displayed chlorpyrifos oxon, a photocatalytic derivative (Anirudhan et al. 2021). *A. veronii* exhibited an extended degradation time, with the appearance of DETP after 24 h, Conversely, the same metabolites appeared after 12 h in ARHB treated with CP. This difference in degradation rate suggests that the bacterial system required an extended period for complete degradation, underscoring the efficiency and accelerated degradation capabilities of the ARHB system.

In the soil system, LC MS analysis detected the presence of TCP at m/z = 195.9 (M-H)–, 197.9 (M-H)–, and 199.9 (M-H)– after remediation **(Figure 8.12c).** TCP is known for its high persistence in soil (Das and Adhya 2015a), but remediation studies revealed a 92.4 % removal of CP using ARHB. ARHB showcased significant advantages in chlorpyrifos degradation in soil matrices by providing adsorption sites for the enrichment of pesticides from soil aggregates, serving as a suitable habitat and nutrient source for bacterial growth, and positively affecting soil microbes. The plant growth study showed that CP affected the growth of plants in contaminated soil, while they had no impact on the early plant growth in soil treated with ARHB.

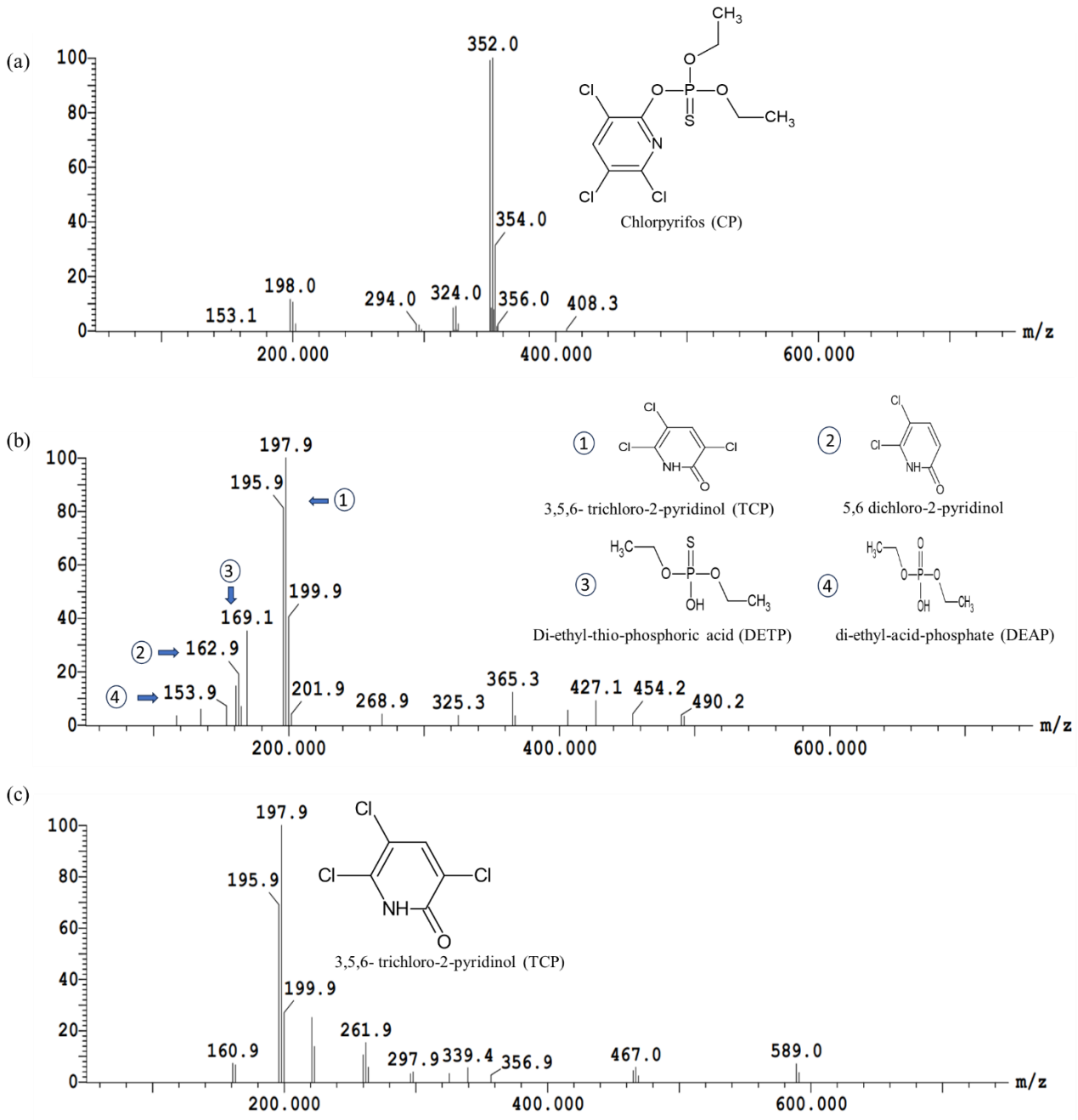

Figure 8.12. LC-MS spectrum of CP and degraded products. **(a)** Mass spectrum of the standard CP, mass spectra of metabolites in **(b)** water and **(c)** soil.

8.12 MECHANISM OF CP REMOVAL FROM WATER AND SOIL BY ARHB

The overall mechanism of CP removal by ARHB can be elucidated based on the major findings obtained from FESEM, LCMS, and FTIR studies. The results revealed a synergistic effect of biochar-bacteria system, leading to a 31 % and 48 % higher removal rate compared to free strain and

RHB, respectively, demonstrating the most effective CP removal with a maximum rate of 96.25 %. FESEM analysis confirms the presence of CP on ARHB, causing depositions and clogging of pores. CP also affects *A.veronii*, evidenced by coverage on both bacteria and biochar surfaces **(Figure 8.13a).** The FTIR results of ARHB before and after CP removal **(Figure 8.13b)** signify that CP adsorption onto ARHB involves hydrogen bonding (O, N and S anions in CP with OH functional groups in RHB), π-π interactions (OH, C-H, C-O groups in RHB with benzene ring of CP) and electrostatic interactions (OH, C-H, C-O, and C-N groups in RHB with anionic species of CP). Hydrophobic interactions occur, leading to moderate aggregation of CP molecules in organic fractions of RHB and it prevails over electrostatic interactions (Supreeth and Raju 2017). Multiple mechanisms responsible for CP sorption have been demonstrated by Hao et al. (2019) utilizing giant reed-derived biochar, including the hydrophobic effect, π–π interaction, pore filling, and hydrogen bonding. There is a greater sorption capacity and affinity toward chlorpyrifos owing to more aromatic units and pores.

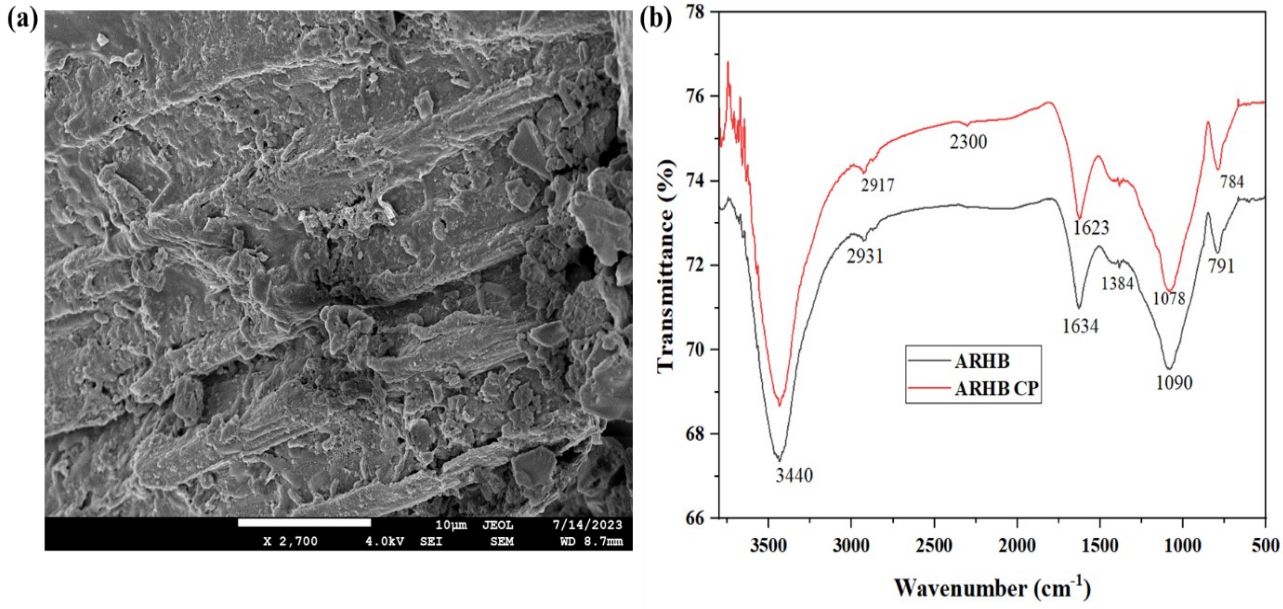

Figure 8.13. (a) FESEM analysis of ARHB after CP removal **(b)** Analysis of infrared spectral bands of ARHB before and after CP removal from water medium.

XPS was used to investigate the chemical structures of ARHB before and after CP removal. Spectral analysis further verifies the adsorption of CP onto ARHB. In the overall spectra, peak belonging to C 1s (285 eV), O 1s (533 eV), N 1s (400 eV), P 2p (132 eV), Si 2p (106 eV) and S 2p

(175.1 eV) Cl 2p (192 eV) indicating the surface elemental compositions include C, O, N, P, Si, S and Cl of ARHB. The deconvolution spectra of C at 284 and 286.1eV, may be due to C−H and C−O carbons, respectively **(Figure 8.14a)** (Bootharaju and Pradeep 2012). Compared with the C1s spectra of ARHB, CP-treated ARHB showed another peak appears at 285.1 eV, which may be related to the generation of new C-N bonds due to CP, and the peak at 287 eV is related to O-C=O **(Figure 8.14d)**. Suo et al. (2019) found that -COOH and C=O on biochar is essential for the adsorption of pollutants. These groups may also be beneficial for CP adsorption. XPS spectrum of N 1s deconvoluted into peaks at 399.9 eV and 401.3 eV **(Figure 8.14b)**. These peaks correspond to sp3 C–N bonds and amino groups with a hydrogen atom (C–N–H) and a new peak formed at 398 eV after treatment due to adsorbed CP **(Figure 8.14e)**. The deconvolution spectra of P 2p peak are well fitted at 133.4, 134.8 and 136.4 eV **(Figure 8.14c)** and the **Figure 8.14f** shows that the P 2p peaks was significantly different after CP treatment indicating that the adsorption of CP on the ARHB surface and CP interacts with the phosphate group of ARHB. These peaks may be due to the organophosphate group in chlorpyrifos. The presence of Cl 2p peaks at 192 eV may be due to organic chlorides. After CP treatment the elements change in peak spectra observed in C, N, and P indicating the successful degradation of the pesticide CP.

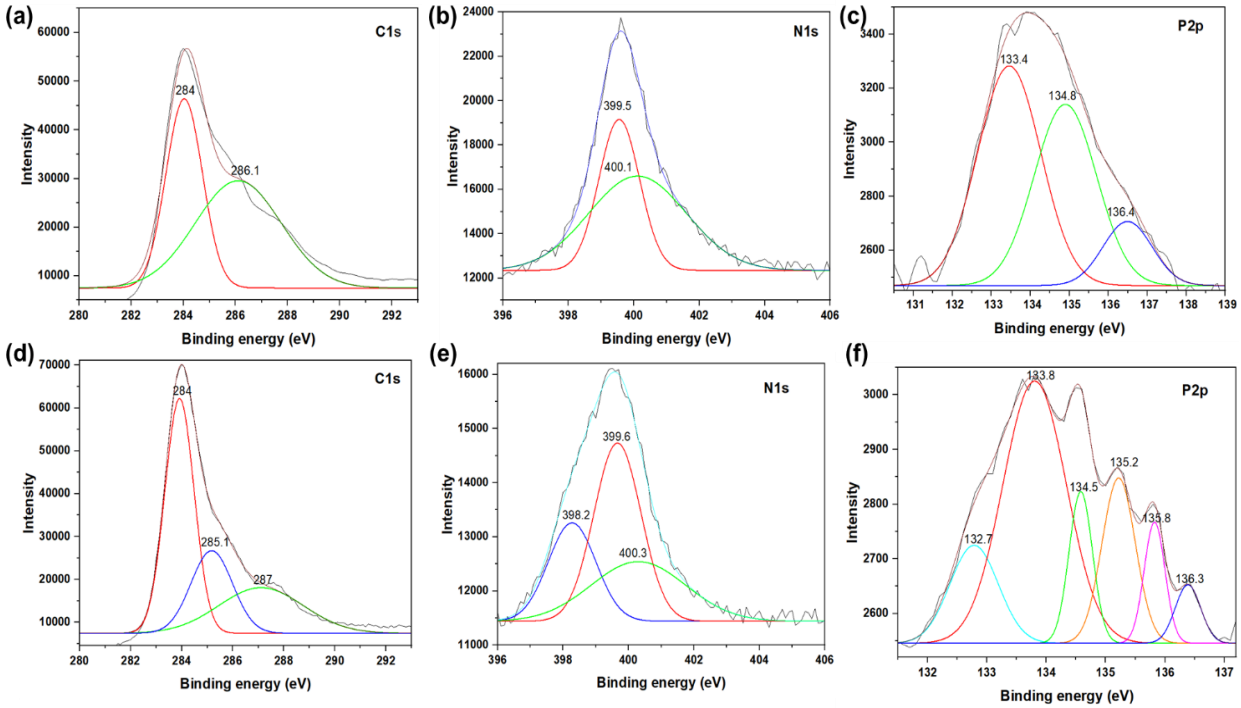

Figure 8.14. XPS of ARHB before (a, b and c) and after treatment with CP (d, e and f).

Analysing toxic intermediate metabolites during microbial bioremediation is crucial. Based on the identified metabolites from LC MS, a potential degradation pathway of CP by ARHB was elucidated **(Figure 8.14)** and explained in section 8.11. ARHB not only degrades CP but also converts TCP into non-toxic forms.

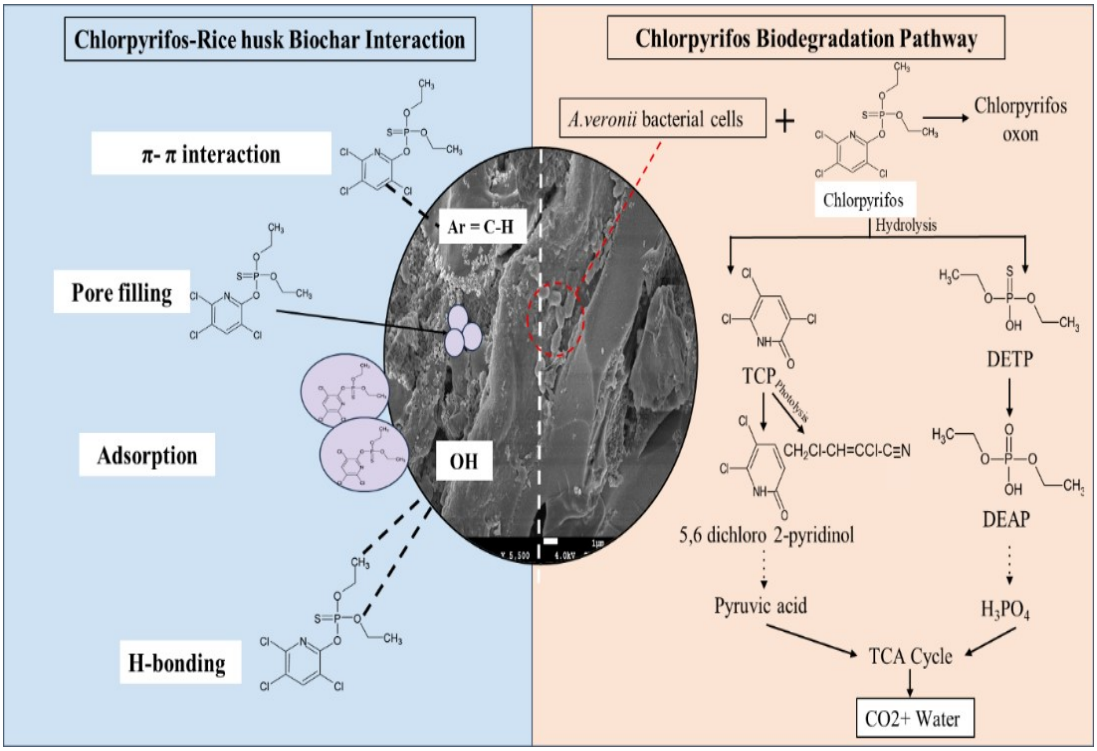

Figure 8.15. ARHB mediated CP removal mechanism.

.

CHAPTER 9

SUMMARY AND CONCLUSIONS

9.1 SUMMARY OF THE WORK

The study focused on the development of microbial cell immobilized biochar catalytic material for effective removal of heavy metals and pesticide from water and soil medium. The work explores the individual as well as the synergistic role of the bacteria and biochar in the remediation process. Biochars from different biomass materials were prepared at different pyrolysis temperature and time periods. The selection of the biochar prepared at different pyrolysis conditions was based on the bacterial immobilization studies. The subsequent exploration of different biochar types revealed RHB as the most effective carrier for *P. stutzeri* immobilization. RHB produced at 500 °C for 30 min exhibited superior bacterial cell immobilization capacity attributed to its well-defined pores, specific surface area, distinctive surface functional groups and nutrient content. In the heavy metal removal studies in water, PRHB demonstrated exceptional efficiency in removing Cd and Ni under optimized conditions, including specific parameters such as incubation time, pH, temperature, and biocatalyst dosage. Significantly, consistent and high removal efficiency of PRHB over multiple cycles, highlighting its reusability. The research also explored the mechanisms involved, identifying processes such as adsorption, ion exchange, complexation, and precipitation. Moving from water to soil, the application of PRHB showed significant efficacy in reducing Cd concentration, altering Cd speciation, and positively influencing soil properties. These findings were supported by a plant growth study, showcasing effectiveness of PRHB in promoting the growth of *Spinacia oleracea* L. and reducing Cd levels in plant shoots.

The research expanded its scope to explore other bacterial cell immobilized biochar catalysts which include *P. stutzeri* immobilized sawdust biochar for Cd and Ni removal from water, *Bacillus* sp immobilized rice husk biochar for Cd removal from soil, *P. stutzeri* immobilized coconut shell

biochar for Cd removal from soil and *A. veronii* immobilized on rice husk biochar for CP removal from water and soil. The porous surface texture and functional groups of sawdust biochar facilitated *P. stutzeri* cell immobilization, resulting in superior efficiency for Cd and Ni removal under optimized conditions. PSDB demonstrated good reusability over consecutive cycles, attributed to the sawdust biochar adsorption and *P. stutzeri*-mediated bioaccumulation. Another aspect of the study focused on BRHB and its significant efficacy in reducing Cd concentration in soil, positively influencing soil health indicators, and promoting *Spinacia oleracea* L. growth. Additionally, the application of CSB for soil enhancement and Cd removal is explored, highlighting its positive impact on soil water-holding capacity and early seedling growth of *Solanum lycopersicum* L. The remediation potential of ARHB for CP removal from water and soil was studied. ARHB demonstrates efficient removal of CP, with optimized conditions determined through RSM. The application of ARHB in reducing CP levels in soil shows promise for long-term soil remediation and positive effects on plant health of *Vigna unguiculata* L, underscoring the efficacy of the developed remediation approach. Overall, the research presents a promising approach for the sustainable remediation of heavy metal and pesticide-contaminated environments. The comprehensive summary of the pollutant removal efficiency achieved through microbial cell immobilization on various biochar materials is represented in **Table 9.1**.

Table 9.1. Summary of pollutant removal efficiency achieved through microbial cell immobilization on various biochar materials

Pollutant	Biochar	Bacteria	Operating Condition	Medium	Efficiency (%)
Cd	Rice husk	*P. stutzeri*	Temperature 37 °C, pH 7, biocatalyst dosage 2 g L^{-1} Incubation time 36 h, Cd concentration 10 mg L^{-1}	Water	95
	Sawdust	*P. stutzeri*	Temperature 37 °C, pH 7, biocatalyst dosage 2 g L^{-1} Incubation time 36 h, Cd concentration 10 mg L^{-1}	Water	86.20
	Rice husk	*P. stutzeri*	Biocatalyst dosage 2 g kg^{-1}, Incubation time 42 days, Cd concentration 10 mg kg^{-1}	Soi	78.20
	Rice husk	*Bacillus* sp	Biocatalyst dosage 2 g kg^{-1}, Incubation time 42 days, Cd concentration 10 mg kg^{-1}	Soil	72
	Coconut shell	*P. stutzeri*	Biocatalyst dosage 5 g kg^{-1}, Incubation time 21 days, Cd concentration 2 mg kg^{-1}	Soil	83
Ni	Rice husk	*P. stutzeri*	Temperature 37 °C, pH 7, biocatalyst dosage 2 g L^{-1} Incubation time 36 h, Ni concentration 10 mg L^{-1}	Water	92
	Sawdust	*P. stutzeri*	Temperature 37 °C, pH 7, biocatalyst dosage 2 g L^{-1} Incubation time 36 h, Ni concentration 10 mg L^{-1}	Water	82.87
CP	Rice husk	*A.veronii*	Temperature 30 °C, pH 6.5, biocatalyst dosage 1.3 g L^{-1} Incubation time 24 h, CP concentration 30 mg L^{-1}	Water	96.45
	Rice husk	*A.veronii*	Biocatalyst dosage 2 g kg^{-1}, Incubation time 42 days, CP concentration 10 mg kg^{-1}	Soil	92.4

9.2 CONCLUSIONS

Microbial cell immobilization and optimization of biochar conditions

- The relationship between pyrolysis temperature and microbial cell immobilization suggests that lower temperatures favor enhanced adherence of cells onto biochar surfaces, emphasizing the critical role of temperature control in optimizing biochar properties for effective immobilization.
- The absence of toxicity towards *P. stutzeri* cells and the observed growth support provided by biochar underscore its biocompatibility and potential as a conducive environment for microbial activity, highlighting its promising application in facilitating microbial processes without adverse effects on microbial viability and growth.

Cd and Ni removal using *P. stutzeri* immobilized rice husk biochar from water

- *P. stutzeri* demonstrated remarkable tolerance to Cd and Ni, showing optimal growth up to 50 mg L^{-1} concentrations.
- The optimized conditions included a temperature of 37 °C, incubation time 36 h, pH of 7.0, and PRHB dosage of 2 g L^{-1} resulted in efficient Cd and Ni removal.
- PRHB outperformed *P. stutzeri* by achieving exceptional metal ion removal rates, with a 95 % removal of Cd and a 92 % removal of Ni within 36 h.
- PRHB showcased consistent and high removal efficiency over five cycles, highlighting its reusability.
- Data from Cd and Ni removal studies successfully fit the pseudo-second-order kinetic and Langmuir isotherm models.
- FTIR, XPS, XRD and ICP-OES indicated that metal ion removal mechanisms involved adsorption, ion exchange, complexation, and precipitation, with functional groups like -OH, C=O, -CN, and C=C playing crucial roles.
- FESEM analysis revealed a synergistic effect between the RHB carrier and *P. stutzeri*, enhancing both adsorption and bioaccumulation.

Cd removal using *P. stutzeri* immobilized rice husk biochar from soil

- PRHB induced a transformation of acid-soluble Cd into less toxic oxidizable and residual fractions, highlighting its effectiveness in altering Cd speciation and reducing soil toxicity.
- PRHB significantly increased soil pH, SOM and soil enzyme activities indicating its potential to modify soil properties and create a more favourable environment for plant growth.
- PRHB positively influenced the initial growth of *Spinacia oleracea* L., improving germination parameters.
- 94 % increase in plant biomass and an 87.5 % reduction in Cd content in shoots, suggesting the potential of PRHB in mitigating Cd-induced stress and enhancing plant health.

Cd and Ni removal using *P. stutzeri* immobilized sawdust biochar from water

- The SDB prepared at 500 °C for 60 min showed higher immobilization capacity.
- PSDB demonstrated superior Cd and Ni removal under optimized conditions of incubation time 36 h, pH 7.0, temperature at 37 °C, and PRHB dosage of 2 g $L^{-1.}$
- Enhanced Cd and Ni removal with PSDB is attributed to mechanisms including adsorption, precipitation, ion exchange by metal cations (K^+ and Mg^{2+}), and complexation by functional groups present in the SDB.
- PSDB revealed good reusability, maintaining a steady removal efficiency over five consecutive cycles.

Cd removal using *Bacillus* sp immobilized rice husk biochar from soil

- BRHB demonstrated significant efficacy in reducing Cd concentration in soil, with a significant reduction of 62.58 % compared to control conditions.
- Increase in soil pH, enzyme activities (phosphatase and β-glucosidase) and organic matter content after BRHB amendment indicating improved soil health.
- BRHB positively influenced the initial growth of *Spinacia oleracea* L., improving germination rates, seed vigour index, and plant growth parameters.

- Spinach plants treated with BRHB exhibited a 58 mg plant $^{-1}$ of dry biomass and reduced Cd content to 0.35 mg kg^{-1} in shoots, suggesting efficacy in alleviating Cd-induced stress.

Cd removal using *P. stutzeri* immobilized coconut shell biochar from soil

- CSB with a particle size of <1 mm demonstrated a significant water-holding capacity of 41.5 %, supporting germination (90.47 %) and seed viguor (464.25) of *Solanum lycopersicum* L. suggesting efficacy as a soil enhancer.
- Pot experiments with CSB enhanced soil enzyme activity and growth of *Solanum lycopersicum* L.
- The application of PCSB demonstrated an effective reduction in the phytoavailability of Cd in soil, decreasing from 1.3 mg kg^{-1} to 0.34 mg kg^{-1} within 21 days showcasing its potential for soil remediation.

CP removal using *A.veronii* immobilized rice husk biochar from water and soil

- The CP-tolerant strain, isolated through enrichment and domestication, was identified as *A. veronii* and subsequently employed for CP remediation.
- Rice husk biomass pyrolysed at 500 °C for 30 min proved effective in enhancing both CP removal capacity and the immobilization of *A. veronii.*
- ARHB achieved 96.25 % CP removal within 24 h based on an optimization study using RSM, showcasing rapid and efficient remediation in comparison to *A. veronii* and RHB.
- The reusability study displayed consistent CP removal over multiple cycles, affirming the viability of immobilized cells.
- ARHB application in soil led to a 92.4 % CP removal rate within 42 days.
- Plant growth studies using *Vigna unguiculata* L. highlighted the positive impact of ARHB on seed germination, seedling growth, and overall plant health.
- Mechanistic insights from FTIR, SEM, and LC-MS analyses revealed the synergy between biochar-mediated adsorption and bacterial metabolism in the remediation process.

9.3 FUTURE PERSPECTIVES

1. Utilize different biomass and microorganisms to develop an efficient microbial cell immobilized biochar-based method for removing heavy metals and pesticides.
2. Explore diverse indigenous bacterial strains to discover new potent agents for heavy metal and pesticide removal.
3. Apply microbial cell-immobilized biochar technology to wastewater treatment for industrial and agricultural effluents.
4. Conduct field-scale studies to validate effectiveness in remediating contaminated sites and soils.
5. Assess long-term stability and performance under various environmental conditions.
6. Address the removal efficiency of emerging contaminants like dyes, motor oil, pharmaceutical residues, and microplastics.
7. Investigate the simultaneous removal efficiency of mixed pollutants using microbial cell-immobilized biochar.
8. Explore the use of microbial consortia immobilized on biochar to target mixed pollutants.
9. Conduct a comparative analysis of microbial cell-immobilized biochar against existing remediation methods.
10. Conduct techno-economic analysis for cost-effectiveness and scalability.

APPENDIX I

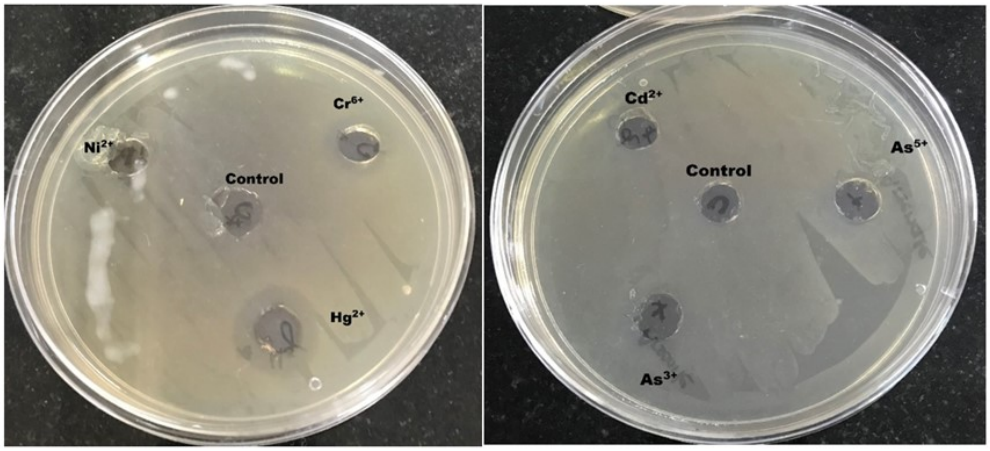

Figure A1. Metal ion tolerance study using *P. stutzeri* plate assay.

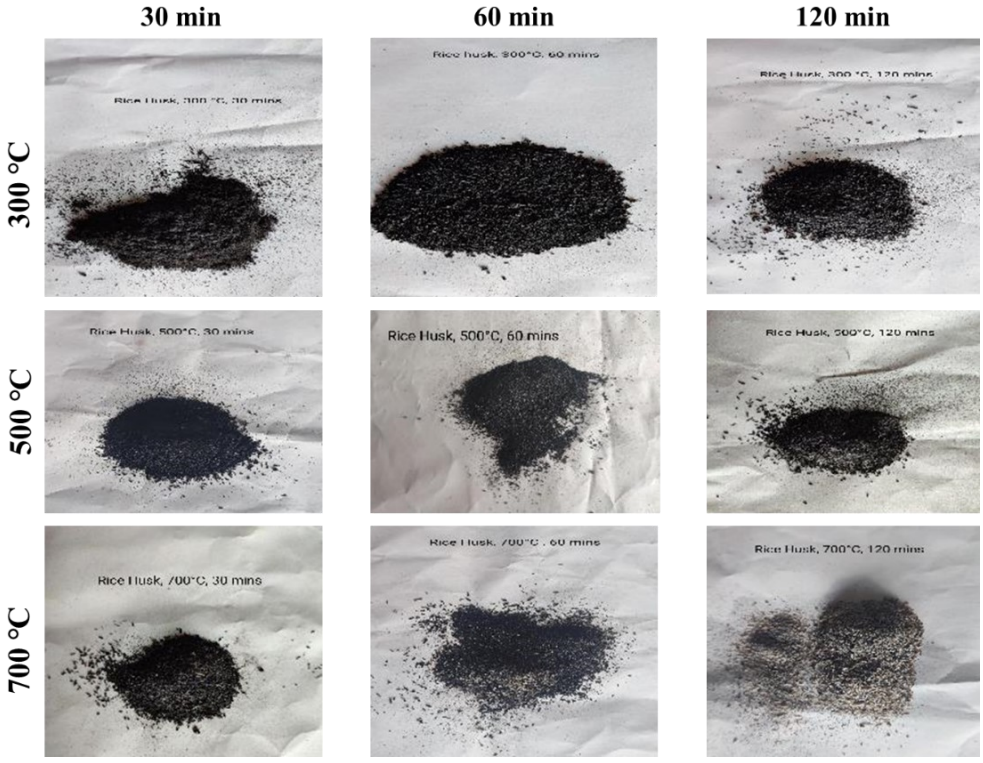

Figure A2. Biochar yield at different temperatures and time for rice husk.

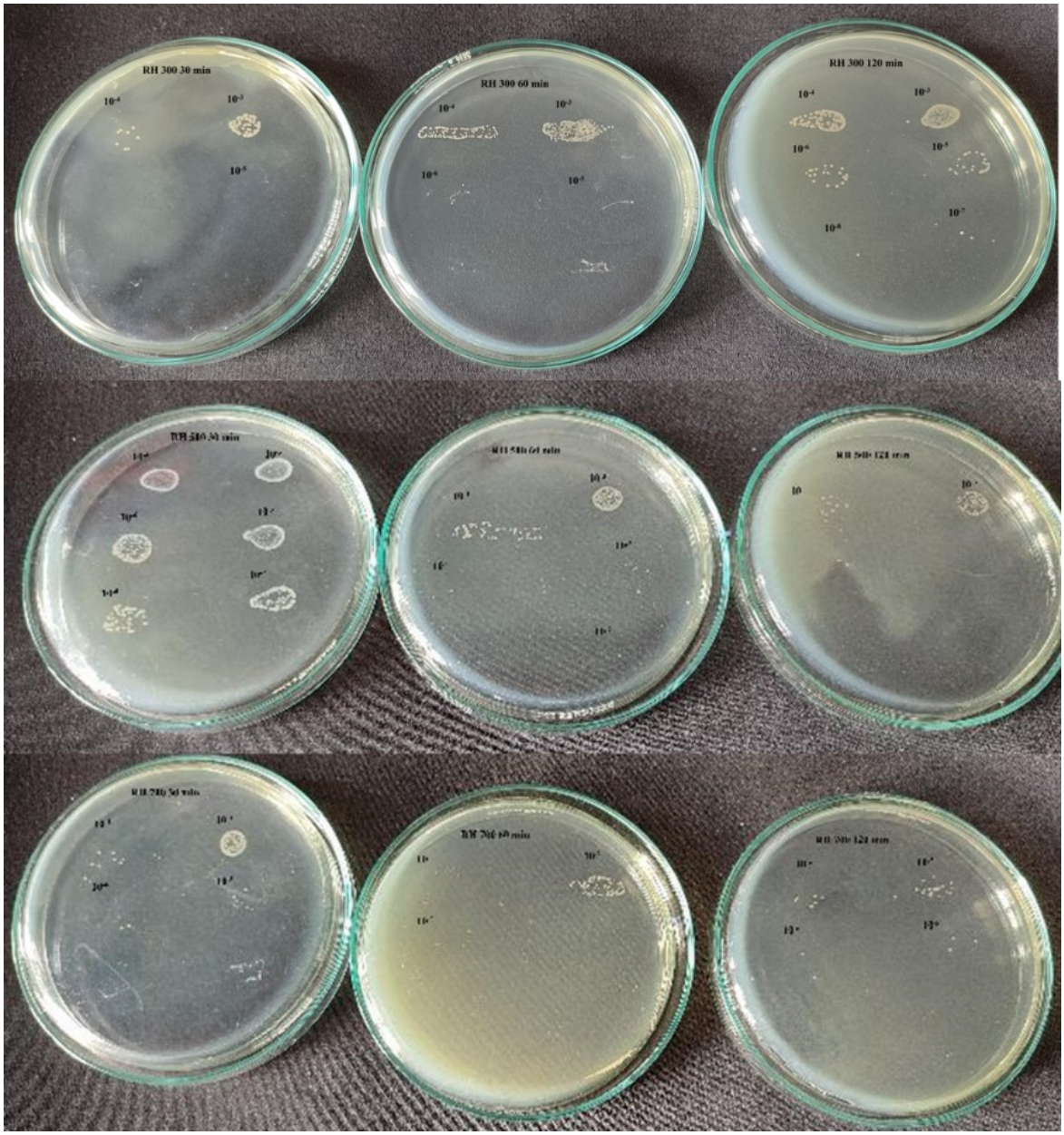

Figure A3. Immobilization of *P. stutzeri* on RHB.

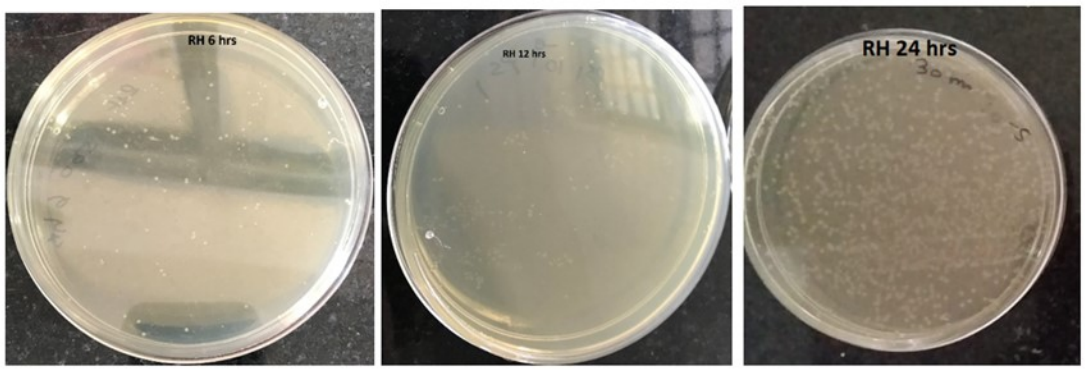

Figure A4. Growth of *P. stutzeri* on RHB at 6, 112 and 24 h.

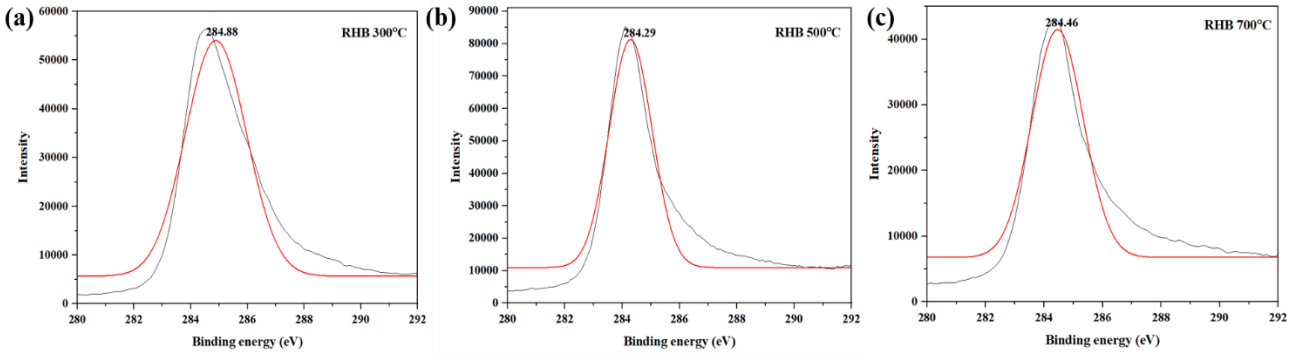

Figure A5. XPS spectra of C1s RHB.

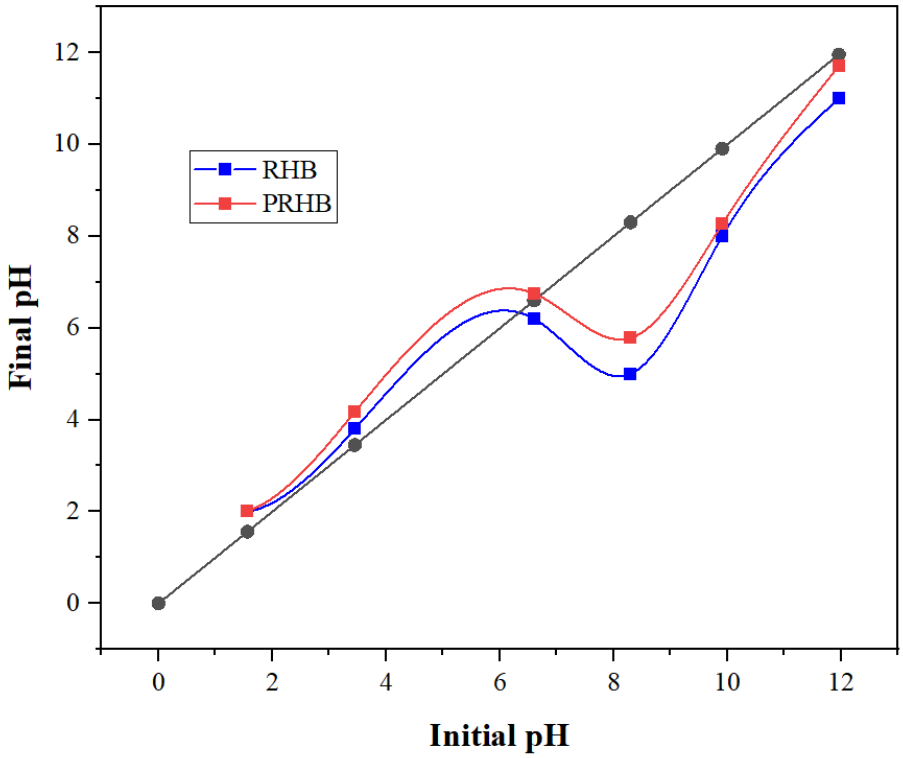

Figure A6. Zero-point charge of RHB and PRHB.

APPENDIX II

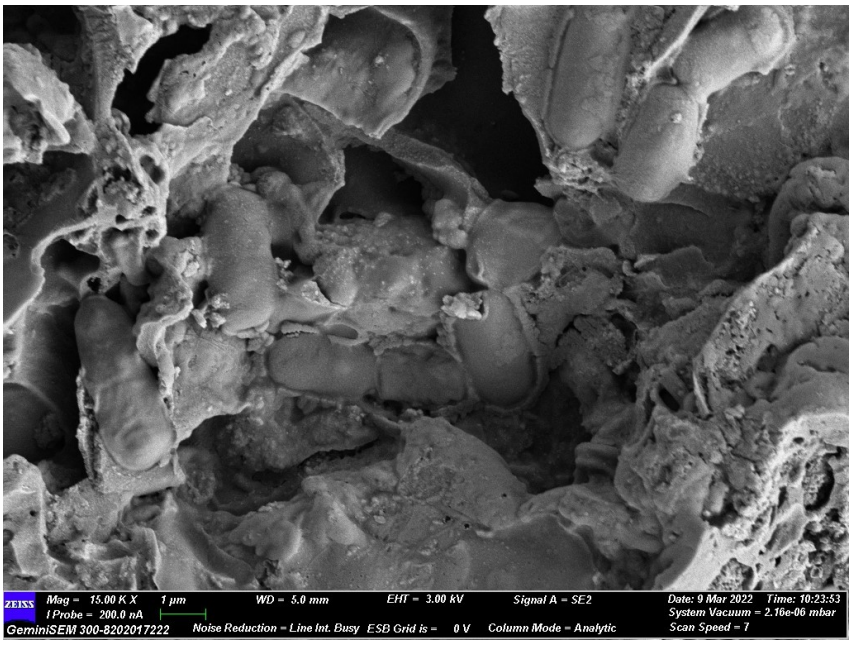

Figure A1. FE-SEM image of PRHB after Ni removal.

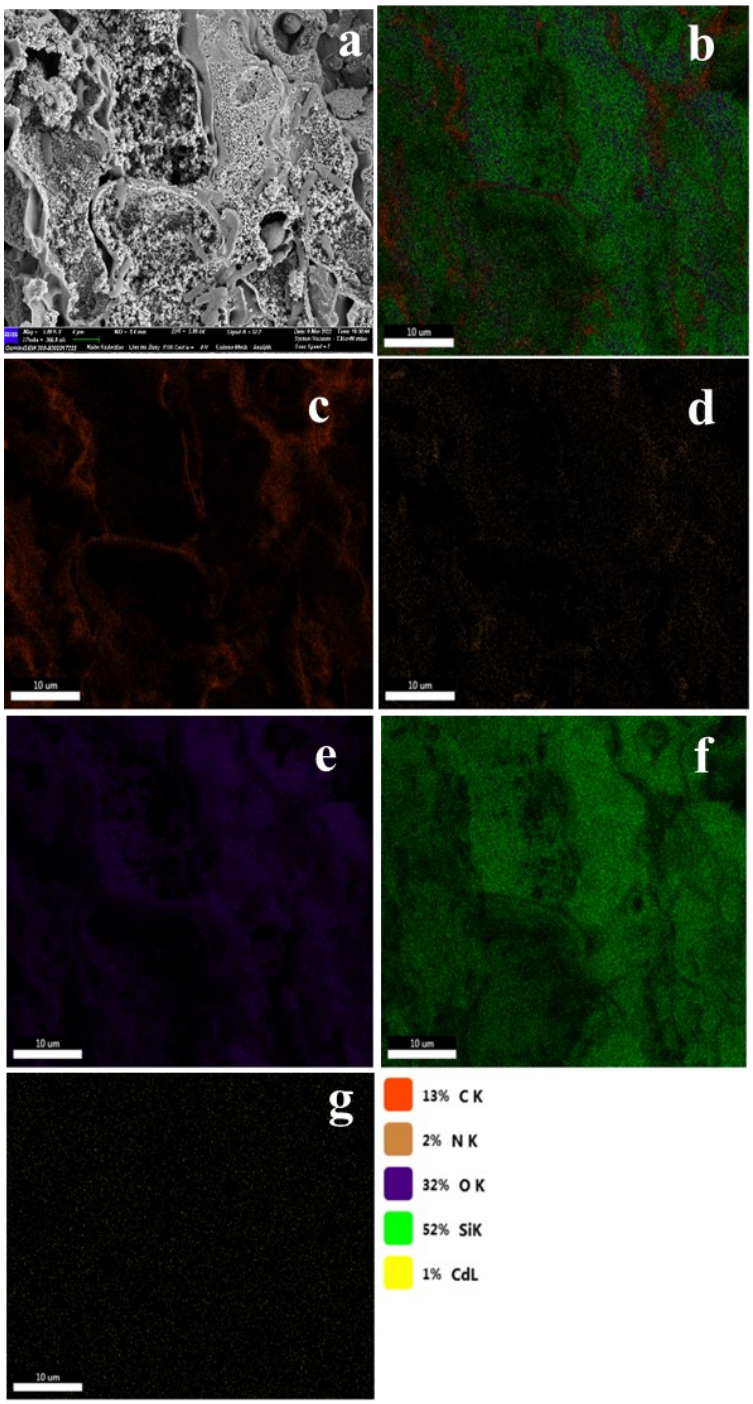

Figure A2. (a) FE SEM image of PRHB after Cd removal **(b)** distribution of all the elements **(c)** elemental mapping of carbon **(d)** nitrogen **(e)** oxygen **(f)** silica and **(g)** cadmium.

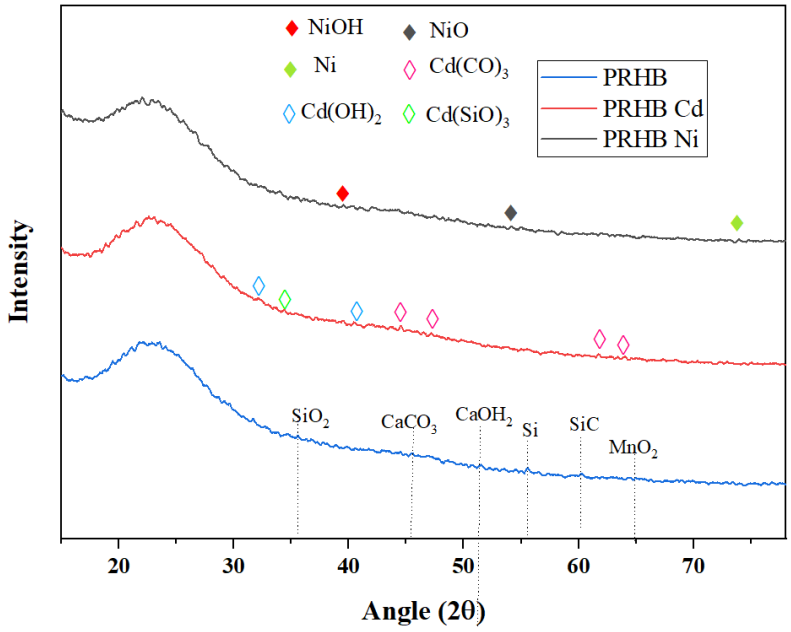

Figure A3. XRD spectra of PRHB before and after Cd and Ni treatment.

APPENDIX III

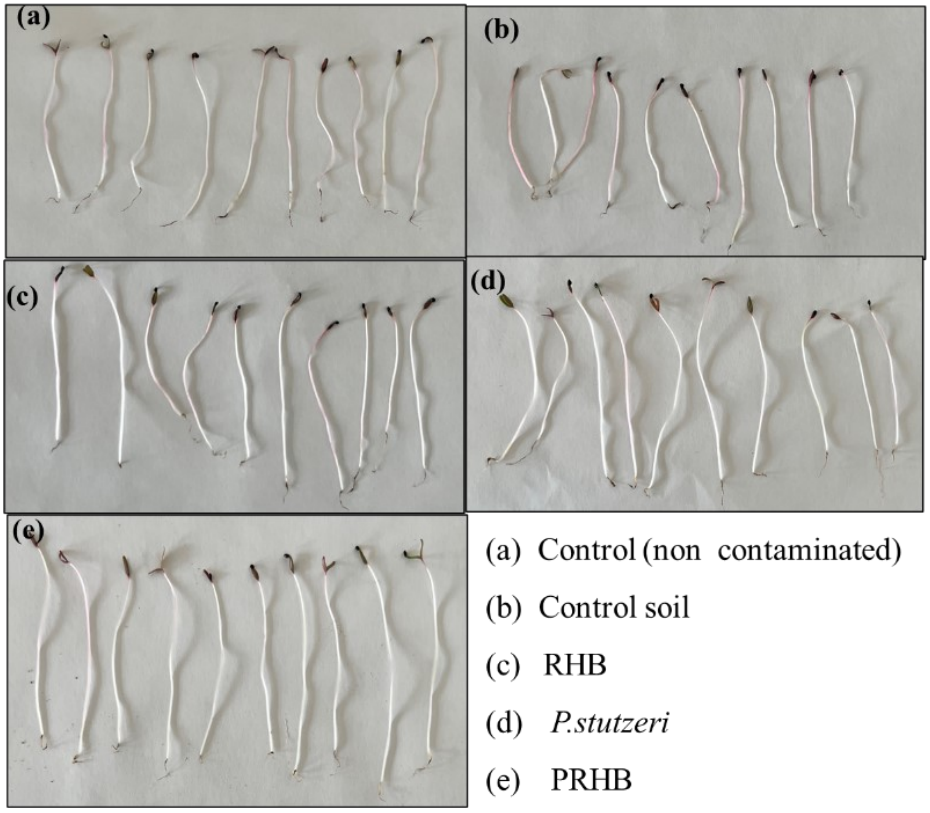

Figure A1. Growth of *Spinacia oleracia* L. seedlings in protray.

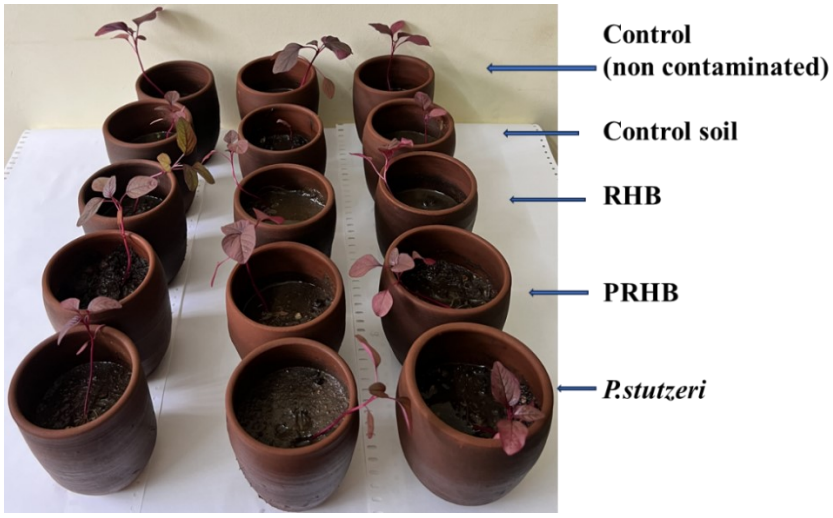

Figure A2. Pot study of *Spinacia oleracia* L. plants.

APPENDIX IV

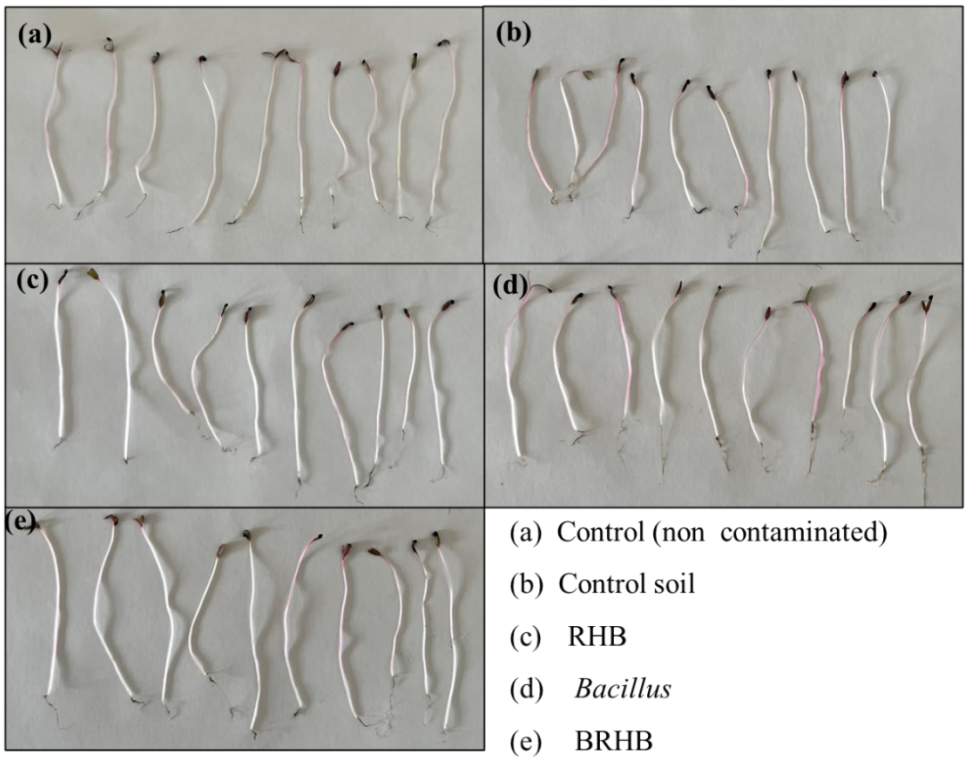

Figure A1. Growth of *Spinacia oleracia* L. seedlings in protray.

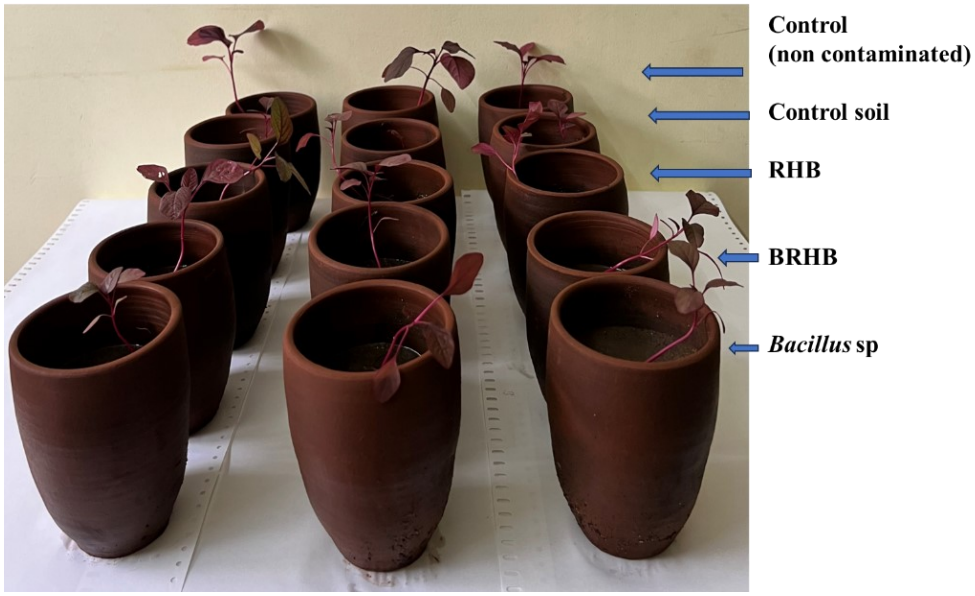

Figure A2. Pot study of *Spinacia oleracia* L. plants.

Figure A3. *Solanum lycopersicum* L. growth in control soil and soil treated with 5% CSB

APPENDIX V

Table A1 ANOVA analysis.

Source	Sum of Squares	df	Mean Square	F-value	p-value	
Model	17708.02	9	1967.56	1135.29	< 0.0001	significant
A-Chlorpyrifos concentration	1188.77	1	1188.77	685.93	< 0.0001	
B-ARHB dosage	875.50	1	875.50	505.17	< 0.0001	
C-Incubation time	4719.55	1	4719.55	2723.20	< 0.0001	
AB	66.42	1	66.42	38.33	0.0004	
AC	367.11	1	367.11	211.82	< 0.0001	
BC	697.22	1	697.22	402.30	< 0.0001	
A^2	2238.47	1	2238.47	1291.61	< 0.0001	
B^2	4485.70	1	4485.70	2588.27	< 0.0001	
C^2	2080.68	1	2080.68	1200.56	< 0.0001	
Residual	12.13	7	1.73			
Lack of Fit	8.21	3	2.74	2.79	0.1734	not significant
Pure Error	3.92	4	0.9806			
Cor Total	17720.15	16				
Adj. R^2	0.998					
Pred. R^2	0.992					
Adeq precision	82.39					

REFERENCES

Abd El-Mageed, T. A., Abdelkhalik, A., Abd El-Mageed, S. A., and Semida, W. M. (2021). "Co-composted poultry litter biochar enhanced soil quality and eggplant productivity under different irrigation regimes." *J. Soil Sci. Plant Nutr.*, 21(3), 1917–1933.

Abdullah, N., Yusof, N., Lau, W. J., Jaafar, J., and Ismail, A. F. (2019). "Recent trends of heavy metal removal from water/wastewater by membrane technologies." *J. Ind. Engg. Chem.*, 76, 17-38.

Abinandan, S., Subashchandrabose, S. R., Venkateswarlu, K., Perera, I. A., and Megharaj, M. (2019). "Acid-tolerant microalgae can withstand higher concentrations of invasive cadmium and produce sustainable biomass and biodiesel at pH 3.5." *Bioresour. Technol.*, 281, 469–473.

Abraham, J., and Silambarasan, S. (2013). "Biodegradation of chlorpyrifos and its hydrolyzing metabolite 3,5,6-trichloro-2-pyridinol by *Sphingobacterium* sp. JAS3." *Process Biochem.*, 48(10), 1559–1564.

Abu Talha, M., Goswami, M., Giri, B. S., Sharma, A., Rai, B. N., and Singh, R. S. (2018). "Bioremediation of Congo red dye in immobilized batch and continuous packed bed bioreactor by *Brevibacillus parabrevis* using coconut shell bio-char." *Bioresour. Technol.*, 252, 37–43.

Adnan, M., Xiao, B., Xiao, P., Zhao, P., Li, R., and Bibi, S. (2022). "Research Progress on Heavy Metals Pollution in the Soil of Smelting Sites in China." *Toxics*, 10, 231.

Agoro, M. A., Adeniji, A. O., Adefisoye, M. A., and Okoh, O. O. (2020). "Heavy metals in wastewater and sewage sludge from selected municipal treatment plants in eastern cape province, south africa." *Water*, 12, 2746.

Ahmad, M., Rajapaksha, A. U., Lim, J. E., Zhang, M., Bolan, N., Mohan, D., Vithanage, M., Lee, S. S., and Ok, Y. S. (2014). "Biochar as a sorbent for contaminant management in soil and water: A review." *Chemosphere*, 99, 19-33.

Ahmed, M. J., and Hameed, B. H. (2020). "Insight into the co-pyrolysis of different blended feedstocks to biochar for the adsorption of organic and inorganic pollutants: A review." *J. Clean Prod.*, 265, 121762.

Ajeng, A. A., Abdullah, R., Ling, T. C., Ismail, S., Lau, B. F., Ong, H. C., Chew, K. W., Show, P. L., and Chang, J. S. (2020). "Bioformulation of biochar as a potential inoculant carrier for sustainable agriculture." *Environ. Technol. Innov.*, 20, 101168.

Ajiboye, T. O., Kuvarega, A. T., and Onwudiwe, D. C. (2020). "Recent strategies for environmental remediation of organochlorine pesticides." *Appl. Sci.,* 10(18), 6286.

Akhil, D., Lakshmi, D., Kartik, A., Vo, D.-V. N., Arun, J., and Gopinath, K. P. (2021). "Production, characterization, activation and environmental applications of engineered biochar: a review". *Environ. Chem.,* 19, 2261-2297.

Alboghobeish, H., Tahmourespour, A., and Doudi, M. (2014). "The study of Nickel Resistant Bacteria (NiRB) isolated from wastewaters polluted with different industrial sources." *J. Environ Health Sci. Eng.*, 12(1), 1–7.

Alburquerque, J. A., Calero, J. M., Barrón, V., Torrent, J., Campillo, M. C. del, Gallardo, A., and Villar, R. (2014). "Effects of biochars produced from different feedstocks on soil properties and sunflower growth." *J. Soil Sci. Plant Nutr.*, 177(1), 16–25.

Alengebawy, A., Abdelkhalek, S. T., Qureshi, S. R., and Wang, M. Q. (2021). "Heavy metals and pesticides toxicity in agricultural soil and plants: Ecological risks and human health implications." *Toxics*, 9, 42.

Ali, N. S., Jabbar, N. M., Alardhi, S. M., Majdi, H. S., and Albayati, T. M. (2022). "Adsorption of methyl violet dye onto a prepared bio-adsorbent from date seeds: isotherm, kinetics, and thermodynamic studies." *Heliyon*, 8(8).

Amin, M., and Chetpattananondh, P. (2019). "Biochar from extracted marine Chlorella sp. residue for high efficiency adsorption with ultrasonication to remove Cr(VI), Zn(II) and Ni(II)." *Bioresour. Technol.*, 289, 121578.

Anirudhan, T. S., Shainy, F., Sekhar, V. C., and Athira, V. S. (2021). "Highly efficient photocatalytic degradation of chlorpyrifos in aqueous solutions by nano hydroxyapatite modified CFGO/ZnO nanorod composite." *J Photochem Photobiol A Chem*, 418.113333.

Apori, S. O., Byalebeka, J., Murongo, M., Ssekandi, J., and Noel, G. L. (2021). "Effect of co-applied corncob biochar with farmyard manure and NPK fertilizer on tropical soil." *Resour. Environ. Sustain.*, 5, 100034.

Argun, M. E. (2008). "Use of clinoptilolite for the removal of nickel ions from water: Kinetics and thermodynamics." *J. Hazard. Mater.*, 150(3), 587–595.

Arias, A. H., Oliva, A. L., Ronda, A. C., Tombesi, N. B., Macchi, P., Solimano, P., Abrameto, M., and Migueles, N. (2023). "Large-scale spatiotemporal variations, sources, and risk assessment of banned OCPs and PAHs in suspended particulate matter from the Negro River, Argentina." *Environ. Pollut.*, 320, 121067.

Asai, H., Samson, B. K., Stephan, H. M., Songyikhangsuthor, K., Homma, K., Kiyono, Y., Inoue, Y., Shiraiwa, T., and Horie, T. (2009). "Biochar amendment techniques for upland rice production in Northern Laos. 1. Soil physical properties, leaf SPAD and grain yield." *Field Crops Re.s*, 111(1–2), 81–84.

Aslam, F., Yasmin, A., and Sohail, S. (2020). "Bioaccumulation of lead, chromium, and nickel by bacteria from three different genera isolated from industrial effluent." *Int. J. Microbiol.*, 23(2), 253–261.

Aswathi, A., Pandey, A., and Sukumaran, R. K. (2019). "Rapid degradation of the organophosphate pesticide – Chlorpyrifos by a novel strain of Pseudomonas nitroreducens AR-3." *Bioresour. Technol.*, 292, 122025.

Ayangbenro, A. S., and Babalola, O. O. (2020). "Genomic analysis of *Bacillus cereus* NWUAB01 and its heavy metal removal from polluted soil." *Sci.Rep.*, 10(1), 1–12.

Ayranci, E., and Hoda, N. (2005). "Adsorption kinetics and isotherms of pesticides onto activated carbon-cloth." *Chemosphere*, 60(11), 1600–1607.

Azimi, A., Azari, A., Rezakazemi, M., and Ansarpour, M. (2017). "Removal of Heavy Metals from Industrial Wastewaters: A Review." *Chem.Bio.Eng. Reviews*, 4(1), 37-59.

Aziz, H., Murtaza, G., Saleem, M. H., Ali, S., Rizwan, M., Riaz, U., Niaz, A., Abualreesh, M. H., and Alatawi, A. (2021). "Alleviation of chlorpyrifos toxicity in maize (*Zea mays* L.) by

reducing its uptake and oxidative stress in response to soil-applied compost and biochar amendments." *Plants*, 10(10).

Bahemmat, M., Farahbakhsh, M., and Kianirad, M. (2016). "Humic substances-enhanced electroremediation of heavy metals contaminated soil." *J. Hazard. Mater.*, 312, 307–318.

Bakshi, P., Chouhan, R., Sharma, P., Mir, B. A., Gandhi, S., Landi, M., Zheng, B., Sharma, A., and Bhardwaj, R. (2021). "Amelioration of chlorpyrifos-induced toxicity in *Brassica juncea* L. by combination of 24-Epibrassinolide and plant-growth-promoting rhizobacteria." *Biomolecules*, 11(6).

Bansod, B. K., Kumar, T., Thakur, R., Rana, S., and Singh, I. (2017). "A review on various electrochemical techniques for heavy metal ions detection with different sensing platforms." *Biosens Bioelectron*, 94, 443-455.

Bashir, A., Malik, L. A., Ahad, S., Manzoor, T., Bhat, M. A., Dar, G. N., and Pandith, A. H. (2019). "Removal of heavy metal ions from aqueous system by ion-exchange and biosorption methods." *Environ Chem Lett*, 17, 729-754.

Bautista-Hernández, D. A., Ramírez-Burgos, L. I., Duran-Páramo, E., and Fernández-Linares, L. (2012). "Zinc and Lead Biosorption by Delftia tsuruhatensis: A Bacterial Strain Resistant to Metals Isolated from Mine Tailings." *J. Water Resour. Prot.*, 04(04), 207–216.

Beesley, L., and Marmiroli, M. (2011). "The immobilisation and retention of soluble arsenic, cadmium and zinc by biochar." *Environ. Pollut.*, 159(2), 474–480.

Bhatt, P., Zhou, X., Huang, Y., Zhang, W., and Chen, S. (2021). "Characterization of the role of esterases in the biodegradation of organophosphate, carbamate, and pyrethroid pesticides." *J. Hazard. Mater.*, 411, 125026.

Bian, R., Joseph, S., Cui, L., Pan, G., Li, L., Liu, X., Zhang, A., Rutlidge, H., Wong, S., Chia, C., Marjo, C., Gong, B., Munroe, P., and Donne, S. (2014). "A three-year experiment confirms continuous immobilization of cadmium and lead in contaminated paddy field with biochar amendment." *J. Hazard. Mater.*, 272, 121–128.

Bigley, A. N., Desormeaux, E., Xiang, D. F., Bae, S. Y., Harvey, S. P., and Raushel, F. M. (2019). “Overcoming the challenges of enzyme evolution to adapt phosphotriesterase for V-agent decontamination.” *Biochemistry*, 58(15), 2039–2053.

Binh, Q. A., and Nguyen, H. H. (2020). “Investigation the isotherm and kinetics of adsorption mechanism of herbicide 2,4-dichlorophenoxyacetic acid (2,4-D) on corn cob biochar.” *Bioresour. Technol. Rep.*, 11, 100520.

Binh, Q. A., Tungtakanpoung, D., and Kajitvichyanukul, P. (2020). “Similarities and differences in adsorption mechanism of dichlorvos and pymetrozine insecticides with coconut fiber biowaste sorbent.” *J. Environ. Sci. Health B.*, 55(2), 103–114.

Bogusz, A., Nowak, K., Stefaniuk, M., Dobrowolski, R., and Oleszczuk, P. (2017). “Synthesis of biochar from residues after biogas production with respect to cadmium and nickel removal from wastewater.” *J. Environ. Manage.*, 201, 268–276.

Bootharaju, M. S., and Pradeep, T. (2012). “Understanding the degradation pathway of the pesticide, chlorpyrifos by noble metal nanoparticles.” *Langmuir*, 28(5), 2671–2679.

Boros-Lajszner, E., Wyszkowska, J., and Kucharski, J. (2018). “Use of zeolite to neutralise nickel in a soil environment.” *Environ. Monit. Assess.*, 190, 1-13.

Bradford, M. M. (1976). “A Rapid and Sensitive Method for the Quantitation of Microgram Quantities of Protein Utilizing the Principle of Protein-Dye Binding.” *Anal. Biochem.*, 72(1-2), 248-254.

Burachevskaya, M., Minkina, T., Bauer, T., Lobzenko, I., Fedorenko, A., Mazarji, M., Sushkova, S., Mandzhieva, S., Nazarenko, A., Butova, V., Wong, M. H., and Rajput, V. D. (2023). “Fabrication of biochar derived from different types of feedstocks as an efficient adsorbent for soil heavy metal removal.” *Sci. Rep.*, 13(1).

Calcan, S. I., Pârvulescu, O. C., Ion, V. A., Răducanu, C. E., Bădulescu, L., Madjar, R., Dobre, T., Egri, D., Moț, A., Iliescu, L. M., and Jerca, I. O. (2022). “Effects of biochar on soil properties and tomato growth.” *Agronomy*, 12(8).

Carles, L., Joly, M., Bonnemoy, F., Leremboure, M., Donnadieu, F., Batisson, I., and Besse-Hoggan, P. (2018). "Biodegradation and toxicity of a maize herbicide mixture: mesotrione, nicosulfuron and S-metolachlor." *J. Hazard. Mater.*, 354, 42–53.

Castilla-Caballero, D., Barraza-Burgos, J., Gunasekaran, S., Roa-Espinosa, A., Colina-Márquez, J., Machuca-Martínez, F., Hernández-Ramírez, A., and Vázquez-Rodríguez, S. (2020). "Experimental data on the production and characterization of biochars derived from coconut-shell wastes obtained from the Colombian Pacific Coast at low temperature pyrolysis." *Data Brief*, 28, 1–11.

Carrasco Cabrera, L., and Medina Pastor, P. (2022). "The 2020 European Union report on pesticide residues in food." *EFSA J*, 20(3), e07215.

Castro, C., Urbieta, M. S., Plaza Cazón, J., and Donati, E. R. (2019). "Metal biorecovery and bioremediation: Whether or not thermophilic are better than mesophilic microorganisms." *Bioresour. Technol.*, 279, 317–326.

Chauhan, P. S., and Jha, B. (2018). "Pilot scale production of extracellular thermo-alkali stable laccase from Pseudomonas sp. S2 using agro waste and its application in organophosphorous pesticides degradation." *J Chem Technol Biotechnol*, 93(4), 1022–1030.

Chen, B., Yuan, M., and Qian, L. (2012). "Enhanced bioremediation of PAH-contaminated soil by immobilized bacteria with plant residue and biochar as carriers." *J Soils Sediments*, 12(9), 1350–1359.

Chen, F., Sun, J., Han, Z., Yang, X., Xian, J. A. A., Lv, A., Hu, X., and Shi, H. (2019a). "Isolation, Identification and Characteristics of *Aeromonas veronii* from diseased crucian carp (*Carassius auratus gibelio*)." *Front Microbiol*, 10.491277.

Chen, Q., Yao, Y., Li, X., Lu, J., Zhou, J., and Huang, Z. (2018). "Comparison of heavy metal removals from aqueous solutions by chemical precipitation and characteristics of precipitates." *J Water Process Eng*, 26, 289–300.

Chen, R., Zhao, X., Jiao, J., Li, Y., and Wei, M. (2019). "Surface-modified biochar with polydentate binding sites for the removal of cadmium." *Int J Mol Sci*, 20(7).

Chen, S., Li, Y., Fan, Z., Liu, F., Liu, H., Wang, L., and Wu, H. (2021). “Soil bacterial community dynamics following bioaugmentation with Paenarthrobacter sp. W11 in atrazine-contaminated soil.” *Chemosphere*, 282, 130976.

Cheng, J., Yin, W., Chang, Z., Lundholm, N., and Jiang, Z. (2017). “Biosorption capacity and kinetics of cadmium(II) on live and dead Chlorella vulgaris.” *J Appl Phycol*, 29(1), 211–221.

Chi, T., Zuo, J., and Liu, F. (2017). “Performance and mechanism for cadmium and lead adsorption from water and soil by corn straw biochar.” *Front Environ Sci Eng*, 11(2).

Chishti, Z., Hussain, S., Arshad, K. R., Khalid, A., and Arshad, M. (2013a). “Microbial degradation of chlorpyrifos in liquid media and soil.” *J Environ Manage*, 114, 372–380.

Choińska-Pulit, A., Sobolczyk-Bednarek, J., and Łaba, W. (2018). “Optimization of copper, lead and cadmium biosorption onto newly isolated bacterium using a Box-Behnken design.” *Ecotoxicol Environ Saf*, 149, 275–283.

Chojnacka, K. (2010). “Biosorption and bioaccumulation - the prospects for practical applications.” *Environ Int*, 36(3), 299–307.

Choleva, T. G., Tsogas, G. Z., Vlessidis, A. G., and Giokas, D. L. (2020). “Development of a sequential extraction and speciation procedure for assessing the mobility and fractionation of metal nanoparticles in soils.” *Environ Pollut*, 263, 114407.

Chuaphasuk, C., and Prapagdee, B. (2019a). “Effects of biochar-immobilized bacteria on phytoremediation of cadmium-polluted soil.” *Environ Sci Pollut Res*, 26(23), 23679–23688.

Congeevaram, S., Dhanarani, S., Park, J., Dexilin, M., and Thamaraiselvi, K. (2007). “Biosorption of chromium and nickel by heavy metal resistant fungal and bacterial isolates.” *J Hazard Mater*, 146(1–2), 270–277.

Cuixia, Y., Yingming, X., Lin, W., Xuefeng, L., Yuebing, S., and Hongtao, J. (2020). “Effect of different pyrolysis temperatures on physico-chemical characteristics and lead(II) removal of biochar derived from chicken manure.” *RSC Adv*, 10(7), 3667-3674.

Cycoń, M., Mrozik, A., and Piotrowska-Seget, Z. (2017). “Bioaugmentation as a strategy for the remediation of pesticide-polluted soil: A review.” *Chemosphere*, 172, 52–71.

Dar, M. A., Kaushik, G., and Villarreal-Chiu, J. F. (2019). “Pollution status and bioremediation of chlorpyrifos in environmental matrices by the application of bacterial communities: A review.” *J Environ Manage*, 239, 124-136.

Das, S., and Adhya, T. K. (2015). “Degradation of chlorpyrifos in tropical rice soils.” *J Environ Manage*, 152, 36–42.

Das, S. K., Das, A. R., and Guha, A. K. (2007). “A study on the adsorption mechanism of mercury on Aspergillus versicolor biomass.” *Environ Sci Technol*, 41(24), 8281–8287.

Das, S. K., and Ghosh, G. K. (2022). “Soil hydro-physical properties affected by biomass-derived biochar and organic manure: a low-cost technology for managing acidic mountain sandy soils of north eastern region of India.” *Biomass Convers Biorefin*, 1-15.

Das, S. K., Ghosh, G. K., Avasthe, R., Kundu, M. C., Choudhury, B. U., Baruah, K., and Lama, A. (2021). “Innovative biochar and organic manure co-composting technology for yield maximization in maize-black gram cropping system.” *Biomass Convers Biorefin*, 13(9), 7797-7809.

Dash, D. M., and Osborne, W. J. (2020). “Rapid biodegradation and biofilm-mediated bioremoval of organophosphorus pesticides using an indigenous Kosakonia oryzae strain - VITPSCQ3 in a Vertical-flow Packed Bed Biofilm Bioreactor.” *Ecotoxicol Environ Saf*, 192, 110290.

Deb, S., Ahmed, S. F., and Basu, M. (2013). “Metal accumulation in cell wall: A possible mechanism of cadmium resistance by pseudomonas stutzeri.” *Bull Environ Contam Toxicol*, 90(3), 323–328.

de-Bashan, L. E., and Bashan, Y. (2010). “Immobilized microalgae for removing pollutants: Review of practical aspects.” *Bioresour Technol*, 101(6), 1611–1627.

Deng, J., Li, X., Wei, X., Liu, Y., Liang, J., Shao, Y., Huang, W., and Cheng, X. (2020). “Different adsorption behaviors and mechanisms of a novel amino-functionalized hydrothermal biochar for hexavalent chromium and pentavalent antimony.” *Bioresour Technol*, 310, 123438.

Deng, S., Ren, B., Hou, B., Deng, R., and Cheng, S. (2023). “Antimony-complexed heavy metal wastewater in antimony mining areas: Source, risk and treatment.” *Environ Technol Innov*, 103355.

Dey, U., Chatterjee, S., and Mondal, N. K. (2016). “Isolation and characterization of arsenic-resistant bacteria and possible application in bioremediation.” *Biotechnology Reports*, 10, 1–7.

Dhaliwal, S. S., Singh, J., Taneja, P. K., and Mandal, A. (2020). “Remediation techniques for removal of heavy metals from the soil contaminated through different sources: a review.” *Environ Sci Pollut Res*, 27, 1319-1333.

Ding, T., Huang, T., Wu, Z., Li, W., Guo, K., and Li, J. (2019a). “Adsorption-desorption behavior of carbendazim by sewage sludge-derived biochar and its possible mechanism.” *RSC Adv*, 9(60), 35209–35216.

Dong, D., Feng, Q., McGrouther, K., Yang, M., Wang, H., and Wu, W. (2015). “Effects of biochar amendment on rice growth and nitrogen retention in a waterlogged paddy field.” *J Soils Sediments*, 15(1), 153–162.

Ekram, M. A. E., Sarker, I., Rahi, M. S., Rahman, M. A., Saha, A. K., and Reza, M. A. (2020). “Efficacy of soil-borne Enterobacter sp. for carbofuran degradation: HPLC quantitation of degradation rate.” *J Basic Microbiol*, 60(5), 390–399.

El-Naggar, A., Shaheen, S. M., Ok, Y. S., and Rinklebe, J. (2018). “Biochar affects the dissolved and colloidal concentrations of Cd, Cu, Ni, and Zn and their phytoavailability and potential mobility in a mining soil under dynamic redox-conditions.” *Sci Total Environ*, 624, 1059–1071.

Escudero, L. B., Quintas, P. Y., Wuilloud, R. G., and Dotto, G. L. (2019). “Recent advances on elemental biosorption.” *Environ Chem Lett*, 17(1), 409–427.

Esfandiar, N., Suri, R., and McKenzie, E. R. (2022). “Competitive sorption of Cd, Cr, Cu, Ni, Pb and Zn from stormwater runoff by five low-cost sorbents; Effects of co-contaminants, humic acid, salinity and pH.” *J Hazard Mater*, 423, 126938.

Essandoh, M., Wolgemuth, D., Pittman, C. U., Mohan, D., and Mlsna, T. (2017). "Adsorption of metribuzin from aqueous solution using magnetic and nonmagnetic sustainable low-cost biochar adsorbents." *Environ Sci Pollut Res*, 24(5), 4577–4590.

Fan, J., Cai, C., Chi, H., Reid, B. J., Coulon, F., Zhang, Y., and Hou, Y. (2020). "Remediation of cadmium and lead polluted soil using thiol-modified biochar." *J Hazard Mater*, 388, 122037.

Fan, S., Wang, Y., Wang, Z., Tang, J., Tang, J., and Li, X. (2017). "Removal of methylene blue from aqueous solution by sewage sludge-derived biochar: Adsorption kinetics, equilibrium, thermodynamics and mechanism." *J Environ Chem Eng*, 5(1), 601–611.

Farooque, A. A., Zaman, Q., Abbas, F., Hammad, H. M., Acharya, B., and Esau, T. (2020). "Correction to: How can potatoes be smartly cultivated with biochar as a soil nutrient amendment technique in Atlantic Canada." *Arabian Journal of Geosciences*, 13, 1-9.

Ferguson, T. L., and Wilkinson, R. R. (1984). "Incineration of pesticide wastes." *ACS Symposium Series*, ACS, 181–191.

Filip, Z., and Hermann, S. (2001a). "An attempt to differentiate Pseudomonas spp. and other soil bacteria by FT-IR spectroscopy." *Eur J Soil Biol*, 37(3), 137–143.

Fu, F., and Wang, Q. (2011). "Removal of heavy metal ions from wastewaters: A review." *J Environ Manage*, 92(3), 407-418.

Gangola, S., Sharma, A., Bhatt, P., Khati, P., and Chaudhary, P. (2018). "Presence of esterase and laccase in Bacillus subtilis facilitates biodegradation and detoxification of cypermethrin." *Sci Rep*, 8(1), 1–11.

Gao, X., Peng, Y., Guo, L., Wang, Q., Guan, C. Y., Yang, F., and Chen, Q. (2020). "Arsenic adsorption on layered double hydroxides biochars and their amended red and calcareous soils." *J Environ Manage*, 271, 111045.

Gebre, M. G., and Earl, H. J. (2020). "Effects of Growth Medium and Water Stress on Soybean [Glycine max (L.) Merr.] Growth, Soil Water Extraction and Rooting Profiles by Depth in 1-m Rooting Columns." *Front Plant Sci*, 11, 487.

Geetha, P., and Sureshkumar, P. (2018). “Aerobic Rice for Nutrient and Water Use Efficiency in Lateritic Soils of Kerala.” *Int J. Bioresour Stress Manag*, 9(5), 562–567.

Ghorbani, M., Neugschwandtner, R. W., Konvalina, P., Asadi, H., Kopecký, M., and Amirahmadi, E. (2023). “Comparative effects of biochar and compost applications on water holding capacity and crop yield of rice under evaporation stress: a two-years field study.” *Paddy and Water Environment*, 21(1), 47–58.

González-Delgado, A. D., Villabona-Ortíz, A., and Tejada-Tovar, C. (2022). “Evaluation of Three Biomaterials from Coconut Mesocarp for Use in Water Treatments Polluted with an Anionic Dye.” *Water*, 14(3), 408.

Govarthanan, M., Ameen, F., Kamala-Kannan, S., Selvankumar, T., Almansob, A., Alwakeel, S. S., and Kim, W. (2020). “Rapid biodegradation of chlorpyrifos by plant growth-promoting psychrophilic Shewanella sp. BT05: An eco-friendly approach to clean up pesticide-contaminated environment.” *Chemosphere*, 247, 125948.

Guidi, P., Bernardeschi, M., Palumbo, M., Genovese, M., Scarcelli, V., Fiorati, A., Riva, L., Punta, C., Corsi, I., and Frenzilli, G. (2020). “Suitability of a cellulose-based nanomaterial for the remediation of heavy metal contaminated freshwaters: A case-study showing the recovery of cadmium induced dna integrity loss, cell proliferation increase, nuclear morphology and chromosomal alterations.” *Nanomaterials*, 10(9), 1–15.

Gumpu, M. B., Sethuraman, S., Krishnan, U. M., and Rayappan, J. B. B. (2015). “A review on detection of heavy metal ions in water - An electrochemical approach.” *Sens Actuators B Chem*, 213, 515-533.

Guo, J., Yan, C., Luo, Z., Fang, H., Hu, S., and Cao, Y. (2019). “Synthesis of a novel ternary HA/Fe-Mn oxides-loaded biochar composite and its application in cadmium(II) and arsenic(V) adsorption.” *J Environ Sci*, 85, 168–176.

Guo, Z. Q., Li, P., Yang, X. M., Wang, Z. H., Lu, B. B., Chen, W. J., Wu, Y., Li, G. W., Zhao, Z. W., Liu, G. bin, Ritsema, C., Geissen, V., and Xue, S. (2022). “Soil texture is an important factor determining how microplastics affect soil hydraulic characteristics.” *Environ Int*, 165, 107293.

Gupta, A., Singh, U. B., Sahu, P. K., Paul, S., Kumar, A., Malviya, D., Singh, S., Kuppusamy, P., Singh, P., Paul, D., Rai, J. P., Singh, H. V., Manna, M. C., Crusberg, T. C., Kumar, A., and Saxena, A. K. (2022). "Linking Soil Microbial Diversity to Modern Agriculture Practices: A Review." *Int J Environ Res Public Health*, 19(5), 3141.

Gupta, J., Rathour, R., Singh, R., and Thakur, I. S. (2019). "Production and characterization of extracellular polymeric substances (EPS) generated by a carbofuran degrading strain Cupriavidus sp. ISTL7." *Bioresour Technol*, 282, 417–424.

Gupta, P., and Diwan, B. (2017). "Bacterial Exopolysaccharide mediated heavy metal removal: A Review on biosynthesis, mechanism and remediation strategies." *Biotechnol Rep*, 13, 58–71.

Ha, N. T. H., Toan, N. C., and Kajitvichyanukul, P. (2021). "Enhanced paraquat removal from contaminated water using cell-immobilized biochar." *Clean Technol Environ Policy*, 1-13.

Hadzi, G. Y., Essumang, D. K., and Ayoko, G. A. (2024). "Assessment of contamination and potential ecological risks of heavy metals in riverine sediments from gold mining and pristine areas in Ghana." *Journal of Trace Elements and Minerals*, 7, 100109.

Hafeez, Y., Iqbal, S., Jabeen, K., Shahzad, S., Jahan, S., and Rasul, F. (2017). "Effect of biochar application on seed germination and seedling growth of glycine max (l.) Merr. Under drought stress." *Pak. J. Bot*, 49(15), 7-13.

Hamadeen, H. M., and Elkhatib, E. A. (2022). "Nanostructured modified biochar for effective elimination of chlorpyrifos from wastewater: Enhancement, mechanisms and performance." *J Water Proc. Eng*, 47, 102703.

Han, J., Zhang, J., Meng, J., Cai, Y., Cheng, M., Wu, S., and Li, Z. (2023). "Characterization of modified rice straw biochar in immobilizing *Bacillus subtilis* 168 and evaluation on its role as a novel agent for zearalenone-removal delivery." *J Hazard Mater*, 453.

Han, Y., Song, L., Zou, N., Chen, R., Qin, Y., and Pan, C. (2016). "Multi-residue determination of 171 pesticides in cowpea using modified QuEChERS method with multi-walled carbon nanotubes as reversed-dispersive solid-phase extraction materials." *J Chromatogr B Analyt Technol Biomed Life Sci*, 1031, 99–108.

Hansda, A., Kumar, V., and Anshumali. (2016). “A comparative review towards potential of microbial cells for heavy metal removal with emphasis on biosorption and bioaccumulation.” *World J Microbiol Biotechnol*, 32(10), 1–14.

Hassani, S., Momtaz, S., Vakhshiteh, F., Maghsoudi, A. S., Ganjali, M. R., Norouzi, P., and Abdollahi, M. (2017). “Biosensors and their applications in detection of organophosphorus pesticides in the environment.” *Arch Toxicol*, 91, 109-130.

He, R., Peng, Z., Lyu, H., Huang, H., Nan, Q., and Tang, J. (2018). “Synthesis and characterization of an iron-impregnated biochar for aqueous arsenic removal.” *Sci Total Environ*, 612, 1177–1186.

Herniter, I. A., Muñoz-Amatriaín, M., and Close, T. J. (2020). “Genetic, textual, and archeological evidence of the historical global spread of cowpea (*Vigna unguiculata* [L.] Walp.).” *Legum Sci*, 2(4), e57.

Hossain, N., Nizamuddin, S., Griffin, G., Selvakannan, P., Mubarak, N. M., and Mahlia, T. M. I. (2020). “Synthesis and characterization of rice husk biochar via hydrothermal carbonization for wastewater treatment and biofuel production.” *Sci Rep*, 10(1), 18851.

Hassani, S., Momtaz, S., Vakhshiteh, F., Maghsoudi, A. S., Ganjali, M. R., Norouzi, P., and Abdollahi, M. (2017). “Biosensors and their applications in detection of organophosphorus pesticides in the environment.” *Arch Toxicol*, 91,109-130.

Hu, N., Xu, Y., Sun, C., Zhu, L., Sun, S., Zhao, Y., and Hu, C. (2021). “Removal of atrazine in catalytic degradation solutions by microalgae Chlorella sp. and evaluation of toxicity of degradation products via algal growth and photosynthetic activity.” *Ecotoxicol Environ Saf*, 207, 111546.

Huang, F., Guo, C. L., Lu, G. N., Yi, X. Y., Zhu, L. D., and Dang, Z. (2014a). “Bioaccumulation characterization of cadmium by growing *Bacillus cereus* RC-1 and its mechanism.” *Chemosphere*, 109, 134–142.

Huang, J., Wang, J., Wang, S., and Guo, S. (2020a). “Different biochars as microbial immobilization substrates for efficient copper II removal.” *Spectroscopy Letters*, 53(9), 712–725.

Huang, S. W., Chen, X., Wang, D. D., Jia, H. L., and Wu, L. (2020c). “Bio-reduction and synchronous removal of hexavalent chromium from aqueous solutions using novel microbial cell/algal-derived biochar particles: Turning an environmental problem into an opportunity.” *Bioresour Technol*, 309, 123304.

Igalavithana, A. D., Mandal, S., Niazi, N. K., Vithanage, M., Parikh, S. J., Mukome, F. N. D., Rizwan, M., Oleszczuk, P., Al-Wabel, M., Bolan, N., Tsang, D. C. W., Kim, K. H., and Ok, Y. S. (2017). “Advances and future directions of biochar characterization methods and applications.” *Crit Rev Environ Sci Technol*, 47(23), 2275–2330.

Ilyas, S., Srivastava, R. R., and Ilyas, N. (2020). “Biosorption of strontium from aqueous solutions.” *Handbook of Environl Chem*, 88, 65–83.

Imran, M., Iqbal, M. M., Iqbal, J., Shah, N. S., Khan, Z. U. H., Murtaza, B., Amjad, M., Ali, S., and Rizwan, M. (2021). “Synthesis, characterization and application of novel MnO and CuO impregnated biochar composites to sequester arsenic (As) from water: Modeling, thermodynamics and reusability.” *J Hazard Mater*, 401, 123338.

Inyang, M. I., Gao, B., Yao, Y., Xue, Inthama, P., Pumas, P., Pekkoh, J., Pathom-aree, W., and Pumas, C. (2021). “Plant Growth and Drought Tolerance-Promoting Bacterium for Bioremediation of Paraquat Pesticide Residues in Agriculture Soils.” *Front Microbiol*, 12, 604662.

Irfan, M., Hayat, S., Ahmad, A., and Alyemeni, M. N. (2013). “Soil cadmium enrichment: Allocation and plant physiological manifestations.” *Saudi J Biol Sci*, 20(1), 1-10.

Ismail, I., and Moustafa, T. (2016). “Biosorption of heavy metals.” *Heavy Metals: Sources, Toxicity and Remediation Techniques*, 3, 131–174.

J. Mwenye, O., Rensburg, L. Van, Biljon, A. Van, and Merwe, R. Van der. (2019). “Seedling Shoot and Root Growth Responses among Soybean (*Glycine max*) Genotypes to Drought Stress.” *Soybean - Biomass, Yield and Productivity*.

Jacob, M. M., Ponnuchamy, M., Kapoor, A., and Sivaraman, P. (2020). “Bagasse based biochar for the adsorptive removal of chlorpyrifos from contaminated water.” *J Environ Chem Eng*, 8(4), 103904.

Javed, M. B., Malik, Z., Kamran, M., Abbasi, G. H., Majeed, A., Riaz, M., Bukhari, M. A., Mustafa, A., Ahmar, S., Mora-Poblete, F., Rafay, M., and Bukhari, S. A. H. (2021). "Assessing yield response and relationship of soil boron fractions with its accumulation in sorghum and cowpea under boron fertilization in different soil series." *Sustainability*, 13(8), 4192.

Jia, Y., Shi, S., Liu, J., Su, S., Liang, Q., Zeng, X., and Li, T. (2018). "Study of the effect of pyrolysis temperature on the Cd2+ adsorption characteristics of biochar." *Appl Sci*, 8(7), 1019.

Joo, J. ock, Choi, J. H., Kim, I. H., Kim, Y. K., and Oh, B. K. (2015). "Effective bioremediation of Cadmium (II), nickel (II), and chromium (VI) in a marine environment by using Desulfovibrio desulfuricans." *Biotechnol Bioprocess Eng*, 20(5), 937–941.

Joseph, C. G., Li Puma, G., Bono, A., and Krishnaiah, D. (2009). "Sonophotocatalysis in advanced oxidation process: A short review." *Ultrason Sonochem*, 16(5), 583-589.

Kammann, C. I., Linsel, S., Gößling, J. W., and Koyro, H. W. (2011). "Influence of biochar on drought tolerance of Chenopodium quinoa Willd and on soil-plant relations." *Plant Soil*, 345(1), 195–210.

Karimi, A., Moezzi, A., Chorom, M., and Enayatizamir, N. (2020). "Application of biochar changed the status of nutrients and biological activity in a calcareous soil." *J Soil Sci Plant Nutr*, 20(2), 450–459.

Karimi, H., Mahdavi, S., Asgari Lajayer, B., Moghiseh, E., Rajput, V. D., Minkina, T., and Astatkie, T. (2021). "Insights on the bioremediation technologies for pesticide-contaminated soils." *Environ Geochem Health*, 44(4), 1329-1354.

Kaur, P., and Balomajumder, C. (2020). "Effective mycoremediation coupled with bioaugmentation studies: An advanced study on newly isolated *Aspergillus* sp. in Type-II pyrethroid-contaminated soil." *Environl Pollut*, 261, 114073.

Kazimierski, P., Januszewicz, K., Godlewski, W., Fijuk, A., Suchocki, T., Chaja, P., Barczak, B., and Kardaś, D. (2022). "The course and the effects of agricultural biomass pyrolysis in the production of high-calorific biochar." *Materials*, 15(3), 1038.

Khalili-Zanjani, M. R., Yamini, Y., Yazdanfar, N., and Shariati, S. (2008). "Extraction and determination of organophosphorus pesticides in water samples by a new liquid phase

microextraction-gas chromatography-flame photometric detection." *Anal Chim Acta*, 606(2), 202–208.

Khan, I., Iqbal, B., Khan, A. A., Inamullah, Rehman, A., Fayyaz, A., Shakoor, A., Farooq, T. H., and Wang, L. X. (2022). "The interactive impact of straw mulch and biochar application positively enhanced the growth indexes of maize (Zea mays L.) crop." *Agronomy*, 12(10), 2584.

Khan, Z. H., Gao, M., Qiu, W., and Song, Z. (2020). "Properties and adsorption mechanism of magnetic biochar modified with molybdenum disulfide for cadmium in aqueous solution." *Chemosphere*, 255, 126995.

Khatoon, H., and Rai, J. P. N. (2020). "Optimization studies on biodegradation of atrazine by *Bacillus badius* ABP6 strain using response surface methodology." *Biotechnol Rep*, 26, e00459.

Kim, H. S., Kim, K. R., Kim, H. J., Yoon, J. H., Yang, J. E., Ok, Y. S., Owens, G., and Kim, K. H. (2015). "Effect of biochar on heavy metal immobilization and uptake by lettuce (*Lactuca sativa* L.) in agricultural soil." *Environ Earth Sci*, 74(2), 1249–1259.

Kim, J., Kim, S. Y., Yang, C. M., and Lee, G. W. (2019). "Possibility of Recycling SiOx particles collected at silicon ingot production process as an anode material for Lithium-Ion batteries." *Sci Rep*, 9(1), 13313.

Kodom, K., Preko, K., and Boamah, D. (2012). "X-ray Fluorescence (XRF) Analysis of Soil Heavy Metal Pollution from an Industrial Area in Kumasi, Ghana." *Soil Sediment Contam*, 21(8), 1006–1021.

Koippully, S., Pattnaik, S. S., and Busi, S. (2018). "Isolation, identification and substrate specificity of a nitrilase producing bacteria, *Acidovorax* sp. SK1." *J Microbiol Biotechnol Food Sci*, 8(2), 788–793.

Kolekar, P. D., Patil, S. M., Suryavanshi, M. V., Suryawanshi, S. S., Khandare, R. V., Govindwar, S. P., and Jadhav, J. P. (2019). "Microcosm study of atrazine bioremediation by indigenous microorganisms and cytotoxicity of biodegraded metabolites." *J Hazard Mater*, 374, 66–73.

Kostas, E. T., Durán-Jiménez, G., Shepherd, B. J., Meredith, W., Stevens, L. A., Williams, O. S. A., Lye, G. J., and Robinson, J. P. (2020). "Microwave pyrolysis of olive pomace for bio-oil and bio-char production." J *Chem Eng*, 387, 123404.

Kumar, M., Yadav, A. N., Saxena, R., Paul, D., and Tomar, R. S. (2021). "Biodiversity of pesticides degrading microbial communities and their environmental impact." *Biocatal Agric Biotechnol*, 31, 101883.

Kumaresan Sarankumar, R., Arulprakash, A., Devanesan, S., Selvi, A., AlSalhi, M. S., Rajasekar, A., and Ahamed, A. (2020). "Bioreduction of hexavalent chromium by chromium resistant alkalophilic bacteria isolated from tannery effluent." *J King Saud Univ Sci*, 32(3), 1969–1977.

Kumas, A., Ertekin, S. G., Gurbanov, R., Simsek, Y. E., Kocak, F. O., and Degirmenci, L. (2021). "Effect of Micromonospora sp. KSC08 on nitrogen conservation throughout composting." *Biomass Convers Biorefin*, 1-16.

Kurniawan, T. A., Chan, G. Y. S., Lo, W. H., and Babel, S. (2006). "Physico-chemical treatment techniques for wastewater laden with heavy metals." J *Chem Eng*, 118(1–2), 83–98.

Kwak, J. H., Islam, M. S., Wang, S., Messele, S. A., Naeth, M. A., El-Din, M. G., and Chang, S. X. (2019). "Biochar properties and lead(II) adsorption capacity depend on feedstock type, pyrolysis temperature, and steam activation." *Chemosphere*, 231, 393–404.

Lai, W., Wu, Y., Zhang, C., Dilinuer, Y., Pasang, L., Lu, Y., Wang, Y., Chen, H., and Li, Z. (2022). "Combination of biochar and phosphorus solubilizing bacteria to improve the stable form of toxic metal minerals and microbial abundance in lead/cadmium-contaminated soil." *Agronomy*, 12(5), 1003.

Lashari, M. S., Liu, Y., Li, L., Pan, W., Fu, J., Pan, G., Zheng, J., Zheng, J., Zhang, X., and Yu, X. (2013). "Effects of amendment of biochar-manure compost in conjunction with pyroligneous solution on soil quality and wheat yield of a salt-stressed cropland from Central China Great Plain." *Field Crops Res*, 144, 113–118.

Leng, L., Xiong, Q., Yang, L., Li, H., Zhou, Y., Zhang, W., Jiang, S., Li, H., and Huang, H. (2021). "An overview on engineering the surface area and porosity of biochar." *Sci Total Environ*, 763, 144204.

Li, H., Dong, X., Silva, E. B. da, Oliveira, L. M. de, Chen, Y., and Ma, L. Q. (2017a). "Mechanisms of metal sorption by biochars: Biochar characteristics and modifications." *Chemosphere*, 178, 466-478.

Li, M., Zhao, Z., Wu, X., Zhou, W., and Zhu, L. (2017b). "Impact of mineral components in cow manure biochars on the adsorption and competitive adsorption of oxytetracycline and carbaryl." *RSC Adv*, 7(4), 2127–2136.

Li, W., Chen, Y., and Wang, T. (2021a). "Cadmium biosorption by lactic acid bacteria *Weissella viridescens* ZY-6." *Food Control*, 123, 107747.

Li, Y., Xin, M., Xie, D., Fan, S., Ma, J., Liu, K., and Yu, F. (2021b). "Variation in extracellular polymeric substances from *Enterobacter* sp. And Their Pb^{2+}adsorption behaviors." *ACS Omega*, 6(14), 9617–9628.

Lin, X. W., Xie, Z. B., Zheng, J. Y., Liu, Q., Bei, Q. C., and Zhu, J. G. (2015). "Effects of biochar application on greenhouse gas emissions, carbon sequestration and crop growth in coastal saline soil." *Eur J Soil Sci*, 66(2), 329–338.

Liu, J., Cheng, W., Yang, X., and Bao, Y. (2020a). "Modification of biochar with silicon by one-step sintering and understanding of adsorption mechanism on copper ions." *Sci Total Environ*, 704, 135252.

Liu, J., Ding, Y., Ma, L., Gao, G., and Wang, Y. (2017a). "Combination of biochar and immobilized bacteria in cypermethrin-contaminated soil remediation." *Int Biodeterior Biodegradation*, 120, 15–20.

Liu, J., Xue, J., Wei, X., Su, H., and Xu, R. (2020b). "Optimization of Cr^{6+} Removal by Bacillus subtilis Strain SZMC 6179J from Chromium-Containing Soil." *Indian J Microbiol*, 60(4), 430–435.

Liu, L., Fang, W., Yuan, M., Li, X., Wang, X., and Dai, Y. (2021). “Metolachlor-adsorption on the walnut shell biochar modified by the fulvic acid and citric acid in water.” *J Environ Chem Eng*, 9(5), 106238.

Liu, L., Yang, X., Ahmad, S., Li, X., Ri, C., Tang, J., Ellam, R. M., and Song, Z. (2023). “Silicon (Si) modification of biochars from different Si-bearing precursors improves cadmium remediation.” J *Chem Eng*, 457, 141194.

Liu, S., Li, J., Xu, S., Wang, M., Zhang, Y., and Xue, X. (2019). “A modified method for enhancing adsorption capability of banana pseudostem biochar towards methylene blue at low temperature.” *Bioresour Technol*, 282, 48–55.

Liu, X., Wang, Y., Gui, C., Li, P., Zhang, J., Zhong, H., and Wei, Y. (2016). “Chemical forms and risk assessment of heavy metals in sludge-biochar produced by microwave-induced low temperature pyrolysis.” *RSC Adv*, 6(104), 101960–101967.

Liu, Y., Alessi, D. S., Owttrim, G. W., Petrash, D. A., Mloszewska, A. M., Lalonde, S. V., Martinez, R. E., Zhou, Q., and Konhauser, K. O. (2015a). “Cell surface reactivity of *Synechococcus* sp. PCC 7002: Implications for metal sorption from seawater.” *Geochim Cosmochim Acta*, 169, 30–44.

Liu, Y., Tie, B., Peng, O., Luo, H., Li, D., Liu, S., Lei, M., Wei, X., Liu, X., and Du, H. (2020c). “Inoculation of Cd-contaminated paddy soil with biochar-supported microbial cell composite: A novel approach to reducing cadmium accumulation in rice grains.” *Chemosphere*, 247, 125850.

Lopes, C. S. C., Teixeira, D. B., Braz, B. F., Santelli, R. E., Castilho, L. V. A. de, Gomez, J. G. C., P. V. Castro, R., Seldin, L., and Freire, D. M. G. (2021). “Application of rhamnolipid surfactant for remediation of toxic metals of long- and short-term contamination sites.” *Int J Environ Sci Technol*, 18(3), 575–588.

Lu, P., Li, Q., Liu, H., Feng, Z., Yan, X., Hong, Q., and Li, S. (2013). “Biodegradation of chlorpyrifos and 3,5,6-trichloro-2-pyridinol by *Cupriavidus* sp. DT-1.” *Bioresour Technol*, 127, 337–342.

Lu, Y., Liang, X., Niyungeko, C., Zhou, J., Xu, J., and Tian, G. (2018). “A review of the identification and detection of heavy metal ions in the environment by voltammetry.” *Talanta*, 178, 324-338.

Lukyanenko, K. A., Denisov, I. A., Sorokin, V. V., Yakimov, A. S., Esimbekova, E. N., and Belobrov, P. I. (2019). “Handheld enzymatic luminescent biosensor for rapid detection of heavy metals in water samples.” *Chemosensors*, 7(1), 16.

Ma, H., Wei, M., Wang, Z., Hou, S., Li, X., and Xu, H. (2020). “Bioremediation of cadmium polluted soil using a novel cadmium immobilizing plant growth promotion strain *Bacillus* sp. TZ5 loaded on biochar.” *J Hazard Mater*, 388, 122065.

Ma, J., Huang, W., Zhang, X., Li, Y., and Wang, N. (2021). “The utilization of lobster shell to prepare low-cost biochar for high-efficient removal of copper and cadmium from aqueous: Sorption properties and mechanisms.” *J Environ Chem Eng*, 9(1), 104703.

Major, J., Rondon, M., Molina, D., Riha, S. J., and Lehmann, J. (2010). “Maize yield and nutrition during 4 years after biochar application to a Colombian savanna oxisol.” *Plant Soil*, 333(1), 117–128.

Mali, H., Shah, C., Patel, D. H., Trivedi, U., and Subramanian, R. B. (2022). “Degradation insight of organophosphate pesticide chlorpyrifos through novel intermediate 2,6-dihydroxypyridine by *Arthrobacter* sp. HM01.” *Bioresour Bioprocess*, 9(1), 1-14.

Malik, L. A., Bashir, A., Qureashi, A., and Pandith, A. H. (2019). “Detection and removal of heavy metal ions: a review.” *Environ Chem Lett*, 17, 1495-1521.

Malla, M. A., Dubey, A., Kumar, A., Yadav, S., and Kumari, S. (2023). “Modeling and optimization of chlorpyrifos and glyphosate biodegradation using RSM and ANN: Elucidating their degradation pathways by GC-MS based metabolomics.” *Ecotoxicol Environ Saf*, 252, 114628.

Manikandan, S. K., Giannakoudakis, D. A., Prekodravac, J. R., Nair, V., and Colmenares, J. C. (2023). “Role of catalyst supports in biocatalysis.” *J Chem Technol Biotechnol*, 98(1), 7-21.

Manikandan, S. K., and Nair, V. (2022). "*Pseudomonas stutzeri* Immobilized Sawdust Biochar for Nickel Ion Removal." *Catalysts*, 12(12), 1495.

Manikandan, S.K., Shilli, A., Noronha, F.R. and Nair, V. (2022). "Soil toxicity and remediation techniques". Pesticides remediation technologies from water and wastewater, 411-429.

Manikandan, S. K., and Nair, V. (2023a). "Dual-role of coconut shell biochar as a soil enhancer and catalyst support in bioremediation." *Biomass Convers Biorefin*, 1-12.

Manikandan, S. K., Pallavi, P., Shetty, K., Bhattacharjee, D., Giannakoudakis, D. A., Katsoyiannis, I. A., and Nair, V. (2023b). "Effective usage of biochar and microorganisms for the removal of heavy metal ions and pesticides." *Molecules*, 28(2), 719.

Manikandan, S. K., and Nair, V. (2023c). "Developing a biocatalyst showcasing the synergistic effect of rice husk biochar and bacterial cells for the removal of heavy metals." *New J. Chem*, *47*(46), 21199-21213.

Marican, A., and Durán-Lara, E. F. (2018). "A review on pesticide removal through different processes." *Environ Sci Pollut Res*, 25(3), 2051–2064.

Mašek, O., Brownsort, P., Cross, A., and Sohi, S. (2013). "Influence of production conditions on the yield and environmental stability of biochar." *Fuel*, 151–155.

Mehmood, A., Naveed, K., Ayub, Q., Alamri, S., Siddiqui, M. H., Wu, C., Wang, D., Saud, S., Banout, J., Danish, S., Datta, R., Hammad, H. M., Nasim, W., Mubeen, M., Shah, F., and Fahad, S. (2021). "Exploring the potential of moringa leaf extract as bio stimulant for improving yield and quality of black cumin oil." *Sci Rep*, 11(1), 24217.

Mehrotra, T., Dev, S., Banerjee, A., Chatterjee, A., Singh, R., and Aggarwal, S. (2021). "Use of immobilized bacteria for environmental bioremediation: A review." *J Environ Chem Eng*, 9(5), 105920.

Meng, R., Zhu, Q., Long, T., He, X., Luo, Z., Gu, R., Wang, W., and Xiang, P. (2023). "The innovative and accurate detection of heavy metals in foods: A critical review on electrochemical sensors." *Food Control*, 109743.

Menzies Pluer, E. G., Schneider, R. L., Morreale, S. J., Liebig, M. A., Li, J., Li, C. X., and Walter, M. T. (2020). “Returning degraded soils to productivity: An examination of the potential of coarse woody amendments for improved water retention and nutrient holding capacity.” *Water Air Soil Pollut*, 231(1), 1-14.

Mezynska, M., and Brzóska, M. M. (2018). “Environmental exposure to cadmium—a risk for health of the general population in industrialized countries and preventive strategies.” *Environ Sci Pollut Res*, 25(4), 3211–3232.

Mishra, S., Lin, Z., Pang, S., Zhang, Y., Bhatt, P., and Chen, S. (2021). “Biosurfactant is a powerful tool for the bioremediation of heavy metals from contaminated soils.” *J Hazard Mater*, 418, 126253.

Mohan, D., Abhishek, K., Sarswat, A., Patel, M., Singh, P., and Pittman, C. U. (2018). “Biochar production and applications in soil fertility and carbon sequestration-a sustainable solution to crop-residue burning in India.” *RSC Adv*, 8(1), 508–520.

Mukherjee, S., Sarkar, B., Aralappanavar, V. K., Mukhopadhyay, R., Basak, B. B., Srivastava, P., Marchut-Mikołajczyk, O., Bhatnagar, A., Semple, K. T., and Bolan, N. (2022). “Biochar-microorganism interactions for organic pollutant remediation: Challenges and perspectives.” *Environ Pollut*, 308, 119609.

Muniswami, D. M., Buvaneshwari K, Fathima Rosa Mystica L, Naveena T, Pabitha B, Reshma S, Rangila D, Santhiya P, Sharmila Devi N, Ahamed Rasheeq A, Sampathkumar P, and Dineshkumar R. (2021). “Comparative assessment of different biofertilizers in maize (Zea mays L.) cultivation.” *Biomass Convers Biorefin*, 1-19.

Murthy, T. P. K., Hari Krishna, R., Chandraprabha, M. N., Divyashri, G., Vanessa, C., Dhanyatha, S. V., Megha, S., and Swarnima, P. (2020). “Glycerol mediated solution combustion synthesis of nano magnesia and its application in the adsorptive removal of anionic dyes.” *Nano Express*, 1(3), 030018.

Mwandira, W., Nakashima, K., Kawasaki, S., Arabelo, A., Banda, K., Nyambe, I., Chirwa, M., Ito, M., Sato, T., Igarashi, T., Nakata, H., Nakayama, S., and Ishizuka, M. (2020). “Biosorption

of Pb (II) and Zn (II) from aqueous solution by *Oceanobacillus profundus* isolated from an abandoned mine." *Sci Rep*, 10(1), 1–9.

Nabieh, K. A., Mortada, W. I., Helmy, T. E., Kenawy, I. M. M., and Abou El-Reash, Y. G. (2021). "Chemically modified rice husk as an effective adsorbent for removal of palladium ions." *Heliyon*, 7(1).

Nam, S. N., Cho, H., Han, J., Her, N., and Yoon, J. (2018). "Photocatalytic degradation of acesulfame K: Optimization using the Box–Behnken design (BBD)." *Process Saf. Environ. Prot*, 113, 10–21.

Nandhini, A. R., Harshiny, M., and Gummadi, S. N. (2021). "Chlorpyrifos in environment and food: A critical review of detection methods and degradation pathways." *Environ Sci Process Impacts*, 23(9), 1255-1277.

Naseem, S., Hamza, S., Nawaz-ul-Huda, S., Bashir, E., and ul-Haq, Q. (2014). "Geochemistry of Cd in groundwater of Winder, Balochistan and suspected health problems." *Environ Earth Sci*, 71(4), 1683–1690.

Nduka, J. K., Kelle, H. I., and Amuka, J. O. (2019). "Health risk assessment of cadmium, chromium and nickel from car paint dust from used automobiles at auto-panel workshops in Nigeria." *Toxicol Rep*, 6, 449–456.

Nguyen, B. T., Trinh, N. N., Le, C. M. T., Nguyen, T. T., Tran, T. Van, Thai, B. V., and Le, T. Van. (2018). "The interactive effects of biochar and cow manure on rice growth and selected properties of salt-affected soil." *Arch Agron Soil Sci*, 64(12), 1744–1758.

Nguyen, C. T., Nguyen, T. H. H., Tra, V. T., Tungtakanpoung, D., Tran, C. S., Vo, T. K. Q., and Kaewlom, P. (2023). "Paraquat removal by free and immobilized cells of *Pseudomonas putida* on corn cob biochar." *Case Stud Chem Environ Eng*, 8, 100376.

Nicodemus, T. J., DiRusso, C. C., Wilson, M., and Black, P. N. (2020). "Reactive Oxygen Species (ROS) mediated degradation of organophosphate pesticides by the green microalgae *Coccomyxa subellipsoidea*." *Bioresour Technol Rep*, 11, 100461.

Nie, F., Guan, K., Zou, C., Xu, Z., and Liu, Z. (2023). “Synthesis of magnetic rice husk biochar and its application in the adsorption of Ni(II) from aqueous solutions.” *Biomass Convers Biorefin*.1-13.

Noronha, F. R., Manikandan, S. K., and Nair, V. (2022). “Role of coconut shell biochar and earthworm (*Eudrilus euginea*) in bioremediation and palak spinach (*Spinacia oleracea* L.) growth in cadmium-contaminated soil.” *J Environ Manage*, 302(PA), 114057.

Novak, J. M., Busscher, W. J., Laird, D. L., Ahmedna, M., Watts, D. W., and Niandou, M. A. S. (2009). “Impact of biochar amendment on fertility of a southeastern coastal plain soil.” *Soil Sci*, 174(2), 105–112.

O’Connell, D. W., Birkinshaw, C., and O’Dwyer, T. F. (2008). “Heavy metal adsorbents prepared from the modification of cellulose: A review.” *Bioresour Technol*, 99(15), 6709–6724.

Ogura, A. P., Lima, J. Z., Marques, J. P., Massaro Sousa, L., Rodrigues, V. G. S., and Espíndola, E. L. G. (2021). “A review of pesticides sorption in biochar from maize, rice, and wheat residues: Current status and challenges for soil application.” *J Environ Manage*, 300, 113753.

Ölmezoğlu, E., Kiratli Herand, B., Öncel, M. S., Tunç, K., and Özkan, M. (2012). “Copper bioremoval by novel bacterial isolates and their identification by 16S rRNA gene sequence analysis.” *Turkish J. Bio*, 36(4), 469–476.

Ormanci, S., and Yucel, N. (2017). “Biofilm formation on polystyrene and glass surface by Aeromonas species isolated from different sources.” *J Food Process Preserv*, 41(6),e13223.

Othmani, A., John, J., Rajendran, H., Mansouri, A., Sillanpää, M., and Velayudhaperumal Chellam, P. (2021). “Biochar and activated carbon derivatives of lignocellulosic fibers towards adsorptive removal of pollutants from aqueous systems: Critical study and future insight.” *Sep Purif Technol*, 274, 119062.

Ouallal, I., Abbas, Y., Elyacoubi, H., Imtara, H., Zain, M. N. Al, Ouajdi, M., Goumi, Y. El, Alzamel, N. M., Noman, O. M., and Rochdi, A. (2022). “Effects of arbuscular mycorrhizal

inoculation by indigenous fungal complexes on the morpho-physiological behavior of *Argania spinosa* subjected to water deficit stress." *Horticulturae*, 8(4), 280.

Ouyang, L., Tang, Q., Yu, L., and Zhang, R. (2014). "Effects of amendment of different biochars on soil enzyme activities related to carbon mineralisation." *Soil Research*, 52(7), 706–716.

Oyewole, O. A., Zobeashia, S. S. L. T., Oladoja, E. O., Raji, R. O., Odiniya, E. E., and Musa, A. M. (2019). "Biosorption of heavy metal polluted soil using bacteria and fungi isolated from soil." *SN Appl Sci*, 1(8), 1–8.

Oza, S., Kodgire, P., and Kachhwaha, S. S. (2022). "Analysis of RSM Based BBD and CCD techniques applied for biodiesel production from waste cotton-seed cooking oil via ultrasound method." *Anal. Chem. Lett*, 12(1), 86–101.

Pandey, D., Daverey, A., and Arunachalam, K. (2020). "Biochar: Production, properties and emerging role as a support for enzyme immobilization." *J Clean Prod*, 255, 120267.

Park, J. H., Wang, J. J., Kim, S. H., Kang, S. W., Jeong, C. Y., Jeon, J. R., Park, K. H., Cho, J. S., Delaune, R. D., and Seo, D. C. (2019). "Cadmium adsorption characteristics of biochars derived using various pine tree residues and pyrolysis temperatures." *J Colloid Interface Sci*, 553, 298–307.

Park, S. J., Lee, Y. J., Kang, J. K., Lee, J., and Lee, C. G. (2021). "Application of Fe-impregnated biochar from cattle manure for removing pentavalent antimony from aqueous solution." *Applied Sciences (Switzerland)*, 11(19), 9257.

Pretti Ogura, A., Zanin Lima, J., Pelinsom Marques, J., Massaro Sousa, L., Guimarães Silvestre Rodrigues, V., and Luiz Gaeta Espíndola, E. (2021). "A Review of Pesticides Sorption in Biochar from Maize, Rice, and Wheat Residues : current status and challenges for soil application." *J Environ Manage*, 300, 113753.

Prieto, P., Nistor, V., Nouneh, K., Oyama, M., Abd-Lefdil, M., and Díaz, R. (2012). "XPS study of silver, nickel and bimetallic silver-nickel nanoparticles prepared by seed-mediated growth." *Appl. Surf. Sci.*, 258(22), 8807–8813.

Priyadarshanee, M., and Das, S. (2021). “Biosorption and removal of toxic heavy metals by metal tolerating bacteria for bioremediation of metal contamination: A comprehensive review.” *J. Environ. Chem. Eng.*, 9(1), 104686.

Pua, F. L., Sajab, M. S., Chia, C. H., Zakaria, S., Rahman, I. A., and Salit, M. S. (2013). “Alkaline-treated cocoa pod husk as adsorbent for removing methylene blue from aqueous solutions.” *J. Environ. Chem. Eng.*, 1(3), 460–465.

Qi, W.-Y., Chen, H., Wang, Z., Xing, S.-F., Song, C., Yan, Z., and Wang, S.-G. (2023). “Biochar-immobilized *Bacillus megaterium* enhances Cd immobilization in soil and promotes *Brassica chinensis* growth.” *J. Hazard. Mater.*, 458, 131921.

Qi, X., Gou, J., Chen, X., Xiao, S., Ali, I., Shang, R., Wang, D., Wu, Y., Han, M., and Luo, X. (2021). “Application of mixed bacteria-loaded biochar to enhance uranium and cadmium immobilization in a co-contaminated soil.” *J. Hazard. Mater.*, 401, 123823.

Qiu, B., Tao, X., Wang, H., Li, W., Ding, X., and Chu, H. (2021). “Biochar as a low-cost adsorbent for aqueous heavy metal removal: A review.” *J. Anal. Appl. Pyrolysis.*, 155, 105081.

Rabbi, S. M. F., Minasny, B., Salami, S. T., McBratney, A. B., and Young, I. M. (2021). “Greater, but not necessarily better: The influence of biochar on soil hydraulic properties.” *Eur. J. Soil. Sci.*, 72(5), 2033-2048.

Rahman, A., Haque, M. A., Ghosh, S., Shinu, P., Attimarad, M., and Kobayashi, G. (2023). “Modified shrimp-based chitosan as an emerging adsorbent removing heavy metals (chromium, nickel, arsenic, and cobalt) from polluted water.” *Sustainability*, 15(3).

Rahman, K., Menon, U., Sivasubramanian, V., and Ranjitha, J. (2022). “Removal of cadmium by heavy metal–resistant bacteria isolated from Hussain Sagar Lake—Hyderabad.” *Biomass Convers Biorefin*, 12(5), 1703–1713.

Rahman, M. A., Lamb, D., Rahman, M. M., Bahar, M. M., Sanderson, P., Abbasi, S., Bari, A. S. M. F., and Naidu, R. (2021). “Removal of arsenate from contaminated waters by novel zirconium and zirconium-iron modified biochar.” *J. Hazard. Mater.*, 409, 124488.

Ranal, M. A., Santana, D. G. de, Ferreira, W. R., and Mendes-Rodrigues, C. (2009). "Calculating germination measurements and organizing spreadsheets." *Revista Brasileira de Botânica*, 32(4), 849–855.

Rao, M. M., Meena, A. K., and Galib. (2011). "Detection of toxic heavy metals and pesticide residue in herbal plants which are commonly used in the herbal formulations." *Environ Monit Assess*, 181(1–4), 267–271.

Rawtani, D., Khatri, N., Tyagi, S., and Pandey, G. (2018). "Nanotechnology-based recent approaches for sensing and remediation of pesticides." *J. Environ. Manage.*, 206, 749–762.

Ray, S., and Shaju, S. T. (2023). "Bioaccumulation of pesticides in fish resulting toxicities in humans through food chain and forensic aspects." *Environ Anal Health Toxicol*, 38.

Razzak, S. A., Faruque, M. O., Alsheikh, Z., Alsheikhmohamad, L., Alkuroud, D., Alfayez, A., Hossain, S. M. Z., and Hossain, M. M. (2022). "A comprehensive review on conventional and biological-driven heavy metals removal from industrial wastewater." *Environ Adv*, 7, 100168.

Rehman, I., Riaz, M., Ali, S., Arif, M. S., Ali, S., Alyemeni, M. N., and Alsahli, A. A. (2021). "Evaluating the effects of biochar with farmyard manure under optimal mineral fertilizing on tomato growth, soil organic c and biochemical quality in a low fertility soil." *Sustainability*, 13(5), 1–19.

Ren, L. ying, Hong, Z. neng, Liu, Z. dong, and Xu, R. kou. (2018). "ATR–FTIR investigation of mechanisms of *Bacillus subtilis* adhesion onto variable- and constant-charge soil colloids." *Colloids. Surf. B. Biointerfaces.*, 162, 288–295.

Ren, W., Chen, L., Wang, Q., and Ren, Y. (2022). "Transcriptome and metabolome analysis of upland cotton (*Gossypium hirsutum*) seed pretreatment with $MgSO_4$ in response to salinity stress." *Life*, 12(6), 921.

Rinklebe, J., and Shaheen, S. M. (2017). "Redox chemistry of nickel in soils and sediments: A review." *Chemosphere*, 179, 265–278.

Robles-Fernández, A., Areias, C., Daffonchio, D., Vahrenkamp, V. C., and Sánchez-Román, M. (2022). “The role of microorganisms in the nucleation of carbonates, environmental implications and applications.” *Minerals*,12,1562.

Rombel, A., Krasucka, P., and Oleszczuk, P. (2022). “Sustainable biochar-based soil fertilizers and amendments as a new trend in biochar research.” *Sci. Total Environ*, 816, 151588.

Rondon, M. A., Lehmann, J., Ramírez, J., and Hurtado, M. (2007). “Biological nitrogen fixation by common beans (*Phaseolus vulgaris L.*) increases with bio-char additions.” *Biol. Fertil. Soils.*, 43(6), 699–708.

Roy, S., Gupta, S. K., Prakash, J., Habib, G., and Kumar, P. (2022). “A global perspective of the current state of heavy metal contamination in road dust.” *Environ. Sci. Pollut. Res*, 29, 33230–33251.

Rugnini, L., Costa, G., Congestri, R., and Bruno, L. (2017). “Testing of two different strains of green microalgae for Cu and Ni removal from aqueous media.” *Sci. Total Environ*, 601–602, 959–967.

Saavedra, R., Muñoz, R., Taboada, M. E., Vega, M., and Bolado, S. (2018). “Comparative uptake study of arsenic, boron, copper, manganese and zinc from water by different green microalgae.” *Bioresour. Technol.*, 263, 49–57.

Sahoo, D., and Remya, N. (2022). “Influence of operating parameters on the microwave pyrolysis of rice husk: biochar yield, energy yield, and property of biochar.” *Biomass Convers Biorefin*, 12(8), 3447–3456.

Sakulthaew, C., Watcharenwong, A., Chokejaroenrat, C., and Rittirat, A. (2021). “Leonardite-derived biochar suitability for effective sorption of herbicides.” *Water. Air. Soil. Pollut.*, 232(2), 36.

Saleem, M., Pirzada, T., and Qadeer, R. (2007). “Sorption of acid violet 17 and direct red 80 dyes on cotton fiber from aqueous solutions.” *Colloids. Surf. A. Physicochem. Eng. Asp.*, 292(2–3), 246–250.

Saleh, M. E., El-Refaey, A. A., and Mahmoud, A. H. (2016). “Effectiveness of sunflower seed husk biochar for removing copper ions from wastewater: A Comparative Study.” *Soil Water Res*, 11(1), 53–63.

Saletnik, B., Bajcar, M., Zaguła, G., Saletnik, A., Tarapatskyy, M., and Puchalski, C. (2019). “Biochar as a stimulator for germination capacity in seeds of *Virginia mallow* (*Sida hermaphrodita (L.) Rusby*).” *Applied Sciences (Switzerland)*, 9(16), 3213.

Sandaa, R. A., Torsvik, V., and Enger. (2001). “Influence of long-term heavy-metal contamination on microbial communities in soil.” *Soil. Biol. Biochem.*, 33(3), 287–295.

Santos, E. V. Dos, Sáez, C., Martínez-Huitle, C. A., Cañizares, P., and Rodrigo, M. A. (2015). “The role of particle size on the conductive diamond electrochemical oxidation of soil-washing effluent polluted with atrazine.” *Electrochem. Commun.*, 55, 26–29.

Saravanan, A., Kumar, P. S., Jeevanantham, S., Harikumar, P., Bhuvaneswari, V., and Indraganti, S. (2022). “Identification and sequencing of bacteria from crop field: Application of bacteria — agro-waste biosorbent for rapid pesticide removal.” *Environ. Technol. Innov.*, 25, 102116.

Sarker, A., Lee, S. H., Kwak, S. Y., Nandi, R., and Kim, J. E. (2020). “Comparative catalytic degradation of a metabolite 3,5-dichloroaniline derived from dicarboximide fungicide by laccase and MnO_2 mediators.” *Ecotoxicol. Environ. Saf.*, 196, 110561.

Sasikala, C., Jiwal, S., Rout, P., and Ramya, M. (2012). “Biodegradation of chlorpyrifos by bacterial consortium isolated from agriculture soil.” *World J. Microbiol. Biotechnol.*, 28(3), 1301–1308.

Satapute, P., and Jogaiah, S. (2022). “A biogenic microbial biosurfactin that degrades difenoconazole fungicide with potential antimicrobial and oil displacement properties.” *Chemosphere*, 286(P1), 131694.

Sathishkumar, K., Murugan, K., Benelli, G., Higuchi, A., and Rajasekar, A. (2017). “Bioreduction of hexavalent chromium by *Pseudomonas stutzeri* L1 and *Acinetobacter baumannii* L2.” *Ann. Microbiol.*, 67(1), 91–98.

Schaumlöffel, D. (2012). “Nickel species: Analysis and toxic effects.” *Journal of Trace Elements in Medicine and Biology*, 26(1), 1–6.

Sethu, V. S., Aziz, A. R., and Aroua, M. K. (2008). “Recovery and reutilisation of copper from metal hydroxide sludges.” *Clean. Technol. Environ. Policy.*, 10(2), 131–136.

Severo, F. F., Silva, L. S. da, Moscôso, J. S. C., Sarfaraz, Q., Rodrigues Júnior, L. F., Lopes, A. F., Marzari, L. B., and Molin, G. D. (2020). “Chemical and physical characterization of rice husk biochar and ashes and their iron adsorption capacity.” *SN Appl. Sci.*, 2(7), 1-9.

Shabbir, M., Singh, M., Maiti, S., Kumar, S., and Saha, S. K. (2018). “Removal enactment of organo-phosphorous pesticide using bacteria isolated from domestic sewage.” *Bioresour. Technol.*, 263, 280–288.

Shangdiar, S., Lin, Y. C., Cheng, P. C., Chou, F. C., and Wu, W. D. (2021). “Development of biochar from the refuse derived fuel (RDF) through organic / inorganic sludge mixed with rice straw and coconut shell.” *Energy*, 215, 119151.

Shariff, A., Mohamad Aziz, N. S., Md Saleh, N., and Ruzali, N. S. I. (2016). “The effect of feedstock type and slow pyrolysis temperature on biochar yield from coconut wastes.” *Int. J. Chem. Molecular Eng*, 10(12), 1410–1414.

Sharma, B., and Shukla, P. (2021a). “Lead bioaccumulation mediated by *Bacillus cereus* BPS-9 from an industrial waste contaminated site encoding heavy metal resistant genes and their transporters.” *J. Hazard. Mater.*, 401, 123285.

Sharma, B., and Shukla, P. (2021b). “A comparative analysis of heavy metal bioaccumulation and functional gene annotation towards multiple metal resistant potential by *Ochrobactrum intermedium* BPS-20 and *Ochrobactrum ciceri* BPS-26.” *Bioresour. Technol.*, 320(P2), 124330.

Sharma, R., Jasrotia, T., Sharma, S., Sharma, M., Kumar, R., Vats, R., Kumar, R., Umar, A., and Akhtar, M. S. (2021). “Sustainable removal of Ni (II) from waste water by freshly isolated fungal strains.” *Chemosphere*, 282, 130871.

Shen, L., Li, Z., Wang, J., Liu, A., Li, Z., Yu, R., Wu, X., Liu, Y., Li, J., and Zeng, W. (2018). "Characterization of extracellular polysaccharide/protein contents during the adsorption of Cd (II) by *Synechocystis* sp. PCC6803." *Environ. Sci. Pollut. Res*, 25, 20713–20722.

Shen, X., Huang, D. Y., Ren, X. F., Zhu, H. H., Wang, S., Xu, C., He, Y. B., Luo, Z. C., and Zhu, Q. H. (2016). "Phytoavailability of Cd and Pb in crop straw biochar-amended soil is related to the heavy metal content of both biochar and soil." *J Environ Manage*, 168, 245–251.

Shen, Y., Li, H., Zhu, W., Ho, S. H., Yuan, W., Chen, J., and Xie, Y. (2017a). "Microalgal-biochar immobilized complex: A novel efficient biosorbent for cadmium removal from aqueous solution." *Bioresour. Technol.*, 244, 1031–1038.

Shi, Q., Zhang, H., Shahab, A., Zeng, H., Zeng, H., Bacha, A. U. R., Nabi, I., Siddique, J., and Ullah, H. (2021). "Efficient performance of magnesium oxide loaded biochar for the significant removal of Pb^{2+} and Cd^{2+} from aqueous solution." *Ecotoxicol. Environ. Saf.*, 221, 112426.

Shi, T., Fang, L., Qin, H., Chen, Y., Wu, X., and Hua, R. (2019). "Rapid biodegradation of the organophosphorus insecticide chlorpyrifos by *cupriavidus nantongensis* x1T." *Int. J. Environ. Res. Public. Health.*, 16(23), 4593.

Shilli, A., Manikandan, S. K., and Nair, V. (2023). "Application of Box-Behnken Design in optimization of the okra (*Abelmoschus esculentus* L.) plant growth in loamy sand soil." *J. Soil. Sci. Plant. Nutr.*, 23(2), 2625–2636.

Shoiful, A., Ueda, Y., Nugroho, R., and Honda, K. (2016). "Degradation of organochlorine pesticides (OCPs) in water by iron (Fe)-based materials." *J. Water Process Eng*, 11, 110–117.

Silambarasan, S., and Abraham, J. (2013). "Ecofriendly method for bioremediation of chlorpyrifos from agricultural soil by novel fungus *Aspergillus terreus* JAS1." *Water. Air. Soil. Pollut.*, 224, 1369.

Singh, B. K., Walker, A., and Wright, D. J. (2006). "Bioremedial potential of fenamiphos and chlorpyrifos degrading isolates: Influence of different environmental conditions." *Soil Biol Biochem*, 38, 2682–2693.

Singh, R., Singh, P., Singh, H., and Raghubanshi, A. S. (2019). “Impact of sole and combined application of biochar, organic and chemical fertilizers on wheat crop yield and water productivity in a dry tropical agro-ecosystem.” *Biochar*, 1(2), 229–235.

Singh, R., Srivastava, P., Bhadouria, R., Yadav, A., Singh, H., and Raghubanshi, A. S. (2020). “Combined application of biochar and farmyard manure reduces wheat crop eco-physiological performance in a tropical dryland agro-ecosystem.” *Energy. Ecol. Environ.*, 5(3), 171–183.

Sirajuddin, S., Khan, M. A., Qader, S. A. U., Iqbal, S., Sattar, H., and Ansari, A. (2020). “A comparative study on degradation of complex malathion organophosphate using of *Escherichia coli* IES-02 and a novel carboxylesterase.” *Int. J. Biol. Macromol.*, 145, 445–455.

Soares, P. R. S., Birolli, W. G., Ferreira, I. M., and Porto, A. L. M. (2021). “Biodegradation pathway of the organophosphate pesticides chlorpyrifos, methyl parathion and profenofos by the marine-derived fungus *Aspergillus sydowii* CBMAI 935 and its potential for methylation reactions of phenolic compounds.” *Mar. Pollut. Bull.*, 166, 112185.

Sobiecka, E., Mroczkowska, M., and Olejnik, T. P. (2022). “The influence of chlorpyrifos on the nonenzymatic antioxidants content in macrophytes leaves.” *Antioxidants*, 11(4), 684.

Song, X. D., Xue, X. Y., Chen, D. Z., He, P. J., and Dai, X. H. (2014). “Application of biochar from sewage sludge to plant cultivation: Influence of pyrolysis temperature and biochar-to-soil ratio on yield and heavy metal accumulation.” *Chemosphere*, 109, 213–220.

Souza Pinheiro, A. de, and Andrade, J. B. de. (2009). “Development, validation and application of a SDME/GC-FID methodology for the multiresidue determination of organophosphate and pyrethroid pesticides in water.” *Talanta*, 79(5), 1354–1359.

Sun, L., Zhang, G., Li, X., Zhang, X., Hang, W., Tang, M., and Gao, Y. (2023). “Effects of biochar on the transformation of cadmium fractions in alkaline soil.” *Heliyon*, 9(1), e12949.

Sun, T., Miao, J., Saleem, M., Zhang, H., Yang, Y., and Zhang, Q. (2020a). “Bacterial compatibility and immobilization with biochar improved tebuconazole degradation, soil microbiome composition and functioning.” *J. Hazard. Mater.*, 398, 122941.

Suo, F., You, X., Ma, Y., and Li, Y. (2019). “Rapid removal of triazine pesticides by P doped biochar and the adsorption mechanism.” *Chemosphere*, 235, 918–925.

Supreeth, M., Chandrashekar, M. A., Sachin, N., and Raju, N. S. (2016). "Effect of chlorpyrifos on soil microbial diversity and its biotransformation by *Streptomyces sp*. HP-11." *3 Biotech*, 6(2), 147.

Supreeth, M., and Raju, N. (2017). "Biotransformation of chlorpyrifos and endosulfan by bacteria and fungi." *Appl. Microbiol. Biotechnol*., 101(12), 5961-5971.

Talebi, P., Singh, H., Rani, E., Huttula, M., and Cao, W. (2021). "Surface plasmon-driven photocatalytic activity of Ni@NiO/$NiCO_3$ core-shell nanostructures." *RSC Adv.*, 11(5), 2733–2743.

Tao, Y., Han, S., Zhang, Q., Yang, Y., Shi, H., Akindolie, M. S., Jiao, Y., Qu, J., Jiang, Z., Han, W., and Zhang, Y. (2020). "Application of biochar with functional microorganisms for enhanced atrazine removal and phosphorus utilization." *J Clean Prod*, 257,120535.

Tariq, M., Waseem, M., Rasool, M. H., Zahoor, M. A., and Hussain, I. (2019). "Isolation and molecular characterization of the indigenous *Staphylococcus aureus* strain K1 with the ability to reduce hexavalent chromium for its application in bioremediation of metal-contaminated sites." *PeerJ*, 10, 1–20.

Tekaya, N., Saiapina, O., Ouada, H. Ben, Lagarde, F., Namour, P., Ouada, H. Ben, and Jaffrezic-Renault, N. (2014). "Bi-Enzymatic conductometric biosensor for detection of heavy metal ions and pesticides in water samples based on enzymatic inhibition in *Arthrospira platensis" J Environ Prot*, 5, 441–453.

Teng, Z., Shao, W., Zhang, K., Yu, F., Huo, Y., and Li, M. (2020a). "Enhanced passivation of lead with immobilized phosphate solubilizing bacteria beads loaded with biochar/ nanoscale zero valent iron composite." *J. Hazard. Mater.*, 384, 121505.

Thangalazhy-Gopakumar, S., Adhikari, S., Ravindran, H., Gupta, R. B., Fasina, O., Tu, M., and Fernando, S. D. (2010). "Physiochemical properties of bio-oil produced at various temperatures from pine wood using an auger reactor." *Bioresour. Technol.*, 101(21), 8389–8395.

Tian, X., Li, C., Zhang, M., Wan, Y., Xie, Z., Chen, B., and Li, W. (2018). “Biochar derived from corn straw affected availability and distribution of soil nutrients and cotton yield.” *PLoS One*, 13(1), e0189924.

Tsai, Y.-P., You, S.-J., Pai, T.-Y., and Chen, K.-W. (2006). “Effect of Cd(II) on different bacterial species present in a single sludge activated sludge process for carbon and nutrient removal.” *J. Environ. Eng*, 132(2), 173–180.

Tu, C., Wei, J., Guan, F., Liu, Y., Sun, Y., and Luo, Y. (2020). “Biochar and bacteria inoculated biochar enhanced Cd and Cu immobilization and enzymatic activity in a polluted soil.” *Environ. Int.*, 137, 105576

Tully, D. B., Collins, B. J., Overstreet, J. D., Smith, C. S., Dinse, G. E., Mumtaz, M. M., and Chapin, R. E. (2000). “Effects of arsenic, cadmium, chromium, and lead on gene expression regulated by a battery of 13 different promoters in recombinant HepG2 cells.” *Toxicol. Appl. Pharmacol.*, 168(2), 79–90.

Tyagi, S., Rawtani, D., Khatri, N., and Tharmavaram, M. (2018). “Strategies for Nitrate removal from aqueous environment using Nanotechnology: A Review.” *J. Water Process Eng,* 21, 84–95.

Uwizeyimana, H., Wang, M., Chen, W., and Khan, K. (2017). “The eco-toxic effects of pesticide and heavy metal mixtures towards earthworms in soil.” *Environ Toxicol Pharmacol*, 55, 22-29.

Velusamy, K. (2017). “Response of relative leaf water content, chlorophyll stability index, proline and yield of cotton to the application of biochar, mulch and PPFM spray under differing moisture regimes.” *Int. J. Agri. Sci,* 9(45), 4753–4756.

Verheijen, F. G. A., Zhuravel, A., Silva, F. C., Amaro, A., Ben-Hur, M., and Keizer, J. J. (2019a). “The influence of biochar particle size and concentration on bulk density and maximum water holding capacity of sandy vs sandy loam soil in a column experiment.” *Geoderma*, 347, 194–202.

Vijayaraghavan, K. (2019). “Recent advancements in biochar preparation, feedstocks, modification, characterization and future applications.” *Environ. Technol. Rev.*, 8(1), 47–64.

Vimal, V., Patel, M., and Mohan, D. (2019). “Aqueous carbofuran removal using slow pyrolyzed sugarcane bagasse biochar: Equilibrium and fixed-bed studies.” *RSC Adv.*, 9(45), 26338–26350.

Wahla, A. Q., Anwar, S., Fareed, M. I., Ikram, W., Ali, L., Alharby, H. F., Bamagoos, A. A., Almaghamsi, A. A., Iqbal, S., and Ali, S. (2022). “Immobilization of metribuzin-degrading bacteria on biochar: Enhanced soil remediation and bacterial community restoration.” *Front Microbiol*, 13, 1027284.

Wahla, A. Q., Anwar, S., Mueller, J. A., Arslan, M., and Iqbal, S. (2020a). “Immobilization of metribuzin degrading bacterial consortium MB3R on biochar enhances bioremediation of potato vegetated soil and restores bacterial community structure.” *J Hazard Mater*, 390, 121493.

Wallace, D. R., and Buha Djordjevic, A. (2020). “Heavy metal and pesticide exposure: A mixture of potential toxicity and carcinogenicity.” *Curr Opin Toxicol*, 19, 72-79.

Wan, S., Qiu, L., Li, Y., Sun, J., Gao, B., He, F., and Wan, W. (2020). “Accelerated antimony and copper removal by manganese oxide embedded in biochar with enlarged pore structure.” J. *Chem. Eng.,* 402, 126021.

Wang, C., Gu, L., Ge, S., Liu, X., Zhang, X., and Chen, X. (2019). “Remediation potential of immobilized bacterial consortium with biochar as carrier in pyrene-Cr (VI) co-contaminated soil.” *Environ. Technol.*, 40(18), 2345–2353.

Wang, H. T., Ding, J., Chi, Q. Q., Li, G., Pu, Q., Xiao, Z. F., and Xue, X. M. (2020). “The effect of biochar on soil-plant-earthworm-bacteria system in metal(loid) contaminated soil.” *Environ. Pollut.,* 263, 114610.

Wang, K., Qiao, Y., Zhang, H., Yue, S., Li, H., Ji, X., and Liu, L. (2018a). “Bioaccumulation of heavy metals in earthworms from field contaminated soil in a subtropical area of China.” *Ecotoxicol. Environ. Saf.*, 148, 876–883.

Wang, P., Yin, Y., Guo, Y., and Wang, C. (2015). “Removal of chlorpyrifos from waste water by wheat straw-derived biochar synthesized through oxygen-limited method.” *RSC Adv*, 5(89), 72572–72578.

Wang, S., Guo, W., Gao, F., Wang, Y., and Gao, Y. (2018b). “Lead and uranium sorptive removal from aqueous solution using magnetic and nonmagnetic fast pyrolysis rice husk biochars.” *RSC Adv*, 8(24), 13205–13217.

Wang, T., Sun, H., Ren, X., Li, B., and Mao, H. (2018c). “Adsorption of heavy metals from aqueous solution by UV-mutant *Bacillus subtilis* loaded on biochars derived from different stock materials.” *Ecotoxicol. Environ. Saf.*, 148, 285–292.

Wang, Z., Ren, D., Wu, J., Jiang, S., Yu, H., Cheng, Y., Zhang, S., and Zhang, X. (2021). “Study on adsorption-degradation of 2,4-dichlorophenol by modified biochar immobilized laccase.” *Int. J. Environ. Sci. Technol.*, 1-14.

Wei, W., Wang, Q., Li, A., Yang, J., Ma, F., Pi, S., and Wu, D. (2016). “Biosorption of Pb (II) from aqueous solution by extracellular polymeric substances extracted from *Klebsiella* sp. J1: Adsorption behavior and mechanism assessment.” *Sci Rep*, 6(1), 31575.

Wu, J., Wang, T., Wang, J., Zhang, Y., and Pan, W. P. (2021). “A novel modified method for the efficient removal of Pb and Cd from wastewater by biochar: Enhanced the ion exchange and precipitation capacity.” *Sci. Total Environ.*, 754.142150.

Xia, Y., Li, Y., Sun, Y., Miao, W., and Liu, Z. (2021). “Co-pyrolysis of corn stover with industrial coal ash for in situ efficient remediation of heavy metals in multi-polluted soil.” *Environ. Pollut.*, 289, 117840.

Xiao, R., Ali, A., Wang, P., Li, R., Tian, X., and Zhang, Z. (2019). “Comparison of the feasibility of different washing solutions for combined soil washing and phytoremediation for the detoxification of cadmium (Cd)and zinc (Zn)in contaminated soil.” *Chemosphere*, 230, 510–518.

Xie, Y., He, N., Wei, M., Wen, T., Wang, X., Liu, H., Zhong, S., and Xu, H. (2021). “Cadmium biosorption and mechanism investigation using a novel *Bacillus subtilis* KC6 isolated from pyrite mine.” *J. Clean. Prod.*, 312, 127749.

Xu, B., Sun, Q. J., Lan, J. C. W., Chen, W. M., Hsueh, C. C., and Chen, B. Y. (2019). “Exploring the glyphosate-degrading characteristics of a newly isolated, highly adapted indigenous bacterial strain, *Providencia rettgeri* GDB 1.” *J. Biosci. Bioeng.*, 128(1), 80–87.

Xu, D., Wang, S., Zhang, J., Tang, X., Guo, Y., and Huang, C. (2015). “Supercritical water oxidation of a pesticide wastewater.” *Chem. Eng. Res. Des.*, 94, 396–406.

Xu, X., Cao, X., and Zhao, L. (2013). “Comparison of rice husk- and dairy manure-derived biochars for simultaneously removing heavy metals from aqueous solutions: Role of mineral components in biochars.” *Chemosphere*, 92(8), 955–961.

Xu, X., Hu, X., Ding, Z., and Chen, Y. (2017). “Effects of copyrolysis of sludge with calcium carbonate and calcium hydrogen phosphate on chemical stability of carbon and release of toxic elements in the resultant biochars.” *Chemosphere*, 189, 76–85.

Xu, Z., He, M., Xu, X., Cao, X., and Tsang, D. C. W. (2021). “Impacts of different activation processes on the carbon stability of biochar for oxidation resistance.” *Bioresour. Technol.*, 338, 125555.

Yaashikaa, P. R., Kumar, P. S., Varjani, S., and Saravanan, A. (2020). “A critical review on the biochar production techniques, characterization, stability and applications for circular bioeconomy.” *Biotechnol. Rep.*, 28, e00570.

Yadav, P., Anu, Kumar Tiwari, S., Kumar, V., Singh, D., Kumar, S., Manisha, Malik, V., and Singh, B. (2022). “Sugarcane bagasse: an important lignocellulosic substrate for production of enzymes and biofuels.” *Biomass Convers Biorefin.*, 1-32.

Yadav, S., Khan, M. A., Sharma, R., Malik, A., and Sharma, S. (2021). “Potential of formulated Dyadobacter jiangsuensis strain 12851 for enhanced bioremediation of chlorpyrifos contaminated soil.” *Ecotoxicol. Environ. Saf.*, 213, 112039.

Yağmur, H. K., and Kaya, İ. (2021). “Synthesis and characterization of magnetic $ZnCl_2$-activated carbon produced from coconut shell for the adsorption of methylene blue.” *J. Mol. Struct.*, 1232, 130071.

Yang, S., Chen, X., Jiang, Z., Ding, J., Sun, X., and Xu, J. (2020). “Effects of biochar application on soil organic carbon composition and enzyme activity in paddy soil under water-saving irrigation.” *Int. J. Environ. Res. Public Health.*, 17(1), 333.

Yang, Y., Wang, X., Wang, Y., Saleem, M., Mu, Y., Zheng, Y., and Zhang, Q. (2023). "Pesticide contamination remediation by biochar-immobilized microorganisms: a review." *Int. J. Envron. Sci. Technol.*, *21*(2), 2225-2238.

Ye, J., Joseph, S. D., Ji, M., Nielsen, S., Mitchell, D. R. G., Donne, S., Horvat, J., Wang, J., Munroe, P., and Thomas, T. (2017). "Chemolithotrophic processes in the bacterial communities on the surface of mineral-enriched biochars." *ISME J.*, 11(5), 1087–1101.

Yin, B., Cao, X., Pan, A., Luo, Z., Dinesh, S., Lin, J., Tang, Y., Liang, S., and Cao, G. (2018). "Encapsulation of CoSx nanocrystals into N/S Co-doped honeycomb-like 3D porous carbon for high-performance lithium storage." *Adv. Sci.*, 5(9). 1800829.

Yin, Z., Xu, S., Liu, S., Xu, S., Li, J., and Zhang, Y. (2020). "A novel magnetic biochar prepared by K_2FeO_4-promoted oxidative pyrolysis of pomelo peel for adsorption of hexavalent chromium." *Bioresour. Technol.*, 300, 122680.

Youngwilai, A., Kidkhunthod, P., Jearanaikoon, N., Chaiprapa, J., Supanchaiyamat, N., Hunt, A. J., Ngernyen, Y., Ratpukdi, T., Khan, E., and Siripattanakul-Ratpukdi, S. (2020). "Simultaneous manganese adsorption and biotransformation by *Streptomyces violarus* strain SBP1 cell-immobilized biochar." *Sci. Total Environ.*, 713, 136708.

Yu, T., Wang, L., Ma, F., Wang, Y., and Bai, S. (2020). "A bio-functions integration microcosm: Self-immobilized biochar-pellets combined with two strains of bacteria to remove atrazine in water and mechanisms." *J. Hazard. Mater.*, 384, 121326.

Yue, C., Jia, N., Lv, X., and Wang, S. (2023). "Identification of two possible metabolic pathways responsible for the biodegradation of 3, 5, 6-trichloro-2-pyridinol in *Micrococcus luteus* ML." *Biodegradation*, 34(4), 371–381.

Zambelli, B., Uversky, V. N., and Ciurli, S. (2016). "Nickel impact on human health: An intrinsic disorder perspective." *Biochim. Biophys. Acta. Proteins. Proteom.*, 1864(12), 1714-1731.

Zamora-Ledezma, C., Negrete-Bolagay, D., Figueroa, F., Zamora-Ledezma, E., Ni, M., Alexis, F., and Guerrero, V. H. (2021). "Heavy metal water pollution: A fresh look about hazards, novel and conventional remediation methods." *Environ. Technol. Innov.*, 22, 101504.

Zeng, S., Qin, X., and Xia, L. (2017). “Degradation of the herbicide isoproturon by laccase-mediator systems.” *Biochem. Eng. J.*, 119, 92–100.

Zhang, D., Yin, C., Abbas, N., Mao, Z., and Zhang, Y. (2020a). “Multiple heavy metal tolerance and removal by an earthworm gut fungus *Trichoderma brevicompactum* QYCD-6.” *Sci.Rep.*, 10(1), 1–9.

Zhang, F., Wang, X., Yin, D., Peng, B., Tan, C., Liu, Y., Tan, X., and Wu, S. (2015a). “Efficiency and mechanisms of Cd removal from aqueous solution by biochar derived from water hyacinth (*Eichornia crassipes*).” *J. Environ. Manage.*, 153, 68–73.

Zhang, H., Yuan, X., Xiong, T., Wang, H., and Jiang, L. (2020b). “Bioremediation of co-contaminated soil with heavy metals and pesticides: Influence factors, mechanisms and evaluation methods.” J. *Chem Eng.,* 398, 125657.

Zhang, J., Kumari, D., Fang, C., and Achal, V. (2019). “Combining the microbial calcite precipitation process with biochar in order to improve nickel remediation.” *Appl Geochem*, 103, 68–71.

Zhang, J., Liu, J., and Liu, R. (2015b). “Effects of pyrolysis temperature and heating time on biochar obtained from the pyrolysis of straw and lignosulfonate.” *Bioresour. Technol.*, 176, 288–291.

Zhang, J., Shao, J., Jin, Q., Zhang, X., Yang, H., Chen, Y., Zhang, S., and Chen, H. (2020c). “Effect of deashing on activation process and lead adsorption capacities of sludge-based biochar.” *Sci. Total Environ.*, 716, 137016.

Zhang, K., Sun, P., Faye, M. C. A. S., and Zhang, Y. (2018). “Characterization of biochar derived from rice husks and its potential in chlorobenzene degradation.” *Carbon.*, 130, 730–740.

Zhang, S., and Wang, J. (2021). “Removal of chlortetracycline from water by *Bacillus cereus* immobilized on Chinese medicine residues biochar.” *Environ. Technol. Innov.*, 24, 101930.

Zhang, S., Zhang, Y., Ren, S., Lu, H., Li, J., Liang, X., Wang, L., Li, Y., Wang, M., and Zhang, C. (2023). “Uptake, translocation and metabolism of acetamiprid and cyromazine by cowpea (*Vigna unguiculata* L.).” *Environ. Pollut.*, 331, 121839.

Zhang, X., Gao, Z., Fan, X., Tan, L., Jiang, Y., Zheng, W., Han, F. X., and Liang, Y. (2022). "A comparative study on adsorption of cadmium and lead by hydrochars and biochars derived from rice husk and Zizania latifolia straw." *Environ. Sci. Pollut Res.,*29(42), 63768-63781.

Zhang, X., Li, Y., and Li, H. (2017). "Enhanced bio-immobilization of Pb contaminated soil by immobilized bacteria with biochar as carrier." *Pol. J. Environ. Stud.*, 26(1), 413–418.

Zhang, X., Wang, Y., Ju, N., Ai, Y., Liu, Y., Liang, J., Hu, Z. N., Guo, R., Xu, W., Zhang, W., Qi, Y., Niu, D., Liang, Q., Sun, H. Bin, and Yang, Y. (2021a). "Ultimate resourcization of waste: crab shell-derived biochar for antimony removal and sequential utilization as an anode for a Li-ion battery." *ACS Sustain. Chem. Eng.*, 9(26), 8813–8823.

Zhang, Y. H., Xu, D., Zhao, X. H., Song, Y., Liu, Y. Le, and Li, H. N. (2016). "Biodegradation of two organophosphorus pesticides in whole corn silage as affected by the cultured *Lactobacillus plantarum*." *3 Biotech*, 6(1), 1-6.

Zhang, Y., Wang, H., Wang, X., Hu, B., Zhang, C., Jin, W., Zhu, S., Hu, G., and Hong, Q. (2017b). "Identification of the key amino acid sites of the carbendazim hydrolase (MheI) from a novel carbendazim-degrading strain *Mycobacterium* sp. SD-4." *J. Hazard. Mater.*, 331, 55–62.

Zhao, L., Hu, G., Yan, Y., Yu, R., Cui, J., Wang, X., and Yan, Y. (2019). "Source apportionment of heavy metals in urban road dust in a continental city of eastern China: Using Pb and Sr isotopes combined with multivariate statistical analysis." *Atmos. Environ.*, 201, 201–211.

Zhao, L., Xiao, D., Liu, Y., Xu, H., Nan, H., Li, D., Kan, Y., and Cao, X. (2020). "Biochar as simultaneous shelter, adsorbent, pH buffer, and substrate of *Pseudomonas citronellolis* to promote biodegradation of high concentrations of phenol in wastewater." *Water. Res.*, 172, 115494.

Zhao, S. X., Ta, N., and Wang, X. D. (2017). "Effect of temperature on the structural and physicochemical properties of biochar with apple tree branches as feedstock material." *Energies*, 10(9). 1293.

Zheng, Y., Han, X., Li, Y., Yang, J., Li, N., and An, N. (2019). “Effects of biochar and straw application on the physicochemical and biological properties of paddy soils in Northeast China.” *Sci. Rep.*, 9(1), 1–11.

Zhen-Yu, W., Ying, X., Hao-Yun, W., Jian, Z., Dong-Mei, G., Feng-Min, L., and Xing, B. (2012). *“*Biodegradation of crude oil in contaminated soils by free and immobilized microorganisms*” Pedosphere* 22, 717-725.

Zhou, S., Li, Y., Chen, J., Liu, Z., Wang, Z., and Na, P. (2014). “Enhanced Cr (VI) removal from aqueous solutions using Ni/Fe bimetallic nanoparticles: Characterization, kinetics and mechanism.” *RSC Adv.*, 4, 50699–50707.

Zhu, C., Zhang, C., Zhang, M., Wu, Y., Zhang, Z., and Zhang, H. (2021). “Degradation characteristics and soil remediation of thifensulfuron-methyl by immobilized *Serratia marcecens* N80 beads.” *Environ. Technol. Innov.*, 24, 102059.

Zhu, X., Chen, B., Zhu, L., and Xing, B. (2017). “Effects and mechanisms of biochar-microbe interactions in soil improvement and pollution remediation: A review.” *Environ. Pollut.*, 227, 98-115.

Zuo, X. J., Liu, Z., and Chen, M. D. (2016). “Effect of H_2O_2 concentrations on copper removal using the modified hydrothermal biochar.” *Bioresour. Technol.*, 207, 262–267.

LIST OF PUBLICATIONS AND CONFERENCES

Research articles

1) Manikandan, S. K., Mariyam, A., Gowda, N., Singh, A., and Nair, V. (2023) "Rice husk biochar-bacteria system for enhanced chlorpyrifos bioremediation: mechanistic understanding and application potential" *Chem Eng J*, 483, 149119.
2) Manikandan, S. K., and Nair, V. (2023) "Developing a biocatalyst showcasing the synergistic effect of rice husk biochar and bacterial cell for the removal of heavy metals" *New J Chem* 48, 416-416.
3) Manikandan, S. K., and Nair, V. (2022). "*Pseudomonas stutzeri* immobilized sawdust biochar for nickel ion removal." *Catalysts*, 12,1495.
4) Manikandan, S. K., and Nair, V. (2023). "Dual-role of coconut shell biochar as a soil enhancer and catalyst support in bioremediation." *Biomass Conv Bioref*, 1-12.

Review articles

- Manikandan, S. K., Pallavi, P., Sujatha, S. K. B., Bhattacharjee, D., Giannakoudakis, D. A., Katsoyiannis, I. A., and Nair, V. (2023). "Effective usage of biochar and microorganism for removal of heavy metal ions and pesticides." *Molecules*, 28,719.
- Manikandan, S. K., Giannakoudakis, D. A., Prekodravac, J. R., Nair, V., and Colmenares, J. C. (2023). "Role of catalyst supports in biocatalysis." *J Chem Technol Biotechnol*, 98, 7-21.

Book chapters

- Manikandan, S.K., Shilli, A.,Noronha F.R., and Nair,V. (2022) "Soil toxicity and remediation techniques" *Pesticides Remediation Technologies from Water and Wastewater*, Elsevier, 411-429.
- Pallavi, P., Manikandan, S.K., and Nair, V. (2023) "Biocatalytic remediation of industrial pollutants" *Green Technologies for Industrial Waste Remediation*, Springer

Other works

- Noronha, F. R., Manikandan, S. K., and Nair, V. (2022). "Role of coconut shell biochar and earthworm (*Eudrilus euginea*) in bioremediation and palak spinach

(*Spinacia oleracea* L.) growth in cadmium-contaminated soil." *J Environ Manage*, 302,114057.

- Shilli, A., Manikandan, S. K., and Nair, V. (2023). "Application of Box-Behnken design in optimization of the Okra (*Abelmoschus esculentus* L.) plant growth in loamy sand soil." *J Soil Sci Plant Nutr*, 23(2), 2625–2636.
- Pallavi, P., Manikandan, S.K., and Nair, V. (2023) "Optimization and mechanistic study on bioremediation of Cr (VI) using microbial cell immobilized sugarcane bagasse biochar" *J Water Process Eng,* 58, 104859.

Conferences

- Manikandan, S, K., and Nair, V. "A sustainable approach to heavy metal wastewater remediation through biochar-bacteria synergy", The International Conference on Desalination, Environment and Sustainability IDEAS 2024, January 22-23, 2024, Abu Dhabi, UAE.
- Manikandan, S, K., and Nair, V. "Biodegradation of chlorpyrifos by *Aeromonas veronii* immobilized rice husk biochar," 4th International Conference on Bioresource Technology for Bioenergy, Bioproducts & Environmental Sustainability, May 14–17, 2023, Lake Garda, Italy.
- Manikandan, S, K., and Nair, V."Optimization and mechanistic study of cadmium removal using novel *Pseudomonas* immobilized sawdust biochar," International Conference on Biotechnology for Sustainable Bioresources and Bioeconomy (BSBB-2022), December 07–11, 2022, Department of Biosciences and Bioengineering, IIT Guwahati, India.
- Manikandan, S, K., and Nair, V. "Effect of coconut shell biochar on tomato (*Solanum lycopersicum* L.) growth in lateritic loam and clay soil", International Conference on Chemical Engineering: Enabiing Transition Towards Sustainable Future, September 08-10, 2022, Department of Chemical Engineering, IIT Roorkee, India
- Singh, A., Manikandan, S, K., and Nair, V. "Harnessing microbial cell -biochar synergy for eco-friendly wastewater treatment", The International Conference on Desalination, Environment and Sustainability IDEAS 2024, January 22-23, 2024, Abu Dhabi, UAE.
- Singh, A., Manikandan, S, K., and Nair, V. "Harnessing microbial cell -biochar synergy

for eco-friendly wastewater treatment", The International Conference on Separation and Purification Technologies (ICSPT), December 07–08, 2023, IIT Patna, India.

- Sreekumar, K., Manikandan, S, K., and Nair, V. "A novel approach on Low density polythene degradation using microbes immobilized on biochar", International conference on Biotechnology, Sustainable Bioresources and Bioeconomy (BSBB-2022), December 7 - 11, 2022, Department of Bioscience and Biotech engineering, IIT Guwahati.
- Noronha, F. R., Manikandan, S, K., and Nair, V. "Role of coconut shell biochar and earthworms (*Eudrilus euginea*) in Palak Spinach (*Spinacia oleracea*) growth studies in cadmium contaminated soil" International Conference on Recent Technologies and Advanced Materials for Green Energy and Sustainable Environment. March 12-13, 2021.

Achievement

- International travel grant support from SERB for attending '4th International Conference on Bioresource Technology for Bioenergy, Bioproducts & Environmental Sustainability', May 14–17, 2023, Lake Garda, Italy.
- Publication titled 'Role of catalyst supports in biocatalysis'. in the Journal of Chemical Technology Biotechnology acknowledged as a top downloaded article by Wiley.

BIODATA

SOUMYA K M

Tharayilpura House

Kanjikode, Palakkad 678621

Contact number: +91 9747525055

E-mail ID: Soumyamanikandan01@gmail.com

EDUCATION

- PhD in Chemical Engineering (CGPA- 7.93) 2019-2023

  Department of Chemical Engineering

  National Institute of Technology Karnataka,

  Surathkal, Mangalore 575025

- Master of Science in Microbiology (CGPA-8.56) 2013-2015

  Department of Microbiology, Pondicherry University,

  Kalapet, Puducherry 605014

- Bachelors of Science in Microbiology (CGPA 8.36) 2011- 2013

  Department of Microbiology, CMS college of Science and Commerce

  Bharathiar University, Coimbatore 641049

PUBLICATIONS

1. Manikandan, S. K., Mariyam, A., Gowda, N., Singh, A., and Nair, V. (2023) "Rice husk biochar-bacteria system for enhanced chlorpyrifos bioremediation: mechanistic understanding and application potential" *Chem Eng J*, 483, 149119.
2. Pallavi, P., Manikandan, S.K., and Nair, V. (2023) "Optimization and mechanistic study on bioremediation of Cr (VI) using microbial cell immobilized sugarcane bagasse biochar" *J Water Process Eng,* 58, 104859.
3. Manikandan, S. K., and Nair, V. (2023). "Developing a biocatalyst showcasing the

synergistic effect of rice husk biochar and bacterial cell for the removal of heavy metals." New J. Chem.

4. Pallavi, P., Manikandan, S.K., and Nair, V. (2023) "Biocatalytic remediation of industrial pollutants" *Green Technologies for Industrial Waste Remediation*, Springer
5. Manikandan, S. K., and Nair, V. (2023). "Dual-role of coconut shell biochar as a soil enhancer and catalyst support in bioremediation." Biomass Convers Biorefin, 1-12.
6. Manikandan, S. K., Pallavi, P., Shetty, K., Bhattacharjee, D., Giannakoudakis, D. A., Katsoyiannis, I. A., and Nair, V. (2023). "Effective usage of biochar and microorganisms for the removal of heavy metal ions and pesticides." Molecules, 28, 719.
7. Manikandan, S. K., and Nair, V. (2022). "Pseudomonas stutzeri immobilized sawdust biochar for nickel ion removal." Catalysts, 12, 1495.
8. Noronha, F. R., Manikandan, S. K., and Nair, V. (2022). "Role of coconut shell biochar and earthworm (*Eudrilus euginea*) in bioremediation and palak spinach (Spinacia oleracea L.) growth in cadmium-contaminated soil." J Environ Manage, 302.
9. Manikandan, S. K., Giannakoudakis, D. A., Prekodravac, J. R., Nair, V., and Colmenares, J. C. (2022). "Role of catalyst supports in biocatalysis." J Chem Technol Biotechnol, 98(1), 7-21.
10. Manikandan, S.K., Shilli, A., Noronha, F.R. and Nair, V., (2022). Soil toxicity and remediation techniques. Pesticides remediation technologies from water and wastewater, 411-429.
11. Shilli, A., Manikandan, S. K., and Nair, V. (2023). "Application of Box-Behnken Design in optimization of the okra (*Abelmoschus esculentus* L.) plant growth in loamy sand soil." J Soil Sci Plant Nutr, 23, 2625–2636.
12. Koippully, S., Pattnaik, S.S. and Busi, S., 2021. Isolation, identification and substrate specificity of a nitrilase producing bacteria, *Acidovorax* sp. SK1. Journal of Microbiology, Biotechnology and Food Sciences, 2021, 788-793.

BOOK CHAPTERS

1. Manikandan, S.K., Shilli, A., Noronha, F.R. and Nair, V., 2022. Soil toxicity and

remediation techniques. Pesticides remediation technologies from water and wastewater, Elsevier, 411-429.

2. Sindhu, R., Shiburaj, S., Sabu, A., Fernandes, P., Singhal, R., Mathew, G.M., Nair, I.C., Jayachandran, K., Vidya, J., de Souza Vandenberghe, L.P. and Deniz, I., 2021. Enzyme technology in food processing: recent developments and future prospects, Elsevier, 191-215.

CONFERENCES

1. Manikandan, S, K., and Nair, V. "A sustainable approach to heavy metal wastewater remediation through biochar-bacteria synergy", The International Conference on Desalination, Environment and Sustainability IDEAS 2024, January 22-23, 2024, Abu Dhabi, UAE.
2. Manikandan, S, K., and Nair, V. "Biodegradation of chlorpyrifos by *Aeromonas veronii* immobilized rice husk biochar," 4th International Conference on Bioresource Technology for Bioenergy, Bioproducts & Environmental Sustainability, May 14–17, 2023, Lake Garda, Italy.
3. Manikandan, S, K., and Nair, V."Optimization and mechanistic study of cadmium removal using novel *Pseudomonas* immobilized sawdust biochar," International Conference on Biotechnology for Sustainable Bioresources and Bioeconomy (BSBB-2022), December 07–11, 2022, Department of Biosciences and Bioengineering, IIT Guwahati, India.
4. Manikandan, S, K., and Nair, V. "Effect of coconut shell biochar on tomato (*Solanum lycopersicum* L.) growth in lateritic loam and clay soil", International Conference on Chemical Engineering: Enabiing Transition Towards Sustainable Future, September 08-10, 2022, Department of Chemical Engineering, IIT Roorkee, India
5. Singh, A., Manikandan, S, K., and Nair, V. "Harnessing microbial cell -biochar synergy for eco-friendly wastewater treatment", The International Conference on Desalination, Environment and Sustainability IDEAS 2024, January 22-23, 2024, Abu Dhabi, UAE.
6. Singh, A., Manikandan, S, K., and Nair, V. "Harnessing microbial cell -biochar synergy for eco-friendly wastewater treatment", The International Conference on Separation and Purification Technologies (ICSPT), December 07–08, 2023, IIT Patna, India.

7. Sreekumar, K., Manikandan, S, K., and Nair, V. “A novel approach on Low density polythene degradation using microbes immobilized on biochar", International conference on Biotechnology, Sustainable Bioresources and Bioeconomy (BSBB-2022), December 7 - 11, 2022, Department of Bioscience and Biotech engineering, IIT Guwahati.
8. Noronha, F. R., Manikandan, S, K., and Nair, V. “Role of coconut shell biochar and earthworms (*Eudrilus euginea*) in Palak Spinach (*Spinacia oleracea*) growth studies in cadmium contaminated soil” International Conference on Recent Technologies and Advanced Materials for Green Energy and Sustainable Environment. March 12-13, 2021.
9. Manikandan, S, K., Abdulhameed, S., and Sugathan, S. “Utilization of cashew apple bagasse for gallic acid production using *Aspergillus niger* TBG-A20” National Seminar on Forestry, Plant Genetics and Improvement, December 03-04,2019, KSCSTE-KFRI Peechi, Kerala, India.
10. Manikandan, S, K., Abdulhameed, S., and Sugathan, S. “Tannin acyl hydrolase activity of *Streptomyces mirabilis* TBGS10” International Workshop on Biology and Applications of Actinomycetes, November 01,2019, Helmholtz Centre for Infection Research, Braunschweig, Germany and University of Mysore, India.
11. Manikandan, S, K., Abdulhameed, S., and Sugathan, S. “Tannin acyl hydrolase activity of *Streptomyces* sp. isolated from shola forests of Munnar wild life sanctuary, Kerala” International symposium on Converging Technologies for Human Welfare Biotechnology, Nanotechnology and Information Technology, July 02, 2019, Department of Biotechnology of Mar Ivanios College, Thiruvananthapuram, India.

ACHIEVEMENTS

- International travel grant support from SERB for attending ‘4th International Conference on Bioresource Technology for Bioenergy, Bioproducts & Environmental Sustainability’, May 14–17, 2023, Lake Garda, Italy.
- Publication titled ‘Role of catalyst supports in biocatalysis’. in the Journal of Chemical Technology Biotechnology acknowledged as a top downloaded article by Wiley.
- Best Poster Award in Louis Pasteur memorial international Symposium conducted at Dr.

NGP College, Coimbatore on "Hen's egg test- chorio allantoic membrane: A reliable human friendly method to replace animal studies"

- Best poster award in International Symposium conducted at Department of Biotechnology Mar Ivanious College, Kerala University on "Tannin acyl hydrolase activity of *Streptomyces* sp. isolated from shola forests of Munnar wildlife sanctuary, Kerala"

Declaration:

I hereby declare that the above particulars are true to the best of my knowledge.

Place: Surathkal, Karnataka, India

Date: 08-04-24

Soumya K M